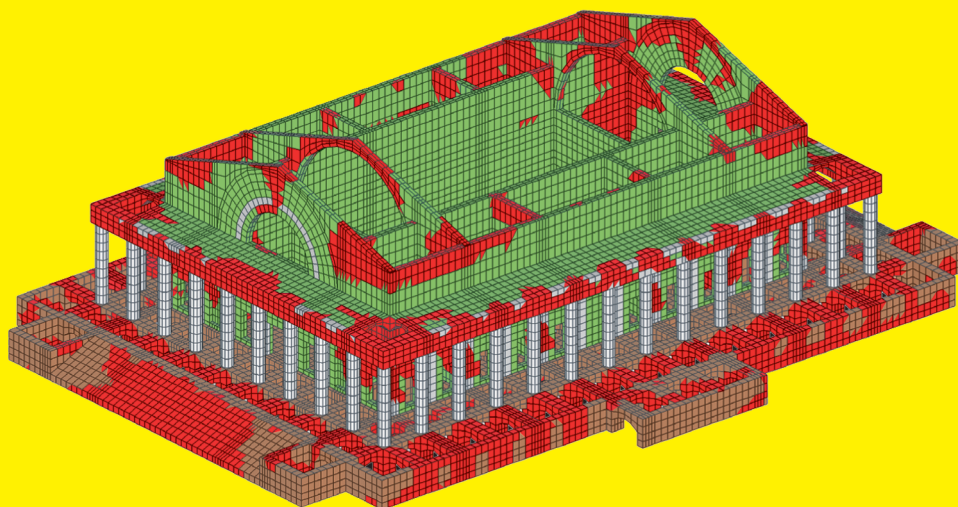PROCEEDINGS
OF THE TECHNICAL MEETING TC207 ISSMGE
DUBROVNIK 2011

WORKSHOP ON SOIL-STRUCTURE INTERACTION AND RETAINING WALLS

6-8 October 2011, Dubrovnik - CROATIA

Croatian Geotechnical Society

TC 207

Technical Committee TC207

SIMSG   ISSMGE

International Society for
Soil Mechanics and
Geotechnical Engineering

PROCEEDINGS
OF THE TECHNICAL MEETING TC207 ISSMGE
DUBROVNIK 2011

WORKSHOP ON SOIL-STRUCTURE INTERACTION AND RETAINING WALLS

6-8 October 2011, Dubrovnik - CROATIA

Edited by:
V.M. Ulitsky
M.B. Lisyuk
I. Sokolić

Zagreb
2011

Proceedings of the Technical Meeting TC207 – Workshop on Soil-Structure Interaction and Retaining Walls

The responsibility for content and editing is placed upon the authors of the papers of this volume.

Front Page: Soil-Structure interaction model for Stock Exchange on Vasilievsky Island, Saint Petersburg (by St. Petersburg State Transport University)

PREFACE

It is a great pleasure that the Croatian Geotechnical Society is organizing the Technical Meeting TC207 – Workshop on Soil-Structure Interaction and Retaining Walls in Dubrovnik, Croatia, from 6th to 8th October 2011. The Meeting gives a good opportunity to all members of the Technical Committee TC207 and their colleagues to exchange their knowledge and experience in the very important and fast growing field of Geotechnics, Soil-Structure Interaction and Retaining Walls.

The Technical Committee TC207 belongs to one of 30 committees of the International Society for Soil Mechanics and Geotechnical Engineering (ISSMGE). The basic field of research of the TC207 Committee covers the problems of Soil-Structure Interaction and Retaining Walls, corresponding to the Application Category of the ISSMGE Committee organization chart. The Committee consists of 44 members from 28 different countries around the world. The current work is focused on the following main three tasks: Guidelines on Soil-Structure Interaction, Retaining Walls and Website of the TC207.

The proceedings of the Workshop include one lecture and 17 delegates' papers from 9 countries. The papers in the proceedings cover a wide range of geotechnical problems: Design of foundation for the high-rise building, Preservation and Reconstruction of Historical Monuments, Strengthening of Old Bridge Foundation, Investigation of Hard Soils, Settlement reduction for the Footings, Modelling of Underline Pipelines and Reservoirs, Microtunnelling, Tunnel-Soil-Pile Interaction Modelling, Constitutive Soil Modelling, Predicting-Monitoring-Controlling of Ground Movements due to Excavation, Influence of the Excavation on the Neighbour Buildings, Geosynthetic Reinforced Retaining Walls and There-dimension Slope Stability Analysis.

We hope that the proceedings will be useful for all experts interested in above mentioned topics.

V. Ulitsky
Chair of TC207

M. Lisyuk
Co-Chair of TC207

I. Sokolić
Secretary of the Technical Meeting TC207

ORGANIZERS

Croatian Geotechnical Society (Hrvatsko Geotehničko Društvo) – www.hgd-cgs.hr

Technical Committee TC207 of International Society for Soil Mechanics and Geotechnical Engineering (ISSMGE) – http://www.tc207ssi.org/main-page.html

ORGANIZING COMMITTEE

V.M. Ulitsky, Chairman of the Technical Committee TC207, Professor, Head of Department, Saint Petersburg State Transport University, Russia

M.B. Lisyuk, Co-Chairmen of the Technical Committee TC207, Director for Development, GRF, Russia

A. Szavits-Nossan, Chairman of the Croatian Geotechnical Society, Professor, University of Zagreb, Faculty of Civil Engineering, Croatia

I. Sokolić, Secretary of the Organizing Committee, Member of ISSMGE, University of Zagreb, Faculty of Civil Engineering, Croatia

MEMBERS OF TECHNICAL COMMITTEE 207
"SOIL-STRUCTURE INTERACTION AND RETAINING WALLS"
ISSMGE

V.M. Ulitsky, Russia (Chairman)
M.B. Lisyuk, Russia (Co-chairman)
W. Van Impe, Belgium
K. Shashkin, Russia
C. Haberfield, Australia
Y. El-Mossallamy, Egypt
R. Katzenbach, Germany
W. Bilfinger, France
L. Andresen, Norway
H. St. John, UK
R. Finno, USA
F. Liu, China
N. Petrović, Croatia
J. Kos, Czech Republic
K. Avellan, Finland
C. Jacquard, France
J. Sze, Hong Kong
V. Balakumar, India
M. Latha, India
N.K. Samadhiya, India
O. al-Farouk Salem al-Damluji, Iraq
H. Hazarika, Japan
G.A. Sultanov, Kazakhstan
M. Korff, Netherlands
G. Horodecki, Poland
F. Roman, Romania
Z.G. Ter-Martirosyan, Russia
V.C.W. Ong, Singapore
A.R. Walker, Singapore
P. Morrison, UK
I. Sokolić, Croatia
M. Favre, France
J.M. Fernández Vincent, Argentina
O. Biligin, USA
J. Couck, Belgium
C. di Prisco, Italy
G. Gottardi, Italy
A.M. Kayana, Norway
B. Moczar, Hungary
J. Moreno, Spain
P. Pantelidis, Greece
L. Vollmert, Germany

CONFERENCE SECRETARIAT

Igor Sokolić – Secretary General,
University of Zagreb, Faculty of Civil Engineering,
Kačićeva 26, 10000 Zagreb, Croatia isokolic@grad.hr

Table of contents

Aspects of soil-structure interaction in design of buildings and geotechnical structures

Retaining walls and structures
Failures of geotechnical structures

Topic 1

Aspects of soil-structure interaction in design of buildings and geotechnical structures

Preservation and reconstruction of historical monuments in Saint Petersburg with account of soil-structure interaction

V.M. Ulitsky
Chair of TC207 "Soil-Structure Interaction and Retaining Walls" ISSMGE
State Transport University, Saint Petersburg, Russia, E-mail ulitsky.vladimir@gmail.com

A.G. Shashkin, K.G. Shashkin, M.B. Lisyuk
Georeconstruction Engineering Co, Saint Petersburg, E-mail Lisyuk@gmail.com

ABSTRACT: Many important historical monuments in Saint Petersburg have been analysed by the authors using soil-structure interaction (SSI) approach. Among them are the Stock Exchange building, Konstantinovsky palace in Strelna, Admiralty building in central Saint Petersburg, St. Nicholas Naval Cathedral in the town of Kronshtadt near Saint Petersburg. These projects are presented in the paper. It is shown that SSI is a very powerful tool in analysing historical monuments. The potential of this method lies in the complete description of the stress-state of the monuments and in possibility to develop measures of the monuments' remediation. To fulfil this method successfully a comprehensive survey of the monuments is needed. Essential parts of this survey are survey of structural elements and foundations, geophysical research, soil sampling and testing. Influence of geotechnologies on adjacent buildings in congested urban conditions is also discussed in the paper.

INTRODUCTION

The lecture deals with preservation and reconstruction of the most valuable historical monuments in St. Petersburg.

Generally, analysis of historical buildings condition is very important for projects dealing with preservation or reconstruction of historical monuments and their foundations (Burghignoli, Jamiolkowski and Viggiani, 2007, Powderham, 2003, Ulitsky et al, 2003).

Such analysis should include the following major steps:

- Analysis of the actual stress - strain conditions of subsoil of preserved buildings, and, if necessary, of adjacent buildings;
- Estimation of the influence of present vibration background on settlement development;
- Estimation of ongoing settlements of buildings (under own weight and outside factors), that is defined through calculations or observations the location of geodetic marks and gauges;
- Estimation of the allowable additional settlement of the existing buildings during reconstruction works or new development.

For important projects it is also necessary to make historical analysis of foundation behaviour of preserved/reconstructed buildings and buildings adjacent to reconstructing object or to new development together with substructure behaviour of the existing buildings;

In all cases the principle of soil-structure interaction analyses was used with account of joint work of subsoil, foundations and superstructure.

1. STOCK EXCHANGE BUILDING ON VASILIEVSKY ISLAND SPIT

First we shall review the building of the Stock Exchange on Vasilievsky Island Spit in Saint Petersburg. This building which has become one of the symbols of Saint-Petersburg was constructed in 1805 according to the design of Thomas de Thomon (Fig. 1) who raised a rectangular ancient temple-style building on a granite rock stylobate formed by a system of massive pillars and walls covered with cross-vaulting. The central hall of the Stock Exchange is capped with a caissonned cylindrical canopy.

Figure 1. Former Stock Exchange on Vasilievsky Island spit: a) cross section; b) the building by the construction completion

In 2002 a large scope of works on the building's elevations was carried out. The cracks developed over two centuries of the building's life were revealed. The restorers expressed their concern regarding the renewed cracks appearing in the new superficial finishes on the gable ends and splitting the building along its longitudinal axis (Fig. 2).
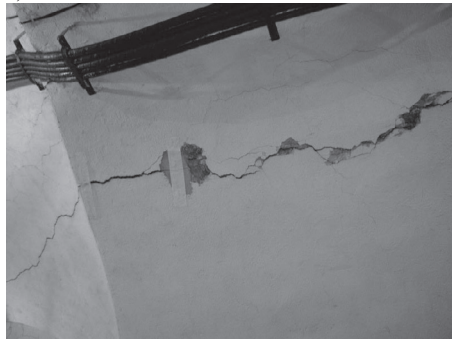
a)

b)

Figure 2 a), b). Development of cracks in the external walls of the building

To identify the reason for the development of these deformations we studied the available historical accounts of the Stock Exchange construction, explored the site conditions, investigated the actual layout of the foundations, measured the accrued settlement differentials, analysed the principal concept behind the superstructure build-up, established the actual subsoil conditions, identified the dynamic background rendered by the nearby traffic, and, finally, conducted a series of soil-structure calculations with the account of all risk factors gleaned through all the above assessment procedures (Ulitsky, 2003).

Unfortunately no geodetic monitoring of the settlement had been previously conducted. Based on the setting-out carried out on all levels of column bases throughout the building perimeter it was possible to establish the settlement differential present between the north and the south elevations amounting to as much as 13-14 cm, whereat the settlement differential along the elevations proved negligible.

The principal feature of the ground conditions was identified as considerable heterogeneity of the soil strata (Fig. 3). The made-up ground is underlain by intermittent sand and soft clayey sand strata with some presence of loam, including a stratum of peaty clay sand whose thickness increases from 0.0 m to 2.0 m directed from north to south elevations.
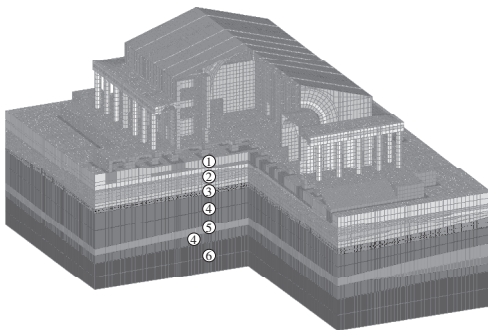
Figure 3. Stock Exchange building and its subsoil. Computer generated outlook. Soil layers:
1 – silty sand, 2 – clayey sand with inclusion of peat,
3 – soft sandy clay, 4 – semi hard clayey sand,
5 – sand with gravel, 6 – dislocated clay

Another possible factor conducive to the actual risk was a possible heterogeneity of the buildings foundations. Thomas de Thomon constructed his building on site of the pulled down Stock Exchange which had been previously built by G. Quarenghi. In construction practice of the time it was a common approach to incorporate old foundations into new structures (which method was implemented by G. Quarenghi himself).

To investigate the matter further the authors carried out a condition survey on the foundations.

The survey displayed the layout where the strip foundations of the exterior stylobate walls (compounded of granite and limestone elements) served as a strengthening embankment for the excavation pit, inside which (over a layer of timber beams) a solid limestone foundation wall was constructed supporting pillar-type rubblework foundations (Fig. 4).

The hypothesis as to discontinuity of the foundation layout was disproved. No rotting of timber beams was observed; fine sand underneath was found to be of mostly firm composition. Therefore it was possible to establish that development of the deformations in the given case was unrelated to either of the two most common causes of foundation failure in Saint-Petersburg, these being, firstly, decomposition of timber elements within foundations and, secondly, washing out of sand fines from subsoils.

The supposition as to unbalanced arc action in the central vault of the Stock Exchange being a contributing factor to the deformations was also discarded. Condition survey showed that the vault was a 'false' one, suspended from the consoles of the reinforced concrete trusses installed in 1914 during reconstruction of the building as per the design submitted by architect Theodore Lidval.

Finally, the list of provisional contributing factors was reduced to the only one remaining possibility i.e. non-homogeneity of the underlying ground composition. We set out to conduct a series of geophysical tests (seismotomography) which confirmed some weaker strata underneath the south part of the building.
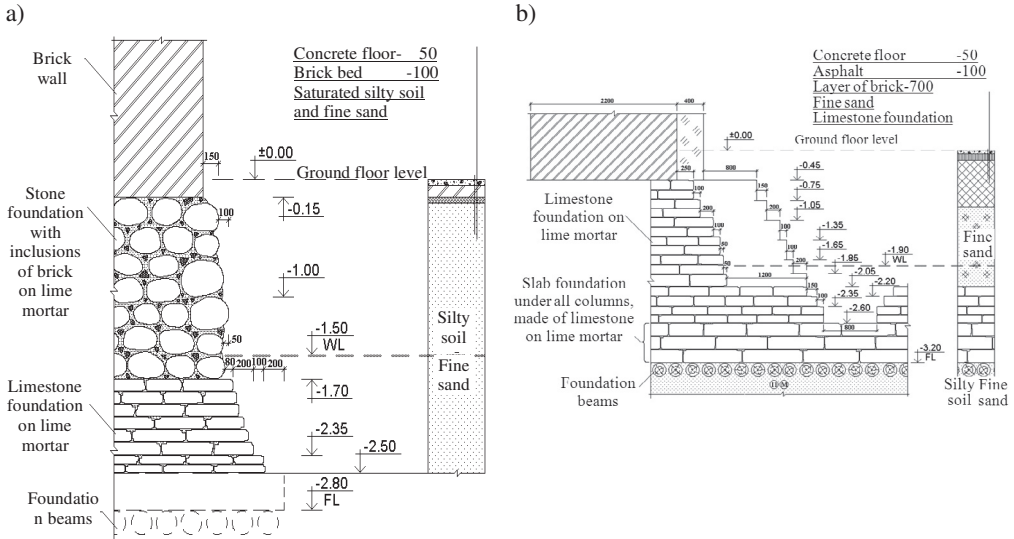
Figure 4. a) Exterior wall foundation of Stock Exchange stylobate; b) Foundations of Stock Exchange pillars

To furnish numerical modelling of the building's behaviour within the scope of *our FEM models* software we used high order elastic rectangular shelled elements to approximate functions of unknown displacement and angles of rotation. We also used volumetric elastic elements, as well as elastic rod elements.

Elasto-plastic soil model for numerical simulation has been chosen. This model presupposes a linear connection between stress and strain within the surface of Coulomb-Mohr criterion, as well as dilatancy-free flow of ground on the limiting surface. To create a subsoil model, spatial character of strata sequence was taken into account (see Fig. 3).

Calculations were carried out in two steps (Fig. 5). The first step featured modelling of the natural stressed subsoil conditions, the second – construction of the building. As was shown by the calculations, the overall settlement of the building throughout the entire period of its life should have been in the order of 26-44 cm.
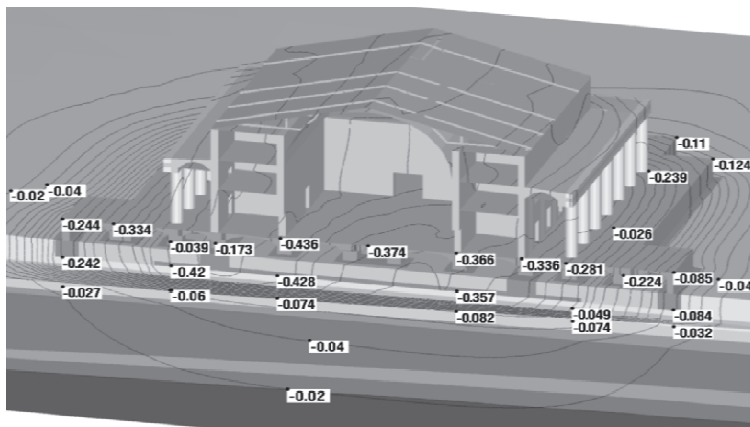
Figure 5. Contours of subsoil settlements (m)

Thereat settlement differential between the corners of the building reached 9-14 cm increasing towards the south wall, which was validated by monitoring. The bulk of compressible strata taken into account was 13-15 m. The most substantial contribution to settlement differential was rendered by the stratum of peaty loam. Considering that the absolute levels of the underside of that stratum vary from -0.8 m to -5.3 m, the foundations of the building fail to reach any reliable support and are embraced by the peaty loam area in the south-east part of the buildings.

As per the calculation results the reason for opening of the cracks lies in development of tensile stress in the upper part of the walls owing to settlement differentials (Fig. 6). The calculation results fully agree with the actual conditions of cracking and deflections of pillar bases (Fig. 7, 8).

a)
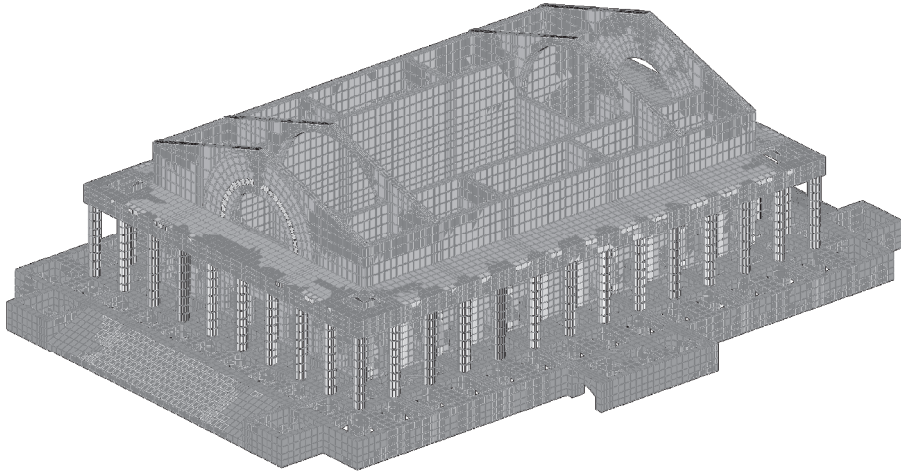
b)
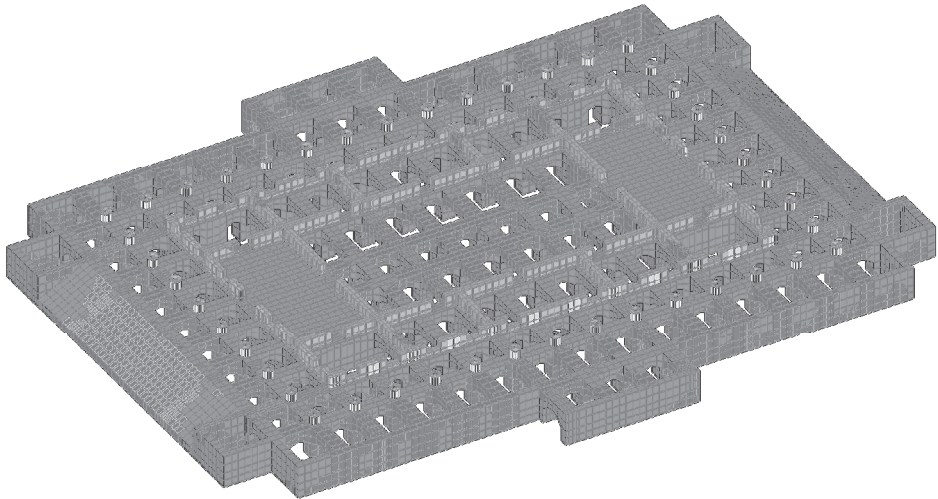
Figure 6. Possible locations of cracks development according to calculations: a) in the bearing walls and structures; b) in the masonry of the ground floor (red areas denote major tensile stresses development)
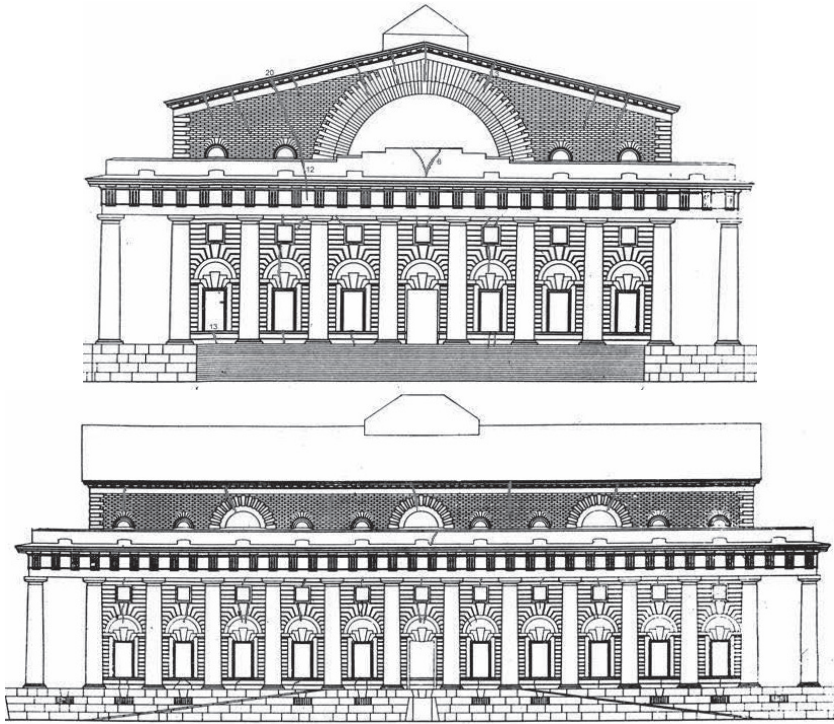
Figure 7. a) Possible locations of cracks development. b) Cracks layout according to condition survey results. c) Locations of possible cracks development in the masonry of the ground floor
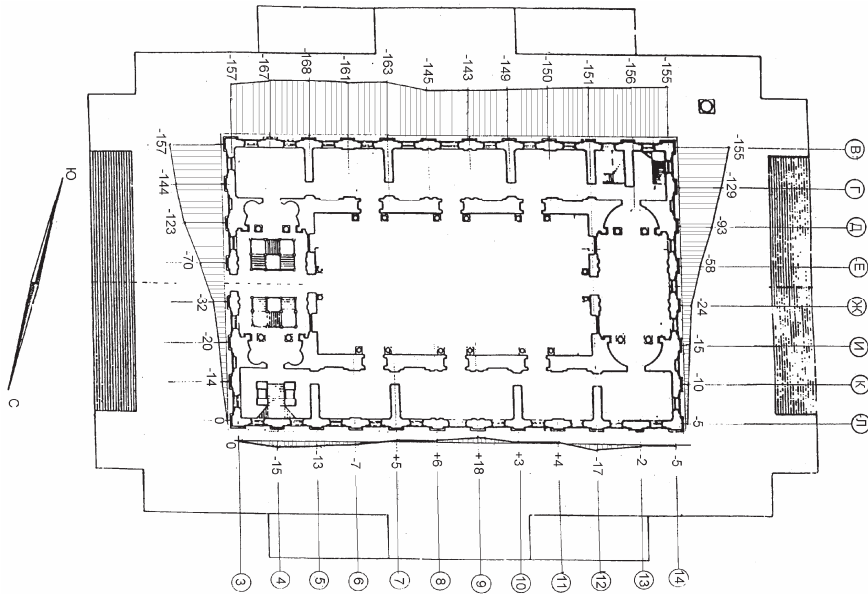
Figure 8. Deflections of the pillar bases from horizontal line as of December 2002 (mm)

The calculation identified the most adverse settlement on the foundations located under the double contour of the building walls. A somewhat smaller settlement of the other sections of the foundation is responsible for development of tensile areas in brickwork vaults of the central and edge zones of the stylobate, also validated by the actually observed situation. The conclusion therefore suggested itself as to the discontinuity of the subsoil strata being responsible for the detrimental settlement differential (Fig. 5).

Geodetic monitoring which has been conducted by ourselves since 2002 shows the current settlement rate on the Stock Exchange approaches 3 mm a year. Such settlement rate is typical for the post-glacial strata of Saint-Petersburg, capable of long-term (so called 'secular') creep under a constant dynamic load.

Measurements of vibration generated by the passing traffic in the structures of the Stock Exchange showed vibration acceleration of 0.035 m/s2 this value being typical for a city with a heavy traffic load.

Thus, there are no grounds to expect any progressive character of deformations and no strengthening or underpinning of the building is required, provided, of course, that the present situation remains unchanged.

The building of the Stock Exchange is currently under constant monitoring. No intensifying deformations have been recently observed.

2. RECONSTRUCTION OF KONSTANTINOVSKY PALACE IN A SUBURB OF SAINT PETERSBURG

2.1. Introduction

Reconstruction of Konstantinovsky Palace was one of the most important projects in Russia in the beginning of the new millennium. This work was stipulated by a ruling passed by the government of the Russian Federation, whereby the palace was to be converted into the Congress Palace. The plan for the Congress Palace project included the following:

1. Reconstruction and restoration of the Konstantinovsky Palace.
2. Reconstruction of the stable quarters, an edifice of dimensions commensurable with the main palace.

3. Reconstruction of two buildings built in the middle of the 20th century: The Engineers' Wing and the Hostelry
4. Construction of the Consuls' Village (comprising 11 cottages).
5. Restoration of the park.
6. Reconstruction of the talks chamber.

The project involved participation of 10 design firms and about 20 subcontractors. The total number of workers simultaneously present at the site reached up to 3,000 people. The entire project was completed in 1.5 years, commencing in November of 2001 and coming to a close in March of 2003.

This article describes the major works on conception and realization of the Konstantinovsky Palace reconstruction project.

The authors of this paper participated in the planning and development of the project, as well as the actual reconstruction of the palace. For his involvement in the project, the first author was awarded the title Russian Civil Engineer of the Year in 2003.

2.2. Historical background

Strelna Palace, more widely known as Konstantinovsky Palace, is a large palace located in the nearest suburb of St. Petersburg on the shore of the Gulf of Finland (Fig. 9-12). Peter the Great was fond of that location where he resolved to construct masonry chambers. Imperial residences in the suburbs of St. Petersburg would commonly begin as modest buildings and at a later date be expanded and reconstructed, graduating to more luxurious edifices. Strelna Palace, however, had from its inception been conceived as a stately and imposing structure. It involved leading European and Russian architects of the time, such as Jean Batiste Leblon, Nicolo Micetti, and Francesco-Bartolomeo Rastrelli.

This palace was situated on the top of the 8-m high slope of the historical Baltic coast, the height being far from insignificant for the typically flat ground of St. Petersburg and the environs. The slope was reinforced with a retaining structure fashioned into a series of loggias (half-sphere niches with the open space towards the park). The front of the palace had been envisaged to provide a majestic fountain cascade, followed by a canal leading to the sea.

Figure 9. Bird's-eye view of Konstantinovsky Palace and the upper and lower parks in Strelna.

Subsequently, the great Russian reformer lost interest in Strelna and shifted his attention to the town of Peterhof as the place for establishing the official suburban residence town. The palace had lost its favour with the emperor. Its construction being very much delayed, the architect Micetti took offence and retired to his motherland to continue the creation of masterpieces there. The palace, having been constructed up to the roof level, remained uncompleted.

It was only following the accession of Empress Catherine that fortune smiled on Strelna Palace once more, and Rastrelli was commissioned to complete its construction. However, the court never moved into the new residence. The luxurious palace was again forgotten for 50 years and, as the case usually is with abandoned buildings, it was decaying quickly due to lack of maintenance and heating.

In 1802, the new owner, Emperor Paul presented the palace to his son Constantine, whereupon it became known as Konstantinovsky Palace. Refinishing of the palace was completed in 1 year. It was designed and supervised by A. Voronikhin. The sumptuous abode of the Grand Duke stood open to welcome its new owner. Fate, however, had no remorse as a large fire broke out on December 28, 1803, destroying the entire artistic decorum of the hapless building. Everything was to be renovated by architect L. Ruska. Architect A. Voronikhin designed a series of grottoes. The roof of the grottoes served as a spacious terraced square facing the palace. The structure of the terrace at the same time functioned as a retainer for the palace, conditioning stability of the entire palatial complex.

The palace was destroyed during World War II, with just the walls remaining in place. During the post-war period the only parts restored to their original condition were the external walls, facades and the two reception halls. More recently, destructive tendencies have prevailed (Fig. 14). The most significant misfortune was the failure of the precipitation sewer. Water from the roof and the terrace found its way into retaining walls, bringing about dampening and partial collapse of the structure. The bearing timber piles were decomposing, and the stone vaults of the terrace suffered from significant masonry fallouts.

10
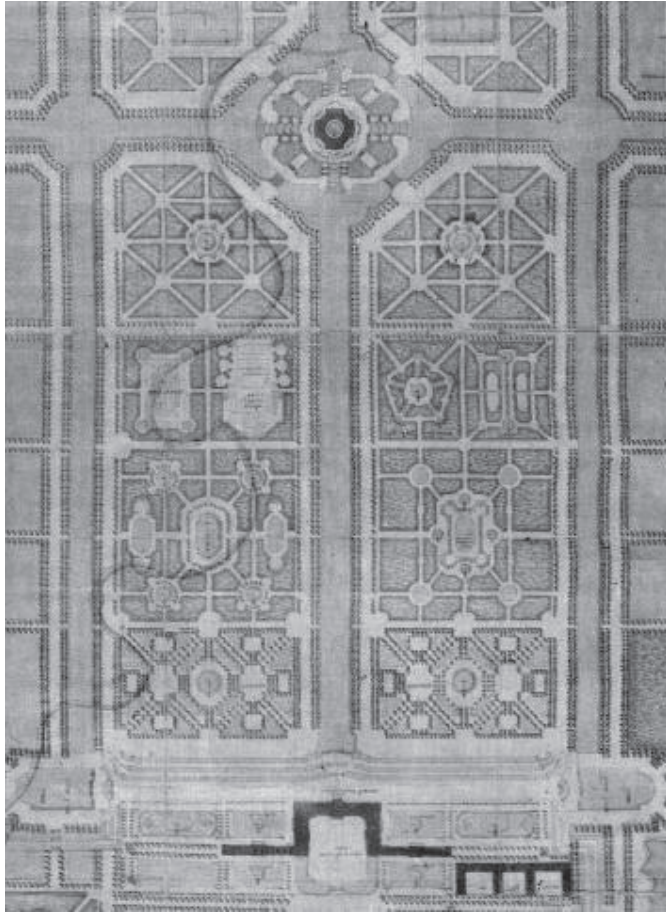
Figure 10. Plan of Konstantinovsky Palace in Strelna. Drawing by Jean Batiste Leblon. Beginning of the 18th century.
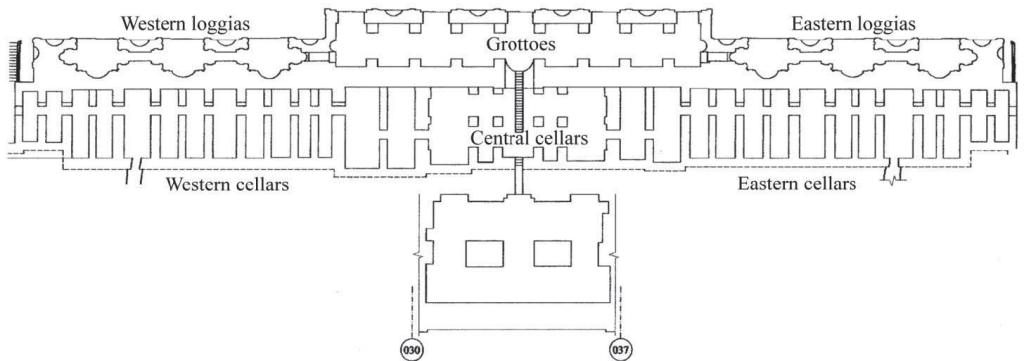
Figure 11. Plan of cellars, grottoes, and loggias of Konstantinovsky Palace.

2.3. Palace condition survey and site investigation

Strelna Palace is a 3-story building on a high basement floor (socle floor). It was constructed on linear rubblework foundations on the crest of a natural slope which descends into Lower Park by three tiers. The natural slope in front of the palace was fashioned into a horizontal area 23 m wide in the middle and 17.3 m wide on the edges. The absolute level of the terrace surface is at 12.7 m Baltic Datum (BD) (see Fig. 12, 13, 16). The vertical terrace ramp (8.0 m high) is retained by a complex system of masonry structures forming grottoes and lateral loggias on the front elevation (Fig. 11), as well as the suite of wine cellars between the grottoes and the palace. The grotto is divided throughout its length into 9 equal bays, each approximately 4.75 m in length.

Symmetrically on each part of the central grotto there are 3 loggias (see Fig. 11 and 12). The gable wall for both the grottoes and the loggias is the actual retaining wall. The loggias retaining wall contains half-sphere niches forming the volume of every loggia. In these locations the retaining wall is especially thin (around 1.5 m), but gradually increases up to 3.2 m elsewhere.

Behind the retaining wall there is a suite of basement premises (former wine cellars) with the absolute floor level of 8.7 m BD. These premises are vaulted with cylindrical brickwork arches supported by transverse walls. The transverse walls are located both in the middle and on the sides of each loggia.

Figure 12. A photograph of Konstantinovsky Palace taken in 1910.
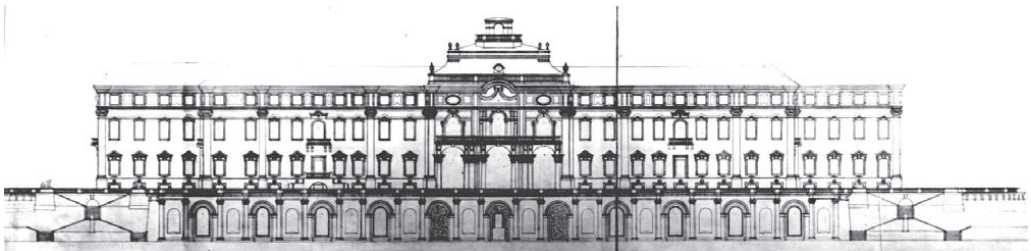
Figure 13. A drawing of the palace made in the first half of the 20th century.

The retaining structure layout of Konstantinovsky Palace in Strelna is a unique feat of engineering of the 18th and19th centuries. It serves not only as a podium for the palace on the Lower Park side, forming a spacious terrace in front of its north elevation, but also as a structure ensuring the building's stability on the brink of an 8-m slope at the historical coast of the Baltic Sea. Stability of the entire palace depends on the technical condition of its retaining structures.

The authors were commissioned by KGIOP (Governmental Monument Preservation Authority) to provide a pertinent condition survey of

this monument or, more precisely, of the structure's areas of critical dilapidation (Fig. 14, 15). What the surveyors saw was an abandoned palace gracing a high slope, strengthened by a retaining structure fashioned into a series of grottoes and loggias. The principal bearing wall, withholding the ground on the slope and the palace on top of it, was considerably damaged in a number of locations. Water had found its way inside, penetrating through fall-outs over piles of brick rubble. Later, as cold weather set in, the water was transformed into ice. Ice stalactites hung on the precipitation drainage (which used to play an important role in dewatering the terrace).

Figure 14. A photograph of Konstantinovsky Palace taken in 2000 before reconstruction.

Figure 15a. Dilapidated structures of the palace: grotto.

Figure 15b. Dilapidated structures of the palace: transverse walls.

The condition survey had to assess the scale of structural dilapidation, identify its causes and mechanism, design ways to eliminate future deformations, and define the methods of bringing the retaining structure back to reasonable functionality.

Complexity of that salvage situation was increased due to the necessity to provide a celebrity vestibule in the basement underneath the central triple arch of the palace and in the grottoes underneath the terrace. For the reconstruction of the subterranean space to be effective, it was necessary to conduct extensive investigations, surveys, and analyses within strict time constraints. The structural layout and condition of all foundations, both of the palace and the retaining structure, were studied and described. To accomplish this, 28 trial pits were excavated, 35 boreholes were drilled through foundation masonry courses, 2 large trenches were excavated on-site, the rigidity characteristics of brickwork were established, moisture conditions of the walls were studied, and the length of timber piles underneath rubblework foundations were defined.

The key issue in ensuring long-term palace and retaining structure preservation was solving the dewatering problem. The dewatering problem was the primary cause of the retaining structure's dilapidation in the first place. It was necessary to compile a detailed historical analysis of the dewatering system (both for groundwater and precipitation water), as well as to define the optimal configuration for the dewatering system to be reconstructed. Bearing in mind the location of the palatial complex on the crest of a natural slope, all contributing architects paid special attention to groundwater and precipitation dewatering. Stability and long life of the entire retaining structure wholly depended on an effective solution in that area.

The old dewatering system had been constructed in the form of a continuous collector made of brickwork courses "for the purposes of intercepting rain water collecting on the entire palace roof, and drying the basement areas" (City Commission on Construction, 1849). Apparently, the contour brickwork collector alongside the palace perimeter was responsible for collecting the water discharged from 35 precipitation drainpipes, whereas the function of the intercepting collector in the north was to divert the water into the canal.

In the west and the east away from the palace in the bulk of the natural terrace ramp, a diverse network of masonry piping was found preserved from times when workers had tried to use it to arrange numerous gallery fountains in the area. The remnants of these pipes were exposed during a palace reconstruction attempt in 1950, and also in 1985 when heating mains was being laid adjacent to an outhouse near the palace.

Dewatering was originally realized in three cardinal points: north, west, and east. It was fashioned as a network of subterranean collectors supplemented with open gutters. In the north, the system was laid as three lines leading from the corners and the centre of the palace to the canal, where it had some vulnerable points in locations of height differential. The historical drainage system in these locations of the gallery collectors consisted of level differential or high-speed water flow installations, such as rough surface gutters on whose finishing courses were installed devices to prevent damage to the network. It is necessary to point out that the old drainage system was mainly precipitation oriented. In the upper terrace area which was compounded of clay soils and characterized by surface water flow, that network exclusively acted as precipitation dewatering (Kliorina, 2004).

To divert precipitation from the terrace surfaces (level 12.7 m BD) above the loggias and the grotto, there were 12 funneltype water receptacles (6 above the grotto and 1 above each loggia). Water was diverted through rectangular ducts constructed of timber planks and embedded into grooves in the brickwork of the retaining walls by one brick-width.

As attested by site investigation in the park, underneath 1 m of fill there is a 3-m layer of soft varved clay loam, underlain by medium stiff moraine clay loam (Fig. 16). Still deeper, at the level of around 14.0 m (absolute – 1.3 m), there are medium stiff and stiff deep Cambrian clays.

The slope incorporating the terrace is compounded by lacustrine-glacial clayey sands followed by silty lacustrine-glacial loams. Straight upon the terrace there is a stratum of man-made ground of sand with admixtures of

lime cement, above which there is 2 m of brickwork (in the section between the palace and the cellars) serving as a base for the terrace. It could not be entirely ruled out that the disco- vered brickwork is demonstrative of a bond between the courtyard foundations and the retaining structure. Above the clayey sand there is a layer of man-made ground about 3 m thick (Fig. 16, layer 1).
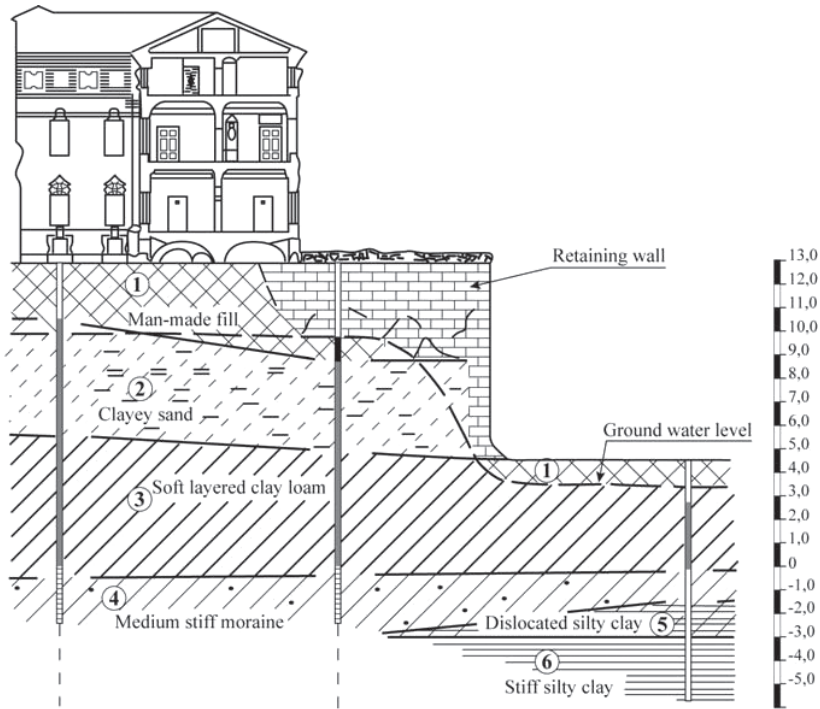
Figure 16. Cross-section of the palace and subsoil profile: 1. Made-up fill, 2. Clayey sand, 3. Soft varved clay loam, 4. Medium-stiff moraine clay loam, 5. Dislocated stiff Cambrian silty clay, 6. Stiff silty Cambrian clay.

Hydro-geological conditions are characterized by the presence of groundwater associated with man-made strata and silty sand inclusions in lacustrine-glacial clay loams which together with clayey sands act as a confining bed. Groundwater is discharged into the Lower Park canal. The groundwater table generally follows surface geometry.

In short, the subsurface of the structures in question is mainly associated with silty clay-like soil that is 3.5 m and 10 m deep in the lower and the upper levels, respectively. The peculiarity of the hydro-geological conditions is mainly that there is considerably lower vertical seepage flow in comparison to horizontal, which means that when water moves towards the discharge point there is pressure on the retaining wall.

Soil properties are given in Table 1.

2.4. Condition survey results

The condition survey confirmed the most negative expectations, postulating a threat of collapse for the historic palace. It was not so much the condition of the building itself but the retaining structure that instilled considerable reservations about the building's life expectancy. Although the condition of the building seemed adequate, the risk of failure appeared to be very significant due to the critical condition of the retaining structure.

Table 1. Soil properties.

Layer No	Soil	Natural water content W	Void ratio e	Unit weight γ (kN/m^3)	Angle of internal friction φ	Cohesion C (MPa)	Young Modulus E (MPa)	Permeability ratio k$_f$ (m/day)
2	Clayey sand	0.26	0.721	19.7	24	0.017	9.8	0.07–0.10
3	Soft varved clay	0.35	0.957	18.8	16	0.019	6.2	0.05
4	Medium stiff moraine clay loam	0.14	0.423	21.8	27	0.020	24.6	0.02-0.03
5	Dislocated stiff Cambrian silty clay	0.22	0.660	20.2	15	0.025	15.2	0.001
6	Stiff silty Cambrian clay	0.19	0.554	21.0	21	0.028	22.2	0.001

The condition survey results were as follows (see Fig. 14, 15, 17, 18):

1. Foundations of the dilapidated retaining walls were constructed of bricks. The foundations were no longer capable of being classified as a structure. There was imminent danger of crushed brickwork movement with formation of local bulges.

2. The entire brickwork structure was soaked in water, causing dilapidation through cycles of freezing and thawing.

3. There were no foundations of the transverse walls of the cellars. Footing was level with the cellar's floor. Decomposed timber pile heads supported the transverse walls.

4. Dilapidated terrace gutters had caused weakening of some retaining wall sections adjacent to niches of the loggias and grottoes.

5. The precipitation sewer consisted of three straight courses underneath the retaining structures, designed to divert precipitation and groundwater from the palace. There was water flow through the ground underneath the cellar walls, and through dilapidated retaining wall sections.

6. Most structural damage (fallouts) was associated with the destroyed drainage sections underlying the retaining structures.
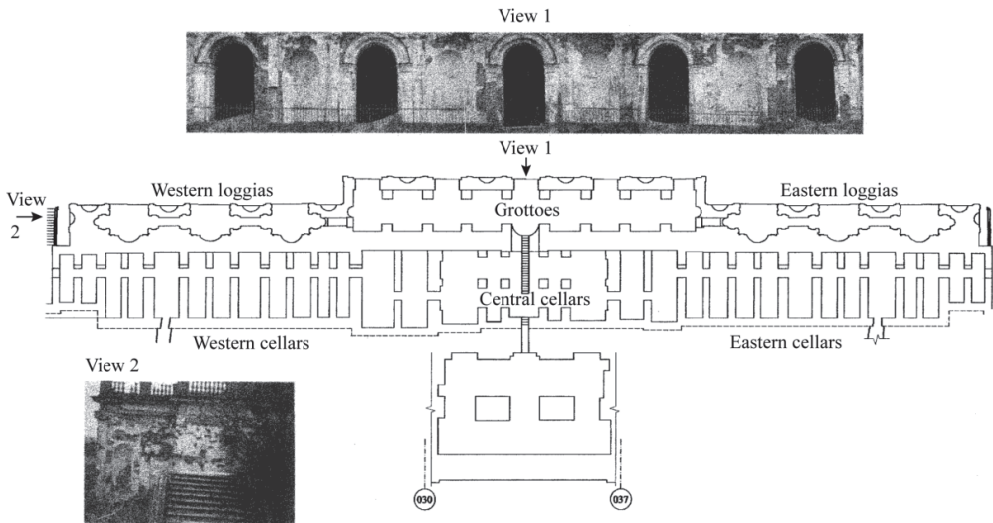

Figure 17. Dilapidated cellars, grottoes, and loggias of Konstantinovsky Palace.

Figure 18. Collapsing cellar wall behind east loggias.

The dilapidation mechanism can be presented as follows. The damaged precipitation sewer caused water discharge from the precipitation water collector adjacent to the gable end of the cellars chamber through the ground underneath the floor and the transverse cellar walls, towards the retaining wall. The drainage pipe under the floor alongside the retaining wall stopped functioning, increasing hydraulic pressure to the retaining wall, and over-dampening the brickwork. Because of the damage to the horizontal waterproofing of the terrace floor, percolating water sufficiently increased, and all cellar structures were finally soaked.

Frost penetration brought about the process of brickwork corrosion accompanied by frost heaving pressure on the retaining wall. At the same time, the vertical terrace drains started malfunctioning, thus thinning and weakening the bearing section of the retaining wall. Cycles of frost penetration into damp brickwork caused destruction thereof by low temperatures. Countless traces of such destruction were observed throughout. Intermittent water discharge into the ground in front of the retaining wall resulted in degradation of the timber pile heads supporting the transverse cellar walls, bringing about their settlement.

Seepage of water through the retaining wall in the weakened section caused suffusion of mortar, formation of seepage passages, and crumbling of brickwork around such passages during frost penetration. Movement of water through the wall caused a flow velocity increase, as well as higher than critical pressure gradients in the subsoil of the transverse walls, washing out of fines from under the transverse cellar walls with corresponding piping, and formation of cavities underneath the walls and the floors.

Piping from under the walls led to their uneven settlement. It also resulted in the subsoil surcharge and generation of additional horizontal pressure on the retaining wall. Gradual dilapidation of the retaining wall brickwork finally resulted in the palace's partial collapse in locations where its bearing section was most weakened by the formation of gaping holes and fallouts (ground and dilapidated brickwork suffusion cones) in the loggia niches. The above description of the dilapidation mechanism was verified by means of detailed geotechnical analyses.

2.5. Analyses of the palace retaining structures

The purpose of the analyses was to: (1) assess the influence of retaining wall dilapidation on groundwater seepage regime, and (2) estimate the stability of the retaining wall.

The Cambrian clays were considered a conventional confining layer. Water pressure corresponded to groundwater levels established

by the site investigation. Wall dilapidation was modeled as a local intensification of cracks and a permeability increase from 0.01 k_f up to 100 k_f, where k_f is permeability ratio of clayey sand layer with (k_f = 0.07–0.10 m/day) (see Fig. 8 and Table 1, soil layer 2). Draining systems were assumed to be out of working order.

Analyses demonstrated that at low permeability of the wall, equal to 0.01 k_f, the wall is capable of functioning in the capacity of a confining layer. It this case, maximum decrease of groundwater level drop behind the wall was 30 cm. Seepage velocity values in the wall are practically zero. If there wasn't any waterproofing behind the wall, the brickwork would be constantly damp.

An increase in dilapidation and permeability leads to a corresponding increase in draining properties of the wall. Water seepage will go on both through subsoil stratum underlying the wall and through the lower part of the wall. This will lead to even greater damage to the material. Further permeability increases of up to 100k_f are conducive to an increase in seepage, and current velocity is realized through the underside of wall, causing its further dilapidation.

The following options of structural analyses were considered (in 3 dimensions) to properly identify the causes of brickwork damage in the loggias and cellars and to select a pertinent strengthening option:
1. with piled foundation underneath cellar walls;
2. without piled foundations underneath cellar walls to account for the timber pile's decomposition;

3. in conditions of soil wash-out from underneath cellar walls and decrease of foundation masonry strength.

To account for the above factors it was necessary to perform soil-structure interaction calculations of subsoil, foundation structures, and superstructures. The calculations were made with the help of FEM models, a software developed by the authors (Ulitsky et al 2003, Shashkin, 2006). This software allows for the calculation of joint stress-strain condition of the superstructure and subsoil by using the finite elements method in 3 dimensions. Numerical analyses are not presented in detail since this is beyond the scope of this paper.

An elasto-viscoplastic hardening model (Shashkin, 2006) was used to model the nonlinear soil behavior, with the limit state surface described by Mohr-Coulomb criterion. Soil properties used in the analyses are provided in Table 1.

Analyses were conducted in two stages: In the first stage, the state of stress under the ground's self weight was calculated. In the second stage, deformations resulting from the weight of the superstructure on the subsoil and foundation were calculated. These calculations showed that:
1. Provided that the piled foundation is kept intact underneath the cellar walls (Fig. 19, 20) and the loggia structures remain in stable condition, with settlement of exterior loggia structures not exceeding 3.4 cm, and the settlement of the cellar walls not exceeding 5.8 cm, the building would be stable.
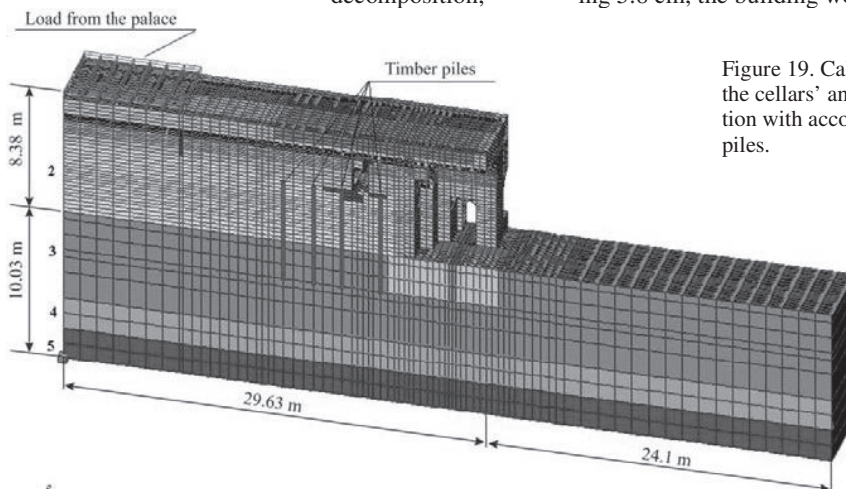
Figure 19. Calculation profile of the cellars' and loggias' deformation with account of intact timber piles.
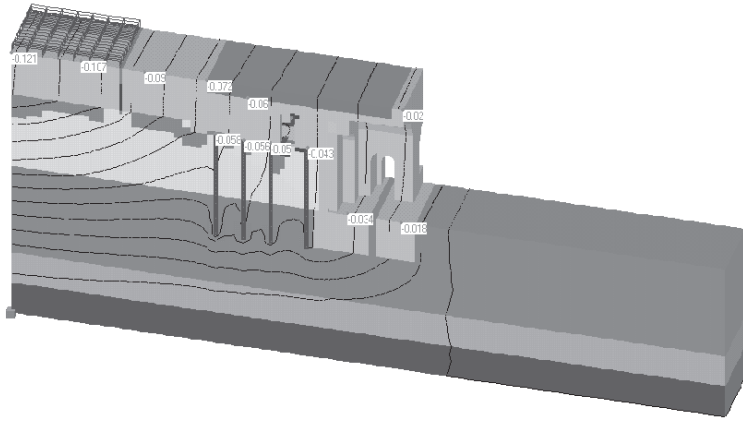
Figure 20. Contours of settlements of the cellars and loggias (m) with account of intact timber piles. Dark red color denotes soil regions reaching the limit state by Mohr-Coulomb criteria.
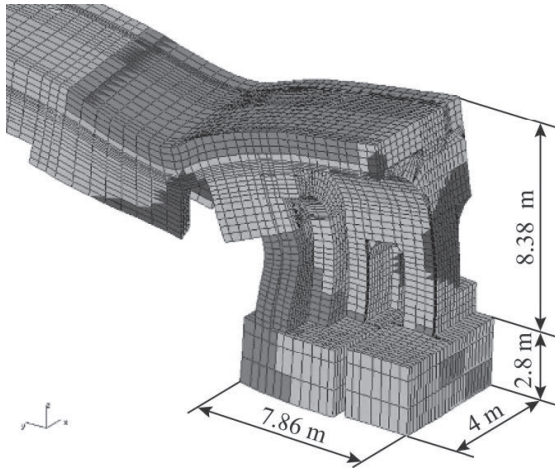
Figure 21. Deformation scheme (scale of deformations enlarged 500 times) and limit state areas in brickwork (defined by Mohr-Coulomb criteria) accounting for subsoil ground wash-out and decomposed timber piles. Shaded sections denote limit state areas generated by compressive and tensile stresses.

2. In the case of the decomposed timber piles, if the cellar wall settlement reached 7.7 cm it would cause the transverse wall's dilapidation. Due to decomposition, the piles were considered inadequate to support the required loads and thus were not included in the analyses.

3. In the case of ground piping and foundation brickwork loosening, if the settlement reached 8.3 cm and the deformation profile resembled that shown in Fig. 21, then the brickwork material would be dilapidated. Observed brickwork dilapidation suggested that this mechanism was actually occurring at the site.

Therefore, the conclusion was that the retaining structure was critically damaged and it would be necessary to carry out complex remedial works.

2.6. Design project of palace reconstruction

The Palace condition demanded immediate rendering of complex strengthening works. Such strengthening had to ensure the following:
1. Reconstruction and subsequent preservation of the brickwork;

19

2. Ability of the retaining wall to sustain horizontal ground pressure;
3. Reliable load transfer onto incompressible subsoil strata to eliminate any subsequent settlement-related deformations which may have arisen owing to dilapidation of the retaining structures and foundations.

The following circumstances had to be taken into account when implementing the above:
1. Complete deterioration of brickwork foundations into a crumbly mass with clayey filling;
2. Most probable prevalence of the same condition on a considerable portion of the subterranean retaining wall;
3. A retaining wall thickness of 3.2 m;
4. The absence of foundations underneath transverse cellar walls.

In such circumstances, the possibility of any local patchwork or consecutive (bay-by-bay) progress of works was precluded by the unsatisfactory condition of the brickwork, danger of local collapse of structures, and complete unavailability of materials for local replacement of the brickwork of those retaining wall sections which were in immediate contact with the ground bank.

In light of the overall surface dilapidation and general weakening of the brickwork, the option of bandages, confining frames, or other structural reinforcement was considered impractical for providing safe retaining structures and would damage the appearance of the historical building. Therefore, the only option that would address all the issues listed previously appeared to be pressure grouting and strengthening of brickwork, with underpinning of all retaining structures with piles embedded into stiff stratum (Fig. 22, 23).
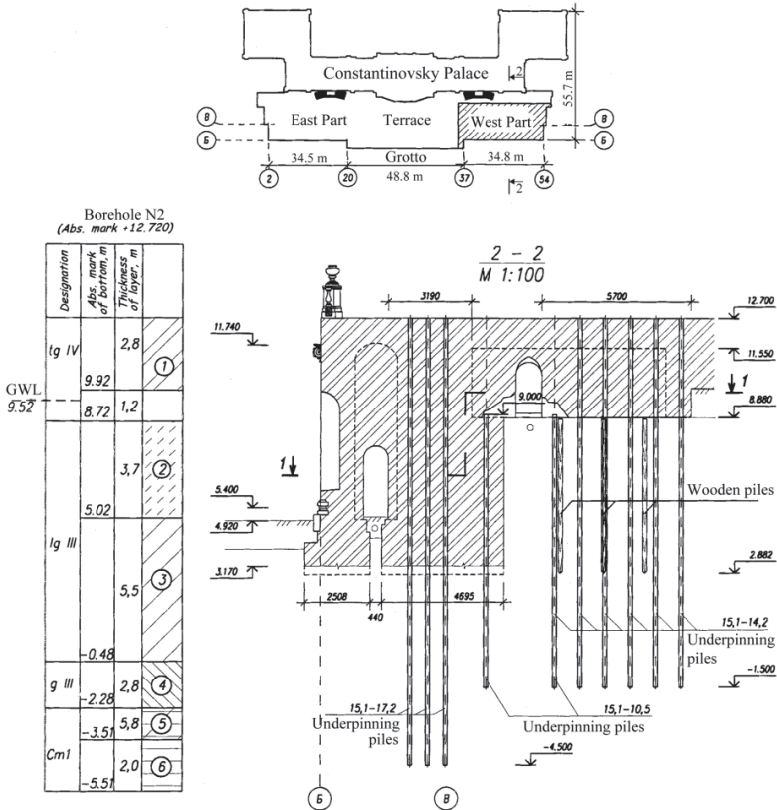

Figure 22. Palace layout in plan – underpinning of the retaining structure. See Fig. 16 for soil stratification.
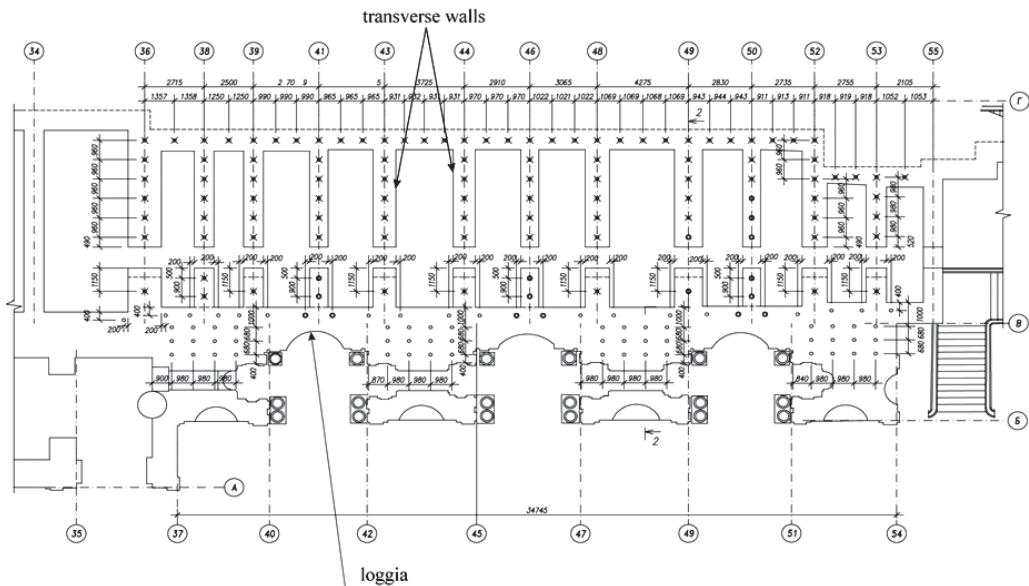
Figure 23. Location of underpinning piles in plan: o, × – underpinning piles.

Grouting of the brickwork was necessary in order to restore its strength and stiffness. Strengthening was required to properly allow the transfer of loads from the entire structure. Finally, underpinning piles had to be constructed in order to transfer the structure loads onto the incompressible subsoil stratum. It needs to be noted that conventional underpinning piles installed at an angle from the level of the lower terrace (around 4.0 m Baltic Datum) would prove ineffective as the dilapidated foundation brickwork was incapable of accommodating the heads of the underpinning piles, and the retaining wall itself was practically unavailable for underpinning.

Based on the above, the foundations underpinning of the retaining structures was carried out in the following sequence (see Fig. 22, 23).

Phase One

1. Strengthening of the critically dilapidated structures (3 left and 3 right loggias).
2. Provision of temporary propping scaffolding in cellar chambers installed on wedges in the cellar floors. Wedging of the scaffolding was regularly inspected. The unsupported spans in locations of the brickwork fallouts were likewise propped.

3. Drilling of 42 mm vertical bores above the partitions of the retaining wall from the terrace in front of the palace down to the brick-wall footing level. Subsequently, the brickwork was grouted by intervals with packing lime mortar until completely permeated.
4. Redrilling of the bores by 151-mm core bores down to the top of the firm Cambrian stratum following 70% setting of the mortar. Drilling below foundation footing was either carried out using thixotropic grout or was casing protected. Cement grout with added plasticizing and shrink-proofing agents was pumped into the subsoil and brickwork at 0.2 and 0.1 MPa respectively, followed by a stain-proof reinforcement casing tube being oscillated into the grout mix. The resulting pile was thus constructed with its toe against the stiff Cambrian stratum reinforcing and underpinning the entire retaining brickwork section. The tube was required to ensure both longer pile life and subsequent possible of deepening of the cellars. Toe levels and bearing of the piles had been previously confirmed based on the static loading tests.
5. Drilling of 42 mm vertical bores paced at approximately 1.0 m from the terrace in front of the palace along each transverse wall down to the brick-wall footing level

21

(absolute level 8.9 m BD) in order to rein-force the transverse walls and rear longitu-dinal wall of the cellars. This was followed by interval grouting and subsequent redril-ling of the bores by 151-mm augers, used in the bored piles construction, down to abso-lute level of 1.5 m BD. Those piles were likewise reinforced through their entire length.

6. Construction of pile heads in the dilapidated areas of the transverse walls at the level of the brickwork footing (absolute level 8.8 m BD), with subsequent construction of the pile caps and masonry courses within the original scope.

Phase Two

1. Completion of the retaining structure streng-thening works.
2. Provision of works described in Stage 1 above for unreinforced sections of the walls.
3. Removal of terrace surface material and construction of a reinforced concrete wall connecting pile heads above the brick vaults.

Phase Three

1. Provision of the terrace surfacing incorporat-ing drainage and snow melting systems, fi-nished by tiling.
2. The provided strengthening should serve to ensure the reliability and long life of the re-taining structures, preserving their appear-ance and historic materials almost complete-ly unscathed by any patchwork or replace-ment of brickwork. Such approach proved most appropriate in relation to this important architectural monument.
3. The constructed strengthening option was successful even when faced with an unex-pected challenge. The architects suddenly decided to provide front access to the palace from the Lower Park and furnish a vestibule underneath the terrace. To do this, all cellars had to be deepened by 1.0-1.5 m and the transverse brick walls were temporarily sus-pended on the thin underpinning piles (Fig. 24, 25, 26). Quality of the strengthening was attested by the fact that not one section of the brickwork was in any way displaced. It was therefore ascertained that the streng-thening was successful.
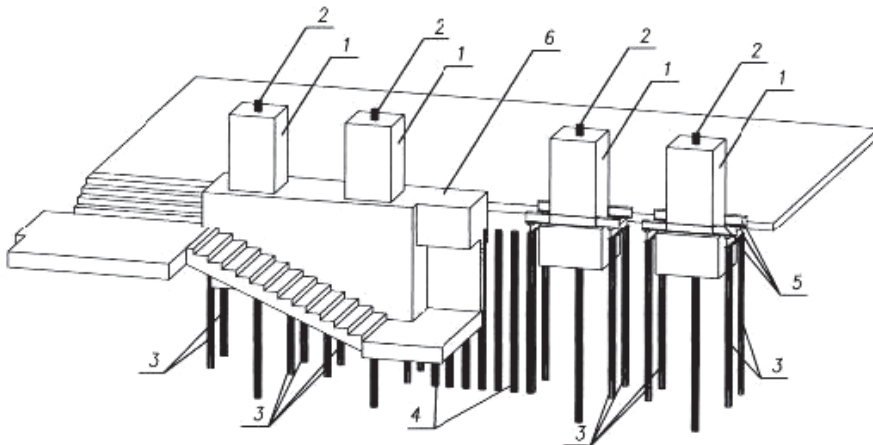
Figure 24. Provision of celebrity entrance overlooking the Lower Park (deepening of the basement down to 5.0 m): 1. existing brickwork pillar, 2. underpinning piles constructed from terrace surface, 3. pile supports for propping brickwork pillars, 4. pile wall, 5. steel waling transmitting loads form pillars onto piles, 6. retaining wall constructed of reinforced concrete.

Figure 25. Deepening of the basements by 1.0-1.5 m.

Figure 26. Bored pile with tube reinforcement viewed from underneath foundation.

It took about 1.5 years to completely reconstruct Konstantinovsky Palace in Strelna (Fig. 27). The palace officially opened as the Congress Palace in 2003 during the tercentenary celebrations of Saint Petersburg (Fig. 28, 29).

Figure 27. Konstantinovsky Palace, south façade. View of a final reconstruction stage (January 2003).

Figure 28. Cellars of Konstantinovsky Palace, 2004 (at the location of reconstructed retaining cellar wall, see Fig. 10).

Figure 29. Konstantinovsky Palace, south facade. View after a final reconstruction stage (July 2003).

2.7. Brief overview of the project

Konstantinovsky Palace, an important historic monument of the early 18th century, underwent almost complete destruction in the first half of the 20th century. Later it was partly restored, but became seriously dilapidated during the past 15-20 years.

A thorough condition survey of the palace showed that due to the dilapidation of the drainage system, the retaining structures had been seriously weakened. Old timber piles had been almost completely decomposed. These factors compromised the structural integrity of the palace and endangered its stability.

Soil-structure interaction analyses of the retaining structures were conducted taking into account the subsoil piping, foundation brickwork loosening, and decomposed state of the timber piles. The calculations showed that the retaining structures of the palace were in critical condition and in need of immediate strengthening.

The complete reconstruction project of Konstantinovsky Palace was developed on the basis of a condition survey and soil-structure interaction analyses. This project envisaged strengthening of the critically dilapidated structures of the palace by pressure grouting of the brickwork and underpinning of the entire range of retaining structures with piles embedded into a stiffer Cambrian clay stratum. The geotechnical part of the project presented the highest challenge and ensured success of the whole project.

The project was successfully realized in 2000-2003. One of the most important features of the project was the detailed soil-structure interaction analysis of the retaining structures.

3. ANALYSIS OF THE ADMIRALTY BUILDING IN CENTRAL SAINT PETERSBURG

Historical analysis of a geotechnical problem is very important for projects dealing with preservation or reconstruction of historical monuments and their foundations (Ulitsky et al, 2003).

Such analysis should include the following steps:

- Analysis of the actual stress - strain conditions of subsoil of preserved buildings, and, if necessary, of adjacent buildings;
- Estimation of the influence of present vibration background on settlement development;
- Estimation of ongoing settlements of buildings (under own weight and outside factors), that is defined through calculations or observations the location of geodetic marks and gauges;
- Estimation of the allowable additional settlement of the existing buildings during reconstruction works or new development.

For important projects it is also necessary to perform the following works:

- Historical analysis of foundation behaviour of preserved/reconstructed buildings and buildings adjacent to reconstructing object or to new development together with substructure behaviour of the existing buildings;
- Calculations of the total assumed deformations and percentage of different causes in settlement development of the existing buildings.

An example of a historical analysis is the Admiralty building in central St. Petersburg (Fig. 30a). The building has well pronounced cracks. The purpose of the historical analysis in this case was to find out the reason of these cracks development to make decision about further strengthening or preservation of the monument.

The Admiralty tower was constructed in 1734 by I. Korobov. In 1811-1823 the Admiralty was reconstructed by A. Zakharov, who enlarged the tower and made some structural rearrangements.

The tower has a rigid structure. It rests on stone foundations supported by wooden piles (Fig 30b). The subsoil under the tower is loaded more than the adjacent lower wings of the building. Therefore the tower suffered bigger settlement than the adjacent wings. The cracks appeared in the wings near the location of windows.

The subsoil of the Admiralty is comprised of fine-grained saturated sand of medium density and soft clayey sands. A thorough survey of the foundation has been made. The stone foundations were inspected by a mini TV camera lowered down the survey holes predrilled through the stone foundations. It was found out

that the average percentage of voids in the foundation body was in the range of 1 to 10%. General condition of the foundations was found to be satisfactory, except for one part of the foundation under a transverse walls of the tower.

a)

b)
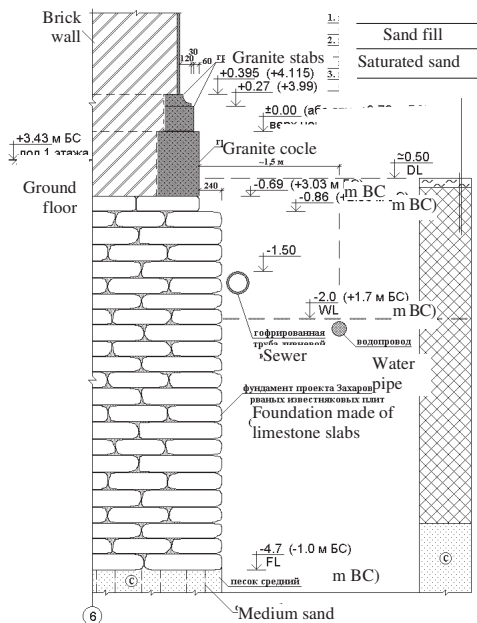
Fig. 30. (*a*) The buildi_ _ _ _ _ _ _ ty, (*b*) historical foundation under the Admiralty tower

The structural survey of the building made it possible to identify all cracks in the walls. It was discovered that many cracks appeared in the bearing walls of the tower.

To find out the reasons of the cracks development in the tower a 3D soil-structure interaction analysis has been performed. All findings made during the geotechnical and structural survey of the building have been taken incorporated into the design scheme.

Initial construction and consequent reconstruction of the building have been modelled. First the deformations of old Korobov's Admiralty tower (1732) have been assessed, and then the modifications of the design scheme have been made with account of the added walls (1816) and additional loads (Fig. 31). Thus, the real construction history had been simulated.

The contours of settlements accumulated after the reconstruction of the building are shown on Fig. 31. The total estimated settlements have a value of about 20 cm. It should be noted that the soil model used in the analysis can take into account a long-term creep of the Admiralty's subsoil.
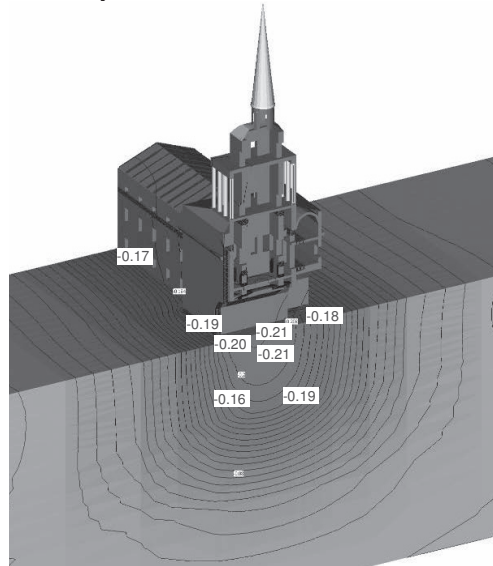
Fig. 31. Contours of computed of settlements of the Admiralty (cross section along the symmetry axis)

The performed analysis has made it possible to identify the reasons of the cracks development in the structural elements of the building. The main crack appeared in the tower wall

a)

b)
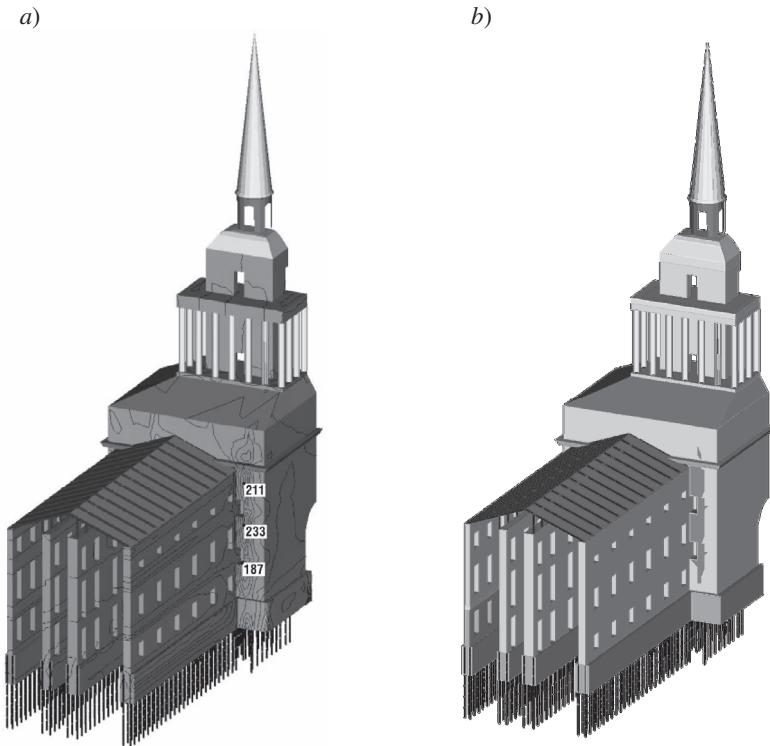
Fig. 32. Calculations of the structure of the building: (a) contours of the shear stresses in the masonry (kPa), caused by the differential settlement of the tower and the lower wing; (b) zones of the possible development of the cracks caused by shear deformations of the transverse wall

adjacent to the lower wing. The reason of this crack development is the non-uniform settlement of the building. The development of settlements may still go on, which can be explained by a long-term creep of the subsoil. The non-uniform settlement leads to the generation of shear stresses in the walls with their maximum values up to 235 kPa (Fig. 32a).

The shear stresses cause the development of the cracks in the tower walls (Fig 32b). There is a good correspondence between the soil-structure interaction calculation results and the observed behaviour of the building (Fig. 33).

Thus, the conducted historical analysis of this geotechnical problem taking into account joint behaviour of the Admiralty' structure and subsoil as well as the construction history helped to identify the reasons of the deformation of this famous monument in the central Saint Petersburg.

Fig. 33. Development of cracks in the Admiralty tower

4. ANALYSIS OF ST. NICHOLAS NAVAL CATHEDRAL IN KRONSHTADT NEAR SAINT PETERSBURG

St. Nicholas Naval Cathedral is located in the town of Kronshtadt (Fig. 34). It was built in 1902-1913 according to the project of V.A. Kossiakoff. In this cathedral an idea of a classical cruciform church with a domed roof was fulfilled. This idea was realized first in the famous St. Sophia Cathedral in Constantinople.

In fulfilling ancient architectural traditions new structural materials, introduced in the beginning of the 20 century, have been used. The main dome is supported by the system of steel beams. The dome is made of the reinforced concrete. Four big pillars are the main supporting elements of the cathedral.

Geological investigations were made in 1897 and 1902. Eighteen boreholes were bored to the depth of 27.7 m. The bearing layer of subsoil is a coarse sand with pebbles (thickness of the layer is 1.1-4.3 m). This layer is underlain by moraine loams with boulders (thickness 6.4 m) and hard clays.

Due to the presence of the boulders the author of the project decided to construct foundations made of cast-in-place reinforced concrete avoiding construction of piles.

Fig. 34. St. Nicholas Naval Cathedral in Kronshtadt

Immediately after the construction completion the differential settlement was recorded with the value of about 4 cm.

During the Cathedral's life a lot of cracks have been developed. In May 2009 a sharp local increase of a crack in one of the abutments was observed. This endangered the stability of the whole structure. A special programme of cathedral structural survey, research and development of salvation measures was put forward. The key issue of this investigation was to find out the reasons of cracks development.

Some dangerous cracks in the cathedral's structures are shown in Fig. 35 and 36.

Fig. 35. Cracks in the vaults of the cathedral

Fig. 36. Cracks in the wall of stairwell passage

The scope of the survey works was the following:

- Full structural survey of the cathedral was completed

- 11 holes have been drilled through the foundations body to the subsoil. Scheme of test boreholes is shown in Fig. 37. The condition of the foundations and subsoil was estimated.

- Dynamic sounding of the subsoil was made

- A detailed geophysical investigation was made. This investigation showed that there are several zones of subsoil local softening due to leakage of water. These zones are located in the vicinity of the engineering networks. Around the cathedral a partially decayed timber sheet pile wall was found out.

- Soil samples from the holes were taken; main properties of soil were determined.

It was found out that the condition of subsoil and foundations was satisfactory.

A series of soil-structure interaction computations has been performed with the help of *FEM models 2.0* software (Ulitsky V.M. et al, 2003). The computation profile is shown in Fig. 38. All main structural elements, foundations, and subsoil layers have been incorporated in the computation profile. All main findings during the condition survey of structural elements, foundations, and subsoil have been taken into account in computations.
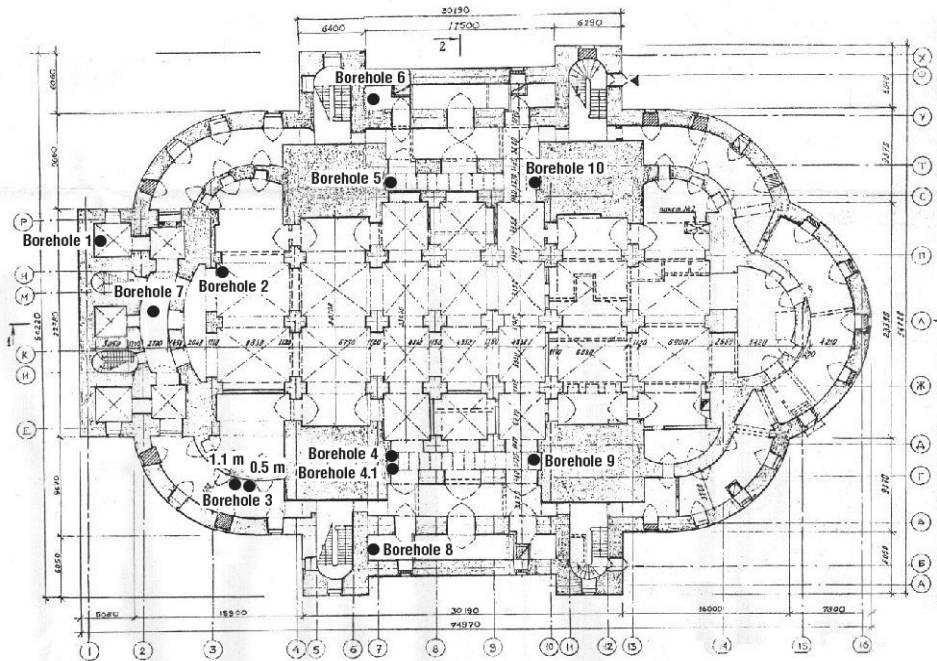
Fig. 37. Location of test boreholes drilled through foundation body to the subsoil

29

Soil-structure interaction calculations showed that the cathedral is subject to non-uniform settlements. The reason of these settlements is the different loads acting to the main bearing structures of the Cathedral (Fig. 39, 40).
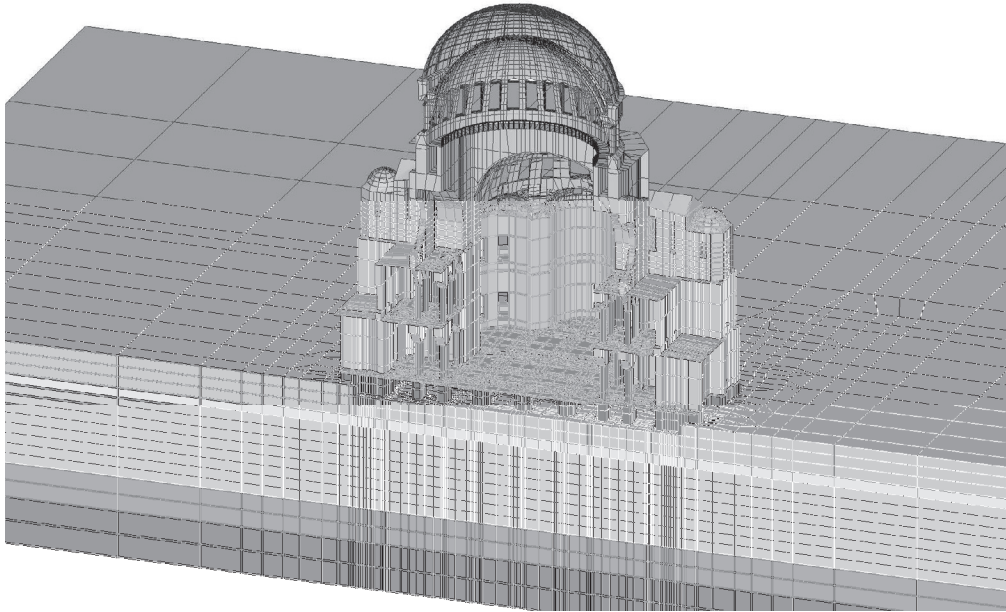
Fig. 38. Computation profile of the cathedral
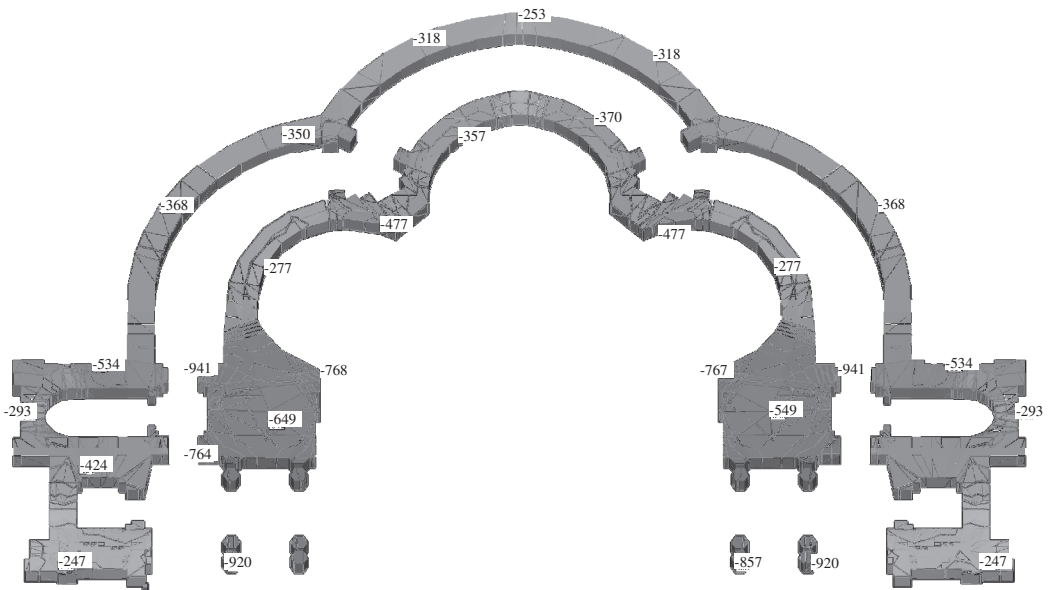
Fig. 39. Distribution of vertical stresses (kPa) in the main bearing structures of the Cathedral on the level of the 1st floor. The most heavily loaded are the main pillars, the least loaded are the walls of the outer galleries
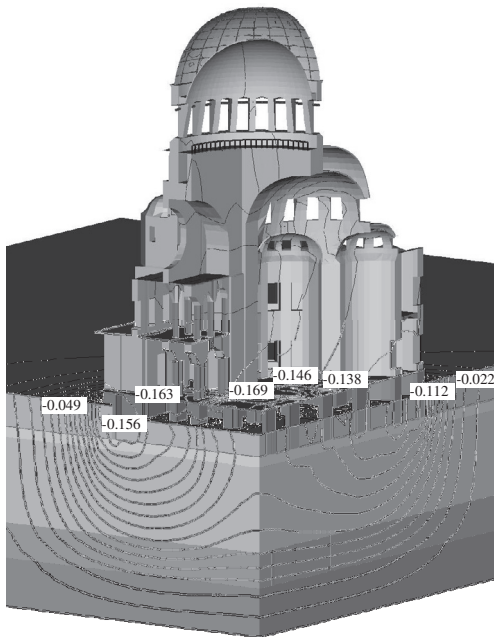
Fig. 40. Contours of computed of settlements of the Cathedral (cm)

ger settlements. The calculated non-uniform settlements (Fig. 40) correspond well to the results of the geodetic measurements. The observed settlement differential is about 13-22 mm.

Computations show that the zones of development of tensile stresses in brickwork well agree with the locations of actual cracks. In particular, taking into account non-uniform settlements we have a characteristic system of cracks in the semi-domes in altar and Western parts of the Cathedral (Fig. 41 and 42).

The main conclusion of the conducted investigations and SSI computations is that currently there is no danger of an immediate collapse of the Cathedral.

Local mostly endangered structural elements are: the main dome, its supporting elements and semi-domes in Eastern and Western parts of the cathedral. Local reinforcement must be provided as soon as possible. This reinforcement must be based on the detailed analysis.

The computations of the system "subsoil-foundations-superstructure" show that all main cracks in the structural elements of the cathedral are caused by differential settlements of the monument (see Fig. 40), conditioned by the non-uniform loading of the subsoil. The most dangerous cracks caused by differential settlements are the cracks in semi-domes in Eastern and Western parts of the cathedral.

Such non-uniformity of loads is quite typical for the temples characterized by cross-cupola structural scheme. The most heavily loaded are central pillars by which the central cupola is supported. Hence, the pillars are subject to big-
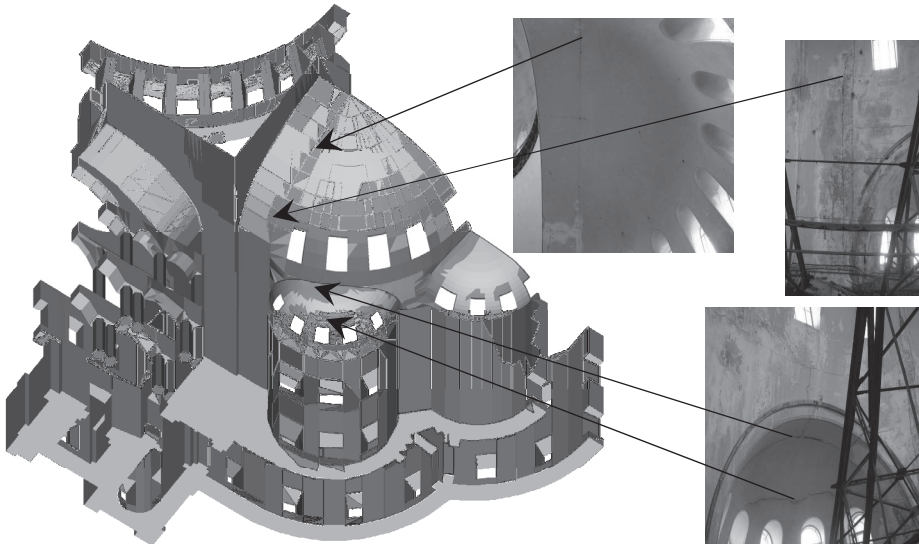
Fig. 41. Location of possible calculated cracks development and real observed crack locations

31
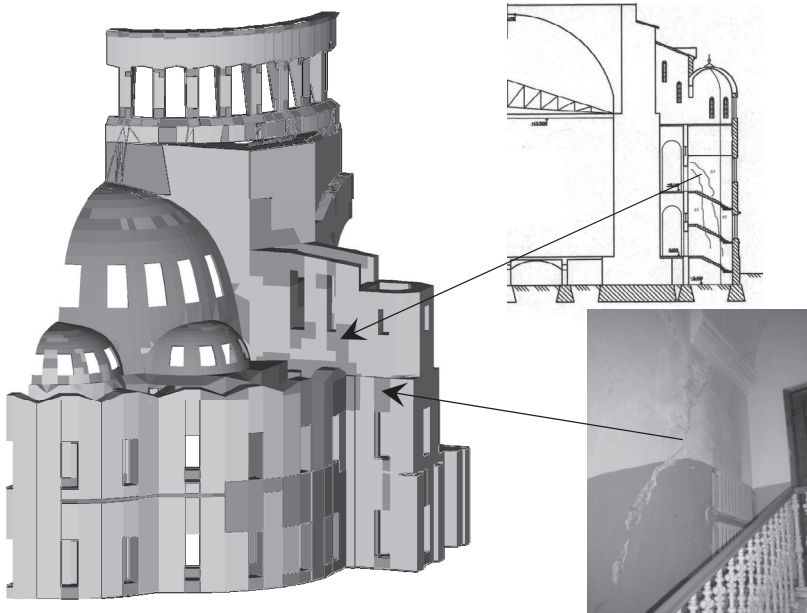
Fig. 42. Location of possible cracks development by calculations as compared with the real observed cracks

5. INFLUENCE OF GEOTECHNOLOGIES ON ADJACENT BUILDINGS IN URBAN AREAS

When considering the issue of neighbouring buildings preservation or strengthening the following rule must applied: means of protection must be adequate to provisional impact.

Usually it is not too difficult to establish impact associated with loading or unloading of subsoil, while the influence rendered by technological factors is much more complicated to define. It is recommended to attempt calculation of impact generated by various piling technologies onto subsoil, to established the importance of relevant technological factors, as well as the dimensions of impact areas, for example, of pile jacking (oscillating), pile driving and vibration techniques of piling and sheet piling in relation to existing structures have been also established (Poulos, 2003, Ulitsky, 2003). It is especially important for urban areas with marine soft soils which often are structurally unstable media inclined to remolding at externally generated impact which procedure is accompanied by reduction of their mechanical properties, such as bearing capacity and strength and increase of their compressibility.

As can be seen from analysis of deformed buildings in central Saint Petersburg, (Fig. 43), the portion of dilapidation brought about by works implementation drawbacks of adjacent construction is 39%.
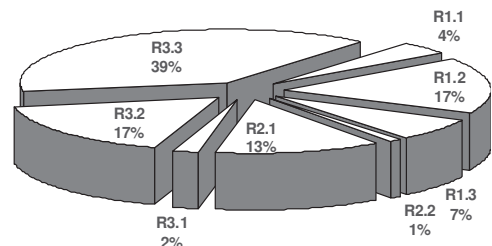
Figure 43. Causes for damage to existing buildings during adjacent construction in St. Petersburg:
R1.1 – deformation causes related to mistakes in site investigation/condition surveying; R1.2 – deformation causes related to faulty design; R1.3 – deformation causes related to faulty works implementation;
R2.1 – deformation causes related to faulty maintenance of building; R2.2 – deformation causes related to faulty maintenance of adjacent area;
R3.1 – prospecting/condition surveying drawbacks of adjacent construction; R3.2 – design drawbacks of adjacent construction; R3.3 – works implementation drawbacks of adjacent construction.

Below we list an example of technological impact to an adjacent buildings. In 1998 one of the world's leading geotechnical companies was carrying out continuous flight auger (CFA) bored piling in central St. Petersburg. Resulting from impossibility to create proper drilling conditions, whereat one turn of the auger would correspond to downward advance of same auger by one flight, remoulding of subsoil of adjacent building was brought about.

Boreholes with geometrical volume of 8 m³ would consume 12 m³ of concrete, sometimes amounting to 24 m³, and in two cases to as much as 50 m³. Resulting from large scale piling the adjacent multi-storey building constructed in 1905 and located at 20 m from the excavation had started developing deformations which exceeded 30 mm by the beginning of 1999 (Fig. 44).

Ligovsky, 44 (Pertsov House) s=f(t) chart (side wall)
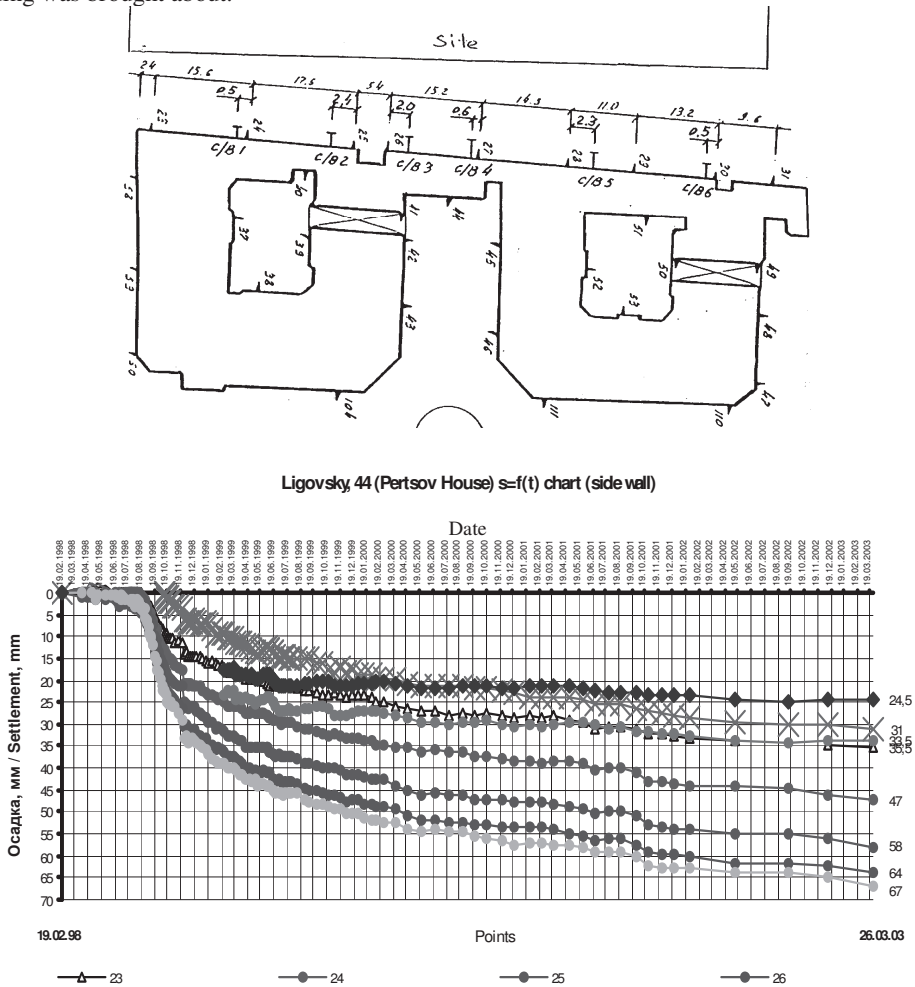
Fig. 44. Settlement development in time resulting from CFA piling (Ulitsky, 2003)

The works were suspended owing to economical reasons and everyone had a possibility to observe 'pure' after effect of such piling. Currently the building has settled by more than

90 mm. Such nature of deformations corresponds quite well to our forecast provided before the works have started. Ground probing conducted prior to commencement of the piling,

during the piling, and following site suspension produced interesting results. Following completion of piles construction the soils considerably reduced their cone resistance properties (Fig. 45).

6. CONCLUSIONS

Four examples of historical monuments are presented in this paper – the Stock Exchange building, Konstantinovsky palace in Strelna, Admiralty building in central Saint Petersburg, St. Nicholas Naval Cathedral in the town of Kronshtadt near Saint Petersburg.

As these examples show, it is very important to use soil-structure interaction approach in design of monuments preservation and renovation in urban areas. SSI approach is a very efficient at all stages of analyses of monuments. It is very powerful tool in prediction of behaviour of preserved buildings and structures.

Successful application of SSI approach requires a very comprehensive survey of the monuments. Essential parts of this survey are: investigation of the structural elements, foundations and subsoil, geophysical research and testing, soil sampling and tesing, in-situ testing of coils. Results of these investigations must be used in SSI analysis.
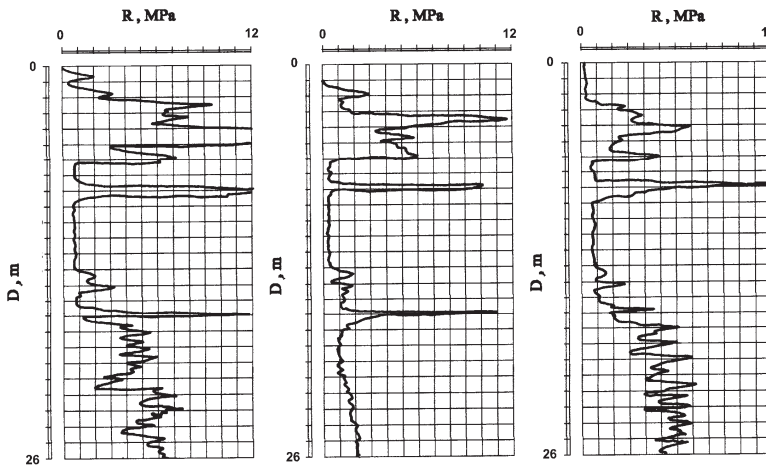
Fig. 45. Change of cone penetration resistance of soils: a) prior to commencement of piling; b) during piling; c) following completion of piling (Ulitsky, 2003)

7. REFERENCES

Burghignoli, A. Jamiolkowski, M., and Viggiani, C. 2007. Geotechnics for the preservation of historic cities and monuments: components of a multidisciplinary approach. General report. *Proc. of XIV European conference on Soil Mechanics and geotechnical Engineering "Geotechnical Engineering in Urban Environments"*, Madrid, Volume 1.

Frank R. 2006. Some aspects of soil-structure interaction according to Eurocode 7 'Geotechnical design', *Engenharia Civil/Civil Engineering*, Universidade do Minho, Portugal , No. 25, pp.5-16.

Powderham, A. 2003. Protecting historical infrastructure using the Observational Method. *Proceedings of the geotechnical conference "Reconstruction of historical cities and geotechnical engineering"*. St. Petersburg, 16-18 September 2003. Vol. 1, pp. 243-250.

TSN 50-302-2004. *Design of foundations for buildings and structures in St. Petersburg*. Local constructional codes for St. Petersburg. Government of Saint Petersburg, 2004.

Ulitsky, V.M., Shashkin, A.G., Shashkin, K.G., and Lisyuk, M.B. 2003. Soil-structure interaction: methodology of analysis and application in design. ASV Publishers. St. Petersburg – Moscow. 40 p. (in English)

Ulitsky, V. 2003. Geotechnical challenges in reconstruction of historical cities (as may be illustrated by St. Petersburg). *Proceedings of the geotechnical conference "Reconstruction of historical cities and geotechnical engineering"*. St. Petersburg, 16-18 September 2003. Vol. 1, pp. 13-28.

Footing Design of the Nakheel Tower, Dubai, UAE

C.M. Haberfield and D.R. Paul

Golder Associates Pty Ltd, Melbourne, Australia; *chaberfield@golder.com.au*

ABSTRACT: The Nakheel Tower in Dubai, UAE, was designed to extend to a height in excess of 1 km. With about 2,000,000 tonnes dead load, the structure would have been one of the heaviest ever built. The bearing pressures applied to the ground coupled with the soft rock ground conditions present at the site provided a significant challenge to the design of the footing system. This paper presents a brief summary of the ground investigation and the foundation structure analyses undertaken for the development of the footing system.

1. INTRODUCTION

The Nahkeel Tower in Dubai was designed to extend to a height in excess of 1 km. With about 2,000,000 tonnes dead load, the structure would have been one of the heaviest ever built. The project was placed on hold in early 2009 at a stage when about half of the foundations had been constructed. As at the date of this paper, construction was yet to recommence. However, ground engineering works undertaken prior to project going on hold included the site investigation and development of site conceptual model, construction and testing of instrumented trial barrettes, assessment of the ground response under the tower loading and the design of a system of barrettes to control ground response, tower settlement and tilt.

The bearing pressures applied to the ground coupled with the soft rock ground conditions present at the site provided a significant challenge to the design of the footing system. This paper briefly discusses the ground investigation undertaken for the project, how the constitutive model for the ground behaviour was developed and the methods used to assess ground structure interaction.

Based on prior but limited knowledge of the ground conditions in Dubai, the foundation system concept adopted for the tower was a piled raft. The raft design had a variable thickness of up to 8 m under the most heavily loaded structural elements. It was to be founded at a depth of about 20 m below ground level at the base of a 120 m diameter excavation supported by a circular, embedded diaphragm wall. Approximately 400 barrettes were proposed, for installation to depths of between approximately 60 m and 80 m below ground level. The design of the barrettes had to consider not only the control of ground response to the tower loading, but also various regulatory requirements and constructability issues.

2. SITE CONDITIONS

2.1 Background and assumed soil behaviour

Another site about 10 km from that eventually chosen and with similar subsurface conditions had previously been proposed for the Tower (Site 1). A geotechnical investigation was completed for this site prior to the location change. Initially, investigation techniques, which were typically used in the UAE were adopted for the investigation at Site 1. Of note, this included double tube drilling, which tended to lead to the recovery of broken core samples (low RQD) and suggested potentially fractured ground. However, a change to triple tube

drilling indicated that this was not that case, and that the ground was relatively homogenous and free of discontinuities.

Based on observations at Site 1, a conceptual constitutive model for the behavior of weak calcareous rock in Dubai was developed and used to help develop the scope of the investigation for Site 2. During the geotechnical investigation at Site 1, a number of observations were made which indicated that samples of soft calcareous rock (calcisiltite) brought to the surface from depth were adversely affected by stress relief. Samples taken from depths in excess of 100 m had a consistency of firm to stiff clay when brought to the surface, unexpected given the overburden stress at that depth. Horizontal cracks (delamination) were seen to develop in core within minutes of it being extracted from the core barrel.

When samples of calicisiltite are subjected to one-dimensional consolidation, the effect of the cementation is apparent. The void ratio changes only slightly with increasing effective stress until the strength of the bonds between the silt sized particles is exceeded. Once this occurs, the rate of consolidation dramatically increases. By taking intact samples from various depths within the deposit and subjecting them to one dimensional consolidation tests, the yield point of the cemented bonds was able to be assessed for samples with various in situ void ratios. This allows a Bond Strength Envelope (BSE) to be plotted in e vs σ'_v space. Figure 1 presents the results of an oedometer test undertaken on a sample recovered from a depth of 182 m at Site 1.
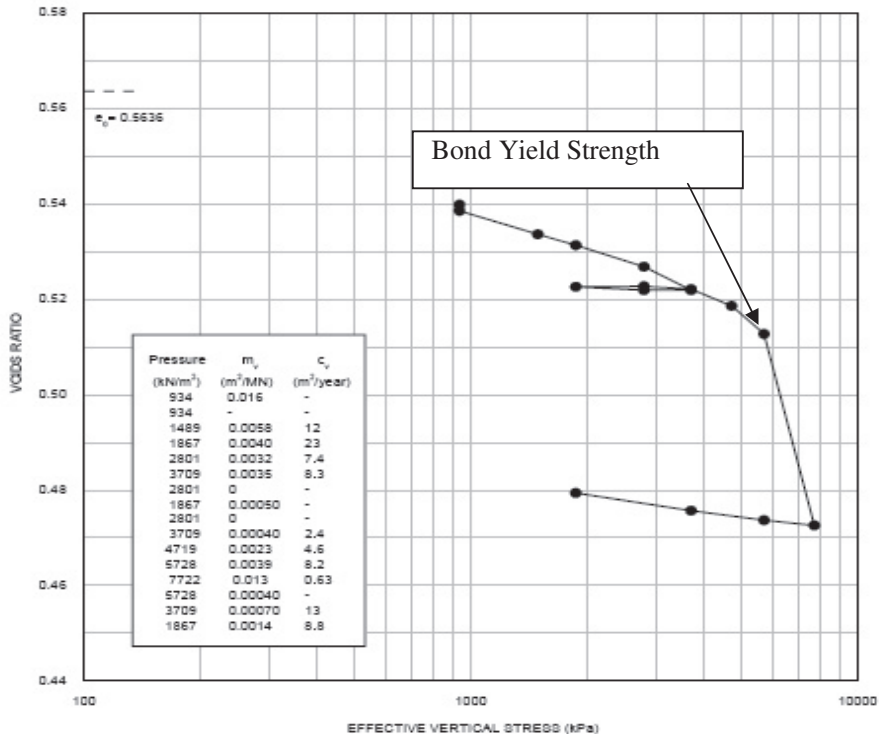

Figure 1: Results of Oedometer test undertaken on sample recovered from 182.5 m. The approximate Bond Yield Strength is indicated.

The stress history of the calcisiltite may be important in defining its behavior. It was postulated that the cementation of the grains occurred during or soon after deposition. As overburden pressure increased during further deposition, the cemented bonds support the increasing stress and the void ratio decreased a minimal amount if at all. This is a 'Metastable State' where the bond strength is supporting most of the overburden load. With increasing effective stress and if the bond strength is exceeded, a rapid decrease in void ratio could occur with associated consolidation and creep.

Given the relatively high carbonate and gypsum contents encountered within the subsurface materials at Site 1, it was inferred that cementation was probably syn-depositional and that the mechanical behavior of these materials, including strength, stiffness, consolidation and creep could be dominated by the bond strength. This was consistent with the observed behavior of this material in laboratory and in situ tests.

The degradation of samples when brought to the surface was inferred to have occurred as a result of stress relief. It was postulated that expansion of dissolved gasses within the pores may be a contributing factor to breaking the cemented bonds and sample degradation.

Based on this assumed constitutive model and the effects on samples of stress relief, the investigation at Site 2 focused on in situ testing in preference to laboratory testing to define the engineering properties, particularly stiffness of the ground beneath the proposed tower.

2.2   *Site Investigation (SITE 2)*

Geotechnical investigation for the proposed tower assumed (based on the Site 1 investigation) that a piled raft foundation system would likely be adopted. The large diameter of the building and high loads would potentially stress the ground to depths in excess of 200 m. Consequently, the investigation focused not only on the stiffness of materials below the raft and within the depth of the barrettes, but also on the ground below the barrettes. A total of nine boreholes of between 120 m and 200 m depth were drilled at Site 2. All boreholes were advanced using PQ, HQ or NQ triple tube drilling techniques, with the borehole diameter varied depending on the type of in situ testing scheduled.

Core recovered from the boreholes was photographed and logged immediately upon its withdrawal from the core barrel. Samples for laboratory testing were selected and removed from the core within 10 minutes of its being brought to the surface. Moisture content testing was undertaken on site at a temporary laboratory established for that purpose. Samples for testing to be undertaken off site were immediately wrapped to preserve moisture content, placed in cardboard tubes and sealed using wax.

Pressuremeter testing was undertaken in three boreholes at depth intervals of about 5 m. The testing was undertaken under the supervision of an experienced engineer using an Oyo Corporation "Elastmeter 2" pressuremeter incorporating pressure measurement within the probe and capable of applying up to 20 MPa. At least one unload/reload loop was incorporated into each test. Creep tests, where pressure was held constant for up to 2 hours whilst displacement was measured, were undertaken as part of about 30% of tests.

Cross-hole seismic testing was undertaken at two locations to depths of 200 m below ground level. Arrays of 3 boreholes with 3 m between each borehole were used for the cross hole seismic testing.

Laboratory testing undertaken on samples recovered from borehole core included moisture content, bulk density, particle density, point load testing, high pressure oedometer, constant normal stiffness direct shear testing, resonant column and cyclic triaxial testing and array of chemical testing on soil and groundwater. Stiffness was measured in the laboratory using primarily Unconfined Compressive Strength Tests with end platen displacement measurement.

2.3   *Geology and stratigraphy*

Drilling undertaken at Site 2 indicated a general subsurface stratigraphy that comprised of:

- An upper 6 m thick layer of loose saturated sand. This unit is subsequently referred to as Unit A. A surficial layer of precipitated gypsum

and other salts forms a thin crust at the surface of the site.

- Recent aeolian deposits comprised of carbonate rich sand with thin, high strength indurated layers. This forms a capping layer over the site. The sand extends from ground surface to a depth of about 20 m. This unit is subsequently referred to as Unit B.

- Shallow marine deposits, inferred to be of Quaternary age and comprised of predominantly calcisiltite unconformably underlie Unit B. This material is a low strength rock with carbonate content typically greater than 70%. It extends to a depth of about 70 m below ground surface.

- A second shallow marine sedimentary sequence underlies Unit C and extends to the maximum depth investigated of about 200 m. This unit is comprised predominantly of calcareous siltstone with some calcisiltite. Although the carbonate content is variable, it is typically lower than that of Unit C. This Unit is characterized by high gypsum content. Gypsum is present as massive layers of up to 2.5 m thick, as well as nodules and veins. Borehole correlation between the massive gypsum layers suggest the bedding within this material has a shallow dip of about 8°.
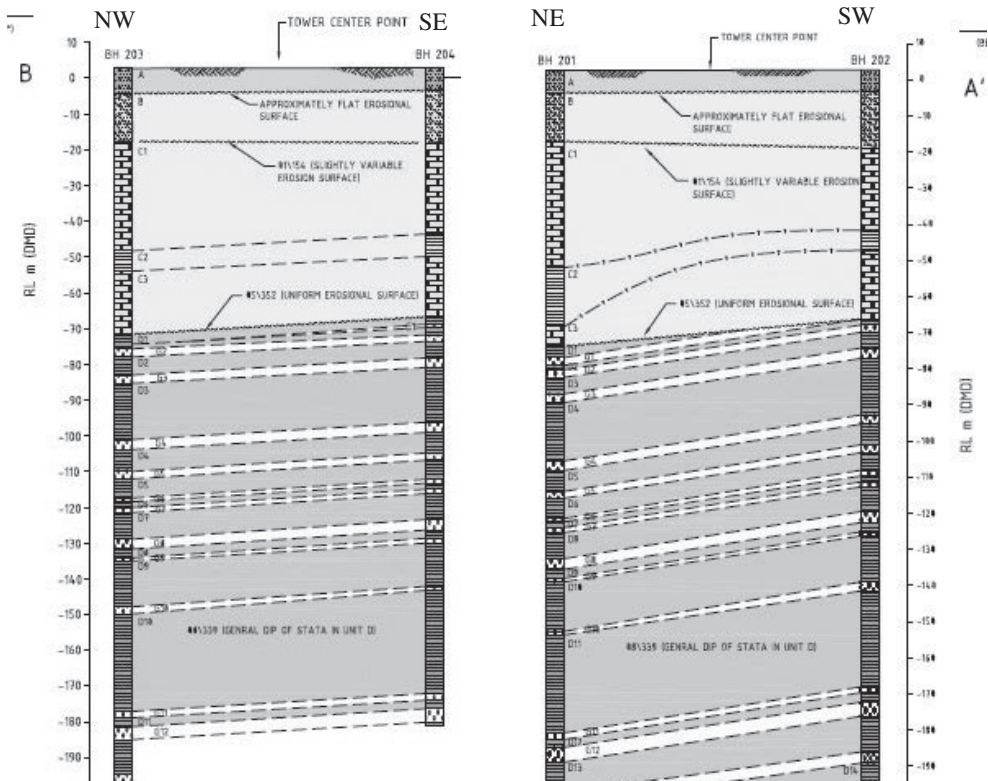
Figure 2: Orthogonal cross sections through the site showing general stratigraphy

Units C and D described above are generally massive. Some tight, closed joints are present within these units which are thought to have formed as a result of stress changes during burial. There were no tectonic induced discontinuities observed. The general site stratigraphy is presented in Figure 2.

2.4   Results of measurement

Small strain stiffness was obtained from the results of the cross-hole seismic testing. Cyclic triaxial testing and resonant column testing was undertaken in the laboratory. Typically, the small strain stiffness measured in the laboratory was about 5 times less than that measured in situ at the location from which the sample was taken, which is consistent with the stress relief and micro-cracking of the laboratory test samples.

Figure 3 presents the initial Young's modulus measured in the pressuremeter testing undertaken in 3 boreholes (BH203, BH204 and BH208). Also shown on the same plot are the results of Young's modulus measured on samples tested in the laboratory in UCS tests with end platen displacement measurement. The general shape of the profiles with depth correlates well between the different boreholes suggesting relatively uniform ground conditions underlying the site. This is consistent with borehole core observations.
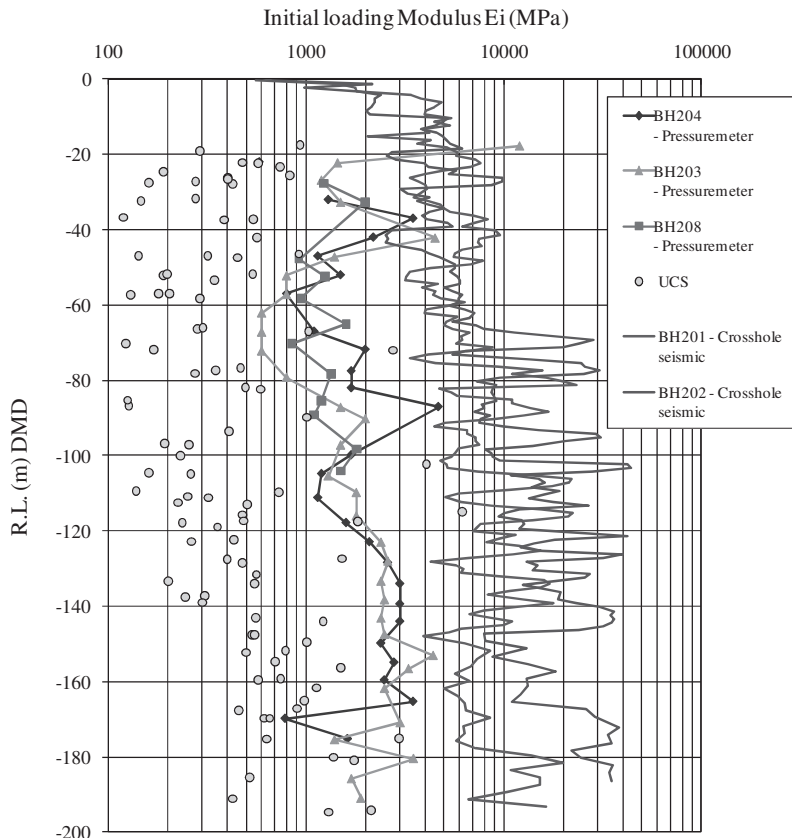
Figure 3: Initial Young's Modulus

The discrepancy between the stiffness measurements made in the field and laboratory for the calcareous materials, Unit C and D was attributed to the effects of stress relief as was noted at Site 1. Greater reliance was therefore placed on the in situ pressuremeter testing for the development of a geotechnical model for analysis.

2.5 Test barrettes

Three test barrettes with cross-sectional dimensions of 1.2 m x 2.8 m were installed to depths of 65 m (TB02 and TB03) and 95 m (TB01) and tested in accordance with specifications provided by the geotechnical engineers. Test barrette TB02 was installed at the same location as the investigation borehole BH208 (Figure 4).
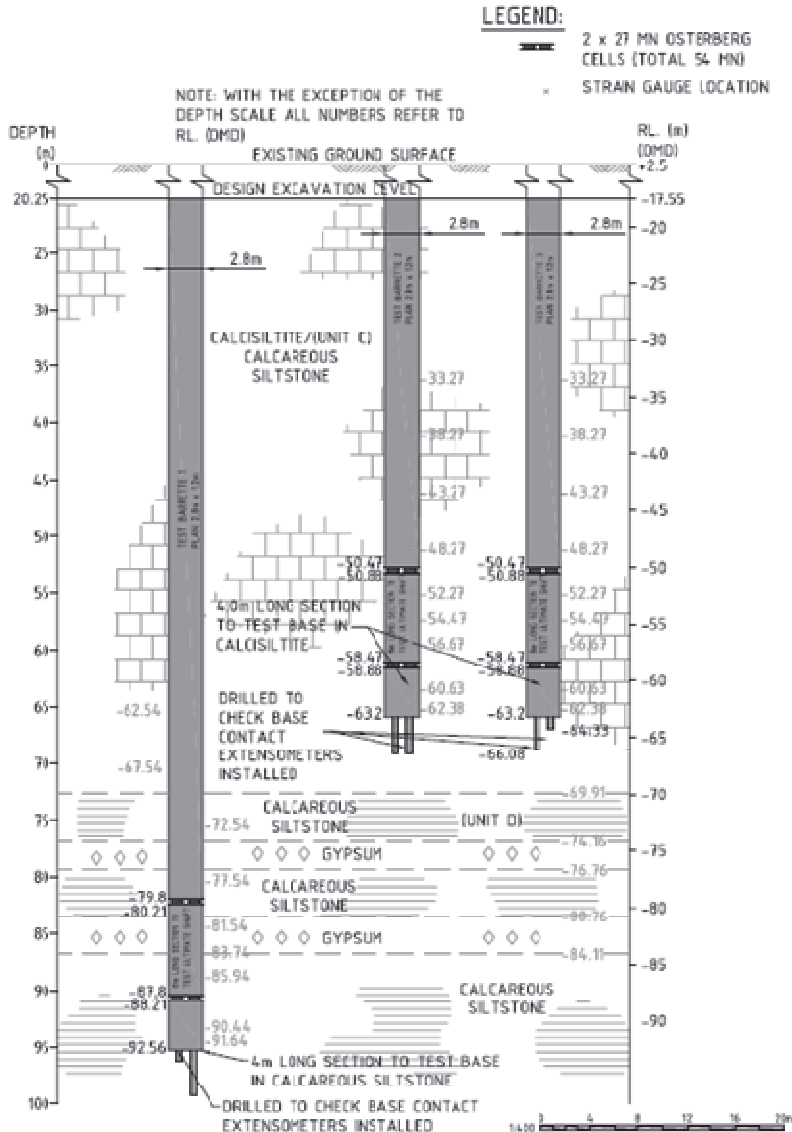
Figure 4: Test Barrette Arrangement

40

Test barrette TB01 was installed about 12 m south east of TB02 and TB03 about 8 m due south of TB02 resulting in a minimum clear distance between test barrettes of about 6 m. The lengths of the barrettes were chosen to provide information on barrette performance in the Unit C and D materials.

The test barrettes were installed using an hydrofraise with polymer support. The hydrofraise cutting action results in a relatively smooth excavated surface and hence a concrete rock interface which is essentially devoid of roughness. High slump concrete was placed by tremie. Concrete design characteristic 28 day strength was 60 MPa. Strengths significantly in excess of 60 MPa were achieved during construction.

Load testing of the barrettes comprised two levels of Osterberg cells in each test barrette as shown in Figure 4. Each level of cells was capable of providing a design bi-directional load of 54 MN. However, during testing loads were increased to the capacity of the equipment resulting in bi-directional loads of up to 83 MN. The Osterberg cells were positioned to measure performance of the lower 20 m or so of the barrettes.

The test barrettes were instrumented with displacement tell-tales and strain gauges. In addition, instrumentation was also located in the rock below the toe of the barrettes to directly measure the displacement of the rock at this location. The arrangement of the test barrettes is presented in Figure 4.

3. STATIC TEST RESULTS

The barrette load tests were used to investigate load deformation behavior of the shaft and base of the barrette under static, cyclic and long term conditions and also as large scale loading tests to confirm modulus estimates. The measured load versus displacement performance of the two shorter test barrettes (TB02 and TB03) for loading at the lower (LOC) and upper (UOC) levels of Osterberg cells are shown in Figures 5 and 6 respectively. Also shown are predictions of the performance. The predictions were obtained on the basis of the adopted design properties for the ground and on the as-constructed barrette geometry. The predictions of performance were completed prior to testing of the barrettes.
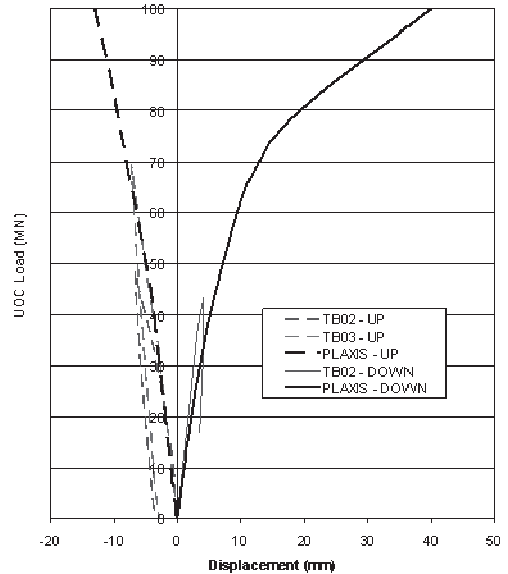
Figure 5: Measured vs predicted performance for loading at upper Osterberg cells.

For the Class A prediction, the rock-socket software ROCKET97 (Seidel, 2000) was used to calculate the performance of the test barrettes. The calculated performance was then used in an axisymmetric PLAXIS 2D V8 model to obtain the calculated load versus displacement response shown in Figures 5 and 6. The comparison between the measured and predicted response is excellent, which provided further confidence that the design properties and constitutive model adopted on the basis of the insitu testing were appropriate. Similar comparisons between measured and predicted results were obtained for the deeper test barrette TB01.

The load test results indicate a significant reduction in shaft resistance during cyclic loading with the reduction in shaft resistance appearing to be dependent on the cycling history. However, full shaft resistance was recovered once displacement of the pile shaft exceeded the displacement experienced during
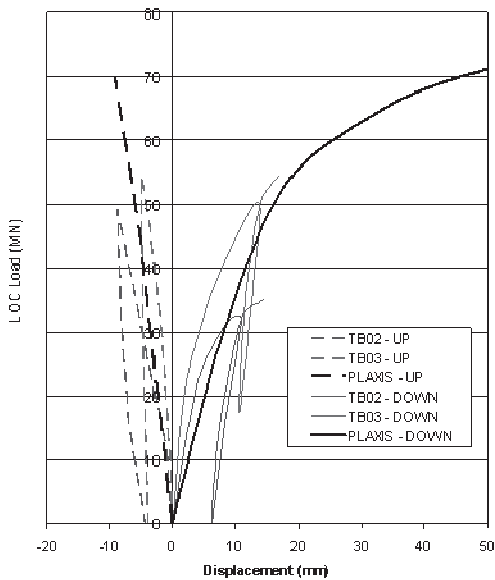
Figure 6: Measured vs predicted performance for loading at lower Osterbeg cells.

the cyclic stage of the test (Haberfield et. al 2010).

Base drilling was also undertaken within the test barrettes through ducts cast into the barrettes. The objective of this drilling was to assess the presence of debris on the base and quality of the contact between the concrete and underlying rock. The drilling suggested that the contact was not clean and that debris was present. The initial response on loading the lower osterberg cells suggested a soft base, possible, given that the base drilling ducts provided a path for soft material and fluid to 'escape' during the barrette loading.

The test barrettes provided confirmation of the constitutive model developed on the basis of the site investigation work. Key elements of the model that influenced the foundation design included:

- If the ground stress exceeds the bond yield strength, a collapse type behaviour resulting in consolidation and creep could ensue.

- There is likely to be poor contact between the barette and ground, possibly due to debris on the base of the barrette.

4. FOUNDATION-STRUCTURE INTERACTION ANALYSIS

4.1.   Basis of foundation design

The proposed footing raft was to have a diameter of about 105 m. A preliminary assessment showed that while the building could be supported on a near-surface raft, the settlements would be excessive. A design based on a pile-supported raft was therefore proposed.

The schematic design for the Nakheel Tower footing system therefore comprised a raft slab generally between 4 m and 8 m thickness. The raft slab was to be founded at about RL -17.5 in the top of the Unit C material, and to be supported by barrettes. The structural engineers, WSP proposed a schematic design for the footing system comprising 184 barrettes of 2.8 m by 1.2 m (plan dimension) and 224 barrettes of about 2.8 m by 1.5 m, a total of 408 barrettes. The final design, as modified by later analyses used 392 barrettes. The number of barrettes was dictated by the ultimate structural load that could be carried by each barrette, and not by geotechnical factors.

The footing layout is shown in Figure 7. Particular concentrations of load occur at the Drum Walls, Hammer Walls and Mega Columns. Analyses were carried out for various combinations of dead load, live load, wind load and earthquake load. Loads and load combinations for these analyses were provided by WSP.

4.2. Two-dimensional analysis of foundation

4.2.1   Design approach

As the first stage of design development, the design performance of the proposed footing system was analysed to:

- calculate settlements of the tower under design dead, live and wind loads
- provide equivalent spring stiffness values for the raft and barrettes that could be used in the structural analysis of the footing system.

At the design development stage, the structural engineers were unable to provide limits on total and differential settlements and allowable tilt. Based on experience with similar buildings,

excavation, dewatering and loading of the footing system. This provided a realistic estimate of the overall load-settlement performance of the Tower from which equivalent spring stiffness values for the barrettes and raft could be calculated for use in structural analyses of the tower. However, because of the two-dimensional nature of the model, it could not model the barrette groups under the mega columns. Additional analyses were therefore carried out with software programme REPUTE to assess the variation of spring stiffness in the
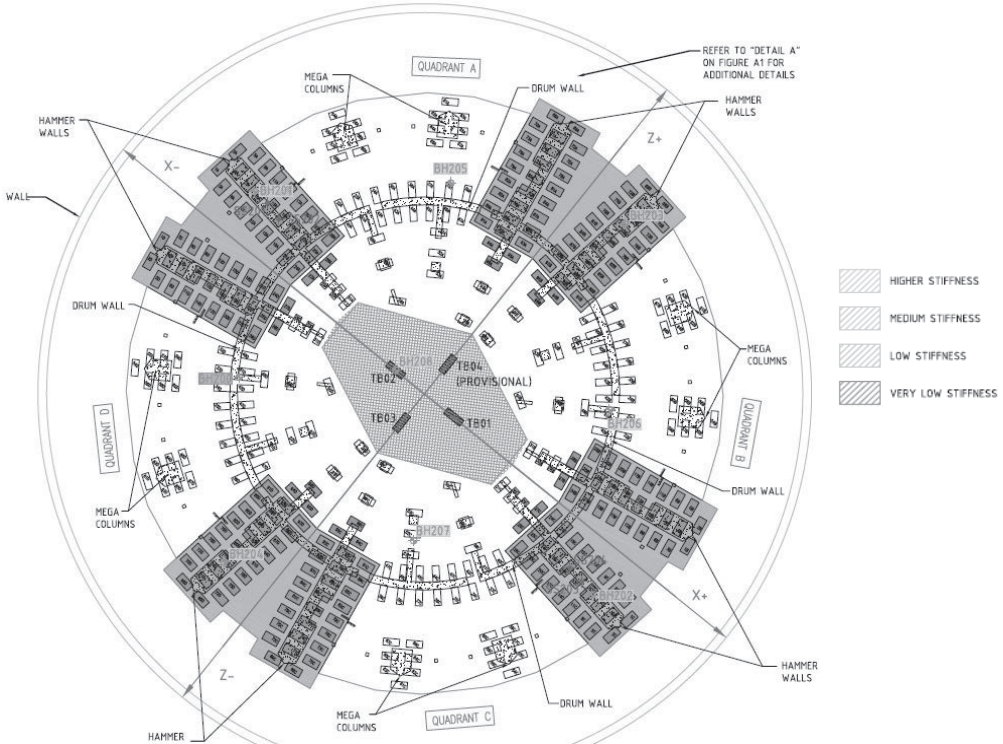
Figure 7: Barrette and layout

it was considered that if the maximum settlement was limited to about 100 mm, it would be likely that differential settlement and tilts would be acceptable. The design proceeded on this basis.

A finite element program PLAXIS 2D was used to model the whole footing system and followed the proposed construction stages from undeveloped site through installation of the basement diaphragm wall and barrettes,

group underlying these columns.

The results from both the PLAXIS 2D and REPUTE analyses were combined to provide representative spring stiffness values for the barrettes and the raft for use in structural models of the Tower footing system. Based on these results, the structural engineers for the project were able to refine the barrette/raft layout and dimensions and the column loads. The footing system was then re-analysed using

the above process to arrive at new spring stiffness values for the new loads. The process was iterated until convergence in loads and deflections was obtained.

4.2.2 Modelling method and assumptions

Axisymmetric modelling was used to analyse the footing response to live and dead loads with PLAXIS 2D Version 8 finite element software. A combination of axisymmetric and plane strain modelling was used to analyse the response to wind loading. Figure 8 shows the finite element mesh used for axisymmetric modelling.
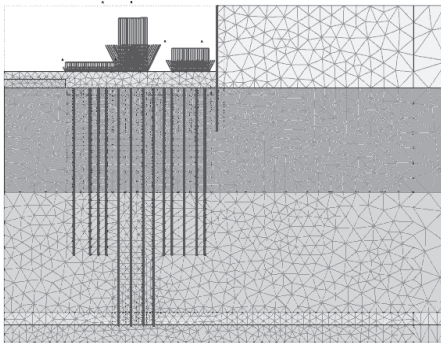
Figure 8: Axisymmetric Model: Barettes Modelled as Structural Elements.

All soil materials were modelled using a purely cohesive constitutive model to simulate the important role played by the interparticle cementation (bond yield strength). Initially, the barrette groups were modelled as a soil element. The equivalent stiffness and the equivalent strength of the barrette-embedded soil mass was estimated by weighting the Young's moduli and strengths of the concrete and rock based on the cross-sectional areas of each. A second method which was considered to give more realistic results was to model the barrettes as concentric rings of structural plate elements. Initial analyses were done with the barrettes supporting the drum wall founded at RL -74.5 m. To investigate the effect of both shorter and longer barrettes supporting other areas of the raft, the barrettes in the remaining rings were founded at RL -57.5 m or RL -42.5 m. The axial and bending stiffnesses of the barrette plate elements were calculated from the barrette cross-sections and average barrette spacings.

The raft slab was assumed to be 2 m or 4 m thick, depending on distance from the centre of the tower. Following initial analyses, the raft thickness was increased to 2.5 m beneath the centre part of the tower and 6 m to 8 m beneath the main structural elements. Further analyses indicated that raft thickness over a reasonable range did not have a significant effect on the geotechnical performance of the footing system and raft thickness was defined by structural rather than settlement considerations.

As part of the site characterisation, three test barrettes were installed and load-tested. The installation allowed construction factors likely to affect the performance to be assessed as well as providing information on the load-settlement behaviour. The construction aspects investigated included barrette verticality, base cleanliness (and the effectiveness of base cleaning methods), degradation of barrette side walls, barrette integrity and concrete placement. The results of base load testing and cross-hole sonic testing indicated the presence of debris between the base concrete and the base of the excavation. Therefore it was essential that analyses be carried out for barrettes with and without debris at the base. The worst case modelling for base debris was to assume a significant thickness of debris extended across the entire base.

4.2.3 Results of 2-D analyses

Calculated maximum total and differential settlements under dead plus live load are shown in Table 1.

The results in Table 1 indicate similar maximum settlements beneath the drum wall of about 82 mm to 86 mm for both methods of modelling the barrettes. For the case of no base debris. the impact of including base debris depends on the modelling method adopted. As the approach using structural plate elements was considered more realistic, it appears that base debris does not have a significant impact on the calculated settlement for the assumptions used.

The increase in vertical stress due to dead and live loading immediately below the toes of the barrettes is shown in Figure 8. The presence

Table 1: Settlement results for axisymmetric PLAXIS 2D analysis – DL + LL only

Barrettte Founding Level (RL m DMD)	Description	Maximum settlement (mm)	Differential settlement* (mm)
-74.5 and -50	Barrettes modelled as soil elements without base debris	86	19
-75.5 and -50	Barrettes modelled as soil elements with base debris	103	26
-62.5 and -50	Barrettes modelled as soil elements with base debris	123	36
.74.5 and -57.5	Barrettes modelled as soil elements without base debris	82	21
-74.5 and -57.5	Barrettes modelled as soil elements with base debris	83	22
-74.5 and -42.5	Barrettes modelled as soil elements without base debris	86	21

of base debris results in locally higher stresses in the ground close to the toe of the barrettes. This is a direct result of load being shed from the base of the barrette to the shaft of the barrette.

Figure 8 shows increases in stress at the toes of individual barrettes from maximum values of 3 MPa and 2.2 MPa to 3.7 MPa and 2.5 MPa respectively under the drum wall and mega columns. These stresses are such that the bond yield strength in the material is likely to be exceeded where base debris is present. This was further investigated in the three-dimensional analyses.

The impact of base debris, should it occur, may be reduced by using the much stronger gypsum layers to spread the load from the barrettes onto the underlying Unit D material. The test barrettes indicated that relatively high shaft resistances (1730 kPa) can be achieved in the gypsum. If the barrettes were founded through the uppermost gypsum layers at about RL -75 m, the shaft resistance developed in the gypsum would off-set the loss of base resistance due to base debris and hence reduce the local areas of high vertical stress in the Unit D material. For the same analyses set out above using barrettes modelled as plate elements, but adopting the design gypsum properties (and not Unit D properties as was used above), the

increase in stresses in the Unit D material due to loading from the Tower were found to be similar to those obtained assuming no base debris.

Spring stiffness value for barrettes located at a given radius from the centre point of the raft were estimated and are shown in Table 2. Figure 9 presents the PLAXIS 2D settlement profile for the raft slab plotted against distance from the Tower centre point (based on the application of dead and live column loads only). For the PLAXIS 2D loading and settlement profile, stiffness values were estimated and are shown in Figure 10. The lower stiffness values in the centre reflect the thinner (2 m) slab there and the absence of applied load in this area.

Analysis under wind loading was carried out using a combination of plane strain and axisymmetric models, and modelling the barrettes as plate elements without base debris (due to the incompressibility of the debris under short term loading). The displacement profile under the raft is shown in Figure 11, using the same modulus values as for Figure 9. The response was also analysed using twice this modulus to represent the short term nature of the wind loading.
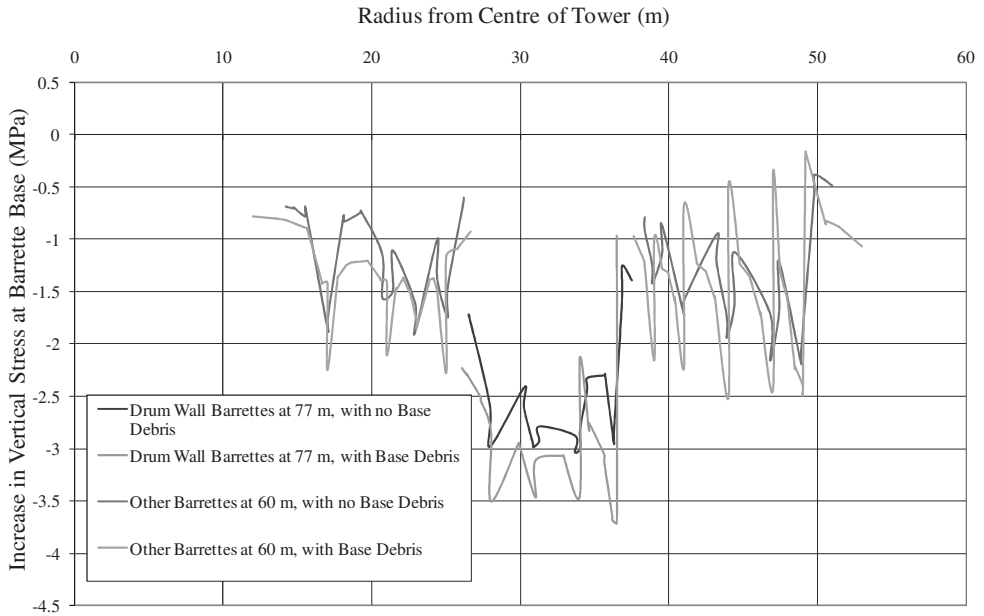
Figure 9: End bearing pressure with barrette groups modelled as structural elements

Table 2: Estimated spring stiffness values of barrettes under DL+LL

Ring	Radius (m)	Spring stiffness MN/mm	Pile Groups
1	49.0	0.56	Mega column 3 x 3 pile group
2	46.5	0.50	
3	44.0	0.52	
4	41.0	0.51	
5	39.0	0.58	
6	36.0	0.78	Inner drum 4 x 3 pile group
7	33.5	0.56	
8	31.8	0.61	
9	28.0	0.65	
10	25.5	0.52	
11	23.0	0.43	
12	20.5	0.29	
13	18.0	0.29	
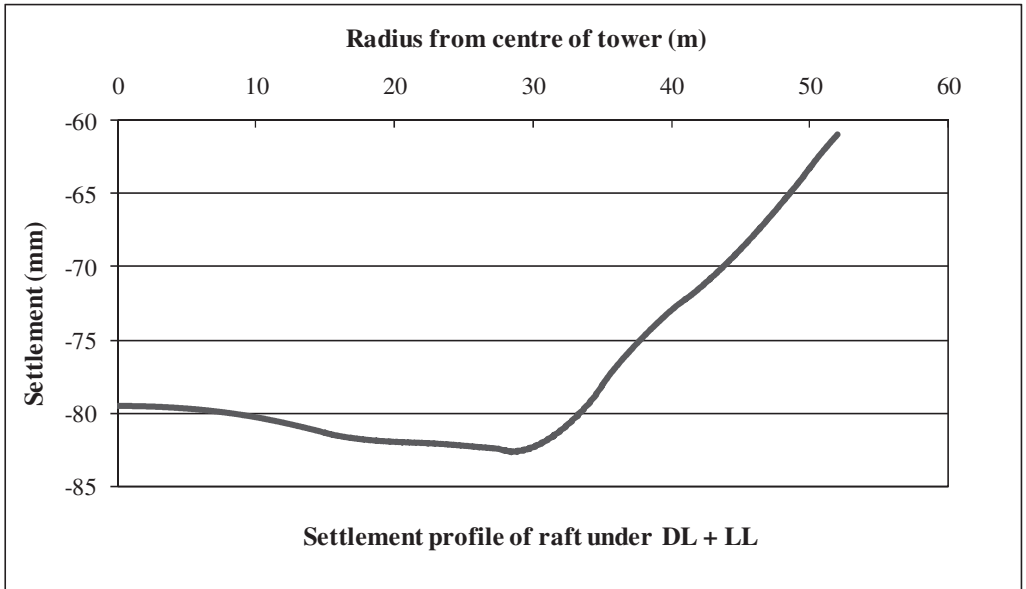
Figure 10: Settlement profile
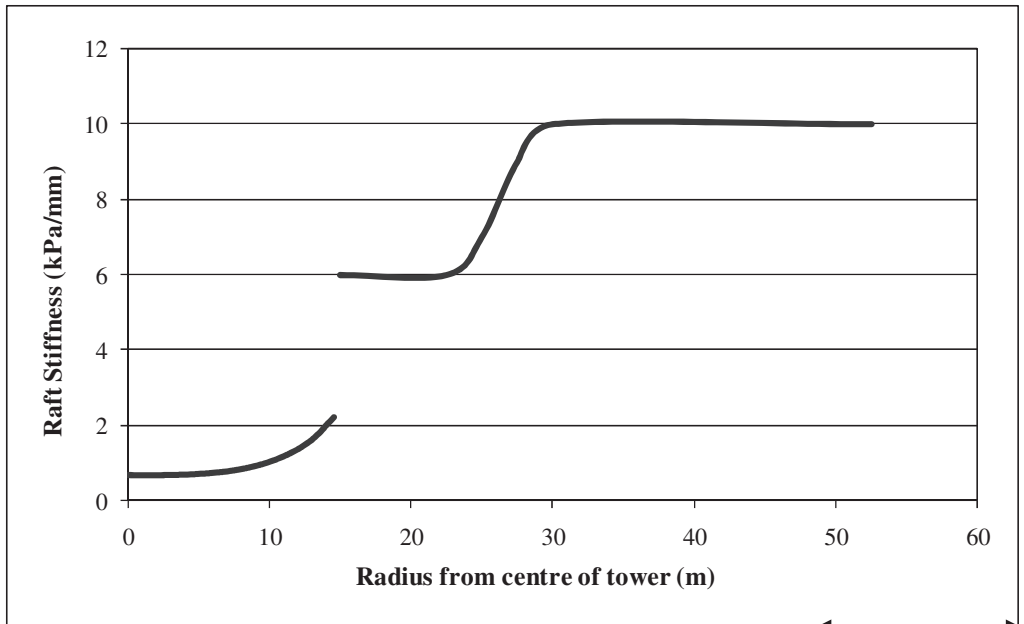
Figure 11: Stiffness profile
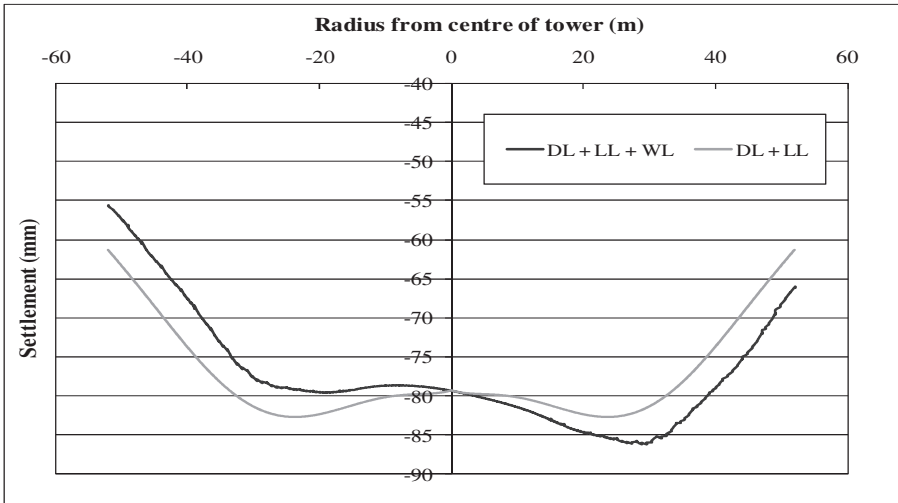
Figure 12: Settlement profile for unfactored ground stiffness

4.2.4 *Barrette founding levels*

The results presented earlier show that where base debris, and therefore poor base contact, is assumed at the toe of the barrettes, the increase in vertical stress applied to the ground near the toe of the barrettes is higher than the case where no base debris is assumed. The consequences of a higher increase in vertical stress near the toe of the barrettes could be exceedence of the bond yield strength of the carbonate cemented materials (Units C and D) and associated time-dependent compression of these materials. There was a risk of greater settlement or tower tilt from this factor.

The risk of higher stresses in the vicinity of the toe of the barrettes could be reduced by adjusting the founding level of the barrettes. Analyses showed that the increase in vertical stress below the base of the barrettes could be reduced by (a) staggering the length of the barrettes beneath the hammer walls and founding the drum wall barrettes through the upper layer of gypsum; (b) increasing the length of the centre row of the barrettes supporting the hammer walls resulting in a more equal share in load between the three rows of barrettes and reducing the risk associated with locally high stresses.

4.3. Three dimensional analysis of foundation

#### 4.3.1 Purpose of analyses

The results of the two dimensional axisymmetric analyses provided the basis for a viable footing system for the Tower. Although versatile and relatively quick to undertake, these analyses only provide an indication of the three dimensional response of the footing system. The two dimensional analyses enabled evaluation of the benefit or otherwise of changing barrette layouts and lengths, and development of the final footing system. Three dimensional analyses using PLAXIS 3D were undertaken to allow a better assessment of the performance of the footing system under non-symmetrical load cases such as wind and earthquake loading. The objectives of the three dimensional analyses were:

- To calculate the settlement profile of the tower raft under gravity and wind working load cases.
- To confirm geotechnical stability of the footing system under ultimate load conditions.
- To calculate the stiffness of the barrettes and the raft for gravity and wind working load cases for use in structural

analysis of the foundation system by WSP.

- To calculate barrette actions (shear force and bending moment) within barrettes for ultimate load cases (including base shear).

- To estimate the impact of debris at the base of the barrettes on the settlement performance of the footing system.

- To estimate the vertical stress increase below the toe of the barrettes under working load and ultimate load conditions for estimation of potential long term settlement (creep).

4.3.2 Loads and load cases

Loads provided by WSP were used in the analyses. In general three working load combinations and two ultimate load combinations as defined below were analysed:

- Working load combinations:
  - i)   DL + LL,
  - ii)   DL + 0.8 WL
  - iii)   DL + 0.75 LL + 0.6 WL
- Ultimate load combinations:
  - iv) 1.2 DL + 0.5 LL + WL
  - v) 1.2 DL + 0.5 LL + E

Analyses were undertaken for each working load combination assuming cases of full base resistance and no base resistance. The analyses assuming full base resistance were considered to provide a reasonable estimate of short term performance while the analyses with no base resistance provided a conservative estimate of long term performance (for the properties and conditions assumed). For each analysis, the following values were evaluated:

- Vertical settlement at the head of the barrettes.

- Vertical load at the head of the barrettes.

- Axial stiffness of each barrette.

- Geotechnical factor of safety for each barrette.

The three dimensional model used in the PLAXIS 3D analyses is shown in Figure 12. As described earlier, the subsurface stratigraphy at the site comprises relatively uniform beds of sedimentary material. The bedding within the different units and the contacts between them are generally sub-horizontal, or with a slight dip. The dip of the beds was modelled in PLAXIS 3D as seen in Figure 12.

Figure 13: Ground Model

The outputs of the analyses were presented in spreadsheets which gave for each of the 392 barrettes the load and settlement estimates. These results were used by the structural engineers as input to their analyses, which resulted initially in revised barrette loads. Further foundation analyses were performed until the calculated barrette head loads and settlements converged with the structural inputs.

4.3.3 Results

The calculated maximum and minimum settlements under working load conditions are summarised in Table 3.

For the dead load plus live load case, the calculated settlements assuming full base resistance were about 10 mm to 15 mm less than those obtained from the analyses assuming no base resistance. It was considered the analyses assuming full base resistance provided a reasonable estimate of settlement performance of the tower footing system in the short-term .

Table 3: Calculated settlements of major columns and walls

Load Case	Full Base Resistance (Short Term)			No Base Resistance (Long Term)		
	Hammer Walls	Drum Wall	Mega Columns	Hammer Walls	Drum Wall	Mega Columns
DL + LL	66 – 72 mm	70 mm	62 mm	82-87 mm	82 mm	74 mm
DL + 0.8WL						
Winward Minimum	34 – 45 mm	46 mm	35 mm	42 – 57 mm	54 mm	45 mm
Leeward Maximum	74 – 80 mm	74 mm	70 mm	90 – 99 mm	93 mm	87 mm
DL + 0.75LL + 0.6 WL						
Winward Minimum	50 – 60mm	56 mm	46 mm	62 – 70 mm	66 mm	58 mm
Leeward Maximum	78 – 82 mm	76 mm	72 mm	96 – 100 mm	90 mm	86 mm

The analyses indicated also that under full design gravity loading of the tower, the bond yield stress immediately below the barrettes was likely to be exceeded and some creep would occur. This would lead to load transfer from the base of the barrettes to the shaft. Alternatively, on the assumption that some debris was present at the base of the barrettes, in the short term the debris would be incompressible and hence the full base resistance may be relevant. However, over time the fluid within the debris would drain and hence load would be transferred from the base to the shaft. It is probable that both mechanisms may occur concurrently.

The consequence is that over time, at least some load would be transferred from the base of the barrettes to the shaft of the barrettes. The extreme end condition of this is that the base of the barrettes may carry little or no load. This condition was modelled by the analyses assuming no base resistance. It was therefore considered that a reasonable upper estimate of the long-term settlement of the tower footing system under the design case parameters was provided by analyses which assumed no base resistance.

Where full base resistance was assumed, barrette axial loads under the dead load plus live load combination varied from 16 MN to 57 MN and from 12 MN to 79 MN for the wind loading cases, with the higher loaded barrettes tending to lie towards the outside of the hammer walls. These loads translated to a geotechnical factor

of safety typically greater than 2.5. Barrette stiffness values ranged between about 0.2 MN/mm and 1 MN/mm.

The maximum axial load in the 1.2 m by 2.8 m and 1.5 m by 2.8 m barrettes under the working load cases analysed were 64 MN and 79 MN respectively. These are less than the barrette structural working load capacities of 64.5 MN and 80.6 MN provided by WSP.

Where no base resistance was assumed, barrette axial loads under the dead load plus live load combination ranged between 13 MN and 47 MN and for the wind load combinations between 7 MN and 56 MN. For the most onerous wind load case analysed, the geotechnical factor of safety was typically greater than 2.5. Barrette stiffness values ranged from 0.16 MN/mm to 0.6 MN/mm.

Where the raft was 4 m thick or greater, the calculated raft stiffness was about 12 MN/mm.

4.4. Probabilistic analysis

The PLAXIS 2D and REPUTE analyses were carried out for a single design set of properties. To investigate the potential range of settlement and tilt that could occur due to variation in the subsurface stratigraphy and variation of the stiffness of the Unit C and D materials, a probabilistic analysis was performed using PLAXIS 2D.

During the field investigation, a correlation between field core hardness and Young's modulus was developed. The mean and standard

deviation values were calculated for each field hardness value and these normal distributions of modulus values were then applied to each of the continuous field hardness profiles at each borehole location.

For every field hardness in each borehole, a Young's modulus was randomly selected from the normal distribution of modulus values for the appropriate field hardness value at that depth. This was repeated 100 times for each

used to define a normal distribution of settlement at each borehole location

The probability/settlement distributions for eight boreholes located within the tower footprint are shown in Figure 14. This also shows the results of analyses using a credible upper and lower bound approach to the estimation of strength and stiffness properties.

The upper and lower bound estimates were based on the highest and lowest credible

Figure 14: Probability curves for settlement at borehole locations
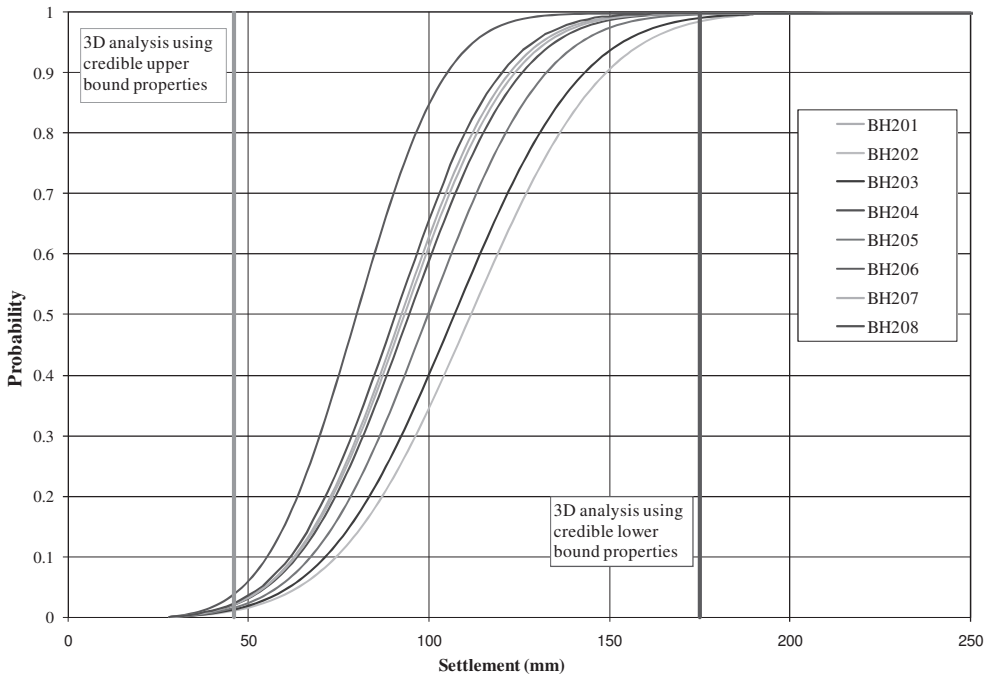
borehole, resulting in 100 possible modulus versus depth, or stiffness profiles at each borehole location.

A simplified model was used to calculate the settlement of the ground below the base of the barrettes. The vertical stress distribution was estimated from the results of the PLAXIS 2D model and applied to the modulus estimates to calculate the settlements. This calculation was repeated for each modulus versus depth profile to give 100 settlement estimates at each borehole location. The mean and standard deviation of these 100 settlement estimates for each borehole location were then calculated and

strength and stiffness data obtained from insitu testing undertaken during the geotechnical investigation. The effects of stress relief on core samples recovered from the boreholes were assessed to be significant, and therefore the strength and stiffness results from laboratory testing were discarded.

5. PRACTICAL FACTORS

5.1. Building code compliance

The local building code does not recognise the concept of a pile raft, where the piles were installed to control settlement and not fully

support the structural load. The code required a minimum geotechnical factor of safety of not less than 2.5 for each pile (barrette). This meant that some barrettes had to be lengthened and they therefore attracted more load.

The code also limited an individual pile structural load to 90 MN. The pile geotechnical capacity was well in excess of this figure. In preliminary discussions with the preferred piling contractors, the contractors proposed shortening the piles, not fully realising that the pile lengths were designed to meet settlement criteria. Although the owner originally proposed that the piles be installed under a design and construct contract, it was eventually recognised that the design intent would be better achieved by a construct-only contract. In this, the contractor would be responsible to install piles to the correct dimensions, lengths and locations, and to the required structural capacities. The geotechnical engineer would be responsible for the settlement performance, geotechnical strength and overall geotechnical performance.

Analyses were required to demonstrate to local authorities that piles would perform satisfactorily without full-length reinforcement cages (which were required by local building codes).

5.2. Construction considerations

Polymer support fluid was used during the construction of the barrettes and, in general, performed satisfactorily. However, a few instances were observed where the upper sand collapsed into an open diaphragm wall panel, requiring backfilling and re-excavation. In each case, the polymer had been in place over the course of a day during which no work had occurred. Therefore the time over which the excavations for the main barrettes were left open should be minimised.

The results of the test barrettes suggested that debris had accumulated on the base of the excavation prior to the placement of concrete. The source of the debris could not be determined definitively. Likely sources include material that could have settled out of the polymer prior to placement of the concrete, material dislodged from the walls of the excavation during placement of the reinforcing cage or during the time that the barrette excavation remained open.

The analyses indicate that although the presence of base debris did not have a significant impact on settlement, it has an influence on the stress that is applied to the ground in the vicinity of the barrette toe and it provides a void into which material can yield. This was considered to be an unacceptable risk to the performance of the footing system. Therefore it is necessary that the barrettes be constructed with as clean a base as is practical. The construction method used to install the barrettes was modified to reduce the potential for base debris.. The primary changes included using the tremie to recirculate the polymer following placement of the reinforcement cage to keep solids which may settle out to form debris in the polymer solution.

7. REFERENCES

Bond, A. J. & Basile, F. 2010. Repute 2.0, Software for pile design and analysis. Reference Manual, Geocentrix Ltd, United Kingdom, 49p.

Brinkgreve, R.B.J, Broere, W. & Waterman, D., 2008. PLAXIS 2D Reference Manual, PLAXIS, The Netherlands.

Brinkgreve, R.B.J, & Swolfs, W.M., 2007. PLAXIS 3D Reference Manual, PLAXIS, The Netherlands.

Haberfield, C.M., Paul, D.R., Ervin, M.C. and Chapman, G.A. (2010), "Cyclic loading of barrettes in calcareous soils using barrettes", Frontiers in Offshore Geotechnics ISFOG 2010: Proceedings of the Second Int. Sym on Frontiers in Offshore Geotechnics, 8-10 November, 2010, Perth, Australia.

Seidel, J. P. 2000. Rocket 3.0 Manual, Monash University, Melbourne.

Strengthening of old bridge foundation using the pile group system

I. Sokolić
University of Zagreb, Faculty of Civil Engineering, CROATIA, *isokolic@grad.hr*

B. Vukadinović
Geotehnički studio d.o.o, CROATIA, *bojan.vukadinovic@geotehnicki-studio.hr*

Ž. Skazlić
University of Zagreb, Faculty of Civil Engineering, CROATIA, *zskoric@grad.hr*

ABSTRACT: Paper describes basic concept for numerical modelling of pile group system used for strengthening of old bridge foundation. The basic design concern is to take into the account interaction between the old pier footing, the new pile group system and surrounding soil. Two different methods were used for soil-structure interaction modelling. The first method, available in computer software Ensoft-GROUP 7.0, is based on semi-empirical correlations to predict nonlinear reaction of the soil due to pile displacement. The second method, available in software PLAXIS 3D Foundation, accounts for full 3D soil-structure interaction. Methods were compared and the effect of old footing on the load transfer distribution is validated.

1. INTRODUCTION

Nowdays there is a constant need for strengthening the old bridge foundations. The main reasons are time degradation effects, higher loads of new traffic and new design codes that must be satisfied. The basic design concern is to take into the account interaction between the old pier footing, the new pile group system and surrounding soil.

The main objective in this paper was to analyze the problem of strengthening of old Railway Bridge foundation in Zagreb. The old pier foundation is huge footing with an area of 17 x 6 m and 8.9 m high. The bearing support on the top of the pier is able to take over both vertical and horizontal actions. The old footing cannot sustain huge moment forces calculated according new traffic loads and new design codes. The critical design situation which was analyzed in this paper is assuming two trains braking at the same time and in the same direction.

The strengthening system consists of 32 piles fully embedded into the new reinforced concrete slab and incorporated into the old pear by the coating. The total length of the piles is approximately 24.5 m. Battered and vertical piles are used with 100 and 40 cm in diameter (Figure 1).
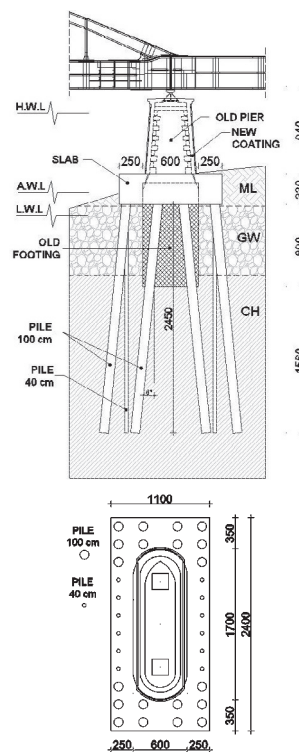

Figure 1. Cross section and top view of the pile group and old pear footing

The soil profile consists of three dominant layers and it is characteristic for alluvium of Sava River in Zagreb. Surface layer consists of low to medium stiffness humus fill, low plasticity clay and sand, and extends to depths of ~3.5 m. The second layer consists of alluvial deposits of dense to very dense gravel, partially mixed with silt, extending down to ~11.0 m. The bottom layer is stiff Pliocene clay.

Geotechnical investigation performed include *in-situ* penetration tests (N_{SPT}) to determine gravel compactness and laboratory tests to determine undrained strength of stiff clay (c_u) and its stiffness (Table 1). The underground water level used in the calculation, correspond to the Average water level of river Sava.

Table 1. Soil parameters and test results.

soil	base [m]	N_{SPT} [blows]	γ [kN/m^3]	ϕ [^{o}]	c_u [kN/m^2]
CL	3.5	4	19	-	20
GW	11.0	21-43	20	35	-
CH	> 20	25-30	20	-	120

The basic pile design concept is that the bridge dead load is sustained by the old footing, while the traffic load is transferred to the pile group. Resulting force at the top of the pile group consist of vertical live load V, horizontal live load H and corresponding moment M. For pile bearing capacity calculation it can be assumed that the moment M is completely taken by the vertical forces in the piles which cause the reduction of the axial force at one side of the pile group and amplification on the other side.

On the other hand, for the design of pile internal stability, the effect of pile embedment must be considered. Due to the horizontal movement of the foundation system, the moment reaction appears at the top of the pile, which is critical for reinforcement design. To validate the amount of action sustained, complex static analysis must be performed, including the effect of old footing.

2. SEMI-EMPIRICAL ANALYSIS

The complete foundation system analysis was carried out using the computer software Ensoft-GROUP 7.0 (Rees et al. 2006). The numerical method used is called '*p-y method*' (Reese & Van Impe, 2011) that consists of Winkler model

of the beam on the ground represented by non-linear springs. The shape and the size of the curves that define secant stiffness of the springs are derived from empirical correlations according to the type of the soil, soil parameters and the soil profile. The similar approach called '*t-z method*' is used for modelling pile settlement curve.

The old footing was modeled using circular pile elements as well. The area and the moment of inertia of the cross section were defined equivalent to the square footing, while the diameter was taken 17.0 m which is the width of the footing in the direction of movement.

Table 2. Reaction forces of footing and piles.

| PILES			Action: H
	H [%H]	V [%H]	M [%Hx1]
Piles	100	-35(-) +35(+)	-210* 210**
			Action: M
	H [%M/1]	V [%M/1]	M [%M]
Piles	-	-11(-) +11(+)	6* 94**
			Action: M,H,V
	H [%H]	V [%V]	M [%M]
Piles	100	-17(-) +117(+)	-10* 110**
PILES + FOOTING (G)		Action: M, H, V (k)	
	H [%H]	V [%V]	M [%M]
Footing	7	2	-2
Piles	93	-18(-) +116(+)	-8* 110**
		Action: M, H, V (d)	
	H [%H]	V [%V]	M [%M]
Footing	3	3	1
Piles	97	-22(-) +119(+)	-8* 107**
PILES + FOOTING (P)		Action: M, H, V (k)	
	H [%H]	V [%V]	M [%M]
Footing	54	16	10
Piles	46	-11(-) +95(+)	-4* 94**
(-) Vertical forces in tension piles (+) Vertical forces in compression piles *Internal moment in piles **Moment by vertical reactions in piles (k) Characteristic value of Action (d) Design value of Action (G) Calculated in program GROUP (P) Calculated in program Plaxis 3D			
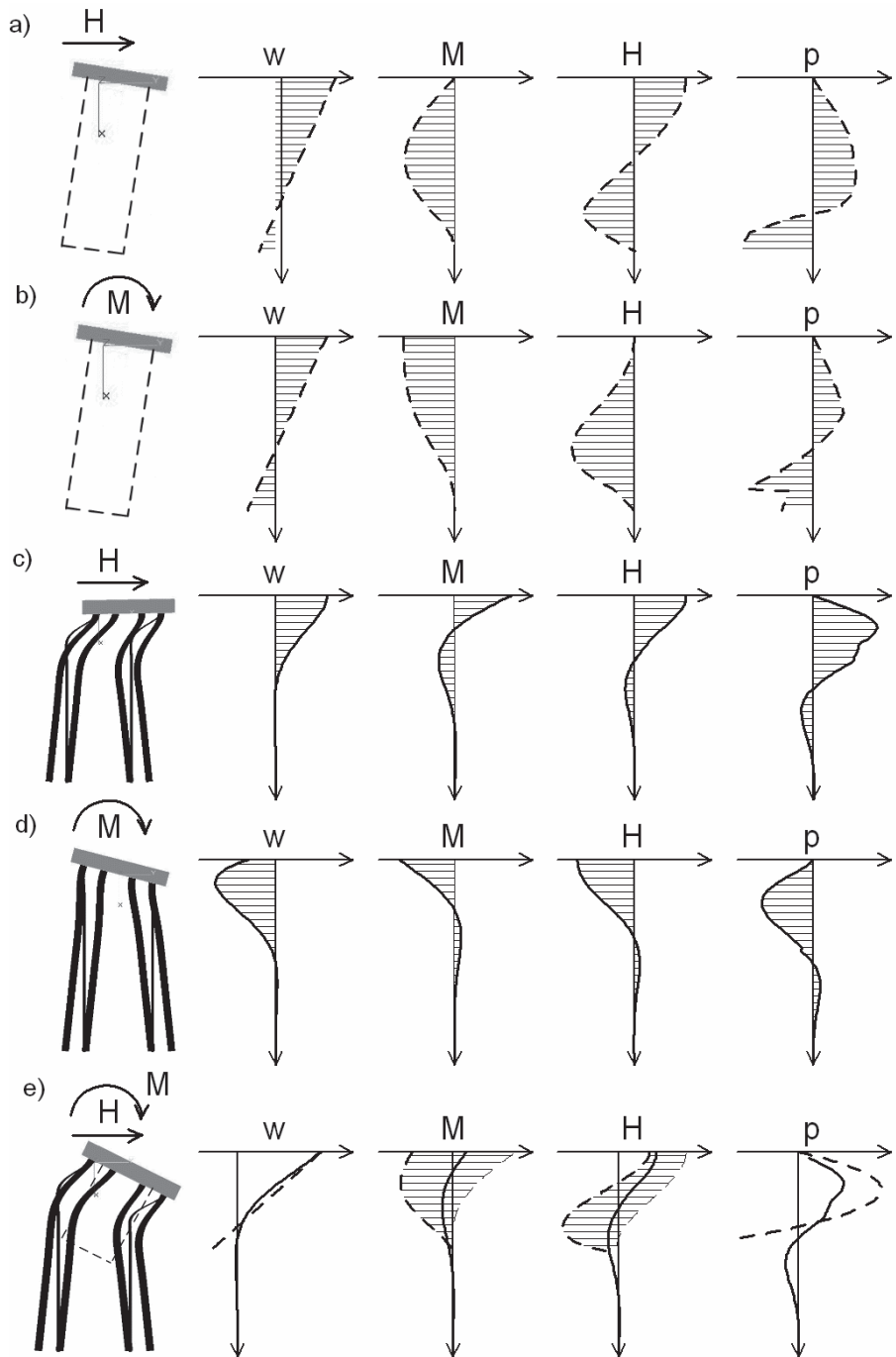
Figure 2. Static analysis of footing and pile group

Totally 10 analysis were performed varying the type of loading and the type of foundation. The shape of the displacement, internal forces and soil reaction diagrams were observed (Figure 2.) together with the reaction forces on the pile caps (Table 2). The soil parameters for calculating '*p-y curves*' and pile '*axial load – settlement curves*' were derived from soil strength parameters and according to recommendations proposed by Rees et al. 2006. The gravel layer was considered as submerged medium to dense sand with starting secant stiffness of spring $k = 20.000$ kN/m^3. The clay layer was considered as stiff clay in the presence of free water with principal strain corresponding to the 50% of the strength, $\varepsilon_{50} = 0.005$.

On Figure 2. a) and b) the results are shown for loading the footing represented by the short, rigid pile, applying separately horizontal and moment action at the pile cap. On the figure c) and d) the foundation system is analyzed only for the pile group, while on the figure e) for the pile group together with the old foundation.

It is important to notice that almost all the moment action on the pile cap is taken by the vertical reactions in the piles (94 to 110 %) while the rest of the moment is taken by the reaction moment of the piles and the footing. It can be seen that total amount of the applied load transmitted to the old footing reach maximum 7% of H, 2% of V and only 2% of M action (Table 2).

Comparing the internal moment diagrams it can be seen that in the case of single rigid pile the internal moment appears on the negative side of the diagram for both positive H and M action. On the other hand in the case of pile group, for H action the internal moment starts on the positive side of diagram, but on the negative side for the M action. For that reason, the reaction moments on the pile caps and the footing for complete system (Footing + Piles) depends both on the character of loading and the stiffness characteristics of all elements in the foundation system. On the Figure 2.e) the results of internal moment are shown for characteristic values of the soil parameters and action forces (tin dashed line) and for the designed parameters (tick dashed line). For serviceability design situation the moment reaction in the old footing is positive, while it is negative for the stability design situation.

3. PLAXIS 3D ANALYSIS

Full 3D soil-structure interaction model was calculated using the PLAXIS 3D Foundation software (Brinkgrawe & Swolfs, 2007). The old footing was modeled with soil elements using the linear-elastic soil model and corresponding parameters for the concrete. The same parameters were used for foundation slab modeled with the 3.3 m thick floor elements. The piles were modeled with embedded pile elements especially available in Plaxis 3D software (Figure 3).

The nonlinear behavior of the soil was modeled using the Hardening soil model (HS) both for gravel and stiff clay (Shanz et al. 1999).
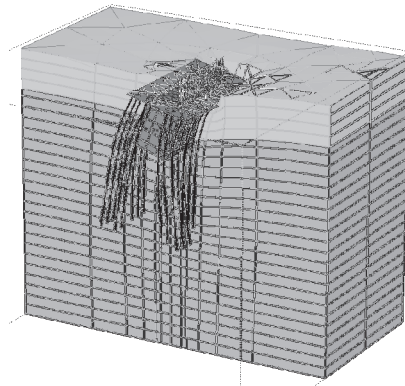

Figure 3. Pile group model with old pier footing in computer software PLAXIS 3D Foundation
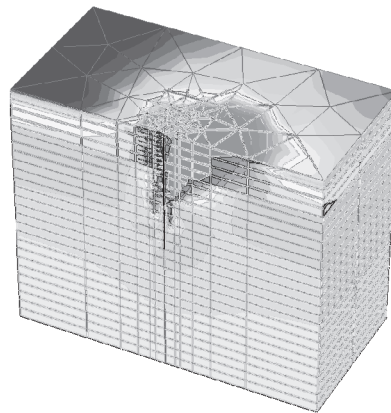

Figure 4. Laterally loaded single pile model in computer software PLAXIS 3D Foundation

The strategy for deriving the parameters for HS soil model was the same as proposed by A. Szavits-Nossan (2008) for numerical modelling of anchored retain structure, for the soil profile typical for the area of Zagreb city. The back analysis of horizontal wall movement, performed on several case histories (A. Szavits-Nossan et al. 2010) show that the reference stiffness of the HS soil model E_{50}^{ref} correlates well with the N_{SPT} values corrected with depth:

$$E_{50}^{ref} = 5x(N_1)_{60} \tag{1}$$

The strength parameter used for the gravel layer is the same as in the GROUP model ($\varphi = 35^o$), while the undrained strength of the clay layer was modeled with effective strength parameters and by performing the undrained type of analysis.

Two additional numerical models were performed to test the performance of the single embedded pile subjected to the vertical and horizontal loading (Figure 4). The former model produced the pile *'vertical load – settlement curves'*, and the latest *'p-y curves'* that can be directly compared to the empirical curves generated by the GROUP software.

4. COMPARISON OF RESULTS

The pile *'vertical load – settlement'* curves are compared on the Figure 5. The full lines represent the empirical results generated by the GROUP software, and the dashed lines the results of the 3D numerical simulation. Both models show the similar shape of the pile settlement curve, and the bearing capacity of the piles correspond quite well, both for $\phi 40$ and $\phi 100$ cm piles. Looking at the footing settlement curves it can be seen that the 3D model reacts much stiffer, which can be due to its huge dimension that are beyond the pile test results analyzed by Rees et al. 2008.

Horizontal displacement *'p-y curves'* are compared for three depths (Figure 6). It can be seen that both models generate similar curves, especially in the small displacement region where the secant stiffness is of great interest for serviceability design analysis. The basic difference is observed in the case of modelling the undrained behavior of stiff clay, while HS soil model is unable to model softening of the soil.

When comparing the results of numerical models for complex foundation system (Footing + Piles) the benefit of the full 3D modelling is evident (Figure 7). The final displacements and the rotation of the system are reduced.
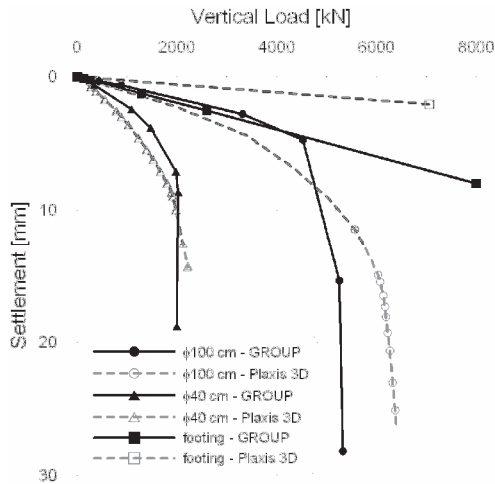

Figure 5. Load-settlement curves for pile $\phi 100$ cm, $\phi 40$ cm and footing, generated by computer program GROUP (full line) and calculated in computer program Plaxis 3D using embedded pile elements
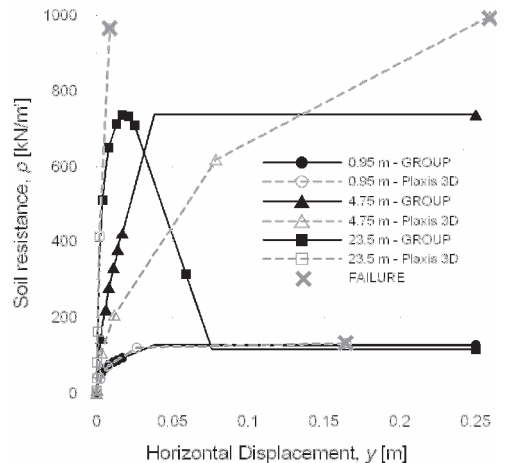

Figure 6. *'p-y curves'* for pile $\phi 100$ cm, generated by computer program GROUP (full line) and calculated in computer program Plaxis 3D using embedded pile elements
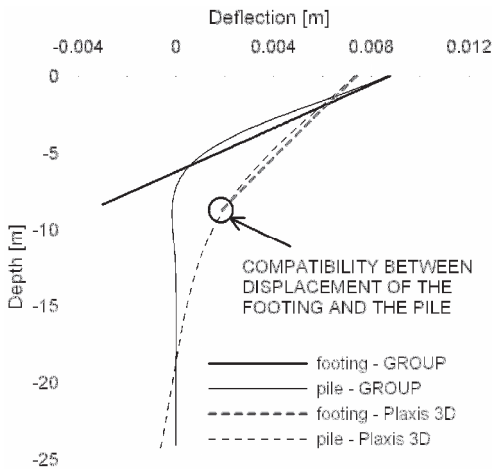
Figure 7. Displacement of the pile and old footing calculated in computer program GROUP 7.0 (full line) and in computer program Plaxis 3D (dashed line)

Compatibility between the displacement of the footing and the piles is achieved at the bottom of the footing. The resulting internal moments in the piles is much smaller then calculated by GROUP software (Figure 8). That can be explained by the fact that GROUP software doesn't account for global movements of the soil that appear around the footing and reduce the final deflection of the piles. Compared to the internal forces in the pile subjected to the equivalent horizontal force at the pile cap, the value calculated by full 3D soil-structure model is more than ten times smaller. Using the full 3D soil-structure interaction model the effect of the footing on the action distribution is high. The footing takes over around 53% of H, 16% of V and 10% of M action.

5. CONCLUSION

The results of the analysis show that using different modelling approaches and different strategy for deriving the soil parameters, the performance of the single pile in both software is very similar. On the other hand, when model-ling the full soil-structure interaction, more realistic and economic results are obtained using the full 3D model.
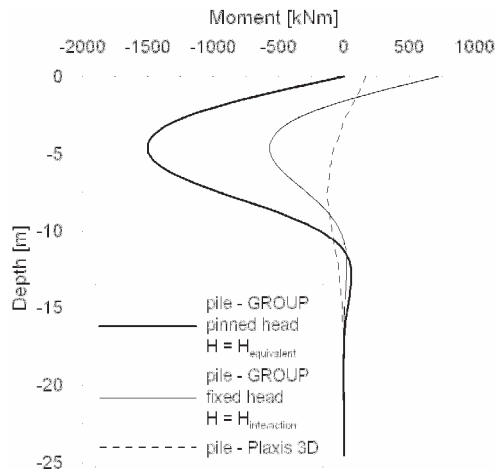
Figure 8. Internal moments of the pile for different soil-structure interaction situations. No interaction (dark full line), partial soil-structure interaction (tin full line), full 3D soil-structure interaction (dashed line)

6. REFERENCES

Reese, L.C., Wang, S.T. & Vasquez, L. 2006. Analysis of Group of Piles Subjected to Axial and Lateral Loading (Technical Manual). *ENSOFT, INC. Austin, Texas.*

Reese, L.C. & Van Impe, W.F. 2001. Single Piles and Pile Groups under Lateral Loading. *Leiden, Balkema.*

Brinkgrave, R.B.J. & Swolfs, W.M. 2007. PLAXIS 3D FOUNDATION Reference Manual V.2. *PLAXIS bv, AN Delft, Netherlands.*

Shanz, T., Vermeer, P.A., Bonnier, P.G. 1999. The hardening soil model – formulation and verifica-tion. *Beyond 2000 in computational geotechnics.*

Szavits Nossan, A. 2008. Advances and uncertainties in the design of anchored retaining walls using numerical modelling. *Acta Geotechnica Sloveni-ca (1): 5-19.*

Szavits-Nossan, A., Sokolić, I. & Plepelić, G. 2009. Design of anchored retaining structures by nu-merical modelling, *17th International Conference on Soil Mechanics & Geotechnical Engineering, Alexandria, Egypt.* Vol. 3.

Vukadinović, B. 2010. Željenzički most Sava, Zagreb – projekt održavanja – stup nepomičnog ležaja. *Design Project T.D.:3608-3/10.GS, Geotehnički studio d.o.o. Zagreb. (in Croatian)*

On the non-linear stiffness of the soil-structure interaction of historical buildings

C. di Prisco
Politecnico di Milano, *cdiprisc@stru.polimi.it*

G. Gottardi
Università di Bologna, *guido.gottardi2@unibo.it*

ABSTRACT: Any integrated structural analysis, especially under seismic loading, requires a suitable understanding and modelling of the soil-structure interaction. Recent developments in modelling soil-foundation behaviour aim at capturing the entire behaviour of a foundation in terms of the combined forces on it and their resultant displacements (known as 'force-resultant' modelling). Highly non-linear features can be thus relatively easily introduced, like soil hardening, creep (time dependent response) as well as dumping effects, in relation to cyclic and seismic loading. The formulation and use of such macro-element modelling (MEM) is herein briefly recalled, together with its relevant implications on the analysis of historical buildings, with special emphasis on tall and slender structures where second-order effects cannot be neglected.

1. INTRODUCTION

In the context of seismic design, according to capacity principles, it is generally recognized that any damage to foundations is to be avoided. This implies that the non-linear capacity of the system is exclusively exploited at the superstructure level, typically allowing energy dissipation at *ad hoc* selected points through either the formation of plastic hinges or the insertion of isolation/dissipation devices. This choice is partially motivated by budget considerations, but it is also justified by the lack of well-established methods to analyse the post-yielding behaviour of soil-foundation systems under strong seismic loading. Conversely, when the seismic performance of already existing buildings is to be assessed, this approach cannot obviously be adopted and performance-based approaches are needed.

Indeed, the interest towards performance-based approaches for seismic design and seismic adequacy assessment is rapidly growing, spreading an increasing awareness about the effects of the interaction between foundation and superstructure. However, while it is widely accepted that the role of foundation on the overall seismic capacity of structures (see e.g. Martin and Lam 2000) cannot be neglected, on the other side a lack of reliable methods for the seismic analysis of foundations is still apparent.

For this purpose, non-linear dynamic finite element (FE) simulations of large numerical models, including the superstructure, the foundation and the surrounding soil, are likely not to be particularly suitable, because of their excessive computational costs when sophisticated soil constitutive laws are adopted. To overcome this shortcoming preserving a satisfactory description of the dynamic soil-structure interaction, the macro-element concept can be fruitfully employed (Nova *et al.*, 1991; Gottardi *et al.*, 1999; Cremer *et al.*, 2002; Randolph *et al.*, 2005). This basically consists in modelling the soil-foundation system as a unique non-linear macro-element with a limited number of degrees of freedom (DOF). However, although the macro-element approach seems to be very promising, it has not been supported so far by adequate experimental evidences, at least for seismic applications. Indeed, few experimental results are available on the non-linear soil-foundation dynamic interaction (Maugeri *et al.,* 2000; Negro *et al.,* 2000; Faccioli *et al.,* 2001; Gajan *et al.,* 2005).

2. MACRO-ELEMENT APPROACH

If the assumption of a perfectly rigid footing is introduced, this allows a significant reduction in the DOF number. For instance, under plane strain conditions, the mechanical interaction can be described in terms of three *generalised stresses* (the vertical load V, the horizontal load H and the overturning moment M), components of vector **Q**, and three *generalised strains* (the vertical displacement v, the horizontal displacement u and the rotation θ), components of vector **q**. Each load component is associated with a specific displacement component, and these must be chosen so that the forces and displacements are work conjugate (Figure 1).
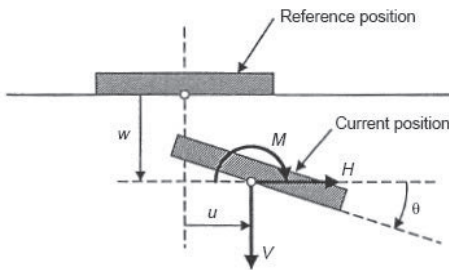

Figure 1. Load and displacement components (from Butterfield *et al.*, 1997)

Under seismic conditions, particularly crucial is to consider the response of the footing both to eccentric and inclined loads, associated with the inertial horizontal forces in the superstructure and, for this reason, some hints inferred from quasi-static experimental results are here below briefly summarised:

– under monotonic loading, the response of the footing is non-linear from the very beginning;
– the coupling between the different generalised stress/strain variables is evident from very low generalised stress levels and gets dominant at failure. For example, when a monotonic horizontal load is applied, vertical displacements develop even for constant vertical load and nil overturning moment;
– bearing capacity is severely affected both by the inclination and the eccentricity of the loads imposed; the so-call *interaction domain* describes this dependence. The in-teraction domain is a function of the nature of the foundation soil (the relative density severely influences its size and shape), as well as of the roughness, shape and embedment of the footing itself;
– the geometry of failure mechanisms severely depends on the combination of generalised stresses: each point of the interaction domain corresponds with a unique failure mechanism;
– the experimental results for strip footings can be easily interpolated in a three dimensional space by employing expressions, quite common in literature (Nova et al., 1991; Gottardi et al., 1999). A possible geometrical representation is reported in Figure 2;
– when overturning moments are applied (or better, under generalised strain controlled conditions, tilting angles are imposed), local measures testify a process of progressive concentration of the vertical stresses under the footing;
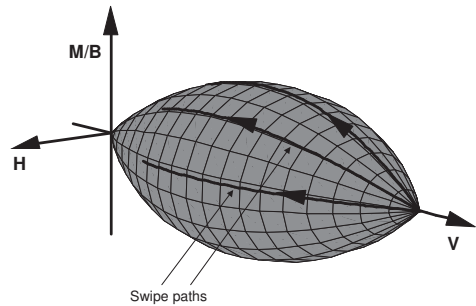
Figure 2. Three-dimensional interaction domain (from Gottardi *et al.*, 1999).

– as is well known, standard general shear failures develop for stiff soils, while, as the soil stiffness reduces (loose sand strata), a punching mechanism is more likely to take place and the corresponding bearing capacity becomes hard to be evaluated. Indeed, owing to second-order effects (the foundation sinking requires large displacements to be accounted for), the corresponding generalised stress-strain curve is characterised by a limitless increase in stress (i.e. no peaks and/or plateaus). A plateau can be envisaged solely if the foundation level is artificially main-

tained coincident with the ground level, as it can be done in the laboratory;

– under cyclic loading, the system dissipates energy and, in general, accumulates irreversible generalised strains (di Prisco *et al.*, 2003).

Once the generalised stresses and strains are defined, the simplest way to describe the previous experimental evidences consists in setting up an homogenized constitutive relationship of elasto-perfectly plastic type. This requires the definition of a suitable failure locus and a plastic potential. Within the failure/yield locus the mechanical behaviour is assumed to be elastic and uncoupled, while coupling exclusively characterises the ultimate conditions.

A more sophisticated modelling approach consists in conceiving strain-hardening elasto-plastic macro-element models. The failure locus is, therefore, the special yield locus for which the hardening variable coincides with the maximum possible load (Nova *et al.,* 1991).

This simple approach allows to satisfactorily reproduce the mechanical response of shallow footings under any monotonic loading path, this statement being supported by the comparisons with both FE analyses and experimental test results.

As undrained tests can be employed to infer the yield locus shape of soils, in a similar fashion the so-called *swipe-tests* have been conceived for shallow foundations (Gottardi *et al.,* 1999; Butterfield *et al.,* 2003). These consist in applying to rigid shallow footings, horizontal/rotational displacements by inhibiting the vertical displacement at rotational/horizontal constant loads (see the corresponding load-path in Figure 2).

3. APPLICATION TO HISTORICAL BUILDINGS: TALL STRUCTURES

As is well known, tall historical buildings very often suffers stability problems against tilting, these being obviously amplified in the presence of significant horizontal loads (seismic, aeolian, etc.) and compliant foundation soils. From this viewpoint, an interesting example is represented by the leaning Ghirlandina tower in Modena (northern Italy, Figure 3a), recently under restoration works.

This example aims at stressing the relevance of soil-structure interaction in seismic analyses, even when standard pseudo-static approaches are adopted. From the rotational equilibrium of the tower under the action of the self-weight F_V and of the horizontal seismic force F_H (Figure 3b), it results that:

$$F_H h + F_V h \sin \theta = k_{\theta\theta}(\theta)\theta \qquad (1)$$

where θ is the rotation angle and $k_{\theta\theta}$ the rotational stiffness of the soil-foundation system. In Eq. [1] the dynamic nature of the interaction problem is neglected, however two essential aspects are accounted for: (i) the influence of the vertical weight F_V as a second-order effect due to large displacements; (ii) the non-linear dependence of $k_{\theta\theta}$ on the unknown rotation θ.

Apparently, the definition of a realistic $k_{\theta\theta}$ - θ relationship is crucial. The use of a macro-element model seems to be very appropriate to this purpose, since the required stiffness $k_{\theta\theta}$ can be extracted from the full elasto-plastic stiffness matrix.
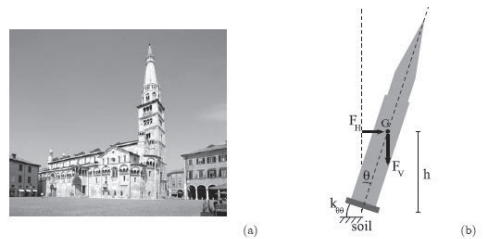
Figure 3. (a) The cathedral and the Ghirlandina bell tower in Modena (Italy), (b)scheme of the pseudo-static seismic analysis (from di Prisco and Pisanò, 2011)

The macro-model can therefore predict not only the moment (generated by tilting) at which a tower will collapse but also provide the rotational stiffness of the soil-foundation system that is the key input to any stability of equilibrium analysis. In a more general case an equilibrium analysis of a tower is best presented in the M-θ plane, in which M_e (external, i.e. overturning, moment) and M_r (resisting moment, i.e. the reaction of the restraint) can be plotted together, as first suggested by Cheney *et al.* (1991). In particular, M_e is a line with slope (Wh), and M_r a curve (Figure 4a) related to the stiffness of the foundation. If the initial slope k

of the M_r curve is equal to or lower than the slope (*Wh*) of the external moment load path M_e, the M_e and M_r paths will never intersect and equilibrium is never possible. On the contrary, if $k > Wh$ (Figure 4c), then, for a given small θ_0, equilibrium can occur at two points on the M_r curve (Figure 4a), that depend on the loading history.

The maximum value of M_e that can be resisted occurs when the M_e line is tangent to the M_r curve; the coordinates of the tangent point then define the critical condition for instability of equilibrium (point E, Figure 4b).

Any situation in which M_e does not intersect M_r is a temporary non-equilibrated state. Figure 4a depicts a tower at a specific, static instant, whereas, in reality, additional creep rotation will usually develop due to viscous behavior of the soil. Such progressive tilting has been incorporated in the above model by treating it analogously to the initial rotation (Cheney *et al.*, 1991; Lancellotta, 1993; Desideri and Viggiani, 1994). In which case any initial rotation (say θ'_0, Figure 4d) will include not only the initial imperfection of the system θ_0, but also any additional rotation due to creep θ_{0creep}.
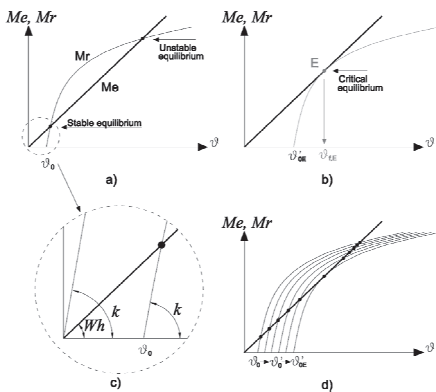

Figure 4. Stability of equilibrium analysis in $M\text{-}\theta$ plane: (a) stable and unstable equilibrium conditions; (b) critical equilibrium condition; (c) detail of relation between external moment slope, *Wh*, and initial rotational stiffness of foundation, *k*; (d) assumed translation of $M–\theta$ curve due to creep (from Marchi *et al.*, 2011).

A crucial step in the analysis is therefore to establish a reliable M_r curve for the tower foundation, as already mentioned, usually not a straightforward task. Strain-hardening plasticity models - developed in relation to the overall soil-footing system - can provide such a relationship directly, starting from the more readily available vertical load-penetration curve. A further advantage and development of such modelling approach is that creep phenomena (time-dependent response) can be equally included into the formulation.

An interesting preliminary application to the well-known case of the leaning Tower of Pisa is reported in Marchi *et al.* (2011).

4. REFERENCES

Butterfield R., Gottardi G., Houlsby G.T., 1997. Standardised sign conventions and notation for generally loaded foundations. *Géotechnique*, vol. n. 47(4), pp. 1051- 1052.

Butterfield R., Gottardi G., 2003. Determination of yield curves for shallow foundations by swipe testing, In *Fondations superficielles*, Magnan and Droniuc (Eds.), Paris, Presses de l'ENPC/LCPC.

Cheney, J., Abghari, A., Kutter, B. L., 1991. Stability of leaning towers. *J. of Geotechnical and Geoenvironmental Eng. (ASCE)* 117, No. 2, pp. 297–318.

Cremer C., Pecker A., Davenne L., 2002. Modelling of nonlinear dynamic behaviour of a shallow strip foundation with macro-element, *International Journal for Numerical and Analytical Methods in Geomechanics*, vol. 25, pp. 1257–1284.

Desideri, A., Viggiani, C., 1994. Some remarks on the stability of towers. *Symp. On Development in Geotechnical Engineering, Bangkok*.

di Prisco C., Nova R., Sibilia A., 2003. Shallow footings under cyclic loading: experimental behaviour and constitutive modeling, In *Geotechnical analysis of seismic vulnerability of historical monuments*, Maugeri M. & Nova R. (Eds.), Patron, Bologna.

Faccioli E., Paolucci R., Vivero G., 2001. Investigation of seismic soil-footing interaction by large scale cyclic tests and analytical models", in *Proceedings 4th International Conference on Recent Advances in Geotechnical Earthquake Engineering and Soil Dynamics*, Special Presentation Lecture, San Diego (USA).

Gajan S., Kutter B., Phalen J., Hutchinson T.C., Martin G.R., 2005. Centrifuge modeling of load deformation behaviour of rocking shallow foun-

dations", *Soil Dynamics and Earthquake Engineering*, vol. 25, pp. 773–783.

Gottardi G., Houlsby G., Butterfield R., 1999. Plastic response of circular footings under general planar loading", *Géotechnique*, vol. 49, no. 4, pp. 453–469.

Lancellotta, R., 1993. Stability of a rigid column with non linear restraint. *Géotechnique* 43, No. 2, 331–332.

Marchi M., Butterfield R., Gottardi G., Lancellotta R., 2011. Stability and strength analysis of leaning towers. *Géotechnique*, Printed *online*. DOI: 10.1680/geot.9.P.054.

Martin G.R., Lam I.P., 2000. Earthquake resistant design of foundations – Retrofit of existing foundations, In *Proceedings GeoEng 2000 Conference*, Melbourne (Australia), pp. 19–24.

Maugeri M., Musumeci G., Novità D., Taylor C.A., 2000. Shaking table test of failure of a shallow foundation subjected to an eccentric load, *Soil Dynamics and Earthquake Engineering*, vol. 20, no. 5-8, pp. 435-444.

Negro P., Paolucci R., Pedretti E., Faccioli R., 2000. Large-scale soil-structure interaction experiments on sand under cyclic loading, In *Proceedings of 12th World Conference on Earthquake Engineering*, Auckland (Australia), paper 1191.

Nova R., Montrasio L., 1991. Settlement of shallow foundations on sand, *Géotechnique*, vol. 41, no. 2, pp. 243–256.

Randolph M.F., Cassidy M.J., Gourvenec S., Erbrich C., 2005. Challenges of offshore geotechnical engineering. *Proc. XVI Int. Conf. Soil Mech. Geotech. Eng., ICSMGE, Osaka, Giappone,* vol. n. 1, pp. 123-176.

Investigation of hard soils for soil-structure interaction analyses

V.M. Ulitsky
St. Petersburg State Transport University, Russia, *ulitsky.vladimir@gmail.com*

V.A. Vasenin, A.G. Shashkin, C.G. Shashkin
Georeconstruction Engineering Co, St. Petersburg, Russia, *mail@georec.spb.ru*

ABSTRACT: Due to increasing height of buildings and development of the underground space hard proterozoic deposits now are used quite often as subsoils of structures in Saint Petersburg. For high-rise buildings embedding pile ends into hard soils often is the only possible option of foundation design, since the depth of rocks in central Saint Petersburg is more than 200 m. One of the main tasks of pile foundation design subjected to big loads is estimation of settlements of such foundation. Meanwhile, deformation properties of hard soils are not studied well yet.

Research of these deposits was conducted by the authors on several sites in Saint Petersburg. It consisted of laboratory testing in triaxial cells, and in-situ tests. Results of investigations on one test site in the centre of Saint Petersburg are presented in the paper. Some results of soil-structure interaction modeling of a high-rise building are also presented.

1. GEOLOGICAL CONDITIONS OF THE SITE

The ground conditions of the site considered in the present paper are characterized by presence of quaternary deposits of variable origin and bedrock of Wendian strata of the Kotlin horizon. The quaternary strata within the boundaries of test areas for testing piles and barrettes extend down to 43 – 45 m. Following those from 45,0 m to 53,0 m stratification consists of bluish-grey laminated clays with thin inclusions of dislocated sandstone (max.1 mm in thickness). Bluish-grey laminated clays continue to follow from 53,0 m down to 127.5 m. Within the boundaries of test areas under consideration, SPT tests on subsoil were conducted – predominantly on quaternary deposits (up to the upper boundary of dislocated Wendian strata, i.e. going down to 40-43 m).

2. RESULTS OF LABORATORY TESTS OF HARD CLAYS

The design for the high-rise building envisages toe levels of deep supports (barrettes) to be located in stiff Wendian clays. Significant attention during laboratory testing was given to strength and strain (deformation) properties of the Wendian clays. The tests were conducted by a professional testing facility according to three testing schemes to comply with requirements expressed in Russian and British Standards. The analysed the test results statistically. Fig. 1 shows strength dependency of hard Wendian clays on depth. Within the interval from 40 to 150 m, shear strength of samples tends to increase. There was, however, no significant difference between the executed testing schemes. Apparently, the difference in strength for hard clays consists only in degree of microcracks closing (the cracks formed in the process of coring and reconstituting samples) during loading at hydrostatic pressure stage, as well as in strain rate at the stage of action along compression paths.

Fig. 2 shows the corresponding change with depth of vertical relative strain value at failure, which reaches about 15% in the area of glacial dislocations at the level of 45 m and reduces with depth to 2-3%.

Fig. 3 shows a dependency of change in water content of Wendian clays samples tested according to various schemes. water content of the tested samples decreases with depth. At depths of around 50 m average water content

65

amounts to approximately 15%, whereas at depths of approximately 150 m average water content reaches roughly 11,5%. Based on triaxial tests results, dependency of strength on natural water content of samples becomes distinctly visible (Fig. 4) for all hard clay strata. The division into various testing schemes (i.e. consolidated-drained, consolidated-undrained, and unconsolidated-undrained schemes) fails to distinguish any other regularity. This may be explained by practical absence of free water in hard clay voids. All pore water in such clays is bound, and it is because of that that the process of the so called "consolidation" in such soil is practically absent and is reduced in all test types to micro-cracks closing.
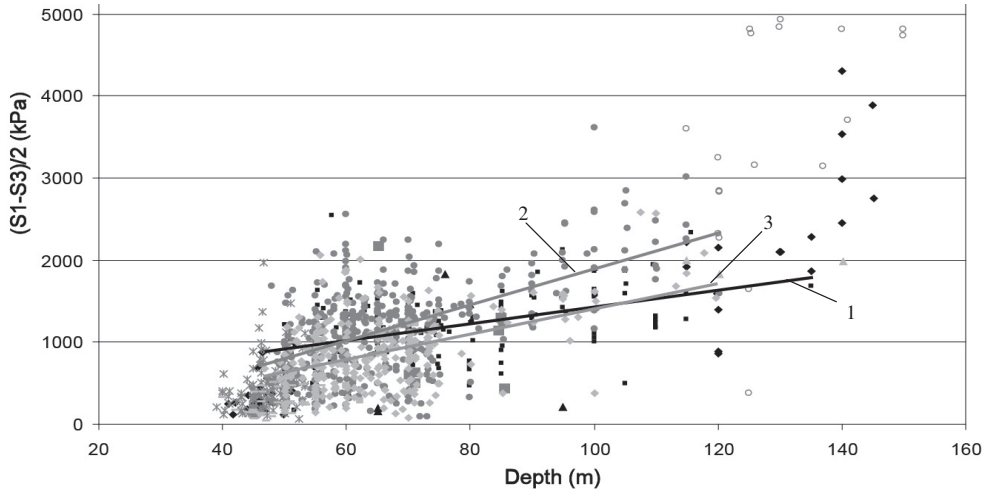
Figure 1. Change of shear strength (kPa) of Wendian clays with depth. According to various test schemes (dots represent soil samples): 1 – Unconsolidated-undrained (UU), 2 – Consolidated-undrained (CU), 3 – Consolidated-drained (CD) tests.

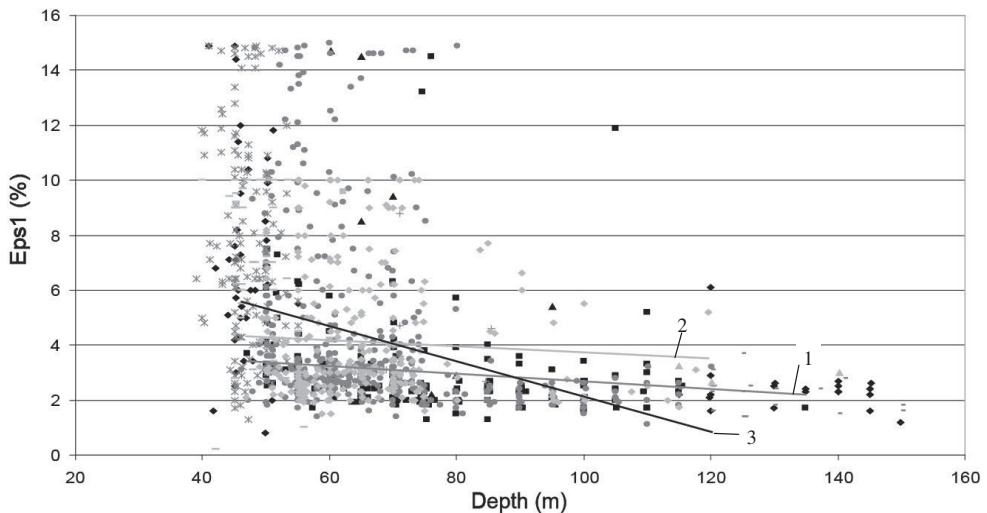Figure 2. Change of vertical relative strain of Wendian clay samples (kPa) at failure with depth. According to various test schemes (dots represent soil samples): 1 – Unconsolidated-undrained (UU), 2 – Consolidated-undrained (CU), 3 – Consolidated-drained (CD) tests.
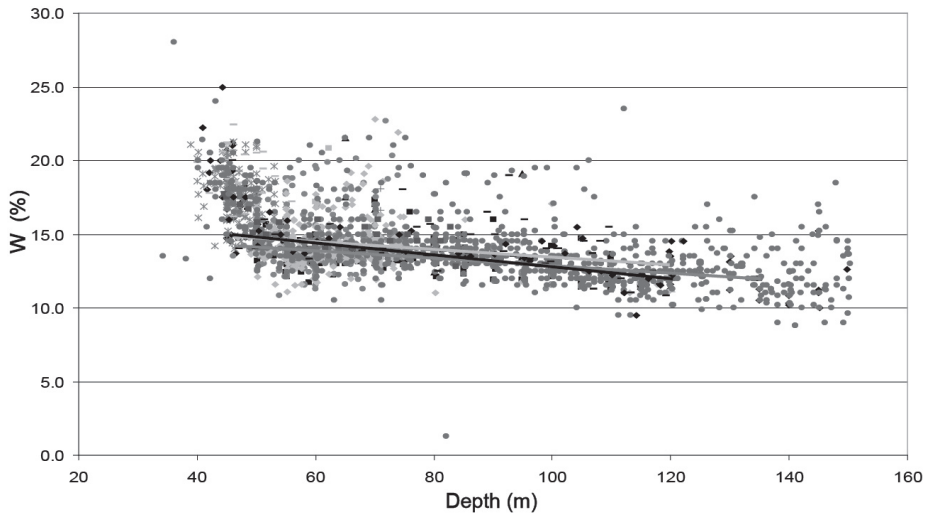
Figure 3. Change of degree of saturation of Wendian clay samples with depth. Variously shaped points corres-
pond to various soil elements and boreholes.
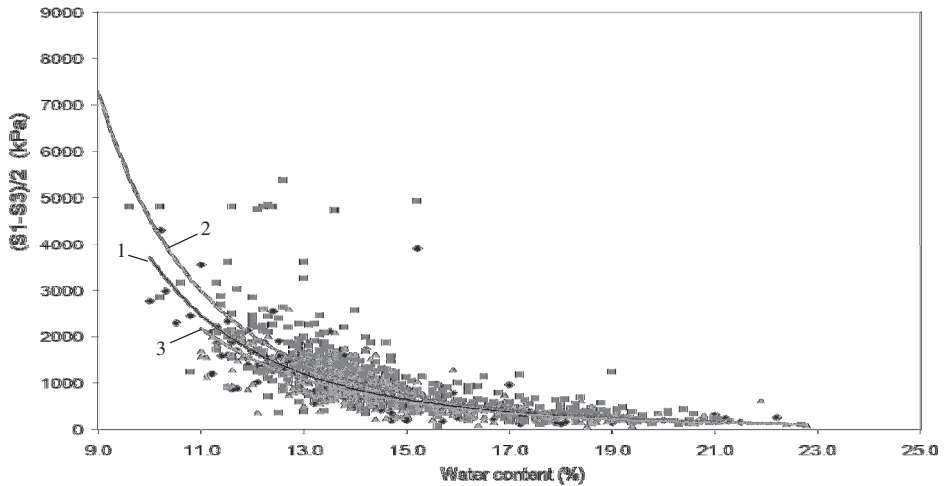
Figure 4. Dependency of strength on saturation in triaxial tests according to various test procedures:
1 – Unconsolidated-undrained (UU). $y = 7E+07x^{-4.3017}$, $R^2 = 0.7152$;   2 – Consolidated-undrained (CU),
$y = 1E+08x^{-4.431}$, $R^2 = 0.7225$;   3 – Consolidated-drained (CD) tests, $y = 5E+07x^{-4.2041}$, $R^2 = 0.6611$.

Fig. 5 shows comparison of dependencies of reached axial strain of samples on water content based on triaxial tests at various schemes of hard clay behaviour. There was no significant difference in strength or deformability of hard clay samples in various testing schemes. Thereat, however, a considerable scatter of both strength, and deformability is observed, which is related, first and foremost, to the scatter of natural physical soil properties.

Absence of significant differences during hard clay tests according to different schemes presumably means that the volumetric strain component is immaterial. Thus, the behaviour of hard clay samples can be described based on various conditions (of both drained and un-drained testing modes).

67

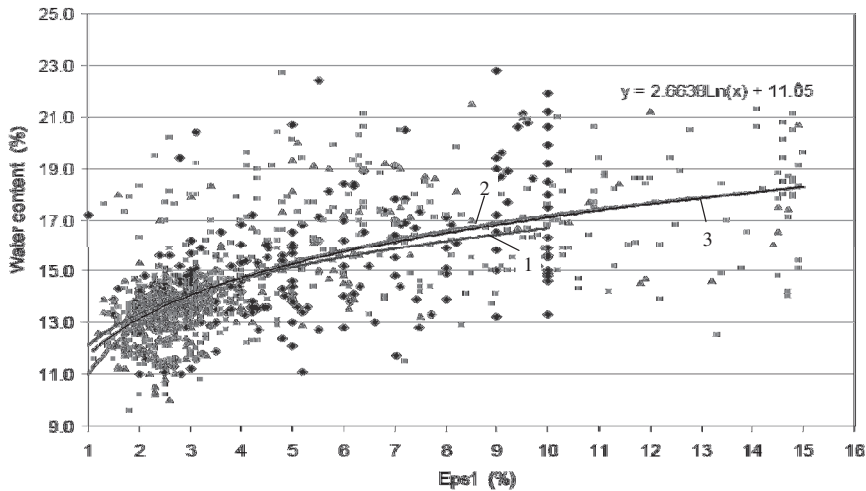Figure 5. Dependency of max. vertical strain on degree of sample saturation in Wendian clays according to various testing procedures: 1 – Unconsolidated-undrained (UU), 2 – Consolidated-undrained (CU), 3 – Consolidated-drained (CD) tests.

3. SOIL-STRUCTURE INTERACTION MODELLING OF A HIGH-RISE BUILDING

The designed high-rise building (having about 80 floors) is of core and frame type. Its overall stability is ensured by joint action of the central monolithic reinforced concrete core and steel columns along the building perimeter, the columns being joined into a single system by means of steel beam cells, along which inter-mediate floor discs are placed; additionally there are special outrigger beams in three levels of maintenance floors. In such a layout the main element responsible for assuming the vertical and horizontal components of the loads is the core. Square area of the central reinforced concrete core decreases with height together with the square area of individual floors, which likewise decreases as the building becomes higher.

As the purpose of our analyses was the con-sideration of interaction of the designed super-structure and the subsoil, the necessity arose to adequately represent the building superstruc-ture, wherewith to ensure the required calcula-tion accuracy (Ulitsky et al, 2005, Shashkin, 2006). Modelling the action of subsoil and barrettes implied obtaining accurate loads distribution onto barrettes, as well as an account of their interaction with the surrounding soil, which made it necessary to model the barrettes

with spatial finite elements. Pressure is trans-ferred onto barrettes through the foundation mat, and considering the thickness of the slab as being 3,6 m, for a reliable assessment of loads distribution onto barrettes, again, it was neces-sary to model the pilecap slab with spatial finite elements. The major portion of loads onto subsoil from the designed high-rise building is generated by concentrated loads from its core. In the underground part of the designed building the thickness of the external core wall is 2 m. Moreover, in places where the core width changes, the width of the core walls reaches 3,5 m.

In this case while constructing a 3-D scheme for the building to perform soil-structure inte-raction analysis it was decided to build up the finite element profile according to the following sequence: modelling behaviour of subsoil, barrettes, pilecap slab and external core walls with spatial finite elements; modelling the internal core walls and intermediate floors with plate finite elements; modelling the columns and beam cells with spatial rod elements.

General outlook for the superstructure calcu-lation profile is presented in Fig. 6 (a).

Soil-structure interaction analysis of the de-signed high-rise building and its subsoil was performed according to several scenarios of subsoil behaviour:

68

1. Calculating structures of the building on elastic subsoil, as per requirements contained in currently applicable codes and in agreement with assumptions adopted on limiting depth of compressible stratum in the subsoil of the designed building.
2. Calculations with account of subsoil behaviour based on non-linear models, which permit automatic limitation of the depth of compressible stratum.

A considerably important issue in assessing settlements of the high-rise building under consideration will be the proportion of subsoil deformation brought about by volumetric and shear strains of hard clays. With this consideration in mind, two conflicting hypotheses in respect of volumetric compressibility of hard clays were used in our analyses:

1. there is no volumetric compressibility at all;
2. volumetric compressibility corresponds to the obtained compression curves within the interval of stresses from natural pressures to acting stresses in subsoil.

The first hypothesis corresponds to an assumption of there being no considerable voids filled with air or free pore water in natural soil. The assumption of overconsolidated state of hard clays can lead to a similar conclusion as well. At overconsolidation ratio OCR=2 or more, additional loading with the building's own weight will not exceed preconsolidation pressure, and, correspondingly, volumetric compressibility will be at its minimum and will be defined by the unloading-reloading modulus.

In respect of strength parameters (as well as of shear deformability) three various hypotheses were put forward:

1. strength depends, largely, on physical properties (natural degree of saturation) of samples and only weakly depends on total pressure; threat strength is defined directly based on triaxial tests (same as in undrained conditions);
2. strength depends on total confining pressure (i.e. increases with depth), in calculations an account is made of angle of internal friction, effective stresses in soil skeleton (considering also the water column in total absence of a confining layer);
3. strength depends on total confining pressure (i.e. increases with depth), in calculations an account is made of angle of internal friction,

stresses in soil skeleton equal total stresses (not accounting for water).

The first assumption, as far as its physical sense is concerned, corresponds to the hypothesis of there being no considerable volumetric compressibility of soil. Indeed, there being a dependency of clay strength on pressure is connected not so much with friction as such, as with soil compaction under load. An increase in density leads to a corresponding increase in quantity and quality of contacts between clay particles and, correspondingly, to an increase in strength. If there is no considerable volumetric compressibility, growth of strength at increasing loads is also hardly probable. In this case strength properties will be defined by natural density of soil, formed at this or that depth by acting natural stresses.

Prior to calculating superstructure of a building on non-linear foundation-subsoil we selected parameters of soil models, with which intention we modelled triaxial tests of soil samples.

Results of calculations performed according to various schemes of subsoil behaviour are contained the following table:

Table 1. Settlement and relative settlement differentials for various foundation options.

Subsoil behaviour scheme	Option with barrette toe level at 105 m from ground surface/ Settlement		
	max., cm	Min., cm	relative differential
Elastic calculation through layer-by-layer summation method (compressible stratum equals ½ of subsoil width)	12,5	9	0,001
1 Unconsolidated-undrained (Cu-lowered)	6,5	5	0.0006
2 Consolidated-drained with account of effective stress	11	9,6	0.00055
3 Consolidated-drained effective stress equals total	6,5	5	0.0006

As can be seen from Table 1, various models of non-linear foundation-subsoil produce provisionally close values of settlement from 7 to 11 cm. Contours of vertical movements in subsoil and superstructure of the designed building, with account of non-linear character of

its subsoil behaviour according to consolidated-drained scheme, are contained in Fig.6 (b) and Fig.7. Differences in settlement values calculated based on possible schemes of subsoil behaviour are conditioned largely by accounting for or disregarding the volumetric component of strain. Here it is necessary to point out that the settlement input contributed by the volumetric portion of strain in hard clays will take a rather long time to develop. As this component of deformations will be entirely defined by consolidation process in hard clays, then, bearing in mind low values of permeability coefficient (approximately 10-6 m/day) and long permeability paths, this settlement component will take a long time to develop, which makes it of secondary importance for consideration over the building lifetime.

The most important for design is distribution of loads unto barrettes and stresses in the superstructure. Based on performed calculations, values of loads in future building structures were chosen as the least favourable for the considered schemes of subsoil behaviour.

One of the important moments in foundation design for high-rise buildings is the criterion of permissible values of absolute subsoil settlement. In this case the ultimate value criterion for foundation settlement was limited to the value of 10 cm. To observe this criterion of ultimate settlement, the barrette toe level in subsoil of the high-rise building must be approximately 100-105 m. If the criterion of ultimate settlement development of the high-rise building is lowered, the length of barrettes can be considerably reduced.

Another not less significant issue defining reliability of foundation-subsoil design is the guarantee of adequate bearing capacity of the barrettes. This issue for the site in question was studied separately and the results of this study are published in a separate paper.

Thus, analyses of various models of subsoil-foundation behaviour provided the possibility to evaluate the possible range of absolute settlements of the high-rise building, as well as the range of relative settlement differential of its individual structures. This in turn allowed definition of loads distribution range onto barrettes and the corresponding loads in the structures of the high-rise building.

(a)

(b)

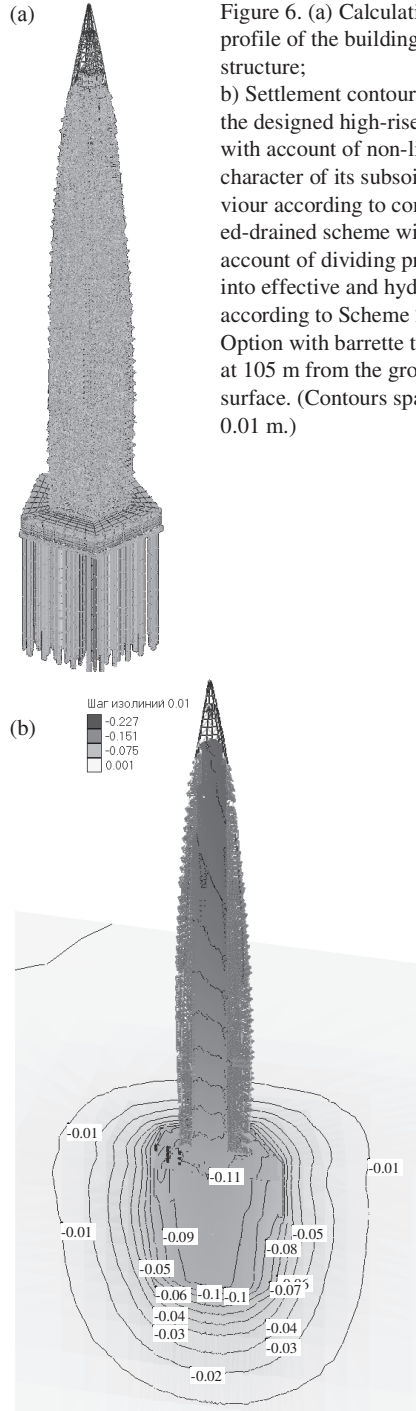Figure 6. (a) Calculation profile of the building super-structure;
b) Settlement contours (m) of the designed high-rise building with account of non-linear character of its subsoil behaviour according to consolidated-drained scheme with account of dividing pressure into effective and hydrostatic – according to Scheme 2 – Option with barrette toe level at 105 m from the ground surface. (Contours spaced at 0.01 m.)

4. CONCLUSIVE REMARKS

Test results of hard Wendian clays and soil-structure interaction analysis of a high-rise building are presented in the paper.

The soils have been tested with different various testing schemes – consolidated-drained, consolidated-undrained, and unconsolidated-undrained. Graphs of dependency of strength on samples natural water content. Absence of significant differences during hard clay tests according to different schemes presumably means that the volumetric strain component could be very small. Thus, the behaviour of hard clay samples can be described based on various conditions (of both drained and un-drained testing modes).

Soil-structure interaction analysis of the designed high-rise building and its subsoil was performed according to several scenarios of subsoil behaviour: with elastic subsoil, with assumptions adopted on limiting depth of compressible stratum in the subsoil of the designed building: and with account of subsoil behaviour based on non-linear models, which permit automatic limitation of the depth of compressible stratum. The computations have made it possible to estimate the settlements of the building with the various foundation options.

REFERENCES

[1] Ulitsky V.M. 2005. The basics of soil-structure interaction. *Proceedings of the International Conference "Soil-structure Interaction: Calculation methods and Engineering Practice"*. St. Petersburg, Vol.1, pp. 3–10.
[2] Shashkin, C. 2006. Basic regularities of soil-structure interaction. *Proceedings of the XIII Danube European Conference on Geotechnical Engineering.* Ljubljana. Vol. 1, pp 179–190.
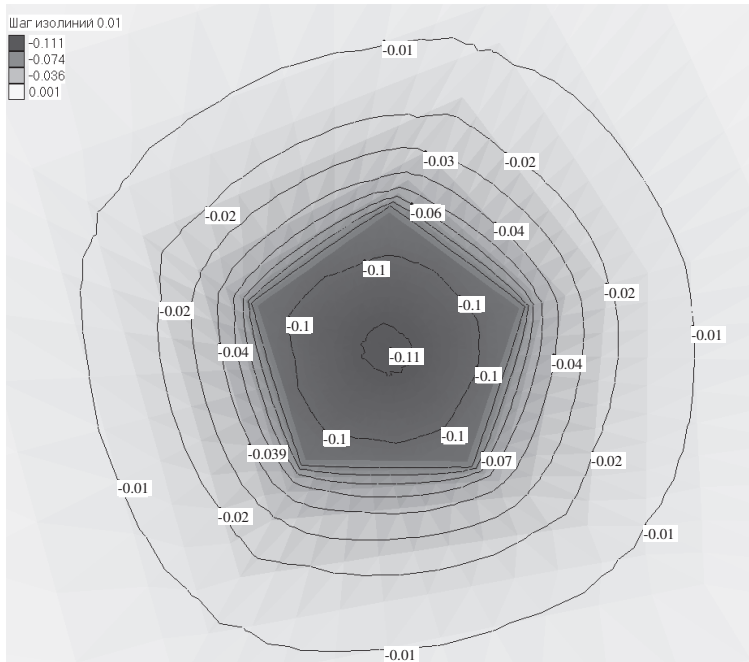
Figure 7. Contours of barrette settlement (m) when calculating building on non-linear subsoil according to consolidated-drained scheme with account of dividing pressure into effective and hydrostatic according to Scheme 2 – Option with barrette toe level at 105 m from the ground surface. (contours spaced at 0.01 m).

Using "Prepack" piles as settlement reduction elements

I. Sorić, A. Hršak,
Geotehnički studio d.o.o., N. Pavića 11, 10090 Zagreb, Croatia
igor.soric@geotehnicki-studio.hr; *ana.hrsak@geotehnicki-studio.hr*

I. Sokolić
University of Zagreb, Faculty of Civil Engineering Zagreb, CROATIA, *isokolic@grad.hr*

ABSTRACT: The paper describes the case history of foundation design for Shopping Center in Zagreb. The soil profile at the site includes weak layers of clay and silt to the depth of ~6.4 m and it is very heterogeneous over the construction area. The settlements of the structure founded on footings were limited up to 2 cm. As the preliminary analyses are showing the average settlement of footing from 17 to 20 cm, *"Prepack"* piles are used to reduce the settlements. Totally 400 piles are distributed under the footings leaving the free contact in between (the pile does not enter the footing). Several methods are used to predict the pile settlement, considering a pile as the rigid body, and as the soil improvement element. Pile tests performed, together with the structure settlement monitoring, are showing good agreement between calculated and measured results.

1. INTRODUCTION

The preliminary design analysis of foundation showed that the footing stability satisfy the design criteria while the settlements are much greater than 2 cm. In the early stage of the design it was obvious that a deep foundation or soil improvement method should be applied.

After several preliminary analysis of different technologies that could be applied, the Client decided to use *"Prepack"* piles as settlement reduction elements. The technology can be used in the soil that allows for stable borehole during the pile installation. After the drilling of the borehole, the grouting tube is placed down to the bottom and the borehole is filled with the gravel. The whole length of the pile is grouted. To improve the performance of the pile it is possible to do additional post grouting.

The area of the construction site is around 100 x 100 m, with an average span of the structure around 8.0 m. Totally 400 "Prepack" piles are distributed under the footings. The layout of the pile disposition is showed on Figure 1 (Hršak, 2010). On several positions of the foundation the higher loads were applied. On those places, the more economic solution was to use post grouted piles rather than more number of piles without post grouting treatment.
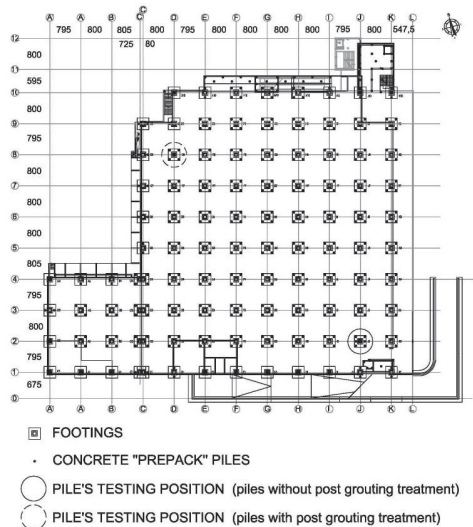

Figure 1. Layout disposition showing raft foundation positions, concrete piles, PG concrete piles and pile testing positions (Hršak, 2010)
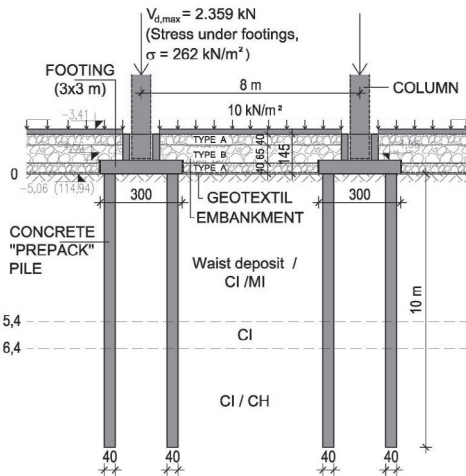
Figure 2. Typical cross-section of foundation

The cross section of foundation is shown on Figure 2. The "Prepack" piles of 40 cm in diameter are installed to the depth of 10 m, and are embedded 4 to 6 m into the bearing stratum. The footings are placed on top of the piles leaving the free contact in between (the pile does not enter the footing). The whole area is covered with 1.5 m tick embankment that transfers the load from the foundation slab and the live load at the top.

2. SOIL PROFILE

The geotechnical investigation was performed in two stages. In the first one, 10 investigation boreholes of various depths (10 – 15 m) have been performed across the construction area (Bradvica, 2007). The result showed significant difference in soil layer distribution and thickness, especially for the first layer of waist deposits. The second investigation stage includes two additional boreholes at the positions of the foundation where higher loads are applied (Goluža, 2010). At the same positions the pile tests were performed afterwards, which enable the quality back analysis of the designed and measured soil parameters.

The soil profile is formed of three dominant layers. The first layer, to the depth of ~5.4 m, consists of intermediate clay and silt with soft to liquid consistency. In the upper part of the layer the soil is mixed with waste deposits of brick, stone and metal fragments. The depth of the

deposit varies between 1.0 and 2.0 m. The second layer is ~1.0 thick and consists of intermediate clay of middle consistency, with the scuds of silt and sand. The third layer, that is considered to be the bearing stratum, consists of hard, high plasticity clay. Underground water level during the investigation works was found 0.5 m below the ground surface. Typical soil profile is shown on Figure 3. and the soil parameters used for calculation in Table 1.
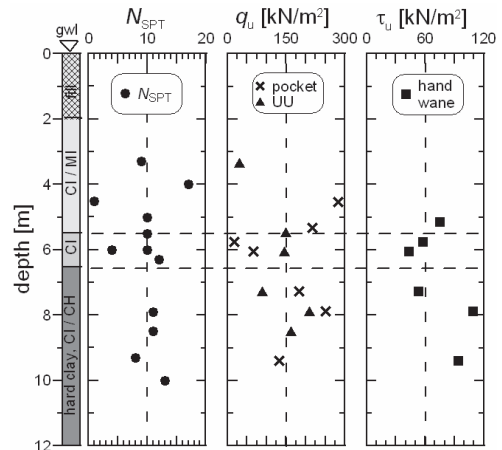

Figure 3. Soil profile

Table 1. Characteristic soil parameters

Soil	base	γ	c	φ	Mv	c_u
	[m]	[kN/m³]	[kPa]	[°]	[MPa]	[kPa]
CI/ML	5.4	18.5	7	18	3.5	5
CI	6.4	20	20	25	8	95
CI//CH	>10	20	24	26	10	130

3. SETTLEMENT ANALYSIS

The first step in the settlement analysis is to validate the boundaries of expected and allowable settlements. The limit settlement allowable is calculated according to the type of the structure. The structure column distance is 8,0 m, leading to maximal acceptable differential settlement (for buildings where cracking is not permissible) of 1,60 cm (l/500 criteria). Consequently, the maximal tolerable total settlement of foundation should remain within the range of 2,0 cm.

Settlement analyses of the footing were performed with the standard Boussinesque method

using the soil parameters given in Table 1. The results showed totally 17 cm of settlement that is well above the allowable 2 cm. However, stability analyses of the footings are showing sufficient bearing capacity of the original soil. Therefore, in order to satisfy the serviceability limit state the "Prepack" piles are used to reduce settlements.

The final settlement of the piles is calculated using three different methods. The first method, developed by Poulos and Davis (1980) calculates the settlement of the pile in a deep layer of uniform elastic material according to following equation (Canadian Committee on Foundation, 1992):

$$S = \frac{Q}{E_s d} I_0 R_k R_\nu \tag{1}$$

where Q is axial load, E_s soil modulus, d pile diameter, I_0 settlement influence factor, R_k compressibility correction factor, R_ν Poisson's ratio correction factor.

The second method, developed by Vesić (1970, 1977) includes empirical equation (Canadian Committee on Foundation, 1992):

$$S = \frac{d}{100} + \frac{QL}{AE} \tag{2}$$

where d is pile diameter, Q axial load, L total length of pile, E modulus of the elasticity of the pile material and A average cross-section of the pile.

The third method, developed by Brinch Hansen (1970), and updated by Meyerhof (1951), Vesić (1973) and Spangler & Handy (1982) is based on Boussinesque approach for calculating the stress distribution below the pile base, that is used to calculate the relative displacement and the final settlement of the pile base. Total settlement of the pile cap is the sum of a pile base settlement, corrected for the depth, plus shortening of the pile (Bowles, 1984). The results of the calculation predict the final settlement of the piles in the range from 6 to 10 mm for the piles without post grouting, and 7 to 14 mm for piles with post grouting.

Table 2. Settlement of the pile [mm]

PILE TYPE	Method used			Pile test
	1.	**2.**	**3.**	test
N. P. G.	10 mm	6 mm	9 mm	6 mm
W. P.G.	14 mm	7 mm	12 mm	4 mm

4. PILE TESTS

Quality control was conducted with two pile tests at the maximally loaded positions. Each test procedure consists of two side tension piles transferring the load to centrally positioned pile (Figure 4). Moreover, one of compression piles has been performed with additional post grouting procedure and another without post grouting ("Prepack" pile technology).

The results of the tests are shown on the Figure 5, and the final settlement, for corresponding working load, in Table 2. Considering the fact that the settlement of the piles for the working is within 0.55 cm (for piles without post grouting) and 0.4 cm (for piles with post grouting) it can be expected that the total settlement of the structure will be less than 2 cm.
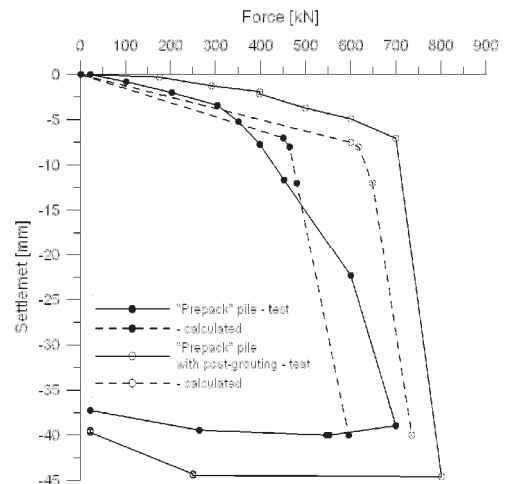

Figure 4. Test pile's construction

Figure 5. Test pile results compared with the calculated load – settlement curves
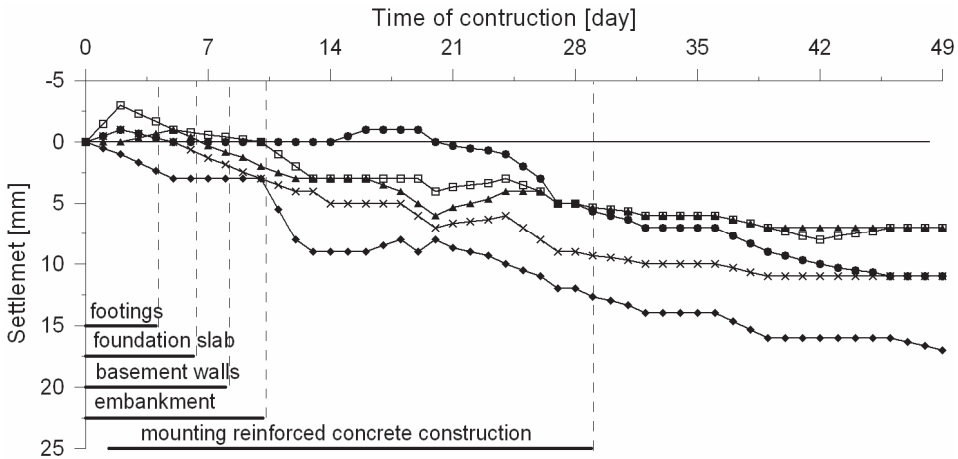
Figure 6. Settlement measurements

The effect of post grouting procedure has been recognized as capable to transfer higher forces. Therefore, this technology option was planned as alternative design option for the positions where column loads are higher. At the pile testing spots additionally performed investigation boreholes describe the particular geotechnical surrounding that enables good back analysis of the soil parameters used for design.

The results of measurements are compared to the calculated load-displacement curves (Figure 5). The calculation is performed according to the DIN standard for piles in cohesive soil. Parameters used are correlated to the undrained strength of the soil c_u. To account for effect of post grouting, the diameter of the pile is modelled larger, according to the additionally amount of grout used. It can be seen that the calculation method used predict well the load – settlement curve both for load capacity for the pile deformation. Also is seams the method to predict the performance of the post grouted pile, by increasing the pile diameter, is quite applicable.

5. SETLLEMENT MEASUREMENTS

Within the quality control procedure, the survey positions (6 survey points located on the footings and 9 survey points located between the footings, below the embankment) has been defined. Total settlements that have been measured are within the expected range, and are showing the chosen design solution as an adequate one (Figure 6). Also, the survey net enables Designer to have prompt deformations control during the embankment placing, and construction performance as well.

6. PILE DESIGN

The particular case is treated as a shallow foundation on footing laying on improved soil. The Designer should strictly follow foundation type calculation for typical shallow foundation. The procedure consists of bearing resistance and serviceability calculations.

Once it has been decided that the concrete piles shall be used as soil improvement solution, one could calculate stiff pile elements as belonging to the soil itself, but also the piles as a particular geotechnical structure element. In accordance with the existing EN1997-1 Design Approach 1 - Combination 2, both calculation approaches have been applied. In addition, the calculation has been carried out due to pile design bearing resistance relevant to the pile testing results. The results of bearing capacity analysis are shown in Table 3. to 5. where:

N.P.G. – piles without post grouting
W.P.G. – piles with post grouting
R_{sk} – characteristic shaft resistance
R_{sd} – design shaft resistance
R_{bk} – characteristic base resistance
R_{bd} – design base resistance
γ_{cu} – partial safety factor for c_u

76

γ_s – partial safety factor for shaft resistance
γ_b – partial safety factor for base resistance
γ_t – partial safety factor for test piles
n – number of pile tests
ξ – safety factor for number of piles tested

Table 3. Bearing resistance design of piles as soil improvement elements

type	R_{sk}	γ_{cu}	R_{sd}	R_{bk}	γ_b	R_{bd}	R_{cd}
N.P.G.	420	**1.4**	300	143	**1.4**	102	**402**
W.P.G	566	**1.4**	404	271	**1.4**	194	**598**

Table 4. Bearing resistance design of piles as geotechnical structure elements

type	R_{sk}	γ_s	R_{sd}	R_{bk}	γ_b	R_{bd}	R_{cd}
N.P.G.	420	**1.3**	323	143	**1.6**	89	**412**
W.P.G	566	**1.3**	435	271	**1.6**	169	**604**

Table 5. Bearing resistance design of piles considering pile test results

type	R_{sk}	n	$\xi / 1.1$	γ_t	R_{cd}
N.P.G.	700	1	**1.4 / 1.1**	**1.5**	**367**
W.P.G	800	1	**1.4 / 1.1**	**1.5**	**420**

7. CONCLUSION

After having passed the entire procedure i.e. Investigation – Design - Pile testing – Monitoring, one can conclude the following:

- The effect of piling as a soil stiffening and its substantial reduction of settlements results in significant soil improvement;
- Monitoring results are close to predicted deformations of improved soil and structure as well;
- Presented Design approaches may open the need for defining stricter procedures aimed to solve such particular foundation cases.

8. REFERENCES

Hršak A. 2010. Trgovačko kulturni centar "Sesvete" – Glavni i izvedbeni project poboljšanja temeljnog tla. Geotehnički studio Zagreb T.D.3640-1/11.GS. (in Croatian).

Bradvica, I. 2007. Trgovački centar Konzum u Sesvetama, Zagreb – Geotehnički elaborat. *IGH Zagreb 29100136 (in Croatian)*

Goluža, D. 2010. Trgovački Centar Konzum, Sesvete Zagreb – Geomehanički elaborate. *Geotehnički studio Zagreb T.D.: 3607 – 4/10G.S. (in Croatiana).*

Canadian Committee on Foundations, 1992. Canadian Foundation Engineering Manual, third edition

J. E. Bowles, 1984. Foundation Analysis and Design, fourth edition, *McGraw-Hill international editions*

N. Janbu, 1967. Settlement Calculations Based on the Tangent Modulus Concept, *the Technical University of Norway, Trotenheim*

N. Janbu, 1967. Settlement Calculations Based on the Tangent Modulus Concept, *the Technical University of Norway, Trotenheim*

J. Feda, 1978. Stresses in Subsoil and Methods of Final Settlement Calculation, *Elsivier Scientific Publishing Company*

E. N. Fox, 1984. The Mean Elastic Settlement of a Uniformly Loaded Area at a Depth Below the Ground Surface, *Proceedings of the Second International Conference on Soil Mechanics and Foundation Engineering, Rotterdam*

Robert W. Day, Sowers, 1962. Geotehnical engineer's portable handbook

Lymon C., Reese, William M. Isenhower and Shin-Tower Wang *Shallow and Deep Foundations*

Soil-structure interaction modelling of underground pipelines behavior in tectonic fault areas of seasonally freezing soils of Sakhalin Island

S.A. Kudryavtsev
Far East State Transport University, Khabarovsk, Russia, kudr@festu.khv.ru

V.N. Paramonov
Georeconstruction Engineering Co, St. Petersburg, Russia, parvn@georec.spb.ru

ABSTRACT: The article contains results of soil-structure interaction modelling of underground pipelines behaviour in tectonic fault areas of seasonally freezing soils of Sakhalin Island. Some structural methods increasing frost resistance and reducing tectonic influence are also proposed.

INTRODUCTION

Throughout its entire route the pipeline of the Sakhalin II Project is laid in tectonic fault areas. Under the circumstances seasonal freezing-thawing of soils renders negative influence on the underground structures. Different configurations of trenches were compared taking into account freezing and thawing of soils, gravitation load consequences, inner pressure and temperature of oil being pumped. It was possible to establish that in order to reduce seismic loads upon the pipeline at places where faults cross it was more advantageous to make trenches with the use of polystyrene isolating slabs instead of soil backfill.

Tectonic areas account for a great deal in formation of Sakhalin Island structure: great faults in longitudinal and latitudinal directions. They were identified based on geological, geophysical and geomorphological investigations. The tectonic faults of Sakhalin Island are classified by activity (highly, normally and mildly active) and by the kinematical type (displacements, dislocations, upcasts, mixed kinematical type). Based on investigations of geological and geotechnical conditions, as well as changing of pipeline route in areas of seismic disturbance, the investigations having been carried out by D.G.Namon, D.G.Honeger and Dr. G.L.Koff, there were designed plans and profiles of pipeline route of the project Sakhalin II at the parts from Boatasino to the River Evay and Nysh-Lynskoe exurbia, where 24 places of crossing the most active tectonic faults were noticed.

1. DESIGN SOLUTION

In the places where pipelines cross active tectonic faults, depending on pipeline diameter, their installation is provided in trenches of typical or trapezoidal shape. Typical trench is one with depth of the surfacing less then a meter to the top of the pipeline across the entire fault area. The belled trench is a trench with flat slopes of trapezoid shape. Backfill is provided by sand, peat or other workable soil. Trench slopes are chosen in such a way that the angle between the line projected through the bottom of the pipe to the point of crossing the surface line and trench line of bevel was 45-φ/2, (approximately 28°, angle of internal fiction $\varphi = 35°$). This flat theoretically determines a wedge-shaped plane of failure under passive soil pressure.

According to the conducted research it was established that special trench configuration could cure maximum displacements ensuring pipeline resistance to extension and compression. Theoretical research of trenches of differ-

ent configurations was carried out, taking into account freezing of soil, gravitational loads, inner pressure and temperature of delivered products. As a result of analytical research it was established that to reduce influence of seismic loads and the climate at pipelines it was necessary to use trapezoid trench configuration with materials like French foamed plastic Supazote EM 26 or similar material with the same mechanical properties.

2. SOIL-STRUCTURE INTERACTION MODELLING

Quantitative valuation of influence of tectonic processes, freezing and thawing at the underground structure with the use of analytical methods is difficult. In order to solve that problem a numerical calculations software with the use of finite elements method was developed. This software allows to solve heat conductivity problems in soils, freeze and thawing, taking into account phase conversion and ground water migration for transient heat state in three-dimensional space.

The software allows to calculate stress-state state of foundations and their subsoil depending on different kind of outer and inner influences. The stress-strain state is determined according to calculated temperature.

Numerical calculations were performed for climatic and geological conditions of the most severe, northern part of the Sakhalin Island.

Geometrical and mechanical properties of underground pipelines in fault areas were assumed according to the data of the Sakhalin II project. As a main variant of damping and heat insulation material for saving the pipelines from tectonic influences at trench bottom a layer of foamed polyester Kompostirol , produced by KNAUF, was considered. At the sides of the pipeline and above it, blocks of French foamed superazote are installed. The space between side blocks of the foam plastic and the pipeline is filled with layer of thin sand. A layer of geotextile is placed onto the damp and heat insulating material. Then the trench is filled with stone or gravel sand. As an alternative to designed pipeline structure a numerical investigation of damp and heat insulation material produced by a Khabarovsk firm *Raduga-Service* was carried out.

This damp and heat insulation material is similar to designed one.

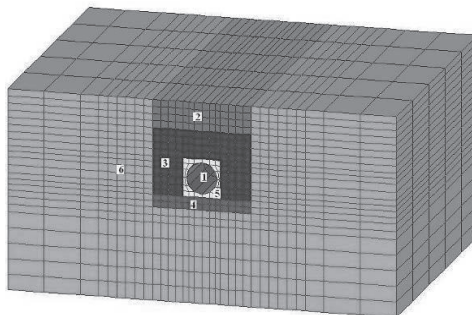The FE scheme of the problem is shown in the Figure 1.

Figure l. FE scheme of the pipeline: 1 – pipeline; 2 –gravel; 3 – foamed polyester Superazote EM26; 4 – foamed polyester *Kompostirol*; 5 – sand filling; 6 – loam.

Thermophysical behaviour of this structure during transportation of petroleum in freezing and thawing soil was modelled for an annual cycle. As an alternative to the designed structure we made numerical calculations of behaviour of heat-insulation material *Raduga-Service*.

Soil temperature change curves in the area of the fault for one year around pipeline are shown in the Figure 2.
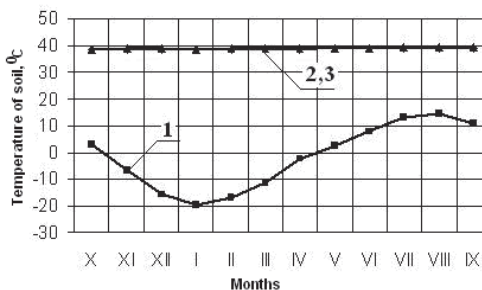

Figure 2. Graphics of temperature changing in soil in the fault area around pipeline for one year; 1 – ground surface; 2,3 – with the use of foamed polyester by the project Sakhalin II local foamed polyester, correspondingly.

The diagrams of soils temperature distribution on March around pipeline with the use of foamed polyester are shown in Figure 3.
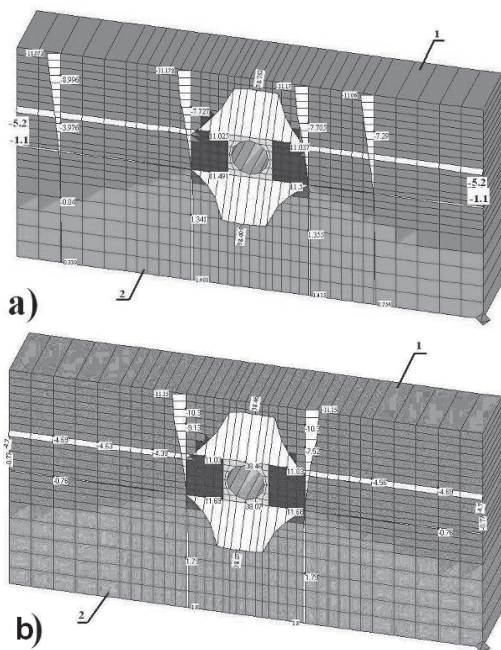

a)

b)

Fig 3. Diagrams of soils temperature distribution in fault soil on March around pipeline with the use of foamed polyester, a) Sakhalin II Project; b) *Raduga-Service* 1 – freezing soil, 2 – thawed soil.

3. ANALYSES OF THE RESULTS OF CALCULATIONS

The results of calculations showed that the depth of soil freezing reached about 1.5 m. Heat insulating material excludes penetration of below zero temperatures to the pipeline. In such cases, temperature of the fine sand, which is used as backfill around the pipeline during a year changes from 38 to 400C, that is to say corresponds to the temperature of the transported petroleum. In order to evaluate behaviour of different construction materials on tectonic influences of fault areas we investigated influence of one-sided shift on underground pipelines.

Diagrams of horizontal displacements of pipelines depending on horizontal pressure, using foamed polyester of different producers, are shown in the Figure 4.
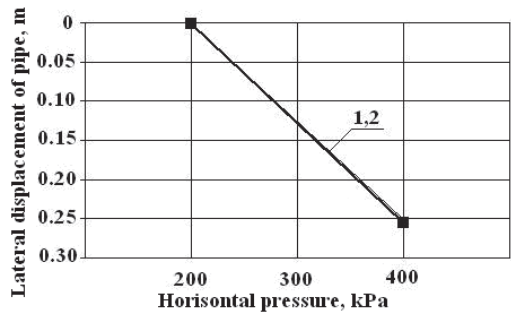

Figure 4. Diagram of lateral displacement of pipeline with the use of polyester in pipeline structure
1) Sakhalin II Project; 2) *Raduga-Service*.

Figure 5 shows contours and diagrams of lateral displacements of soil bulk around pipeline in the fault area with the use of foamed polyester under horizontal pressure P=400 kPa from the assumed displacement of rock.
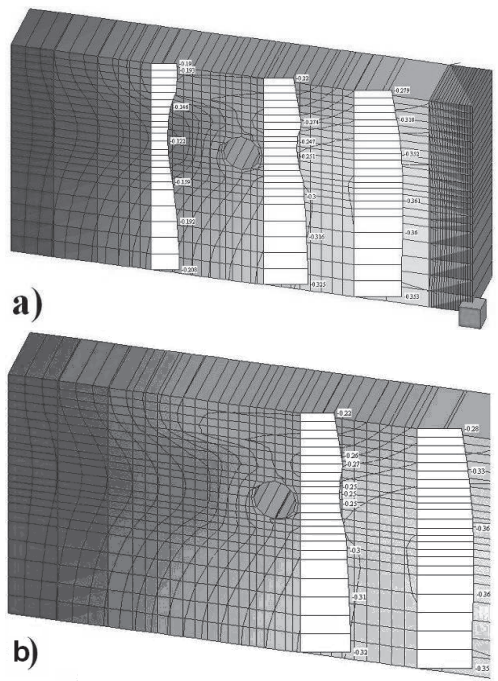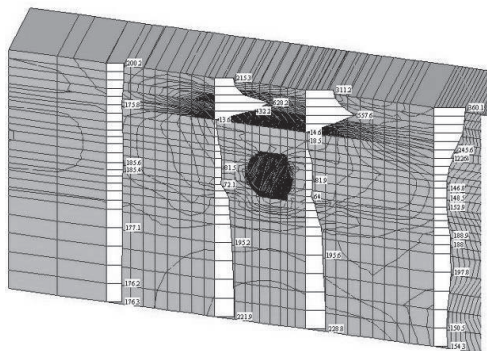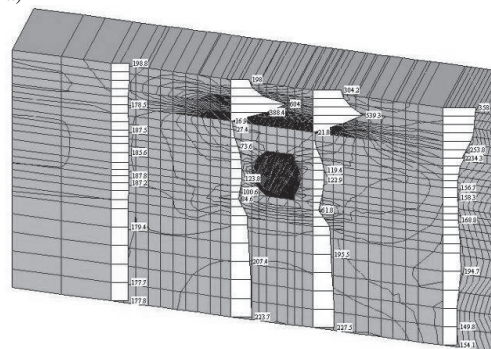

a)

b)

Figure 5. Contours and diagrams of lateral displacements of soil around pipeline in the fault area with the use of foamed polyester under horizontal pressure P=400 kPa from the assumed displacement of ro0ck:
a) Sakhalin II design;
b) *Raduga-Service*, Khabarovsk.

Figure 6 shows contours and diagrams of horizontal stresses in soil around the pipeline with the use of foamed polyester under horizontal pressure P=400 kPa from the assumed displacement of rock.

a)

b)

Figure 6. Contours and diagrams of horizontal stresses in soil around the pipeline with the use of foamed polyester under horizontal pressure P=400 kPa from the assumed displacement of rock, a) Sakhalin II Project, b) *Raduga-Service* , Khabarovsk.

4. CONCLUSION

Results of modelling of thermophysical and stress-strain state of soil in fault areas with structures located therein, like one-sided horizontal displacement of rock, showed that the influence on the foamed polyester by Sakhalin II design is the same as on the *Raduga-Service* polyester. Numerical modelling of freeze and thaw showed that loss of heat during transportation of petroleum is ruled out on account of eliminating influence of freeze pressure on the pipeline. This allows to reduce running costs. These results prove that the expanding foam polyester Kompostirol produced by KNAUF can be substituted for a local one reducing construction costs.

5. REFERENCES

Ulitsky V.M., Paramonov V.N., Kydryavtsev S.A., Shashkin K.G. Automation of soil-structure calculations during deep seasonal freezing. Design automation in civil engineering and hydroengineering. *Proc. of International Geotechnical Conference*, Odessa, 2003 (in Russian).

Tunnel-soil-pile interaction

C.W. Ong
Managing Director, KIMARO Geotechnical Engineering Pte Ltd, Singapore, *ong@kimaro.com.sg*
Executive Director, J.Pro Consulting Engineers LLP, *Singapore, ong1@jproce.com*

C. F. Leung
Professor, Department of Civil Engineering, National University of Singapore, *cvelcf@nus.edu.sg*

K.Y. Yong
Vice President, National University of Singapore, Singapore, *uciyky@nus.edu.sg*
Professor, Department of Civil Engineering, National University of Singapore

ABSTRACT: It is increasingly economically viable to build underground tunnels as precious urban landscan then be utilized for the development of buildings. However, during tunneling, the ground around the tunnel often moves towards the tunnel opening. The resulting ground movements induce additional settlement, axial force, deflection and bending moment on adjacent pile foundations. As a result, the foundations may not be able to resist the loads induced by tunnelling nearby. In this paper, the results of a series of centrifuge model tests conducted to investigate the effects of tunnelling on single piles in clay are presented. The effects of pile-to-tunnel distance due to tunnelling are also examined. In addition, the observed pile behaviours are evaluated against the measured free field soil movements due to tunnelling.

1. INTRODUCTION

It is increasingly advantageous to build transportation tunnels underground as precious urban lands are better utilized for the development of buildings. However it can be challenging to excavate tunnels in urban areas. When a tunnel is excavated, the ground around the tunnel often moves towards the tunnel opening. Soil movements can be very significant if tunnelling is carried out in soft clay.The resulting ground movements induce axial (settlement and axial force) and lateral (deflection and bending moment) responses on adjacent pile foundations, see Figure 1. In addition, pile foundations supporting existing buildings were often designed to resist compression loads only. In such cases, the foundations may not be safe to resist the bending moment induced by tunnelling nearby. In this paper, the study of tunnel-soil-pile interaction is being carried out. The results of a series of centrifuge model tests conducted to investigate the effects of tunnelling on single piles in clay are presented. Besides, the observed pile behaviours are evaluated against the measured free field soil movements due to tunnelling using the Particle Image Velocimetry technique (PIV), an advanced image processing

technique developed for geotechnical research by White et al. (2003).

2. CENTRIFUGE MODEL SETUP

The setup of the centrifuge model package is shown in Figure. The tests were conducted at an acceleration field of 100g on the National University of Singapore (NUS) Geotechnical Centrifuge. The container used is made of stainless steel alloy and has internal dimensions of 525 mm × 200 mm × 490 mm (length × width × height).
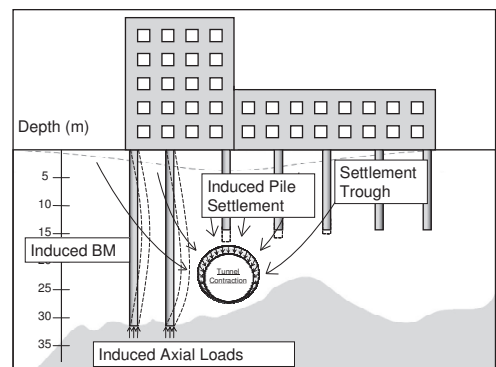

Figure 1 Pile responses caused by tunnel construction

One sidewall of the container is made of transparent Perspex plate, which allows image acquisition by a high resolution CV-M1 camera. To minimize the soil/container side friction, all the inner walls of the container are heavily greased. The set-up essentially comprises a model tunnel surrounded by kaolin clay with instrumented model piles installed nearby. The soil used in the test was prepared from a slurry of Malaysian kaolin clay (Gs=2.65, LL=80%, PL=40%, Cc=0.65, Cs=0.14) at a water content of 120% (1.5 times LL). The Toyoura sand placed beneath the clay serves as a drainage channel. It has an average particle size of 0.2 mmand Gs of 2.65. The minimum and maximum density of the sand is 1335 kg/m^3 and 1645 kg/m^3, respectively. The critical state friction angle is 32°

2.1. Model tunnel & pile

An innovative model tunnelling technique has been developed such that controlled inward tunnel deformation can be achieved. An oval-shape ground deformation pattern is imposed as the boundary condition and the gap parameter (GAP) proposed by Lee et al. (1992) is used to quantify the amount of tunnel over-cut. Loganathan & Poulos (1998) and Park (2005) evaluated that an oval-shape deformation pattern is in reasonable agreement with tunnel deformations observed commonly in the field. The model tunnel comprises a circular rigid outer plate and a hollow metallic circular tube of 60 mm diameter, simulating a 6-m diameter prototype tunnel at 100g. The rigid plate helps to maintain a uniform GAP for the entire model tunnel. There are advantages of such model tunnel. Firstly, the present model tunnel is able to simulate the precise volume loss when the GAP closes up after tunnelling. The percentage of volume loss has been calibrated by calculating the area of surface settlement against the GAP created in the model tunnel at the undrained stage. Secondly, the circular rigid outer plate can provide a very uniform oval-shaped of the GAP throughout the entire length of the model tunnel. As such, a constant volume loss around the model tunnel can be ensured.

Two instrumented model piles were employed in the present tests to study the effects of tunnelling on single free-headed floating piles.

The aluminium model square piles have 9.53 mm external width and 6.35 mm internal width. Ten pairs of strain gauges were attached along the pile shafts to measure the bending moments and axial forces along the piles, see Figures 4(b) & (c). The strain gauges were protected by a thin layer of epoxy resin for waterproofing. The final external width of the pile shafts is 12.6 mm corresponding to 1.26 m in prototype scale. The flexural rigidity, EI, of the model pile, is 3.97×10^6 kNm^2 at 100g, which is equivalent to that of a 1300-mm diameter Grade 40 concrete bored pile.

2.2. Experimental Procedures

The kaolin clay slurry was thoroughly mixed at a water content of 120% and preconsolidated at 20 kPa. The container was then placed on the centrifuge platform and accelerated to 100g. After the ground settlement and pore water pressure readings stabilized, the centrifuge was stopped and the front wall of the container was removed to install the model tunnel, pore pressure transducers (PPTs) and to place marker beads onto the soil facing the Perspex window. The container walls were fixed back to the model container after lubricated with vacuum silicon grease.
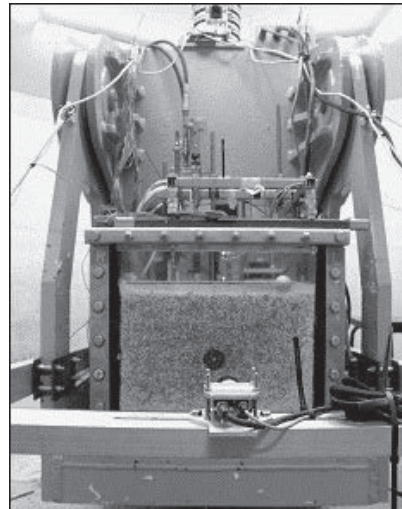

Figure 2 Centrifuge model set-up

The model piles were then installed at a distance of 6 m (in prototype scale) from the tunnel centre. Potentiometers were used to measure the surface settlements and two non-contact laser transducers were used to measure the lateral pile deflection. The pile settlement was measured by a potentiometer resting on the pile head. The entire model package was then spun up to 100g for reconsolidation of the clay. The test began by pushing the sliding rod forward with the small rods lying on the sliding rod dropping onto the thinner part of the sliding rod. As a result, the gap between the rigid aluminium plate and the model tunnel closes and inward tunnel deformation was simulated. The model tunnel was left in place to simulate the tunnel lining to study the post-excavation ground deformation and pile responses. The centrifuge was kept at 100g for 2 hours (2.3 years in prototype scale) and instruments were monitored regularly during this period.

3. TUNNEL-SOIL INTERACTION

The test results are presented in prototype scale hereinafter. The tunnel cover (C) (distance from ground surface to tunnel crown) and tunnel diameter (D) are 12 m and 6 m, respectively. Test 1 examines the free-field soil movements due to tunnelling with a volume loss of 3% but no piles. Tests 2, 3 and 4 investigate the effects of pile-to-tunnel distance on the performance of 22-m long free head friction piles. The terminology "short-term (ST)" refers to the time when tunnel excavation has just been completed. "Long-term (LT)" refers to 720 days after tunnel excavation with negligible change in ground movement and pile responses.

The amount of volume loss depends on soil conditions and method of tunnelling. The Civil Design Criteria for Road and Rail (LTA, 2006) recommended for tunnels up to 6.6-m diameter in marine clay, the selected tunnel volume loss should be in the range of 2% to 3.5%. As such, a tunnel volume loss of 3% is adopted in the present tests. The subsurface soil movements were computed using a deformation measurement system based on PIV by tracking the texture (i.e. the spatial variation of brightness) within an image of soil from high resolution photographs. Texture can be added to an exposed plane of clay by additional marker beads randomly scattered at the front face as to capture the soil deformation, as shown in Figure 3.

Figure 4 shows the displacement vectors obtained using PIV in short and long terms. In the short-term, the principal soil movements are concentrated within a zone extending approximately 45° from the tunnel spring line, see Figure 4(a). This zone can be identified as an 'Immediate Shear Zone' in which the soil within this zone has been 'unloaded' due to tunnel excavation. For clay, the soil does not settle as a rigid body but gradually deforms by arching whereby the radial stress in the immediate shear zone reduces due to stress relief. This leads to the observed soil movement pattern and the settlement trough at the ground surface. On the other hand, the zone outside the immediate shear zone can be identified as the 'Support Zone', as the circumferential soil stresses increase within this zone to support the arches formed in the immediate shear zone.

In the long-term, volumetric soil strain would increase due to soil consolidation and cause the soil movements to increase, see Figure 6. Since the behaviour of clay is time-dependent, the induced pile responses are hence expected to increase with time. A review on the changes of soil displacement vectors over time around the tunnel would shed more light on the behaviour of piles installed at different pile-to-tunnel distances.
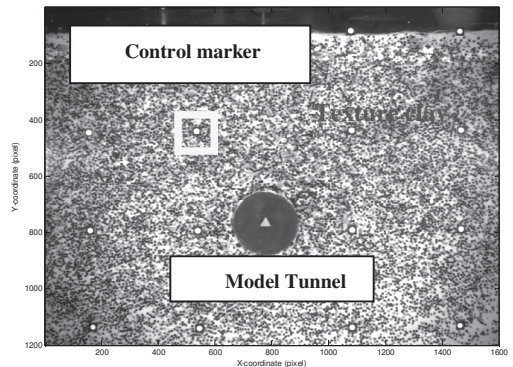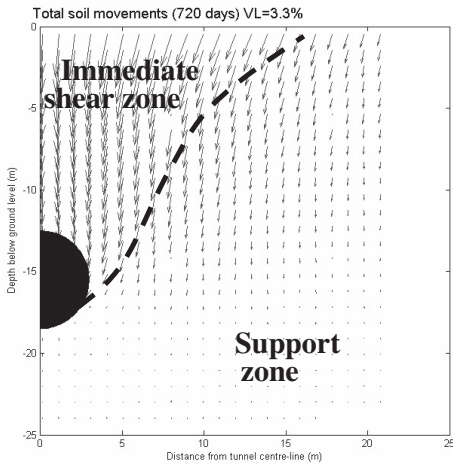

Figure 3 Example of digital image taken during the test for PIV analysis

(a)

(b)

Figure 4 Vector of soil displacement after (a) 2 days (Short-term) and (b) 720 days (Long-term)

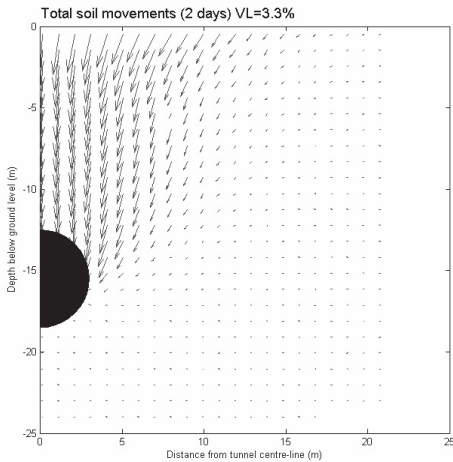## 4. TUNNEL-SOIL-PILE INTERACTION

Three centrifuge model tests (Tests 2, 3 and 4) were performed to study the behaviours of long piles placed at 6 m (or 1D), 9 m (or 1.5D) and 12m (or 2D) from the centre of the tunnel.

4.1. Axial pile responses

The induced pile axial force profiles due to tunnel excavation in Tests 2, 3 and 4 are presented in Figure 5. The results reveal that all the induced axial load profiles are similar with a maximum load at slightly higher than tunnel spring line. The neutral planes shifts lower over time. The induced pile axial forces decrease with increasing pile-to-tunnel distance. This can be attributed to the reduced shaft contact area with soils in the immediate shear zone when the distance of pile-to-tunnel increases. Figure 6 shows the variation of pile head settlement and the free-field vertical soil movement at the respective pile locations. Similar steady decreases in vertical soil settlement with depth and pile-to-tunnel distance are observed. The magnitudes of pile head settlement also decrease with increasing pile-to-tunnel distance. This is consistent with the observed variations of pile axial forces from the three tests. Besides, the smaller magnitudes of soil settlement is expected to induce less negative skin friction (Fig. 5) for the case in which pile tip is below the tunnel invert. Once again, the pile head settlement exhibits time-dependent behaviour and reaches its respective peak value after 720 days. The results suggest that the induced axial pile responses are insignificant when the pile-to-tunnel distance is larger than 2D in the present study.

Axial Force (kN)

Bending Moment (kNm)

Figure 5 Tunnelling-induced pile axial force

Figure 7 Tunnelling-induced pile bending moment

Settlement (mm)

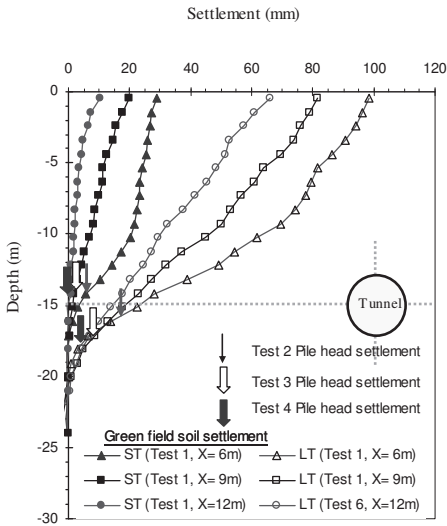Lateral deflection (mm)

Figure 6 Tunnelling-induced pile settlement and soil settlement
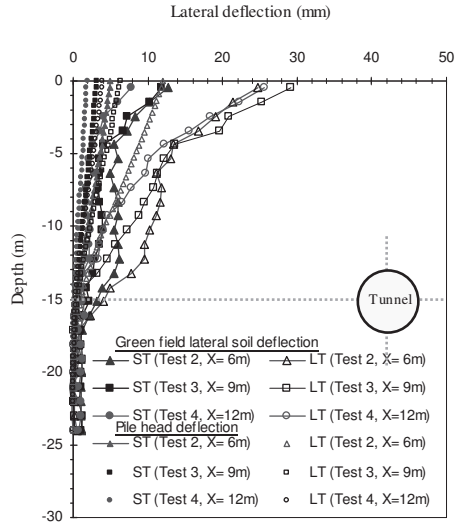

Figure 8 Tunnelling-induced pile deflection and lateral soil movement

4.2. Lateral pile responses

The variations of induced bending moment profile with pile-to-tunnel distance are shown in Figure 7. The induced pile bending moment profiles are similar in all tests with a maximum approximately at the tunnel spring elevation. This is consistent with the numerical predictions reported by Cheng (2003) and field measurements reported by Pang (2006). The maximum induced bending moment generally decreases, as expected, with increasing pile-to-tunnel distance. The induced pile bending moments are generally small when the pile is over 2D from the tunnel centre as the maximum moment is less than 50kNm. It is also evident that regardless of pile-to-tunnel distance, the induced pile response exhibit time-dependent behaviours. In the long-term, the maximum pile bending moment dropped significantly from 1D to 1.5D by almost 80% and the reduction becomes less significant from 1.5D to 2D. The variations of pile deflection and corresponding free-field lateral soil movement profiles are shown in Figure 8. The surface lateral soil movements in the three tests increase with time and decrease with increasing distance between pile and tunnel. Moreover, the pile deflection drops significantly from 1D to 1.5D, with a much smaller decrease from 1.5D to 2D. The observed variation of pile bending moment and deflection with pile-to-tunnel distance is best explained by the soil deflection profiles obtained from Test 1, see Figure 9. The results reveal that at locations near to the tunnel, the lateral soil displacement is prominent at the tunnel spring elevation. However, when the distance is large enough, the lateral soil displacement profile reveals significant soil deflection at the ground surface while the soil movement at the tunnel spring elevation becomes negligible.

5. CONCLUSIONS

A series of centrifuge model tests was conducted to evaluate the tunnel-soil-pile interaction. The time effects of induced lateral and axial behaviour of single free head piles located at 1, 1.5 and 2 tunnel diameters from the tunnel centre line with a tunnel volume loss of 3% are investigated.

For a tunnel volume loss of 3%, the vertical and lateral soil movements due to tunnelling are found to increase with time and the soil move-

Figure 9 Lateral soil displacement profiles at different pile-to-tunnel
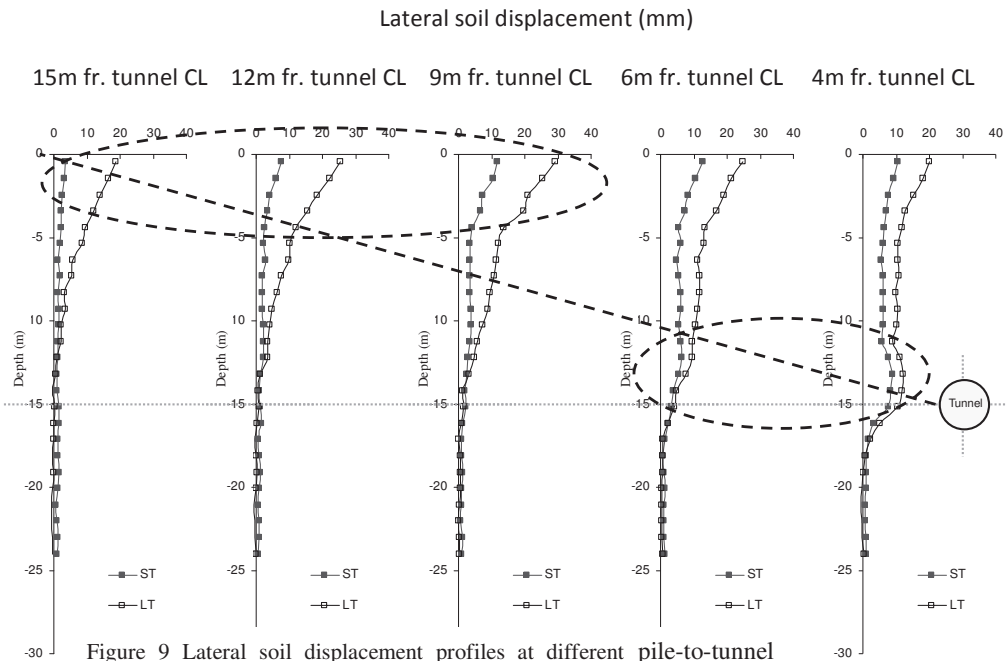
ments stabilise at around 720 days after the completion of tunnel excavation. In the short term, an immediate shear zone with large soil movement above tunnel can be identified. In the long term, the significant soil movement zone extends much wider resulting in a wider surface settlement trough and the soil settlement is noted to be dominant rather than the lateral soil movement.

It is observed that the pile responses decrease with an increase in pile-to-tunnel distance in both short and long terms. Regardless of pile-to-tunnel distance, all pile responses increase over time. It is evident that the pile responses are generally small when the pile-to-tunnel distance is greater than 2D. The results also reveal that at locations close to the tunnel, the lateral soil displacement is prominent at the tunnel spring elevation. However, when the distance is large enough, the lateral soil displacement profile reveals significant soil deflection at the ground surface while the soil movement at the tunnel spring elevation becomes negligible. This finding is consistent with the insignificant pile lateral responses when the pile-to-tunnel distance is over 2D. It thus further illustrates that when the pile-to-tunnel distance increases, a shorter portion of the pile length is inside the immediate shear zone.

6. REFERENCES

Cheng, C. Y. 2003. Finite element study of tunnel-soil-pile interaction.M Eng thesis, National University of Singapore.

LTA, 2006. Civil design criteria for road and rail transit systems revision A5, Rail & Engineering Group, Land Transport Authority, Singapore

Lee, K. M., Rowe, R. K. and Lo, K. Y. 1992. Subsidence due to tunnelling: Part I – Estimating the gap parameter. *Canadian Geotechnical Journal*, Vol. 29, No. 5, 929-940.

Loganathan, N. and Poulos, H. G. 1998. Analytical prediction for tunneling-induced ground movements in clays. *Journal of Geotechnical and Geoenviromental Engineering*, Vol. 124, No. 9, pp. 846-856.

Mair, R. J., Taylor, R. N. and Bracegirdle, A. 1993. Subsurface settlement profiles above tunnels in clay. *Geotechnique*, Vol. 43, No. 2, 315-320.

Park, K. H. 2005. Analytical solution for tunneling-induced ground movement in clays. *Tunneling and Underground Space Technology* Vol. 20, pp. 249-261.

Pang C H. 2006. The effects of tunnel construction on nearby piled foundation. PhD thesis, National University of Singapore.

Ran, X. 2004. Tunnel pile interaction in clay. M Eng thesis, National University of Singapore. White, D.J., Take, W.A. & Bolton, M.D. 2003.Soil deformation measurement using particle image velocimetry (PIV) and photogrammetry. *Geotechnique*, Vol.53, No.7, 619-631.

Design model of long nonlinear deformation of clay soil in a complex stress state

Mirsayapov I.T. , Koroleva I.V.
mirsayapov1@mail.ru
Kazan State University of Architecture and Engineering, Russia

ABSTRACT: The spatial model of dilating soil is proposed. Hypothesis which says that strength dry friction of the Coulomb deflect from platforms of a limiting condition and function on surface slipping was taken as a principle. The strain creep of soil is described according to hereditary creep theory. Volumetric deformation is summed up change of shape and volume.

In standard environment, when ground is situated under the influence of it's own weight and external force, complex is formed where each soil element is under the influence of stress tensor. Soil's deflected mode is defined, if in each of it's volume elements with coordinates X, Y, Z components of normal (σ) and shearing (τ) stresses; angular (γ) and space coordinates (u, v, w) are defined. In a state when ultimate strength is reached shearing surface in every volume element's formed and oriented in particular way to direction of main stresses $\sigma_1 > \sigma_2 > \sigma_3$ [10].

Experimental studies of clay soil in long-term triaxial compression [8, 9] have defined the mechanism of tested specimen's failure. The process can be described in a following way: While pressure is applied, consolidated areas in a form of pyramids are formed, pyramids occur in specimen's upper and lower surface and at specimen's sides (Figure 1a). Geometrical sizes of pyramids mentioned, depends on loading conditions.

To define physical-mechanical properties, soil samples were taken from relevant areas. [9].

As a result of analysis of failure process and areas of different densities, a suggestion was made. Authors state that triaxial compression leads to formation of areas of different deflected state. As a result of gradual increment of load, consolidated pyramids of different shapes and sizes are formed in specimen's upper and lower surfaces and at specimen's sides. Size and shape of pyramids depends on loading conditions (figure 1).
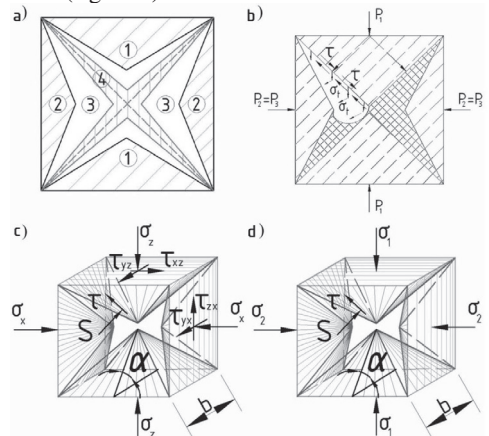
Figure 1. a) – consolidated areas of different density of a specimen in triaxial tests: 1-vertical consolidated pyramids; 2 – consolidated pyramids at specimen's sides; 3 – uniformed deflected state area; 4- area of dilatancy; b) – deformed state of clay between pyramids formed; c) – deflected state of volume element in space in random moment of time at preultimatecondition (stresses and tensions are not shown); d) – deflected state of volume element in space at ultimate condition (stresses and tensions are not shown)

Specimen's deformation occurs as a result of this pyramid's movement, where pyramids are

considered as solid bodies. Authors observe improvement of physical-mechanical properties in consolidated areas mentioned above (increment of density up to 11%; φ – 88%; c – 138%). Negative processes related to reduction of physical-mechanical properties are located in areas between pyramids (area 4, Figure 1a) (density reduction up to 43%; φ – 45%; c – 67%). At the same time Mohr's circles drawn based on results of series of tests conducted, show reduction of internal tension angle φ up to 16% and cohesive force c – 6 % in an integral volume. Visual investigation of shearing surface after specimen's failure, shows that soil at this area is subjected to both detachment and shearing (Figures 1a, 1b).

Similar schemes of failure were observed in surveys done by Boldyrev [1], Kryzhanovskii [5], Higo [12] that correspond to surfaces of normal and shearing stresses described in [11] (Figure 2).

(a)   (b)   (c)   (d)   (f)

Figure 3. (a) – Normal stresses surface during general state of stress in case of same signs of all three main stresses; (b) – Normal stresses surface during general state of stress in case of different signs of main stresses ($\sigma_2=0.5\sigma_1;\sigma_3=-0.5\sigma_1$); (c) – Normal stresses surfacewhen $\sigma_1\backslash=\sigma_2\backslash= \sigma_3$; (d) – Normal stresses surfacewhen $\sigma_1\backslash=\sigma_2= \sigma_3$; (f) –directions with maximal shear displacements: 1 – directions with shear displacement $\gamma_1=\varepsilon_2-\varepsilon_3$; 2 – directions with shear displacement $\gamma_2=\varepsilon_3-\varepsilon_1$; 3-directions with shear displacement $\gamma_3=\varepsilon_1-\varepsilon_2$. [11]
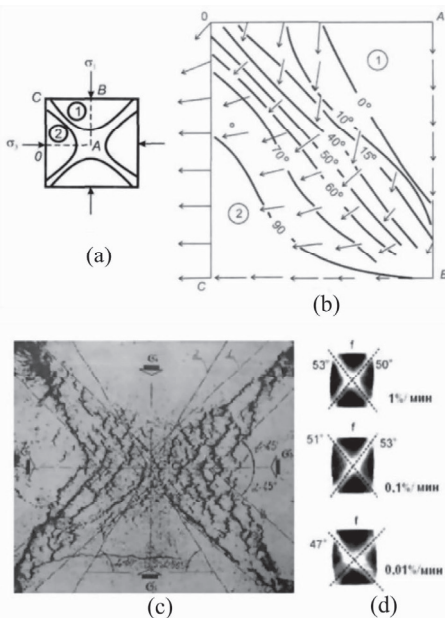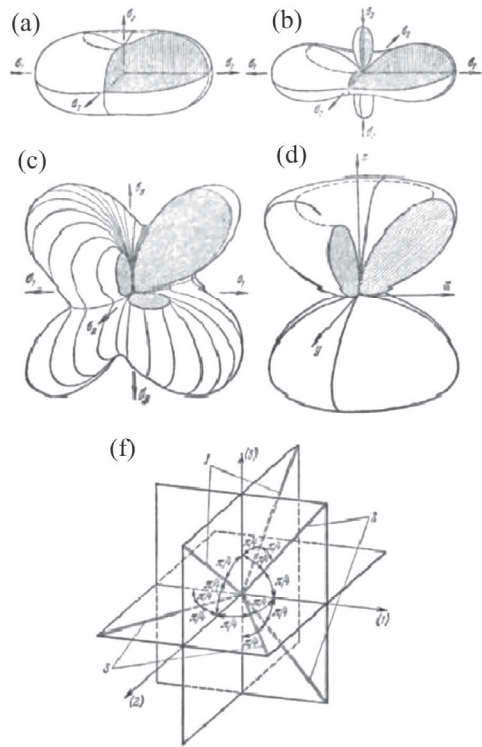

(a)   (b)   (c)   (d)

Figure 2. (a) – Loading and unloading soil specimen (data by Boldyrev); (b) – isolines of displacement vectors' angles of inclination: solid areas in soil specimen; (c) – soil specimen's failure picture in triaxial compression device with flexible walls (data by Kryzhanovskii); (d) – Dense clay test results (Higo)

Results of experimental surveys can be represented as shown below:

$$\varepsilon_V = \varepsilon_V^0 \pm \varepsilon_V^D \qquad (1)$$

where ε_V^0 – volume strain during uniform pressure;

ε_V^D – volume strain caused by stress deviator.

ε_V^0 value does not depend only on σ_m but also on shearing stresses τ , occurring as a result of difference between soil's resistance to compression and tension:

$$\varepsilon_V^0 = f_1^*(\sigma_m, \tau, t) \qquad (2)$$

With the assumption that shearing displace-

ments γ_i depend on intensity of shearing stresses τ_i, normal stresses σ_m and type of deflected state, displacements of forming can be represented as following:

$$\varepsilon_V^D = f_2^*(\sigma_m, \tau_i, t) \tag{3}$$

Taking in consideration the law of volume deformation change, found by authors [8, 9, 6], according to which Poisson's ratio in soil remains constant ($v = const$) during tests on creep age, we suggest that volumetric deformations change and deformations of forming develop in time similarly.

Volumetric deformation of soil in time is described in compliance with Bolzman-Valter's heredity theory, modified by Maslov-Arutunjan in respect to soil. According to this theory, total shear or volume deformation during random way of loading can be represented as following:

$$\varepsilon_i = \frac{\sigma_i(t)}{G(t)} + \frac{1}{G(t)} \int_\tau^t K_j(t,\tau) \cdot \sigma_i(\tau) \cdot d\tau; \tag{4}$$

$$\varepsilon_v = \frac{\sigma(t)}{K(t)} + \frac{1}{K(t)} \int_\tau^t K_V(t,\tau) \cdot \sigma(\tau) \cdot d\tau; \tag{5}$$

where $G(t)$ and $K(t)$ – shear modulus and bulk modulus;

$K_j(t,\tau)$ – creep kernel, represented as velocity of shear deformation with unit value of loading intensity;

$K_V(t,\tau)$ – creep kernel, represented as velocity of volumetric deformation with unit value of mean stress.

Analysis of test data found helped to define creep kernels $K_j(t,\tau)$, $K_V(t,\tau)$ for soil in general state of stress.

While patterning equations of clay soil deformation in general state of stress processes of clay hardening (aging) were taken into account, that is the reason why aging function $\varphi(t)$ is used. Taking hardening process into account, creep kernels can be represented as shown below:

$$K_\gamma(\sigma,t-\tau) = \begin{cases} \varphi_\gamma(\tau) \cdot \dfrac{\delta_{\gamma 1}}{(t-\tau)} \cdot \delta_{\gamma 2} & npu \quad 0 \le t \le t_{нм} \\ \varphi_\gamma(\tau) \cdot C(\sigma) & npu \quad t > t_{нм} \end{cases} \tag{6}$$

$$K_V(\sigma,t-\tau) = \begin{cases} \varphi_V(\tau) \cdot \dfrac{\delta_{V1}}{(t-\tau)} \cdot \delta_{V2} & npu \quad 0 \le t \le t_{нм} \\ \varphi_V(\tau) \cdot C(\sigma) & npu \quad t > t_{нм} \end{cases} \tag{7}$$

where $t_{нм}$ – deformation speed hold start.

Based on suggestions stated above, we can assume that in the beginning stage of long-lasting triaxial stress deflected state of soil specimen is inhomogeneous. Deviator loading and long-term isolation during loading accompanied by initiation and development of set of shear surfaces and specimen uniformity break. Surface positions change in correlation with time and process of deviator increment. Therefore negative dilatancy (aeration) of clay soil during long-term triaxial stress is localized in the range of potentially available areas of limit equilibrium [9]. Since aeration of soil occurs in straitened localized areas, significant values of dilatancy stresses are reached in zones surrounding aeration area, which is considered to be buffer area where stresses are transferred from vertical pyramids to area of undisturbed soil (figure 1a, 1b). Described above is the mechanism of shear and compacted areas correlation. When in limiting state clay soil's failure is localized in areas between pyramids. On this stage deflected state of soil specimen can be assumed as homogeneous.

Under the assumption of determined scheme of failure and deflected state areas general scheme of inelastic long-term clay soil deformation is suggested. Suggested scheme is based on modified model of non associated plastic flow proposed by Nicolaevskii [7], according to which Coulomb's dry friction force is deviated from the platform of limit equilibrium and acting in a direction of tangential glide of physical particles. These platforms' directions can only be defined if soils' deformed state is taken in account.

Taking into consideration, that unrelatedly to the degree of starting uniformity of soil specimen's deflected state, failure always takes place in the space of main stresses, overlapping the space of main stresses σ and space of main deformations ε remaining the principle of stresses and deformation speed's tensors coaxiality [7]. We will assume that Coulomb's dry friction law relates projections of forces acting on platforms of limited equilibrium on its normal and on the platform itself. Thus, condition of long-term loading flow can be represented as above:

$$|t| = S \cdot tg\varphi(t,\tau) + c_0(t,\tau), \tag{8}$$

where $S = \sigma_1 \cdot l \cdot l' + \sigma_2 \cdot m \cdot m' + \sigma_3 \cdot n \cdot n'$

$$t = \sqrt{\begin{array}{l}(\sigma_1 \cdot l \cdot m - \sigma_2 \cdot l \cdot m)^2 + (\sigma_2 \cdot m \cdot n - \sigma_3 \cdot m \cdot n)^2 + \\ + (\sigma_3 \cdot n \cdot l - \sigma_1 \cdot n \cdot l)^2\end{array}}$$

$\varphi(t, \tau)$ – varying internal tension angle;

$c_0(t, \tau)$ – varying cohesive force;

l, m, n – cosines to platforms of limit equilibrium;

$l`, m`, n`$ – cosines to platforms of gliding.

Special orientation of limit equilibrium platforms is defined by equations below:

$$l^2 = \frac{\overline{I_3}}{\overline{I_2} \cdot \overline{\sigma_1}}; \quad m^2 = \frac{\overline{I_3}}{\overline{I_2} \cdot \overline{\sigma_2}}; \quad n^2 = \frac{\overline{I_3}}{\overline{I_2} \cdot \overline{\sigma_3}}; \quad (9)$$

where $\overline{I_2} = \overline{\sigma_1} \cdot \overline{\sigma_2} + \overline{\sigma_2} \cdot \overline{\sigma_3} + \overline{\sigma_3} \cdot \overline{\sigma_1}$ and $\overline{I_3} = \overline{\sigma_1} \cdot \overline{\sigma_2} \cdot \overline{\sigma_3}$ – second and third invariants of tensors of modified main stresses $\overline{\sigma_i} = \sigma_i + H \quad (i = 1, 2, 3)$

$H = c / ctg\varphi$ – uniform compression defined by Mohr-Coulomb's hypothesis

φ – internal tension angle

Expressions for cosines to gliding platform's normal are as in [7]:

$$\left.\begin{array}{l}(l`)^2 = \frac{1}{3} \cdot \frac{3 \cdot d\varepsilon_2 \cdot d\varepsilon_3 - I_2 + \sqrt{I_2^2 - 3 \cdot I_1 \cdot I_3}}{(d\varepsilon_1 - d\varepsilon_2) \cdot (d\varepsilon_1 - d\varepsilon_3)}; \\[3mm] (m`)^2 = \frac{1}{3} \cdot \frac{3 \cdot d\varepsilon_1 \cdot d\varepsilon_3 - I_2 + \sqrt{I_2^2 - 3 \cdot I_1 \cdot I_3}}{(d\varepsilon_2 - d\varepsilon_1) \cdot (d\varepsilon_2 - d\varepsilon_3)}; \\[3mm] (n`)^2 = \frac{1}{3} \cdot \frac{3 \cdot d\varepsilon_1 \cdot d\varepsilon_2 - I_2 + \sqrt{I_2^2 - 3 \cdot I_1 \cdot I_3}}{(d\varepsilon_3 - d\varepsilon_1) \cdot (d\varepsilon_3 - d\varepsilon_2)},\end{array}\right\} \quad (10)$$

where $d\varepsilon_1, d\varepsilon_2, d\varepsilon_3$ – increments of main deformations

$I_1 = d\varepsilon_1 + d\varepsilon_2 + d\varepsilon_3$,

$I_2 = d\varepsilon_1 \cdot d\varepsilon_2 + d\varepsilon_2 \cdot d\varepsilon_3 + d\varepsilon_3 \cdot d\varepsilon_1$,

$I_3 = d\varepsilon_1 \cdot d\varepsilon_2 \cdot d\varepsilon_3$ – first, second and third invariants of deformation increments

As stated above, potentially available platform's orientation is not constant in general, and changes in the process of inelastic deformation of soil according to equation (5):

$$\alpha = \arccos \sqrt{\frac{1}{1 - \frac{de_1^p}{de_3^p}} - \frac{\mu_{d\varepsilon}}{6}}, \quad (11)$$

where $\mu_{d\varepsilon} = \frac{2de_2^p - de_1^p - de_3^p}{de_1^p - de_3^p}$ – deformed state characteristic (Lode-Nadai characteristic),

where

$de_1^p = d\varepsilon_1^p - d\varepsilon_m^p; \quad de_2^p = d\varepsilon_2^p - d\varepsilon_m^p; \quad de_3^p = d\varepsilon_3^p - d\varepsilon_m^p$

– increments of plastic deformations (taking creeping deformations in account);

$\varepsilon_1, \varepsilon_2, \varepsilon_3, \varepsilon_m$ – linear and volumetric deformations.

Taking in account surveys conducted and model described above, long-term strength condition can be represented as follows:

$$4 \cdot [\sigma_V(t) \cdot A_{sh} \cdot \cos\alpha_1(t) + \tau_V(t) \cdot A_{sh} \cdot \sin\alpha_1(t)] \geq \sigma_1 \cdot A_1; (12)$$

where $A_{sh} = \frac{b^2}{4\cos\alpha_2(t)}$;

$A_1 = b^2$ – cube's face area;

α_1 – corner incline of balance`s limit plan;

α_2 – corner incline of shear`s plan;

$\sigma_V(t) = \sigma_1 \cdot l(t) \cdot l`(t) + \sigma_2 \cdot m(t) \cdot m(t) + \sigma_3 \cdot n(t) \cdot n(t) + \sigma_d(t)$ – normal stresses;

$\sigma_d(t) = \frac{E}{(1+\nu) \cdot r} \cdot \Delta\delta_d$ – dilatancy stresses;

$\tau_V(t) = S \cdot tg\varphi_0(t, \tau) + c_0(t, \tau).$ – shear stresses.

Thus, soil's strength, during long-term triaxial compression, depends on variation of internal tension angle, cohesive force and angle of limit equilibrium surface incline.

According to kinetic theory of soil deformation, proposed by Vyalov, Zaretskii [2, 4], failure takes place, when damage level by microfractures in limit equilibrium area reaches its critical value.

Vyalov [2] states that soil strength decrease in time generally occurs as a result of cohesive force lowering, while internal tension angle change is insignificant.

Based on test results [1, 2, 4, 8, 9] following scheme of creeping deformation development and long-term strength change can be suggested. Depending on magnitude and duration of load appliance, two mutually compensated processes occur in multistate clay soil – strengthening conditioned by defect treatment and more compact integrity of particles and weakening conditioned by re-orientation of particles and forming and development of micro and macrofractures (Figure 1b). When weakening prevails over strengthening, phase of failure and progressive creeping occurs. At this stage intensive disintegration of microstructure takes place and particles start to re-direct, though these processes take place onle in limit equilibrium areas where values of strength are lower

and fractures are developed.

Taking in account statements above, expression for varying cohesive force can be represented as follows:

$$c_0(t,\tau) = K_{Ict}^M \cdot q(S), \qquad (13)$$

where $q(S)$ – summary fracture length function;

K_{Ict}^M – soil fracture tip stresses intensity coefficient.

Finding S from (11), taking in account that $K_{Ict}^M = \sqrt{2E\gamma}$ according to [3] S can be represented in relation to external force T as follows:

$$S_* = T^{-1} \cdot \left(T \bigg/ \sqrt{2E\gamma} \right), \qquad (14)$$

where T^{-1} is rising function inverse to T.

Using procedure, suggested in [3] function for soil weakening can be represented as follows:

$$\eta(t,\tau_1) = m(t,\tau_1) \cdot \lambda(t,\tau_1) \cdot \sqrt{\frac{K(\tau_1)}{K(t)} \cdot \frac{1}{1+K(\tau_1) \cdot C(t,\tau_1)}}. \qquad (15)$$

Cohesive force varying in time can be represented as follows:

$$C_0(t,\tau_1) = C_0(\tau_1) \cdot m(t,\tau_1) \cdot \lambda(t,\tau_1) \cdot \sqrt{\frac{K(\tau_1)}{K(t)} \cdot \frac{1}{1+K(\tau_1) \cdot C(t,\tau_1)}}, \qquad (16)$$

where $C(t,\tau_1)$ – volumetric creeping value;

$C_0(\tau_1)$ – initial value of cohesive force during short-term loading;

$m(t,\tau_1)$ – function of soil strengthening in expense of water-colloid bonds;

$\lambda(t,\tau_1)$ – function of soil strengthening in expense of soil bonds during long-term deformation.

Internal tension angle change is defined according to orientation of limit equilibrium platforms' change during long-term inelastic deformation.

REFERENCES

1. Boldyrev G.G. Metods definition mechanical properties of soils. Sostoyanie voprosa. – Penza, 2008. – 696 p.
2. Vyalov S.S. Rheological principles of soil mechanics. – M.: HSPH, 1978. – 447 p.
3. Y.V. Zaytsev. Mechanic destructions for builder. – M.: HSPH, 1991. – 288 p.
4. Zaretskii Yu.K., Vyalov S.S. Structural mechanics of clay soils. // Soil Mechanics and Foundation Engineering. – 1971. – №3.
5. Kryzhanovskii A. L., Vil'gel'm Yu. S., Rakhmanov T. Determination of the angle of friction of granular soils in triaxial apparatus and shear devices // Soil Mechanics and Foundation Engineering. – 1983. – №6. – P.24 – 27.
6. Meschyan S.R. Experimenal rheology of Clayey Soils. – M.: Publishers Nedra, 1985. – 341 p.
7. Mironov V.A., Sof'in O.E. Limiting-yield model for dilating soils in a complex stress state. Budaun. Stroit., №1-2, – Minsk, 2003, P. 71 – 75.
8. Mirsayapov I.T., Koroleva I.V. Deformation of clay soil for long operational triaxial compression. The collection of proceedings/ Saint-Petersburg State University of Architecture and Civil Engineering. – SPb, 2010, P. 253 – 257.
9. Mirsayapov I.T., Koroleva I.V. Pphysic and mechanical properties of clay soils an long triaxial compression. // Bulletin of Civil Engineers. – 2011. – №1(26). – P.82 – 87
10. Ter-Martirosyan Z.G. Soil mechanics. – M.: Publishers ASV, 2005. – 488 p.
11. Filin A.P. Applied mechanics of deformable solid.Vol.1. – M.: HSPH, 1978. – 790 p.
12. Higo Y., Oka F. Kodakat T., Kimoto S. A Three – Dimensional Elasto-Viscoplastic Stran Localization Analysis of Water-Satureted Clay. Geo-Research Institute, Osaka, Japan. – Vol. 86, 2006. – P. 3205 – 3240.

Topic 2

Retaining walls and structures

Failures of geotechnical structures

BEAM-COLUMN METHOD FOR TIEBACK WALLS

By Jean-Louis Briaud,[1] Fellow, ASCE, and Nak-Kyung Kim,[2] Associate Member, ASCE

ABSTRACT: The beam-column method for the design of tieback walls is of intermediate complexity between the pressure diagram methods and the finite-element method (FEM). A set of recommended P-y, F-w, and Q-w curves are presented for the soil model and the P-y path method is described to simulate properly the construction sequence of excavation and tieback stressing. The recommended beam-column method is evaluated by comparing predictions with the measured behavior of four full-scale tieback walls in sand and in clay. The most influencing factors are identified through a parametric analysis and a comparison with four pressure diagram methods is presented. The beam-column method is a deflection-based method that satisfies the vertical, horizontal, and moment equilibrium of the wall. These significant and fundamental advantages over the pressure diagram methods make it a superior method, which should be used anytime the added complexity is warranted. The most severe limitation of the beam-column method is its inability to properly account for mass phenomena, namely, mass movement and downdrag. The most useful aspect of the beam-column method is its ability to give better bending moment profiles than the pressure diagram methods.

INTRODUCTION

Tieback walls have been used for temporary excavations for decades. Their use as permanent retention systems has increased recently and has prompted a corresponding increase in research to improve the general understanding of their behavior as well as refine the existing design methods. This paper is the result of one part of a large research project sponsored by the Federal Highway Administration (FHwA) and Schnabel Foundation aimed at improving the design of tieback walls (Chung and Briaud 1993; Powers and Briaud 1993; Kim and Briaud 1994; Mueller et al. 1994; Mueller 1996; Long et al. 1996). The project started in 1989 and ended in 1996. A follow-up project started under the Texas Department of Transportation sponsorship. The part of the FHwA/Schnabel project reported here deals with the refinement of the beam-column method for the design of tieback walls. The aspects investigated include P-y curves for walls, prediction of the bending moment and horizontal deflection profiles, prediction of the axial-load distribution, influence of the construction sequence, influence of the input parameters, and comparison with case histories and with other methods.

CURRENT PRACTICE

Essentially, there are two types of tieback walls: the slurry wall and the soldier pile and lagging wall. Slurry walls, also called structural slurry walls or diaphragm walls, are built by digging a trench, usually under slurry, lowering the reinforcing cage for the wall, and pumping concrete from the bottom up through a tremie. Anchors are placed as excavation proceeds. The soldier pile and lagging walls are built by driving piles (usually H-piles) in a line with a spacing of approximately 2.5 m. Sometimes bored piles are used by drilling a hole, lowering an H-pile in the center and filling the annulus with low-strength grout. During excavation, wood lagging is placed to retain the soil between the piles and the anchors are installed at regular intervals. One major difference between the two walls from the analysis point of view exists below the excavation level: the slurry wall is a plane strain problem whereas

the soldier pile and lagging wall are a row of widely spaced single piles.

There are three major techniques that can be used to design and analyze such structures: the pressure diagram approach, the beam-column approach, and the finite-element approach. The pressure diagram approach is still the most commonly used approach. It consists of assuming an empirical pressure diagram on the wall (Terzaghi and Peck 1967) or a theoretical active-passive pressure diagram (Canadian Geotechnical Society 1985; Cheney 1988) on the wall, distributing this pressure to the anchors and to the embedment depth by some method such as the tributary method (Terzaghi and Peck 1967), the hinge method (Lambe and Wolfskill 1970), or equilibrium considerations (Canadian Geotechnical Society 1985; Cheney 1988), and then obtaining the bending moment diagram for the wall in order to size the structural elements. No deflection predictions are performed in this approach.

The beam-column approach is becoming increasingly popular. It consists of analyzing the wall as a structural member subjected to horizontal and vertical loads, which depend on deflections. The load-deflection curves are used to represent the soil layers and the anchors. The equilibrium of a wall element (Fig. 1) under the soil and anchor loads leads to the governing differential equations, which are solved by the finite difference technique (Fig. 2). This method finds its root in the work of Winkler (1867) and Hetenyi (1946) but it is Matlock who developed the general computer solution for the beam-column problem (Matlock et al. 1981) and Haliburton (1968) who first applied it to the flexible retaining wall problem. This method leads to the prediction of the bending moment profile, the deflection profile, and the axial-load profile in the wall.

The FEM is used very rarely in practice for this problem. It consists of analyzing the soil mass and the wall by using proper models for the elements of the mesh. The name of Ray Clough is often mentioned when acknowledging the early developments of the FEM, whereas Wayne Clough worked on the particular application of the FEM to tieback walls (Clough and Tsui 1974; Clough 1984). This method leads to the prediction of the bending moment and axial load in the wall, the anchor load distribution, and the deflection of the wall and of the soil surface among other things.

The pressure diagram approach is very simple but it uses restricting and often unrealistic assumptions and does not lead to deflection predictions. The beam-column approach is of intermediate complexity, includes deflection-based pressure determinations, and is theoretically sound but is severely limited when it comes to predicting soil mass phenomena. The FEM approach is very complicated and required extensive training; although it is the way to the future it has not been made simple and rugged enough to be an everyday consulting tool in 1996.

[1]Spencer J. Buchanan Prof., Dept. of Civ. Engrg., Texas A&M Univ., College Station, TX 77843-3136.

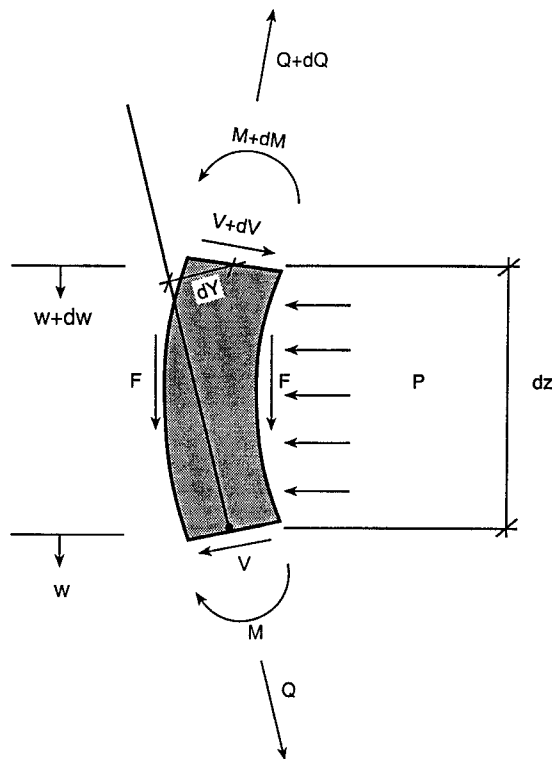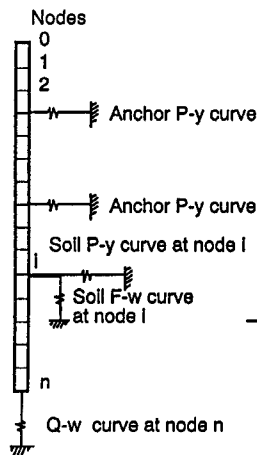[2]Proj. Engr., Geotest Engrg., Inc., 5600 Bintliff Dr., Houston, TX 77036.

99

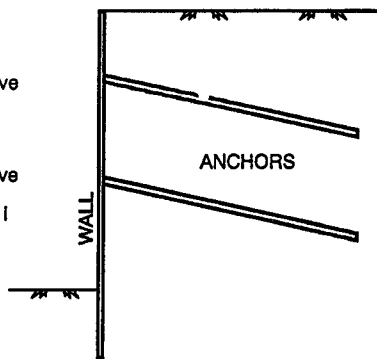**FIG. 1.   Forces Acting on an Element of Wall**

FIG. 2.   Beam-Column Simulation

BEAM-COLUMN METHOD FOR TIEBACK WALLS

It is essential to stress that a general slope stability analysis must be performed in addition to the beam-column analysis of the wall to achieve a proper wall design. This general stability analysis deals with the factor of safety against sliding of the soil mass along a chosen and often circular shearing surface. It influences the embedded depth of the wall and the length of the anchors. On the other hand, the beam-column method for tieback walls deals with the analysis of the wall as a structural element interacting with the soil and the anchors; it leads to sizing the wall and the anchors.

An element of wall (Fig. 1) is considered. Horizontal equilibrium of this element together with the constitutive law for the wall in bending ($M = EId^2y/dz^2$) and the constitutive law for the soil [$P = P(y, z)$] leads to one of the governing differential equations (Matlock et al. 1981)

$$EI \frac{d^4y}{dz^4} + Q \frac{d^2y}{dz^2} - P(y, z) = 0 \qquad (1)$$

where E = wall modulus; I = wall moment of inertia; y = wall horizontal deflection at depth z; Q = axial load in the wall at depth z; and P = horizontal soil reaction for a wall deflection y at a depth z. The soil reaction P is a load per unit height of wall (kN/m, for example).

Vertical equilibrium of the same element together with the constitutive law for the wall in compression ($Q = AEdw/dz$) and the constitutive law for the soil [$F = F(w, z)$] lead to the second governing differential equation (Matlock et al. 1981)

$$AE \frac{d^2w}{dz^2} + F(w, z) = 0 \qquad (2)$$

where E = wall modulus; A = wall cross section; w = wall vertical deflection at a depth z; and F = vertical soil reaction for a wall deflection w at a depth z. The soil reaction F is a load per unit height of wall.

Eqs. (1) and (2) are solved by the finite difference technique after considering that the wall is made of n elements having $n + 1$ nodes (Fig. 2). At the nodes, the $n + 1$ horizontal deflections y_i and the $n + 1$ vertical deflections w_i are the unknowns in the $n + 1$ finite difference versions of (1) and the $n + 1$ finite difference versions of (2) including the boundary conditions. Once the deflections y_i and w_i are known, the bending moment M, the shear V, the soil reaction P, and the axial-load Q can be obtained through their relation to y and w.

One of the critical steps in the beam-column approach is to decide what width of wall will be simulated with a program such as BMCOL76 (Matlock et al. 1981). For the slurry wall type, it is recommended that a width b equal to the horizontal spacing between anchors be used and that this width b be centered around a vertical row of anchors. The moment of inertia I would be equal to $bt^3/12$ where t is the thickness of the slurry wall, the soil reaction P would be equal to pb where p is the pressure behind the wall, and the vertical soil reaction F would be equal to $pb \tan \delta$ where δ is the soil-wall friction angle. For the soldier pile and lagging wall, it is recommended that a width b equal to the horizontal spacing between soldier piles be used and that this width b be centered around a soldier pile. The moment of inertia I would be equal to the moment of inertia of the soldier pile; the horizontal soil reaction P would be equal to pb where p is the pressure behind the wall; and the vertical soil reaction F would be equal to $pb \tan \delta$ with δ being the soil-wall friction angle.

RECOMMENDED WALL P-y CURVES

Several P-y curves are involved for a tieback wall: the wall P-y curves (plane strain) (Fig. 3), the single-pile P-y curves (below excavation level for a soldier pile and lagging wall), and the anchor P-y curves. The following recommendations (Kim and Briaud 1994) come from back calculations using bending moment profiles and cubic spline interpolation for a full-scale experimental wall in sand and comparison of measured and predicted bending moment and deflection profiles for two full-scale walls in clay and one full-scale wall in sand. Because of the limited number of comparisons and the large number of parameters involved, these P-y curves can only be considered as preliminary.

For walls in sand with a vertical face and horizontal ground, the following soil reactions and deflections are used (Coulomb 1776):

$$P_{active} = (K_a \sigma'_{0v} \cos \delta + u)b; \quad P_{passive} = (K_p \sigma'_{0v} \cos \delta + u)b \qquad (3, 4)$$

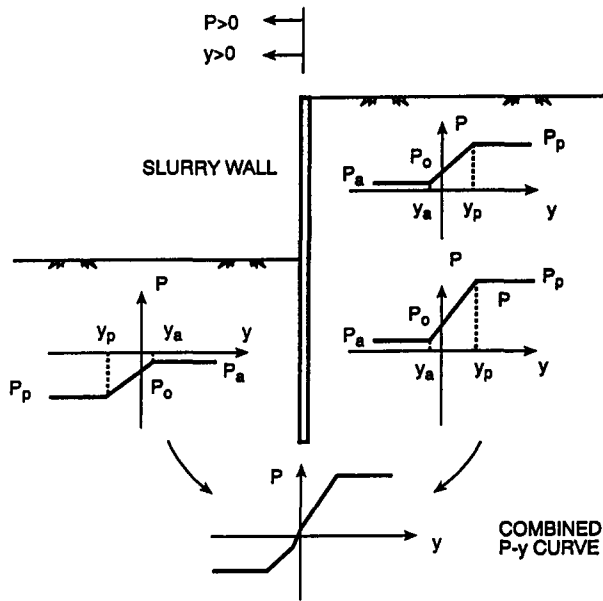$$P_{at\ rest} = [(1 - \sin \phi)\sqrt{OCR}\sigma'_{0v} + u]b \qquad (5)$$

100

FIG. 3. P-y Curves for above and below Excavation Level

TABLE 1. Reference Deflections for Plane Strain P-y Curves in Clay

(mm) (1)	$S_u < 200$ kN/m² (2)	$200 < S_u < 400$ kN/m² (3)	$S_u > 400$ kN/m² (4)
y_a	5	4	3
y_p	25	20	10

$$K_a = \frac{\cos^2\phi}{\cos\delta\left[1 + \dfrac{\sqrt{\sin(\phi + \delta)\sin\phi}}{\cos\delta}\right]^2} \qquad (6)$$

$$K_p = \frac{\cos^2\phi}{\cos\delta\left[1 - \dfrac{\sqrt{\sin(\phi + \delta)\sin\phi}}{\cos\delta}\right]^2} \qquad (7)$$

$$y_a = 1.3 \text{ mm}; \quad y_p = 13 \text{ mm} \qquad (8, 9)$$

where P_{active} = active earth soil reaction; K_a = coefficient of active earth pressure; σ'_{0v} = vertical effective stress at depth z where P_{active} is calculated; δ = wall friction angle; u = pore pressure at depth z against the wall; b = width of wall considered; $P_{passive}$ = passive earth soil reaction; K_p = coefficient of passive earth pressure; $P_{at\ rest}$ = at rest earth soil reaction; ϕ = sand friction angle; OCR = overconsolidation ratio of the sand; y_a = deflection necessary to mobilize P_{active}; and y_p = deflection necessary to mobilize $P_{passive}$. Ignoring the effect of wall friction on K_a was found to give K_a values much higher than the back-calculated ones for the wall experiment described later. Also, y_a and y_p are taken as constant values at this time because such a criterion matches the two case histories. Because P_a and P_p increase with depth, constant values of y_a and y_p imply that the soil stiffness increases with depth as is reasonable to expect.

For the long-term analysis of walls in clay, the following pressures are used:

$$P_{active} = (K_a\sigma'_{0v} - 2c\sqrt{K_a} + u)b \qquad (10)$$

$$P_{passive} = (K_p\sigma'_{0v} - 2c\sqrt{K_p} + u)b \qquad (11)$$

$$P_{at\ rest} = [(1 - \sin\phi)\sqrt{OCR}\sigma'_{0v} + u]b \qquad (12)$$

$$K_p = \tan^2\left(45 + \frac{\phi}{2}\right); \quad K_a = \tan^2\left(45 - \frac{\phi}{2}\right) \qquad (13, 14)$$
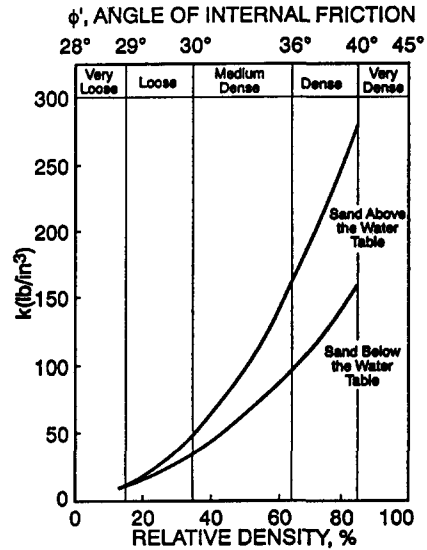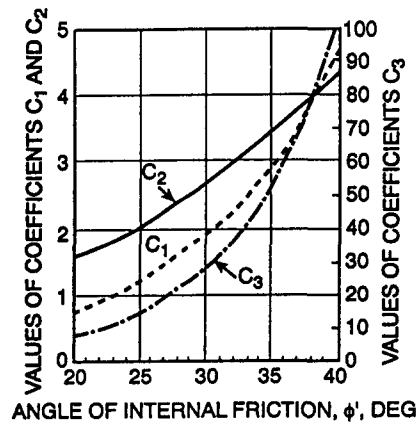

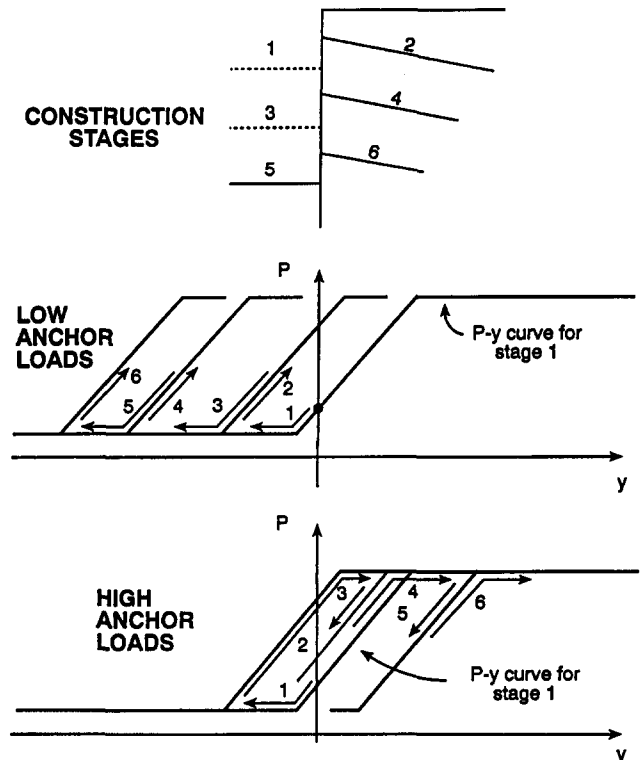FIG. 4. Parameters for Single-Pile P-y Curves in Sand (O'Neill & Murchison 1983)

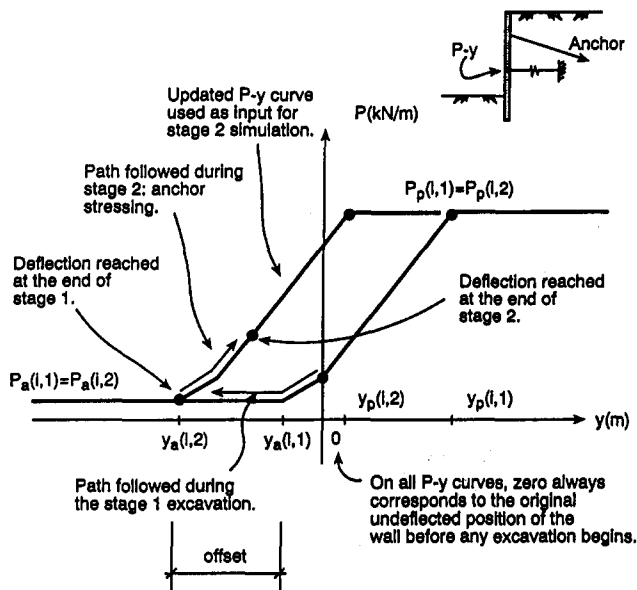FIG. 5. P-y Path Followed during Simulation of Construction Sequence

101

FIG. 6. Example of Updating Process for a *P*-*y* Curve on the Side of Retained Soil
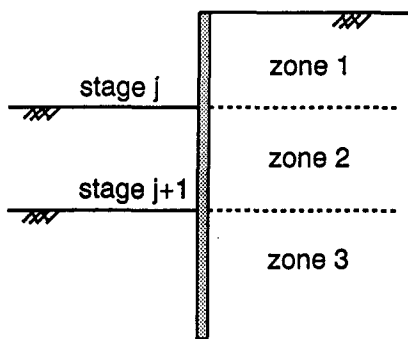

FIG. 7. Three Zones Involved with Sequence Simulation Process

In this case the wall friction is ignored because, although it is logical to expect it, there is no back-calculated *P*-*y* curve to prove its existence and the case histories compared relatively well with the predictions using the foregoing equations. Any negative soil reactions generated from (10) are considered to be zero.

For the short-term analysis of walls in clay, the following soil reactions are used:

$$P_{active} = (\sigma_{0v} - 2s_u)b; \quad P_{passive} = (\sigma_{0v} + 2s_u)b \quad (15, 16)$$

$$P_{at\ rest} = \sigma_{0v}b \quad (17)$$

where σ_{0v} = total vertical stress at depth z where the pressures are calculated; s_u = undrained shear strength of the clay; and b = width of wall considered. Again, any negative soil reactions generated from (15) are considered to be zero. The deflections y_a and y_p for clay are given in Table 1.

Any surcharge at the ground surface is treated as an increase in σ'_{0v} or σ_{0v} next to the wall. The *P*-*y* curves are nonsymmetrical multilinear curves as shown in Fig. 3. The flat plateaus in those *P*-*y* curves should be input with a slight slope to avoid potential convergence problems in computer programs. In the embedded portion of a slurry wall, a *P*-*y* curve is constructed on the active side and one is constructed on the passive side; the resultant *P*-*y* curve is the addition of the curves from both sides (Fig. 3).
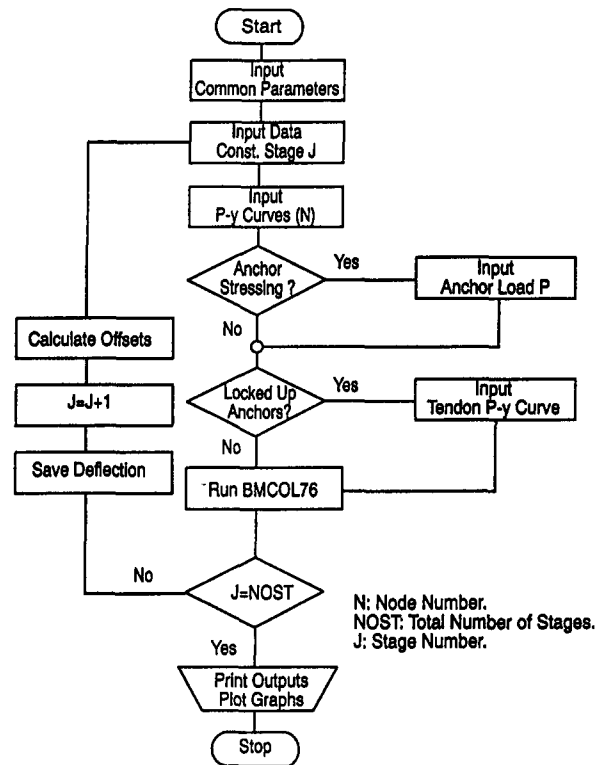
FIG. 8. Flowchart for Construction Sequence

N: Node Number.
NOST: Total Number of Stages.
J: Stage Number.
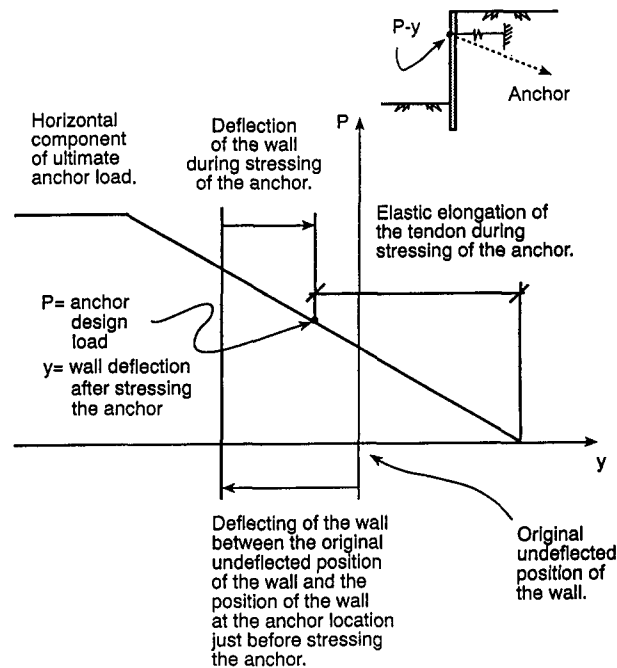
FIG. 9. Example of an Anchor *P*-*y* Curve

RECOMMENDED PILE *P*-*y* CURVES

Below the excavation level of a soldier pile and lagging wall the *P*-*y* curves to be used are those of single piles. The soldier piles are usually approximately 0.3 m in size and installed with a 2.5-m center-to-center spacing or approximately 6-pile diameter. At this large spacing, the piles are considered to be acting individually and single-pile *P*-*y* curves are used.

For soldier piles in sand, the *P*-*y* curves proposed by O'Neill and Murchison (1983) are recommended because of the recent and extensive calibration that led to them. These *P*-*y* curves are modified to take into consideration the fact that the ground surface is not horizontal in this case. Indeed the excavation

102

FIG. 10. Measured and Calculated Response for One-Row Anchor Wall at Texas A&M University (y, M, P, Q)

level is much lower than the ground surface behind the wall and this difference in elevation creates a net pressure on one side of the piles.

$$P_{us} = (C_1 z + C_2 D)\sigma'_{0v} - (-1)^j K_a \sigma'_e b \qquad (18)$$

$$P_{ud} = C_3 D\sigma'_{0v} - (-1)^j K_a \sigma'_e b \qquad (19)$$

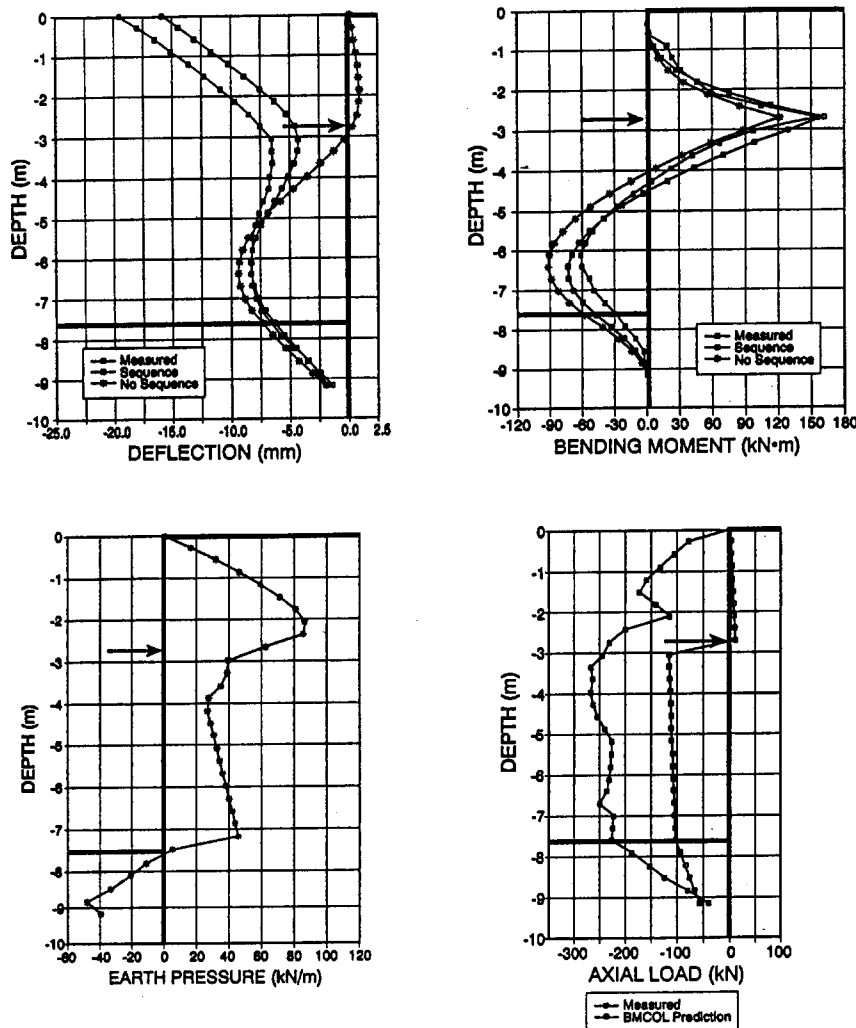$$P = AP_u \tan h\left(\frac{kz}{AP_u} y\right); \quad A = 3 - 0.8\frac{z}{D} \geq 0.9 \qquad (20, 21)$$

where P_{us} = soil reaction above the critical depth z_c; P_{ud} = soil reaction below the critical depth z_c; z_c = critical depth equal to $[(C_3 - C_2)/C_1] \times D$ (the coefficients C_1, C_2, and C_3 are given by Fig. 4); z = depth below the excavation level if the wall moves toward the excavation; z = depth below the top of the wall if the wall moves away from the excavation; D = pile diameter; σ'_{0v} = effective vertical stress at z; $j = 1$ if the wall moves away from the excavation and $j = 2$ if the wall moves toward the excavation; K_a = coefficient of active earth pressure [see (13)]; σ'_e = vertical effective stress at the excavation level behind the wall; b = width of wall being simulated; A = a coefficient defined in (21); $P_u = P_{us}$ or P_{ud}, depending on the depth; k = an initial modulus of subgrade reaction given by Fig. 4; and y = wall deflection.

For soldier piles in clay, the P-y curves proposed by Reese et al. (1975) were selected after trying several others because of the better match with the case histories. As in the case of sand, these P-y curves were modified to account for the une-

venness of the ground surface and to better match the case histories. They are elastic-plastic P-y curves defined by an ultimate value P_u and a deflection y_e necessary to mobilize P_u

$$P_{us} = A(\sigma_{0v} D + 2s_u D + 2.83s_u z) - (-1)^j p_e b \qquad (22)$$

$$P_{ud} = 11 A s_u D - (-1)^j p_e b \qquad (23)$$

$$p_e = K_a \sigma'_e - 2c\sqrt{K_a} \quad \text{for a long-term analysis} \qquad (24)$$

$$p_e = \sigma_e - 2s_u \quad \text{for a short-term analysis} \qquad (25)$$

$$y_c = 18 \text{ mm} \quad \text{if} \quad s_u < 200 \text{ kN/m}^2 \qquad (26)$$

$$y_c = 13 \text{ mm} \quad \text{if} \quad 200 < s_u < 400 \text{ kN/m}^2 \qquad (27)$$

$$y_c = 2.5 \text{ mm} \quad \text{if} \quad s_u > 400 \text{ kN/m}^2 \qquad (28)$$

where P_{us}, P_{ud}, D, z, b, K_a, and σ'_e have been defined for (18)–(21); $A = 0.2$ at $z = 0$, to 0.5 for $0 < z < 2D$, and to 1 for $z > 2D$; σ_{0v} and s_u are defined for (15)–(17); p_e = active horizontal pressure behind the wall at the excavation level; and σ_e = total vertical stress behind the wall at the excavation level.

RECOMMENDED ANCHOR P-y CURVES

One anchor can be simulated as an elastic-plastic spring. The elastic slope is given by the stretch of the steel tendon alone because the movement that takes place at the soil-grout interface is very small compared with the stretch of the tendon. The plastic plateau corresponds to the ultimate capacity of the
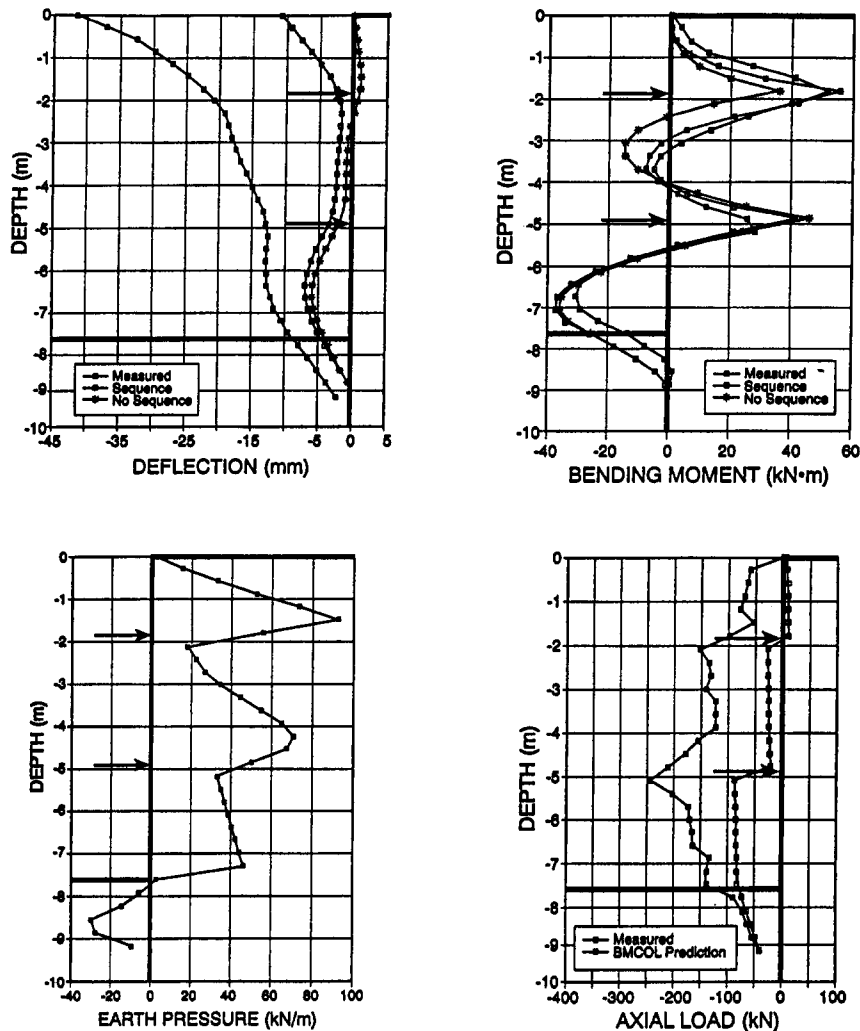
103

FIG. 11.   Measured and Calculated Response for Two-Row Anchor Wall at Texas A&M University (y, M, P, Q)

anchor, which is input as the chosen lock off load times an appropriate factor of safety (Briaud et al. 1996).

$$P_h = \frac{AE}{L_u + \dfrac{1}{2}L_b} y_h \qquad (29)$$

where P_h = horizontal load at the anchor head; A = cross section area of the steel tendon and E its modulus of elasticity; L_u = unbonded length of the anchor whereas L_b is its bonded length; and y_h = horizontal deflection at the anchor head. The ultimate capacity of the anchor is evaluated as for a pile. Note that the anchor P-y curve is offset by the deflection of the wall from the very beginning of construction to just after stressing the anchor as explained later. The length $L_u + 1/2L_b$ is used because it is assumed that the point of fixity is in the middle of the bonded length. Even though the anchor may be inclined, (29) holds true for the horizontal components as well as the vertical components of P and y because P and y are affected equally. Note that there also is a need to put a Q-w curve at the anchor location to simulate the action of the anchor in the vertical direction. This Q-w curve is similar to the P-y curve.

RECOMMENDED F-w AND Q-w CURVES

The soil loads the wall in the vertical direction as well and there is a need to simulate the soil reaction in the vertical direction through the use of F-W curves for side friction and of Q-W curves for point resistance. Those curves are represented by elastic-plastic models. The parameter F is the load

carried in friction per unit height of wall and for the width b of wall considered. The parameter Q is the load carried in point resistance at the bottom of the wall or of the pile.

For walls in sand, the following recommendations are made for the part of the wall that is above the excavation level:

$$F_{max} = 0.65K_a\sigma'_{0v}b \tan \delta; \quad w_f = 5 \text{ mm} \qquad (30, 31)$$

where K_a, σ'_{0v}, δ are those defined for (3)–(9); b = width of wall considered; F_{max} = maximum friction load per unit height of wall; and w_f = vertical displacement necessary to mobilize F_{max}. In (30), use is made of Terzaghi and Peck's (1967) empirical pressure for such walls.

For walls in sand the following recommendations are made for the part of the wall that is below the excavation level [after Briaud and Tucker (1996)]:

$$F_{max} \text{ (kN/m)} = 5N^{0.7}b \quad \text{for continuous walls} \qquad (32)$$

$$F_{max} \text{ (kN/m)} = 5N^{0.7}c \text{ for soldier piles;} \quad w_f = 5 \text{ mm} \qquad (33, 34)$$

$$Q_{max} \text{ (kN)} = 80\sqrt{N}bt \quad \text{for continuous walls} \qquad (35)$$

$$Q_{max} \text{ (kN)} = 100\sqrt{N}A_p \text{ for soldier piles;} \quad w_q = 10 \text{ mm} \qquad (36, 37)$$

where N = standard penetration test blow count in blows/0.3 m; c is the perimeter of the soldier pile in contact with the soil; Q_{max} = maximum point load; t = wall thickness; A_p = point area for the soldier pile; and w_q = vertical displacement necessary to mobilize Q_{max}.
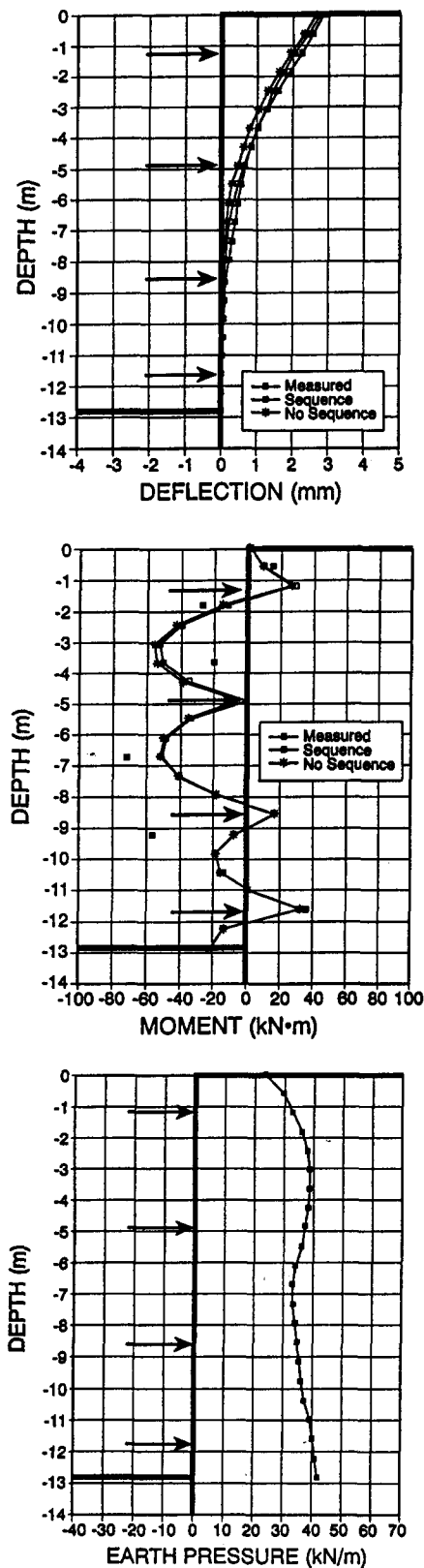
72 / JOURNAL OF GEOTECHNICAL AND GEOENVIRONMENTAL ENGINEERING / JANUARY 1998

104

FIG. 12. Measured and Calculated Response for Bonneville Tieback Wall (y, M, P)

For walls in clay, the following recommendations are made for the part of the wall that is above the excavation level:

$$F_{max} = 0.3\sigma'_{ov}b \tan \delta; \quad w_f = 5 \text{ mm} \quad (38, 39)$$

Here again use is made in (38) of an average Terzaghi and Peck (1967) empirical pressure behind the wall.

For walls in clay, the following recommendations are made

for the part of the wall that is below the excavation level [after American Petroleum Institute (1984)]:

$$F_{max} = \alpha s_u b \quad \text{for continuous walls} \quad (40)$$

$$F_{max} = \alpha s_u c \quad \text{for soldier piles;} \quad w_f = 5 \text{ mm} \quad (41, 42)$$

$$Q_{max} = 7s_u bt \quad \text{for continuous walls} \quad (43)$$

$$Q_{max} = 9s_u A_p \quad \text{for soldier piles;} \quad w_q = 10 \text{ mm} \quad (44, 45)$$

where s_u = clay undrained shear strength; and $\alpha = 1$ for $s_u \leq 25$ kN/m^2 to 0.5 for $s_u \geq 75$ kN/m^2, and varies linearly from 1 to 0.5 when s_u varies from 25 to 75 kN/m^2.

SIMULATING THE CONSTRUCTION SEQUENCE

The first construction stage consists of excavating the soil in front of the wall down to a depth of approximately 2.4 m. The second construction stage consists of installing a row of anchors at a depth of approximately 1.8 m and stressing them at the design load about 1 week later. The third construction stage consists of excavating the soil in front of the wall from 2.4 m down to a depth of approximately 5.5 m. The fourth construction stage consists of installing a row of anchors at a depth of approximately 4.9 m and stressing them approximately 1 week later. The fifth construction stage consists of excavating to approximately 7.6 m, which is the final excavation depth in this example. In the following discussion, the "jth stage" will be used to refer to the wall and loading configurations at the end of the jth construction stage.

With the beam-column approach, the wall behavior can be simulated by ignoring the stages and modeling the wall in its final configuration only; this is the "no-sequence" approach. Alternatively, each stage can be simulated, five in the foregoing example, to arrive at the final configuration; this is the "sequence" approach. The sequence approach is much more complicated and time consuming than the no-sequence approach; the question is: "does it make much difference in the predictions?" This is one of the questions that was investigated.

Note that any time a jth stage is to be simulated, the P-y curves are prepared such that y = 0 corresponds to the undeflected shape of the wall before any excavation begins (Figs. 4 and 5). The updated P-y curves together with the beam-column program lead to the deflections and other parameters corresponding to the jth stage. The deflections obtained after each stage are not the incremental deflections to be added together to obtain the total deflections; instead, the deflections obtained after each stage are the total deflections that can be compared directly with the measurements in the field. The deflections obtained after each stage are used as the starting point on the P-y curves once they are updated for the next stage. The P-y curve updating process is as follows.

During the construction sequence an element of soil next to the wall follows a certain path: the P-y path (Fig. 5). Keeping track of the P-y path and adjusting the P-y curves accordingly from one stage to the next is the key to a proper sequence approach. The input to the first stage simulation is a set of P-y curves as recommended in the previous sections. The output of the first stage simulation is among other things a set of deflections y(i, 1) at the nodes of the wall toward the excavation (path 1 in Fig. 5). During the stressing of the anchor (stage 2), the anchor force causes the wall to move back into the soil mass. Because of the plastic and hysteretic properties of the soil, the path followed on the P-y curve is not the original one but the one shown as path 2 in Fig. 4. This path can be obtained by shifting the original P-y curve by an offset $y_{off}(i, 1)$ equal to the plastic movement that occurred during the first stage (Fig. 6). The updated P-y curve is as shown in

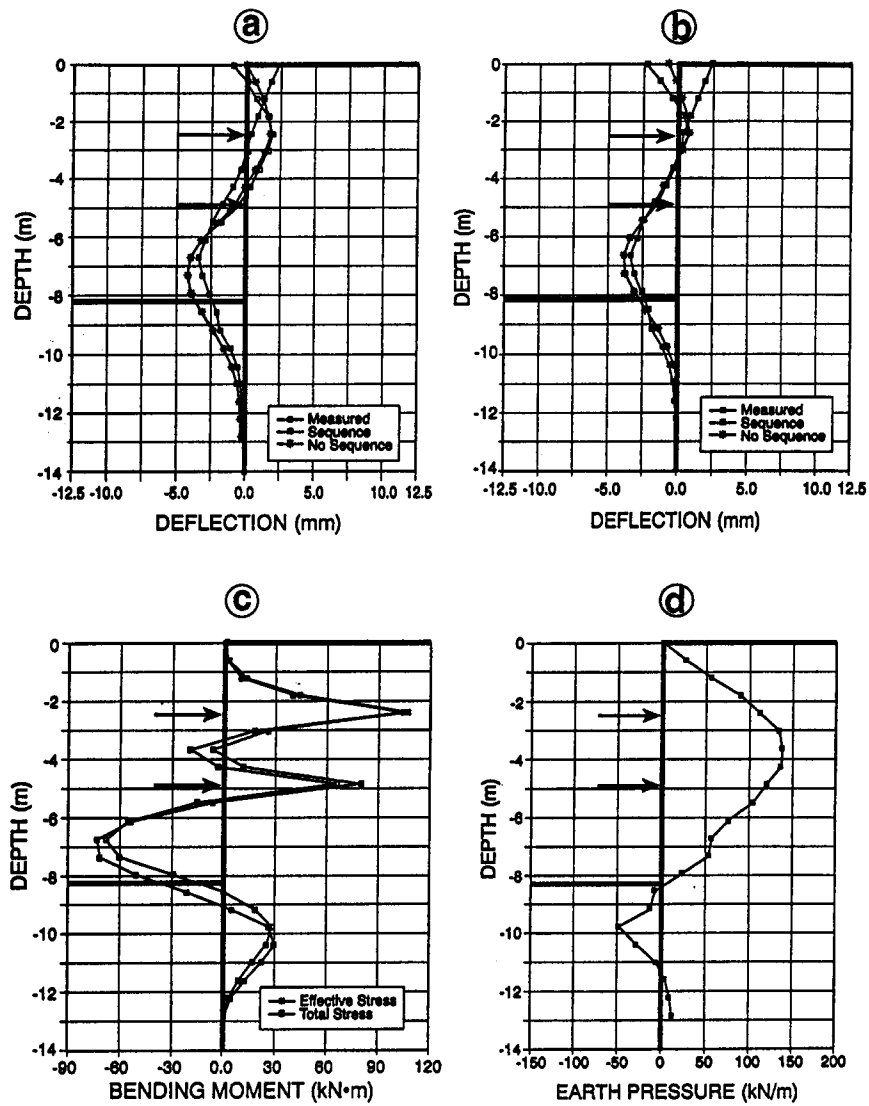JOURNAL OF GEOTECHNICAL AND GEOENVIRONMENTAL ENGINEERING / JANUARY 1998 / 73

105

FIG. 13. Measured and Calculated Response for the Lima Tieback Wall: (a) y for Effective Stress Analysis; (b) y for Total Stress Analysis; (c) Bending Moment; (d) Earth Pressure

Fig. 6 and is used as an input to stage 2. This updating process is followed for all stages and at all nodes.

The offset distance $y_{off}(i, 1)$ is critical to simulating the sequence process. The offset distances $y_{off}(i, 1)$ obtained from the jth stage simulation will be used to prepare the P-y curves to simulate the $(j + 1)$th stage. The offset $y_{off}(i, 1)$ should be calculated by comparing the deflection $y(i, j)$ obtained as an output of the jth stage simulation with the P-y curves used as an input to the jth stage simulation. The following rules govern the offset determination and therefore the P-y path. Three zones must be identified (Fig. 7). Zone 1 is the zone behind the wall above the excavation at the end of the jth construction stage. Zone 2 is the zone that was below the excavation level at the end of the jth construction stage but will be above the excavation level at the end of the $(j + 1)$th construction stage. Zone 3 is the zone that will be below the excavation level at the end of the $(j + 1)$th construction stage. For zone 1

$$\text{if } y(i, j) > y_p(i, j), y_{off}(i, j) = y(i, j) - y_p(i, j) \qquad (46)$$

$$\text{if } y_a(i, j) < y(i, j) < y_p(i, j), y_{off} = 0 \qquad (47)$$

$$\text{if } y(i, j) < y_a(i, j), y_{off}(i, j) = y(i, j) - y_a(i, j) \qquad (48)$$

Note that $y_{off}(1, j)$ is negative for (48). For zone 2

$$y_{off}(i, j) = y(i, j) \qquad (49)$$

For zone 3

$$y_{off}(i, j) = 0 \qquad (50)$$

where i = node number along the height of the wall; j = stage number; $y_a(i, j)$ and $y_p(i, j)$ = deflections required to mobilize the active and passive soil resistances $P_a(i, j)$ and $P_p(i, j)$ on the input P-y curves, respectively; $y_0(i, j)$ = deflection corresponding to the at-rest soil resistance $P_0(i, j)$ on the input P-y curves; $y_{off}(i, j)$ = offset distance used to prepare the P-y curves for the $(j + 1)$th stage simulation; and $y(i, j)$ = output deflection from simulating the jth stage.

The P-y curves for the first stage are the recommended P-y curves presented earlier. After each jth stage, new sets of $y_a(i, j + 1)$, $y_0(i, j + 1)$, and $y_p(i, j + 1)$ are calculated from the deflections obtained at every node i as an output of the jth stage simulation. These new sets are used to prepare the input P-y curves to simulate the $(j + 1)$th stage

$$y_a(i, j + 1) = y_a(i, j) + y_{off}(i, j) \qquad (51)$$

$$y_0(i, j + 1) = y_0(i, j) + y_{off}(i, j) \qquad (52)$$

$$y_p(i, j + 1) = y_p(i, j) + y_{off}(i, j) \qquad (53)$$

recommended P-y curves presented earlier are input for simulating the final excavation stage only. The flow chart of Fig. 8 summarizes the complete process. If the no-sequence option is chosen, the recommended P-y curves presented earlier are input for simulating the final excavation stage only.
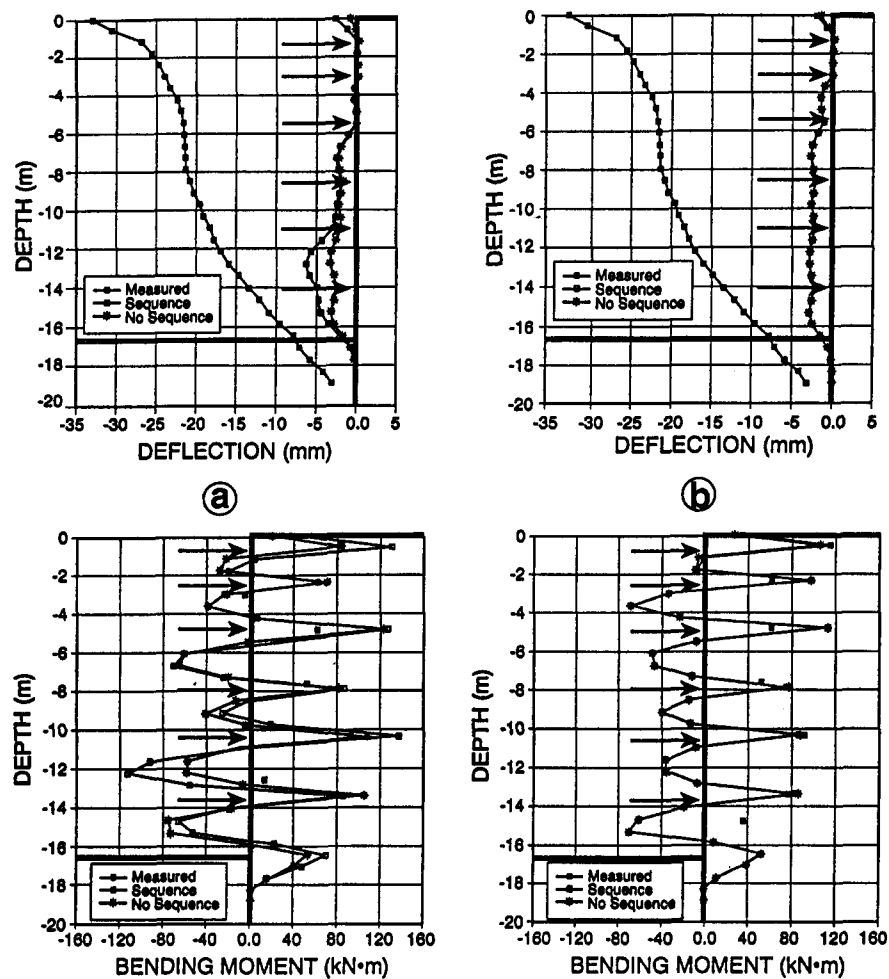
74 / JOURNAL OF GEOTECHNICAL AND GEOENVIRONMENTAL ENGINEERING / JANUARY 1998

FIG. 14. Measured and Calculated Response for the Boston Tieback Wall (y, M): (a) Effective Stress Analysis; (b) Total Stress Analysis

When an anchor is stressed with a load Q, this event is simulated by simply imposing a load Q on the wall at the anchor location. In subsequent stages the anchor force depends on the deflection of the wall at that location; this relationship is given by the anchor P-y curve. This P-y curve is the recommended P-y curve described in a previous section offset by the deflection of the wall from the very beginning of construction to just after the stressing of the anchor (Fig. 9).

COMPARISON WITH CASE HISTORIES

Four case histories are used to calibrate the proposed beam-column method and the associated P-y curves. Note that this is not a prediction of measured performance but the results of trial and error attempts to choose P-y curves to best match four case histories. The case histories include the Texas A&M University tieback wall in sand, the Bonneville tieback wall in sand, the Lima tieback wall in clay, and the Boston tieback wall in clay. The program used for this work was BMCOL76 (Matlock et al. 1981) modified to automate the data input and handle the simulation of the construction sequence.

The Texas A&M University (TAMU) wall is a 7.6-m-high soldier pile and lagging tieback wall built at the National Geotechnical Experimentation Site in a fine silty sand deposit (Chung and Briaud 1993). The sand deposit has the following average properties at the wall location: SPT (standard penetration test) blow count, 15 blows per foot; CPT (cone penetrometer test) point resistance, 6 MPa; PMT (pressuremeter test) limit pressure, 600 kPa, and PMT modulus, 7.5 MPa; BST (borehole shear test) friction angle, 32°; and estimated total unit weight, 18.1 kN/m³. A wall friction angle of 16° was

used in the beam-column predictions. The ground-water level was at a depth of 9.75 m. The wall itself is a soldier pile and lagging wall. The H-piles are 9.15 m long with a spacing of 2.4 m center to center and the wall height is 7.62 m. Half of this 50-m long wall has one row of anchors at a depth of 2.75 m and HP 10 × 57 soldier piles; the other half has two rows of anchors at a depth of 1.8 and 4.9 m and HP 6 × 25 soldier piles. The anchors are inclined downward at 30° and have a 2.4-m spacing. They apply with the wall an average horizontal pressure against the soil of 20 kN/m². Eight of the 22 soldier piles were instrumented with some 450 vibrating wire strain gauges for bending moment and axial-load determination, and 19 inclinometer casings for wall and soil mass movement. Figs. 10 and 11 show a comparison between the predictions by the beam-column method and the observed performance for the one-row and two-row-TAMU walls.

The Bonneville wall is a 12.8-m-high reinforced concrete diaphragm tieback wall built to retain temporarily the Union Pacific Railroad at the Bonneville Lock and Dam near Portland, Oreg. (Munger et al. 1990). The soil at the site is a heterogeneous mixture of alluvial silts, sands, gravels, cobbles, and boulders mixed with angular rock fragments and underlaid by a weak fine-grained sedimentary rock. This soil was classified as a sand and the following properties were used in the beam-column predictions: friction angle, 30°; total unit weight, 19.6 kN/m³; and wall friction angle, 30°. No water pressure was considered because of the dewatering system. The wall itself is a 0.91-m-thick reinforced concrete wall. The total height of the concrete wall is 18.9 m for a final excavation height of 12.8 m. Four rows of anchors were installed at depths

JOURNAL OF GEOTECHNICAL AND GEOENVIRONMENTAL ENGINEERING / JANUARY 1998 / 75

107

of 1.2, 4.9, 8.5, and 11.6 m. The horizontal anchor spacing was 3.35 m and the anchor inclination was 20° downward. The average pressure generated by the anchors and the wall against the soil was 120 kN/m². Deflections and bending moment measurements were reported for this case history. Fig. 12 is a comparison between the predictions by the beam-column method and the observed performance of the wall.

The Lima wall is an 8.2-m-high drilled shaft and wood lagging tieback wall in the city of Lima, Ohio (Lockwood 1988). The soil is a very stiff clay and the following properties were used for the beam-column predictions: undrained shear strength, 158 kN/m²; drained friction angle, 35°; drained cohesion intercept, 16.3 kN/m²; total unit weight, 21.1 kN/m²; OCR, 2.5; and wall friction angle, 12°. The water table was within the excavated depth; however, no water pressure was considered because of the free draining face of the wall. The wall itself is a soldier pile and lagging wall. The soldier piles are drilled shafts of 0.76 m in diameter and 12.8 m long; the reinforcement for the drilled shafts is made of a double channel C-15 × 33.9. The final excavation height is 8.2 m with anchor rows at depths of 2.4 and 4.9 m. The anchors were inclined downward at 20° and had a horizontal spacing of 1.8 m. The average pressure generated by the anchors and the wall against the soil was 50 kN/m². Only deflection measurements were available for this case history. Fig. 13 is a comparison of the measured data with the predictions using an effective stress approach and then an undrained approach.

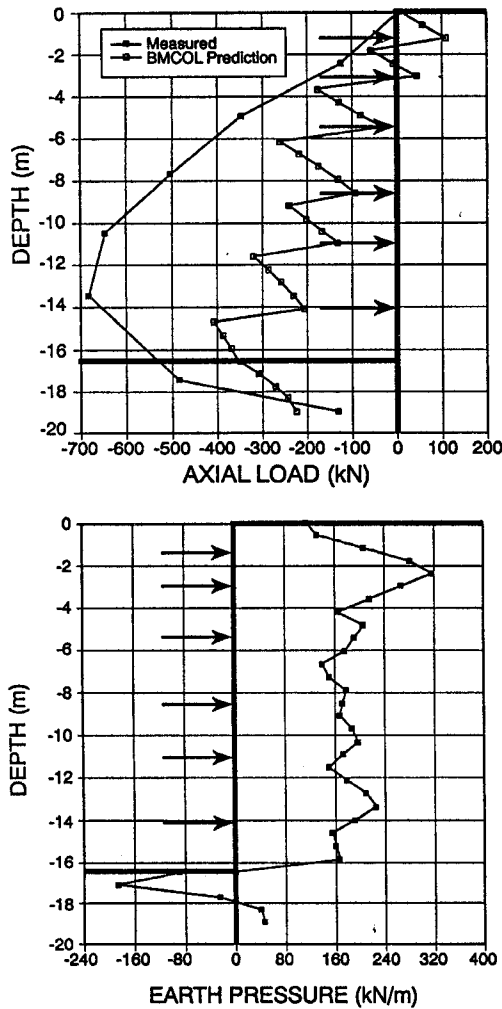The Boston wall is a 16.5-m-high drilled shaft and wood lagging tieback wall in Boston, Mass. (Houghton and Dietz 1990). The soil is a very hard clay or glacial till and the following properties were used for the beam-column predictions: undrained shear strength, 448 kN/m²; drained friction angle, 45°, total unit weight, 21.2 kN/m³; SPT blow count, 75 bpf; and wall friction angle, 23°. The water table condition was unclear and no water pressure was considered because of the free draining face of the wall. The wall itself is a soldier pile and lagging wall. The soldier piles are drilled shafts 0.91 m in diameter and 18.9 m long with a 3-m center-to-center spacing. The reinforcement for the drilled shafts was a pair of W-12 × 30 beams. The final excavation height is 16.5 m with anchor rows at depths of 1.2, 3, 5.5, 8.5, 11, and 14 m. The anchors were inclined downward at 25° and had a horizontal spacing of 3 m. The average pressure generated by the anchors and the wall against the soil was 70 kN/m². Both deflection and bending moments were measured for this case history. Figs. 14 and 15 are a comparison of the measured data with

A) Axial Load due to Anchor Stressing

B) Axial Load due to Downdrag of Soil Mass

C) Axial Load due to Anchor Stressing and Downdrag

D) Axial Load due to Anchor Stressing and Downdrag for Multi-anchored Wall

FIG. 16. Downdrag on Tieback Wall

FIG. 15. Measured and Calculated Response for Boston Tieback Wall (Q, P) Where Earth Pressure is for Total Stress Analysis

108

A) Movement of Anchor Bonded Zone

B) Horizontal Movement due to Settlement
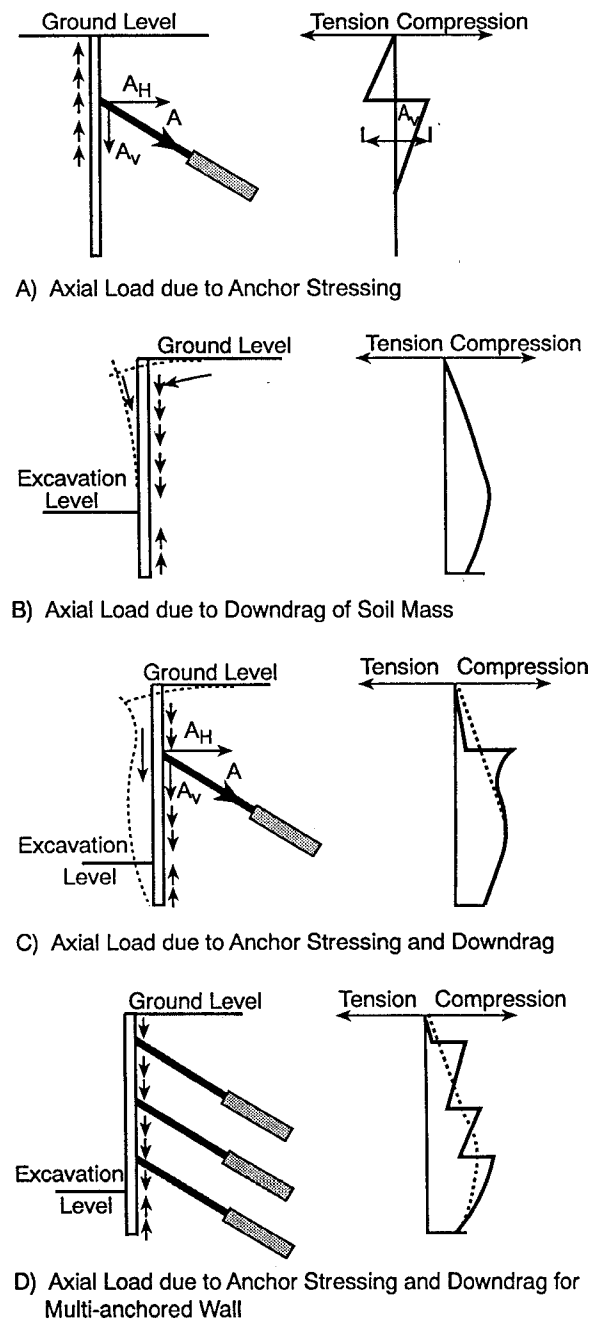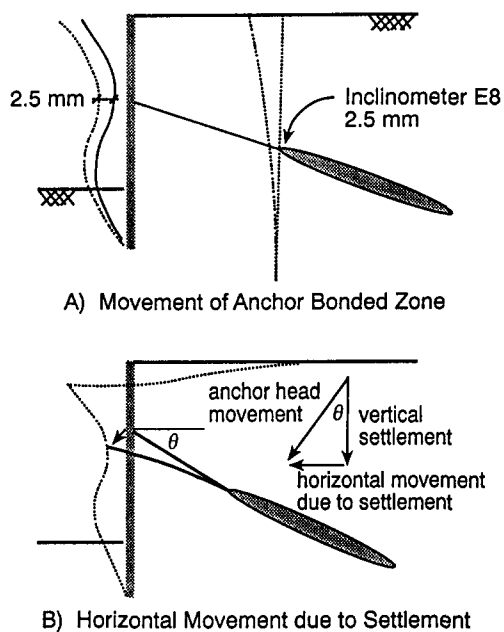
FIG. 17. Horizontal Deflections due to Mass Movement: (a) Movement of Anchor Bonded Zone; (b) Horizontal Movement due to Settlement

the predictions using an effective stress approach and then an undrained approach.

Several observations can be made when studying the comparisons between measured and predicted results for these four case histories. For the bending moments, the predictions are consistently close to the measurements. There is very little difference in bending moment predictions between the sequence and no-sequence runs and very little difference between the effective stress and undrained runs in clay. For the deflections, the predictions are erratic; they are good when the measured deflection is small (less than 5 mm) whereas they underpredict significantly when the measured deflection is large. This is attributed to the inability of the beam-column approach to predict mass movement. There is some difference between the sequence and no-sequence predictions of deflections with the sequence deflections being larger, but there is practically no difference between the effective stress and the undrained predictions in clay. For the axial loads the predictions are consistently too low by a significant amount. This is caused by, in part, the fact that the downdrag load on the wood lagging was ignored [use of D in (30) instead of b]. The downdrag effect is a result of the retained soil mass moving toward the excavation and downward (Fig. 16). This movement is more severe if the anchors are short and do not apply enough pressure to hold the soil back. Note that the vertical movement of the wall induced by the vertical component of the anchor loads and by the general downdrag can induce a significant horizontal movement by rotation around the anchor bulb (Fig. 17). This leads one to think that a wall with a strong point resistance will deflect less horizontally.

INFLUENCING FACTORS

A parametric study was performed with the beam-column method to identify the parameters that influenced the predictions the most. The parameters that were varied were the soil pressure coefficients K_a, K_0, and K_p; the soil reference deflections y_a and y_p; and the wall bending stiffness EI. The sensitivity analysis was performed for the TAMU wall with one row of anchors in sand and for the Lima wall with one row of anchors in clay. The influence of the foregoing parameters

on deflections, bending moments, and earth pressures was studied.

For the deflections, the coefficient K_a is most influential; when K_a was multiplied by 2, the maximum deflection was multiplied by 3 for the more flexible TAMU wall in sand and by 2 for the more rigid Lima wall in clay (effective stress analysis). The bending stiffness EI was the next most influential parameter; when EI was multiplied by 2, the maximum deflection was multiplied by 0.55 for the TAMU wall, by 0.57 for the effective stress analysis of the Lima wall, and by 0.90 for the total stress analysis on the Lima wall. The reference deflection y_a was the next most influential parameter; when y_a was multiplied by 2, the maximum deflection was multiplied by 1.07 for the TAMU wall and by 1.7 for the effective stress and the total stress analysis of the Lima wall. The other parameters, K_0, K_p, and y_p, had negligible influence on the deflections.

For the bending moment, the coefficient K_a and the wall stiffness EI are most influential; when K_a was multiplied by 2, the maximum bending moment was multiplied by 1.6 and occurred at a different location for the TAMU wall and remained unchanged for the Lima wall (effective stress). When EI was multiplied by 2, the maximum bending moment was multiplied by 1.05 for the TAMU wall and by 1.56 for the effective stress and total stress analysis of the Lima wall. The reference deflection y_a had a small influence whereas y_p, K_0, and K_p had negligible influence.

For the earth pressure distribution, only K_a had a significant influence. Note that the influence of these parameters is highly nonlinear for a given wall and also will vary significantly from one wall to another depending on the wall geometry and the anchor location. Therefore the foregoing results can only be used qualitatively.

COMPARISON WITH OTHER METHODS

To evaluate the accuracy of the beam-column method compared with the pressure diagram methods, the case of the TAMU two-row anchor wall in sand was used (Chung and Briaud 1993). The following methods were used: Terzaghi and Peck (1967) combined with the tributary method for anchor
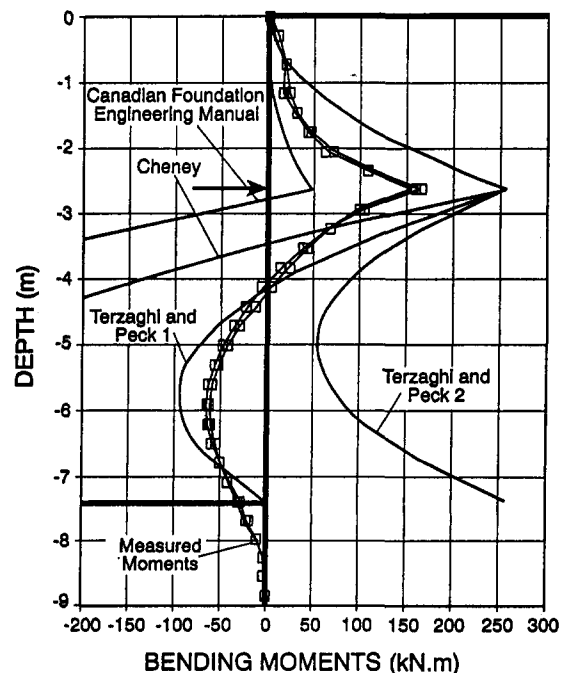

FIG. 18. Measured and Predicted Bending Moment Profiles by Various Methods (One-Row Anchor Wall at Texas A&M University)
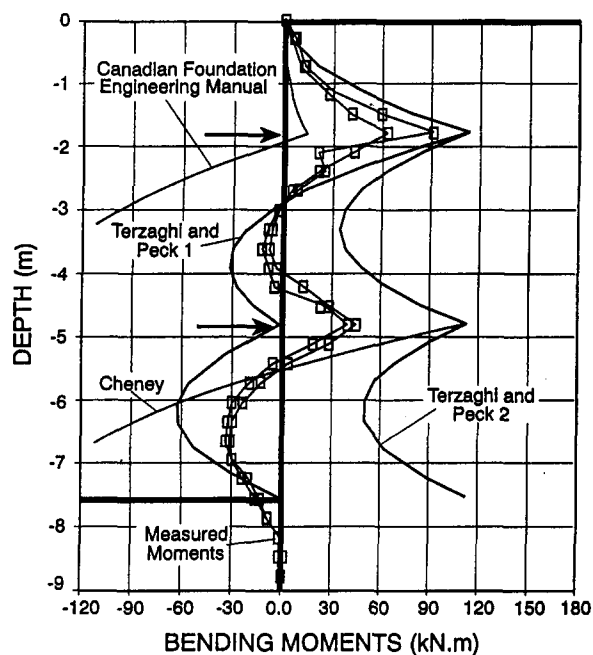
FIG. 19. Measured and Predicted Bending Moment Profiles by Various Methods (Two-Row Anchor Wall at Texas A&M University)

load determination, Terzaghi and Peck (1967) combined with the hinge method for anchor load determination, and the Canadian Geotechnical Society (1985), the Cheney method (1988). Figs. 18 and 19 show a comparison of the bending moment diagrams obtained by the various methods for the one-row and two-row anchor wall at Texas A&M University. It is clear that the beam-column method represents an improvement in the prediction of the bending moment diagram. Note, however, that this is not a fair comparison because the parameters used for the beam-column prediction come in part from back calculations using this case history. Future comparisons against independent case histories are needed. Nevertheless it is obvious that the fundamental approach in the beam-column method is superior to the drastic assumptions of the empirical methods provided the input parameters to the beam-column method have been calibrated against full-scale case histories.

CONCLUSIONS

The basis for these conclusions is the construction, instrumentation, and monitoring of a full-scale research tieback wall in sand, three instrumented production tieback walls in sand and in clay, a sensitivity analysis to evaluate the influence of various input parameters, the development of an excavation sequence simulation technique, and comparison of the beam-column approach and the pressure diagram approach to measured data. On the basis of this evidence, the following conclusions and recommendations are drawn:

1. Recommendations are made concerning the P-y curves, F-w curves, and Q-w curves for use in the beam-column analysis of tieback walls. Considering the small number of case histories used to calibrate those curves compared with the number of parameters involved, these recommendations can be considered only as preliminary. Further comparisons with case histories not involved in the calibration will be particularly useful.
2. The beam-column technique to simulate the construction sequence when building a tieback wall is developed. The P-y path method is used to handle the soil hysteresis

during the excavation steps (unloading) and the anchor stressing steps (reloading).

3. The simulation of the construction sequence is cumbersome and does not appear to be necessary for bending moment predictions. Indeed there is little difference in the predicted bending moment profiles between the sequence and the no-sequence runs. Yet the sequence runs give closer predictions.
4. The simulation of the construction sequence gives a better prediction of the deflection profiles than the no-sequence approach. The predictions are close to the measurements if the measured deflections are small (say less than 25 mm) but the predictions grossly underestimate the measured deflections if the measured deflections are large. This is attributed to the inability of the beam-column method to predict mass movements.
5. The beam-column method does give an idea of the vertical load distribution in the wall. The predictions underestimate the measured vertical loads, however. This is attributed to the sagging of the retained soil mass, which moves downward and toward the excavation. In the process, the soil applied a downdrag load on the wall and this vertical load is not predicted by the beam-column method.
6. The factors that influence the bending moments and deflection predictions the most are the coefficient of active earth pressure K_a and the bending stiffness of the wall EI. The other parameters such as y_a, y_p, K_0, and K_p have little influence.
7. A comparison on a tieback wall in sand of methods based on an assumed pressure diagram is presented. It shows that the Terzaghi and Peck (1967) pressure diagram combined with the hinge method (Lambe and Wolfskill 1970) gives the best results and that methods based on active and passive pressure diagrams lead to unreasonable results. The comparison also shows that the beam-column method gives better results than the best pressure diagram method.
8. The beam-column method is a deflection-based method that satisfies the vertical, horizontal, and moment equilibrium of the wall. These significant and fundamental advantages over the pressure diagram methods make is a superior method, which should be used any time the added complexity is warranted. The most severe limitation of the beam-column method is its inability to properly account for mass phenomena, namely, mass movement and downdrag. The most useful aspect of the beam-column method is its ability to give better bending moment profiles than the pressure diagram methods.

ACKNOWLEDGMENTS

APPENDIX. REFERENCES

American petroleum institute recommended practice 2a for planning, designing, and constructing fixed offshore platforms. (1984). American Petroleum Institute (API), Dallas, Tex.

Briaud, J.-L., Powers, W. F., and Weatherby, D. E. (1998). "Grouted anchors should have short bonded lengths." *J. Geotech. and Geoenvir. Engrg.*, ASCE, 124(2).

Briaud, J.-L, and Tucker, L. M. (1996). "Design and construction guide-

110

lines for downdrag on uncoated and bitumen-coated piles.'' *NCHRP Res. Rep. 393*, Dept. of Civ. Engrg., Texas A&M Univ., College Station, Tex.

Canadian foundation engineering manual (CFEM). (1985). Canadian Geotechnical Society, BiTech Publishers, Vancouver, B.C., Canada.

Cheney, R. S. (1988). "Permanent ground anchors." *Rep. No. FHWA-DP-68-1R*, Federal Highway Administration, Washington, D.C.

Chung, M., and Briaud, J.-L. (1993). "Behavior of a full scale tieback wall in sand." *Res. Rep. to Schnabel Foundation and the Federal Highway Administration*, Dept. of Civ. Engrg., Texas A&M Univ., College Station, Tex.

Clough, W. G. (1984). *User's manual for program SOILSTRUCT.* Department of Civil Engineering, Virginia Polytechnical Institute, Blacksburg, Va.

Clough, W. G., and Tsui, Y. (1974). "Performance of tieback walls in clay." *Proc., J. Geotech. Div.*, ASCE, 12(100), 1259–1273.

Coulomb, C. A. (1776). "Essai sur une Application des Regles des Maximis et Minimis a quelques Problemes de Statique Relatifs a l'Architecture." *Mem. Acad. Roy. des Sciences*, Paris, France, 3, 38.

Haliburton, T. A. (1968). "Numerical analysis of flexible retaining structures." *Proc., ASCE*, 94(6), 1233–1251.

Hetenyi, M. (1946). *Beams on elastic foundations.* University of Michigan Press, Ann Arbor, Mich.

Houghton, R. C., and Dietz, D. L. (1990). "Design and performance of a deep excavation supports system in Boston, Massachusetts." *Proc., ASCE Spec. Conf. on Des. and Perf. of Earth Retaining Struct.*, ASCE, New York, N.Y., 795–816.

Kim, N.-K., and Briaud, J.-L. (1994). "A beam column method for tieback walls." *Res. Rep. to Schnabel Found. and the Fed. Hwy. Admin.*, Dept. of Civ. Engrg., Texas A&M Univ., College Station, Tex.

Lambe, T. W., and Wolfskill, A. L. (1970). "Measured performance of braced excavation." *J. Soil Mech. and Found. Div.*, ASCE, 95(6), 817–836.

Lockwood, M. E. (1988). "Retention system monitoring demonstration project no. 68." *Progress Rep. for the Ohio Dept. of Transp.*, Ohio DOT, Cincinnati, Ohio.

Long, J. H., Cording, E. J., and Mueller, C. G. (1996). "Analysis and behavior of tieback walls." *Rep. to Schnabel Found. Co.*, Dept. of Civ. Engrg., Univ. of Illinois, Urbana, Ill.

Matlock, H., Bogard, D., and Lam, I. (1981). "BMCOL76: a computer program for the analysis of beam-columns under static axial and lateral loading." Program developed at the University of Texas at Austin, under grant from Fugro, Inc., and documented at Ertec, Inc., Long Beach, Calif.

Mueller, C. G. (1996). "Behavior of model-scale tieback walls in sand," PhD dissertation, Department of Civil Engineering, University of Illinois, Urbana, Ill.

Mueller, C. G., Long, J. H., Cording, E. J., and Weatherby, D. E. (1994). "Ground movements from tieback wall construction." *ASCE Conf. on Vertical and Horizontal Deformation for Found. and Embankments, Geotech. Spec. Publ. No. 40*, ASCE, New York, N.Y., 1337–1352.

Munger, D. F., Jones, P. T., and Johnson, J. (1990). "Temporary tieback wall, Bonneville Navigation Lock." *Proc., ASCE Spec. Conf. on Des. and Perf. of Earth Retaining Struct.*, ASCE, New York, N.Y., 778–794.

O'Neill, M. W., and Murchison, J. M. (1983). "An evaluation of *P-y* relationships in sands." *Res. Rep. No. GT-DF02-83*, Dept. of Civ. Engrg., Univ. of Houston, Houston, Tex.

Powers, W. F., and Briaud, J.-L. (1993). "Behavior of 10 full scale ground anchors installed in clay." *Res. Rep. to Schnabel Found. and the Fed. Hwy. Admin.*, Dept. of Civ. Engrg., Texas A&M Univ., College Station, Tex.

Reese, L. C., Cox, W. R., and Koop, F. D. (1975). "Field testing and analysis of laterally loaded piles in stiff clay." *Proc., 7th Annu. Offshore Technol. Conf., Vol. II*, OTC, Richardson, Tex., 671–690.

Terzaghi, K., and Peck, R. B. (1967). *Soil mechanics in engineering practice*, 2nd ed., John Wiley & Sons, Inc., New York, N.Y.

Winkler, E. (1867). *Die Lehre von Elastizitat und Festigkeit.* H. Dominicus, Prague, Czechoslovakia.

111

BEHAVIOR OF FULL-SCALE VERT WALL IN SAND

By Jean-Louis Briaud,[1] Fellow, ASCE, Peter Nicholson,[2] Member, ASCE, and Jonghyub Lee[3]

ABSTRACT: The VERT wall is a new type of top-down retaining wall, which derives its name from the fact that it is vertically reinforced. Typically, three to four rows of 1-m-diameter cemented-soil columns are constructed to the depth of soil to be retained. After curing of the cement, the soil in front of this gravity wall is excavated in one step. To study the viability of this new wall type, a 10-m-high, 40-m-long, and 5.6-m-wide VERT wall was built at the National Geotechnical Experimentation Site at Texas A&M University. The soil is a medium-dense silty sand, and the wall was instrumented for horizontal and vertical movement. One year after excavation the horizontal movement of the wall was 24.6 mm and the settlement was 9.3 mm. These values are very close to the movements of the similar size tieback wall built at the same site. This performance is an indication of the viability of this new wall type.

INTRODUCTION

A new type of top-down retaining wall has been developed. The wall construction consists of drilling several rows of cemented-soil columns down to the depth of soil to be retained, as shown in Figs. 1 and 2. Then, when the cement has cured, excavation proceeds in one step. The columns are built using deep soil mixing equipment and a final ratio of dry cement weight divided by soil weight of about 0.2. The ratio of the volume of cemented soil as compared to the global volume of the vertically reinforced soil mass is about 0.3, and the ratio of the weight of cement used over the weight of the vertically reinforced soil mass is about 0.06.

To study the behavior of this new wall type, Geo-Con built and instrumented a full-scale VERT wall at the National Geotechnical Experimentation site (NGES) at Texas A&M University (TAMU). The university collected the long-term readings of the instrumentation, reduced the data, and analyzed the results. This article presents the results of this large-scale project, including soil properties, wall construction, instrumentation, cemented-soil properties, and observed performance.

SITE AND SOIL PROPERTIES

At NGES-TAMU there are two sites, a sand site and a clay site. The VERT wall was built at the sand site. Geologically the sand is a floodplain deposit of Pleistocene age (Jennings et al. 1996). This sand has a high fine content with occasional clay layers due to the relatively low energy depositional environment. Some cleaner sand layers, which correspond to old river channels, are found from time to time. Below these 200,000-year-old sand layers and about 10 m below the ground surface is the 45,000,000-year-old Eocene bedrock; this bedrock is a dark gray clay shale that was deposited in a series of marine transgressions and regressions.

Many laboratory and in situ tests have been performed on the sand (Briaud 1997). The average properties are as follows: Mean grain size $D_{50} = 0.2$ mm; standard penetration test (SPT) blow count = 18 blows per 0.3 m; cone penetrometer test point resistance = 6 MPa; pressuremeter test limit pressure = 800 kPa; pressuremeter test modulus = 8.5 MPa; dilatometer test

modulus = 30 MPa; borehole shear test friction angle = 32°; estimated total unit weight = 18 kN/m³; and cross-hole shear-wave velocity = 240 m/s. The water table is 7.2-m deep, and the average water content above the water table is 15%. At the specific location of the VERT wall, two borings were drilled and gave the results shown on Figs. 3–5.

WALL CONSTRUCTION

Prior to construction of the VERT wall a 1-m-thick fill was placed on top of the original ground surface. The purpose was to ensure that the final excavation level would remain above the water table. The borings shown in Figs. 3–5 were drilled before the fill was placed. They indicated that, while the deposit is primarily a dirty sand, some clay layers exist within the excavation depth. The sand from the site was used for the fill, which was compacted by rolling over it with construction equipment.

Next the cement-soil columns were drilled with a drilling rig equipped with a 0.91-m-diameter cutting and mixing head. The drilling fluid was a water and cement slurry in the ratio of 1.75 to 1 (weight of water over weight of cement = 1.75), with a wet unit weight of 13.04 kN/m³. The drilling proceeded with the addition of a cement slurry; the cement slurry to soil ratio by weight was approximately 0.55. All columns were drilled to a depth of 8.5 m below the top of the fill. The soil-cement mixing system consisted of a specially designed hollow-stem discontinuous auger fitted with mixing paddles. During the insertion phase, the auger loosened the soil as the cement slurry or grout was pumped through the hollow stem. Mixing bars above the auger blended the grout and the soil into a soilcrete column. Once the drill reached the required depth, the rotation direction of the auger was reversed and a slow withdrawal began as grout continued to be pumped. Approximately 80% of the target volume of slurry was injected during insertion; the balance was injected during withdrawal. The drilling and grouting of one 0.9-m-diameter and 8.5-m-deep column took between 20 and 30 min. During construction of the columns, various drilling parameters were monitored to ensure that the correct amount of cement was used and that the soil and cement were homogeneously mixed.

A front row (Row A) of 43 contiguous columns, 0.91 m in diameter and 8.5-m deep, was constructed (Figs. 6–8). Immediately behind this front row of columns, a second row (Row B) was constructed with a center-to-center column spacing of 1.82 m. A third row (Row C) and a fourth row (Row D) were constructed to maintain the 1.82-m spacing, as shown in Fig. 6. On top of the wall, a 1-m-thick relieving platform was built (Figs. 7 and 8) using the soil slurry spoils ejected from each hole. Note that this platform covered only about 3/4 of the wall (Fig. 8). The global volume of soil treated was 9.5-m high, 5.6-m wide, and 40-m long.

The cement-soil mixing process ended April 17, 1998. On

[1]Spencer J. Buchanan Prof., Dept. of Civ. Engrg., Texas A&M Univ., College Station, TX 77843-3136.

[2]Pres., Geo-Con, 4075 Monroeville Blvd., Corporate 1, Build. 2, No. 400, Monroeville, PA 15136.

[3]Des. Engr., Tensar Earth Technologies Inc., 5775-B Glenridge Dr., Lakeside Ctr., Ste. 450, Atlanta, GA 30328-5363.
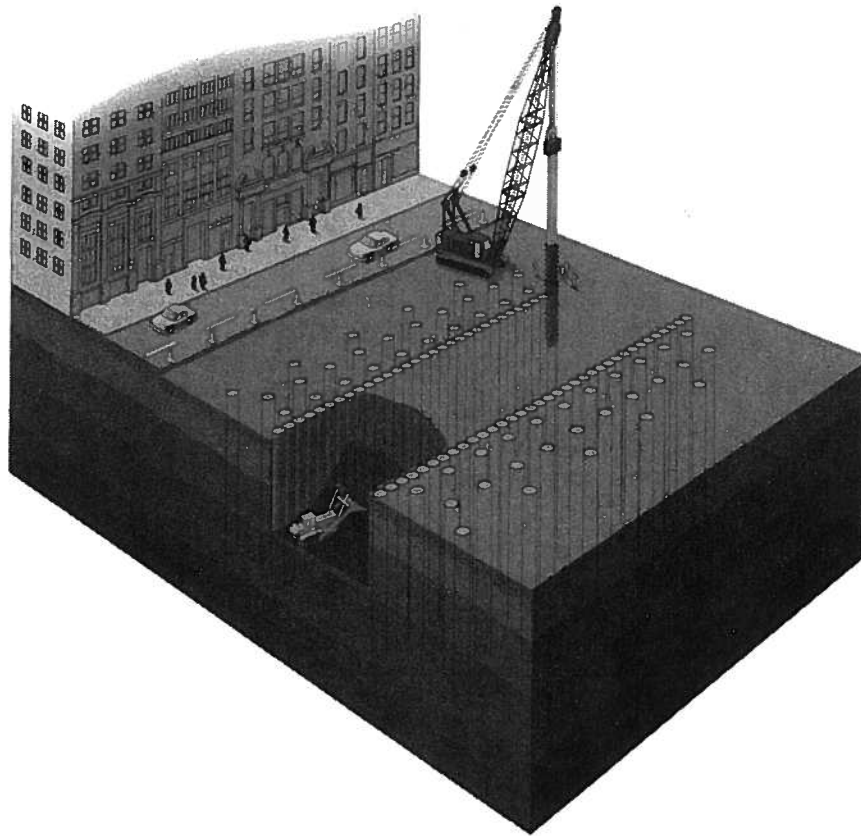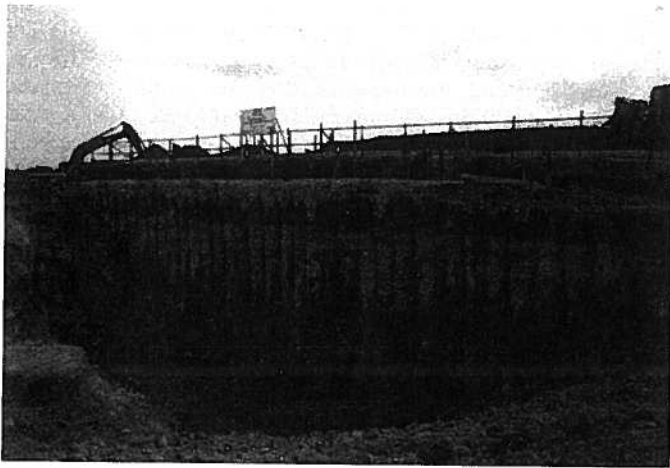
FIG. 1. VERT Wall Concept

FIG. 2. Completed VERT Wall

May 9, 1998, a 1-m-thick surcharge to simulate construction equipment loading was placed on top of the wall at the same time as a 1-m excavation was performed in front of the wall (Fig. 9); this is called Phase I Stage 1. Then excavation proceeded to 4 m below the original ground level; this is Phase I Stage 2. Phase I Stage 3 consisted of excavating to 7 m below the original ground level. Phase II Stage 1-2 consisted of placing a 2-m surcharge behind the wall (Fig. 9) while 1 m more of surcharge was added behind the wall to complete Phase II Stage 3. The final depth of excavation was 10 m below the top of the surcharge, 9 m below the top of the relieving platform, 8 m below the top of the columns or of the fill, and 7 m below the original ground level. The sides of the excavation had a slope of approximately 1.5 horizontal to 1 vertical (Fig. 8). Fig. 2 is a photograph of the completed wall. Note that the soil layering is apparent on the front face of the wall, with the clayey sands at the top and bottom of the

wall (darker zones) and the clean sand in the middle (lighter zone).

INSTRUMENTATION

The wall was instrumented to monitor the horizontal and vertical movements during excavation and surcharge. The instruments included horizontal extensometers, inclinometers, vertical extensometers, and survey targets. Five instrument arrays were installed in the wall at the locations shown on Fig. 6. Table 1 and Fig. 6 give the details of what instrument was placed at what location. Twenty 70-mm-diameter inclinometer casings were grouted in predrilled holes; the bottom of the casings was located 4 m below the final excavation level of the wall. Zero readings were taken after the grout had set. The readings were taken every 0.61 m while pulling the Digitilt probe up. The data was collected with a Digitilt Datamate and reduced using the Digipro software. All are Slope Indicator Inc. products.

Five horizontal extensometers were installed in 0.61-m-deep trenches at the top of the wall and running perpendicular to the wall face. These trenches were backfilled with a soil-cement slurry mixture after installation. Multipoint rod extensometers with groutable anchors (Geokon Model A-3) were selected to measure the horizontal movements at four points. Each horizontal extensometer gave the horizontal movement of points 0.5, 1.5, 3.1, and 4.8 m behind the top of the wall face. The extensometers consisted of steel rods housed in a protective sheath with a spade anchor at the end of the steel rod. At the measuring end, the rod was anchored in the wall, and at the recording end, the rod was free to move with respect to a fixed benchmark. Both ends of the rod moved the same amount thanks to the sheath. The benchmark was placed 16 m behind the front face of the wall. The movement of the rod with respect to the benchmark was measured with a micrometer and represented the horizontal movement of a point in the wall with respect to the benchmark location.

113

Depth in Meters	Penetrometer Readings (100kPa)	Blows / 0.3m	DESCRIPTION OF STRATUM
1	3.0	13	Medium dense, lt. brown, medium to fine SAND; trace silt. (SP)
		21	
2	4.0+	18	Stiff to hard, red-gray mottled to red, sandy CLAY to clayey SAND. (CL/SC)
3	1.5	14	
4		14	Medium dense, lt. brown, medium to fine SAND; some clay. (SC)
		19	
5		24	Medium dense, lt. brown, medium to fine to coarse SAND; little clay. (SC)
6		15	
		17	
7		16	
8	2.5	21	Stiff to very stiff, red, sandy CLAY to clayey SAND with gravel. (CL/SC)
9	1.5	21	
		40	
10		43	
11	4.0+	40	Dense, gray medium to fine, clayey SAND; occasional hard clay seams. (SC)
12		50/9"	
			End of Boring at 12 meters

FIG. 3. Boring Log No. 1

FIG. 5. SPT Results

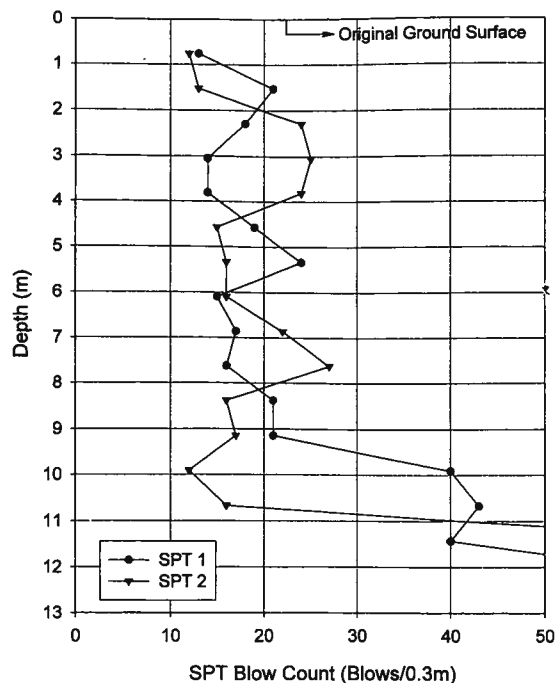| Depth in Meters	Penetrometer Readings (100kPa)	Blows / 0.3m	DESCRIPTION OF STRATUM
1	4.0+	12	Medium dense, lt. brown, medium to fine SAND; trace clay. (SP)
		13	
2	4 0+	24	Hard, gray-red mottled to red, sandy CLAY to clayey SAND; trace gravel. (CL/SC)
3	4.0+	25	
4		24	
		15	
5		16	Medium dense, red to lt. brown, fine to medium SAND; little clay, trace gravel. (SM)
6		16	
		22	
7		27	
8		16	Medium dense, lt. brown, fine to coarse SAND; with gravel, some clay, occasional clay and clayey sand seams. (SM/SC)
9		17	
10		12	
		16	
11		50/8"	Medium dense, gray medium to fine silty SAND; occasional clay seams. (CL/SC)
12		50/8"	
			End of Boring at 12 meters

FIG. 4. Boring Log No. 2

Six vertical extensometers were installed in 14-m-deep, 125-mm-diameter boreholes. These boreholes were grouted after installation of the extensometers. Multipoint rod extensometers with hydraulic anchors (Slope Indicator Inc.) were selected to measure the vertical movements in four depths. Each vertical extensometer gave the vertical movement of points 4.3, 7.0, 10.1, and 13.7 m below the top of the wall. The extensometers are steel rods housed in a protective sheath. At the measuring end, the rod was connected to an anchor that was hydraulically pushed into the soil and looked like a small umbrella flipped inside out by the wind. At the recording end (top of the wall), the rod was free to move with respect to a fixed benchmark made of a shallow casing. Both ends of the rod moved the same amount thanks to the sheath. The movement of the rod with respect to the benchmark was measured with a micrometer and represented the difference in vertical movement between the anchor location and the top of the wall.

MODULUS AND STRENGTH

Immediately after construction of certain columns, fluid samples of the soil cement mixture were collected with a sampler at various depths. Compressive strength tests were performed on the samples at 3, 7, 28, and 56 days. The unconfined compressive strength (UCS) results are shown in Fig. 10. This figure shows the gain in strength as a function of time and the variability of the strength from one sample to the next. This variability was taken into account in the design process; indeed, for this particular wall the target strength for design purposes was 690 kPa at 28 days before starting the excavation. As can be seen, even the lowest measured 28-day UCS was twice the design value. The rate at which a soil-cement mixture gained strength was compared to the rate for concrete. The concrete data from Dobrowolski (1998) is shown in Fig. 11 and compared to the soil-cement mixture of the VERT wall. The rate of strength gain for concrete is appreciably quicker than the soil-cement mixture of this wall. Lin and Wong (1999) performed UCS tests on mixtures of cement and soft clay. Their data indicated an even slower strength gain than for the VERT wall.

Column CW-2 was constructed on April 17, 1998, and core drilling was performed on May 13, 1998, to retrieve in situ
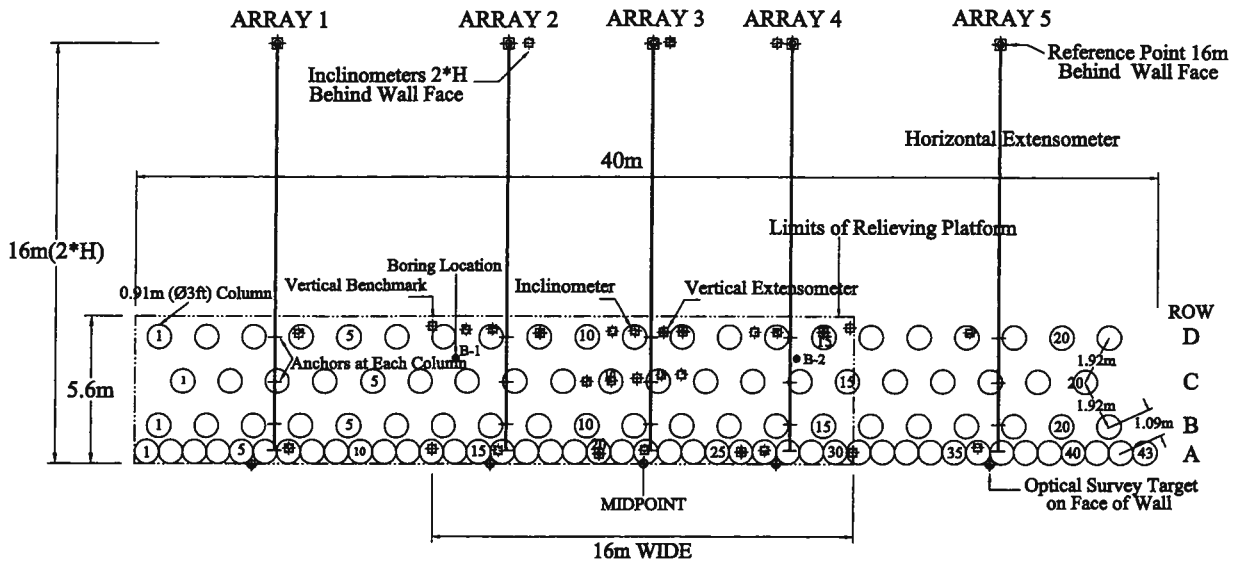
FIG. 6. Plan View of Full-Scale VERT Wall

LEGEND

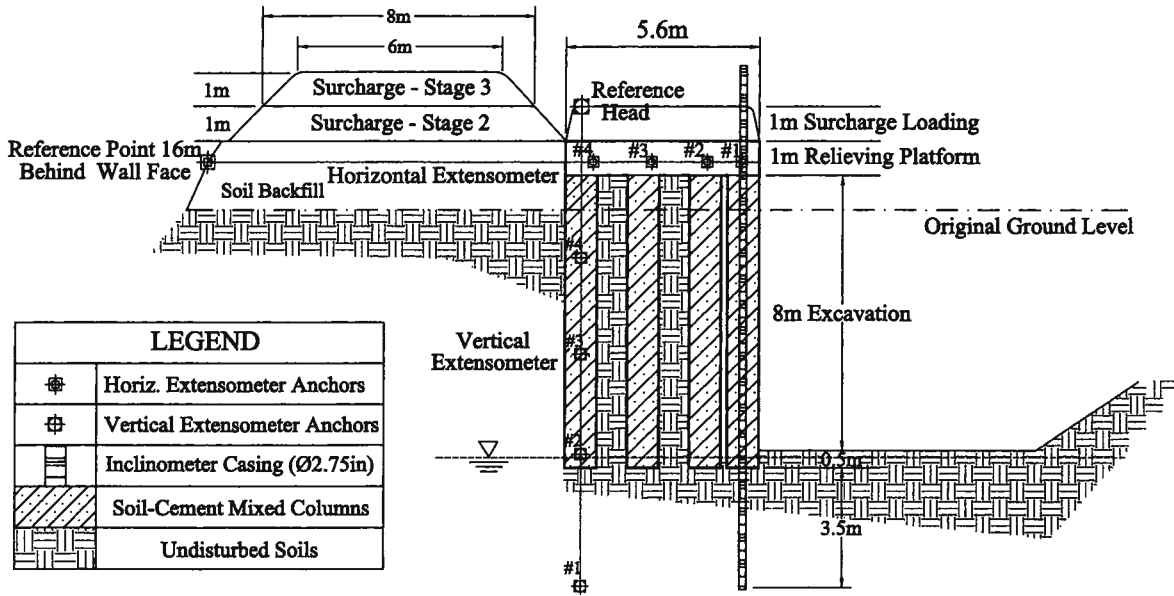|	
⊕	Horiz. Extensometer Anchors
⊕	Vertical Extensometer Anchors
	Inclinometer Casing (Ø2.75in)
	Soil-Cement Mixed Columns
	Undisturbed Soils

FIG. 7. Cross-Section View of Full-Scale VERT Wall
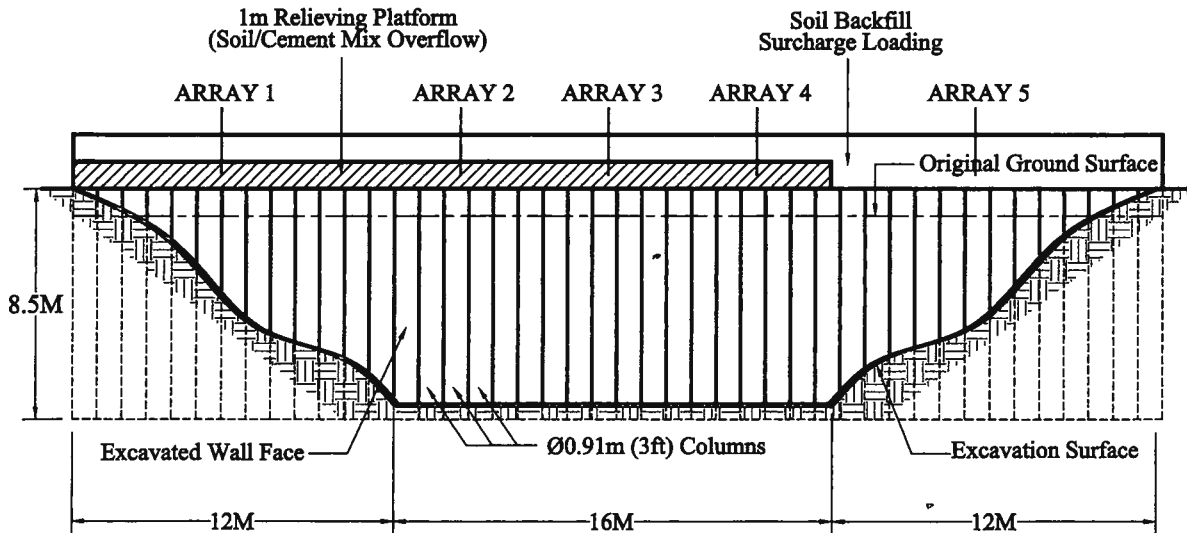
FIG. 8. Front View of Full-Scale VERT Wall

115

Phase & Stage	Schematic of Construction	Date	Symbol	Event
Phase I Stage1	[1m; O.G.L.]	5/12/98	—●—	1m Surcharge on Relieving Platform and 1m Excavation
Phase I Stage 2	[4m]	5/14/98	—○—	4m Excavation Below Original Ground Surface
Phase I Stage 3	[7m]	5/17/98 — 5/19/98	--▼-- ---▽---	7m Excavation, Total 8m Below the Top of the Soil Mixed Columns
Phase II Stage1-2	[7m]	5/20/98	--■--	2m Surcharge Behind wall
Phase II Stage 3	[7m]	5/27/98 6/12/98 7/1/98 10/2/98 1/4/99 4/2/99	----□--- --◆-- —◇— —▲— --△-- --●--	1m Surcharge Behind wall, Total 3m Above Relieving Platform Line

FIG. 9. Construction Stages of Full-Scale VERT Wall

TABLE 1. Location of Instrumentation

Instrumentation/location (1)	Array 1 (2)	2 (3)	3 (4)	4 (5)	5 (6)
Four-point horizontal extensometer	●	●	●	●	●
Inclinometer in front row A column	●	●	●	●	●
Inclinometer in row C column			●		
Inclinometer in unmixed soil in row C			●		
Inclinometer in row D column	●	●	●	●	●
Inclinometer in unmixed soil row D		●	●	●	
Vertical extensometer in front row A column			●	●	
Vertical extensometer in row D column		●	●	●	
Vertical extensometer in unmixed soil in row D			●		
Inclinometer at 16 m behind wall face		●	●	●	
Optical survey targets on front face of wall	●	●	●	●	●

samples to a depth of 6.9 m. The recovery of core was 95%, and the rock quality designation was 74%. The best coring process of the soil-cement columns was achieved when using a triple-tube core barrel and coring 28 days or more after column construction. Compression testing of a representative sample showed a 28-day unconfined compressive strength of 2,069 kN/m². This compares favorably with the mean 28-day strength of the grab samples (Fig. 10).

Stress-strain curves were obtained for samples cored in five columns. The tests were unconfined compression tests. From each curve a secant modulus to 50% of the peak stress E was calculated as well as the unconfined compression strength f'_c. The decimal logarithm of E is plotted against the decimal logarithm of f'_c on Fig. 12 and leads to the regression

$$E(\text{kPa}) = 12,900(f'_c(\text{kPa}))^{0.41} \qquad (1)$$

The relationships proposed by Brandl (1998) and Futaki et al. (1996) for soil-cement mixtures as well as the one for normal concrete, high strength concrete (Oluokun et al. 1991) and steel are shown on Fig. 12 for comparison purposes.

OBSERVED HORIZONTAL MOVEMENTS

The observed behavior is discussed with respect to horizontal movements, vertical movements, rigid body translation and rotation, and bending moment in the columns. A comparison is made with a tieback wall of similar size built at the same site.

The horizontal movement of the front face of the wall was given by the inclinometers. Fig. 13 shows the results for inclinometer 3-A22. This number means that the inclinometer was in instrumentation array 3 along row A in the 22nd column. This inclinometer was in the middle of the front of the wall (Fig. 6). The first six profiles correspond to readings taken during the excavation sequence (up to May 27, 1998, Fig. 9). The next five profiles correspond to the 9-month period following excavation. Fig. 13 shows a maximum deflection of 25 mm; this deflection is very close to the deflection of a similarly large tieback wall built by the Schnabel Foundation in 1990 at the same site (Briaud and Lim 1999). Fig. 13 also shows that the effect of the relieving platform was to create a top deflection that was less than the maximum deflection. Fig. 14 is a plot of the horizontal deflection at the top of the wall as a function of the excavation depth during construction.

The deflection profile of Fig. 13 can be used to calculate the bending moment profile. Indeed

$$M(z) = EI \frac{d^2y}{dz^2} \qquad (2)$$

where $M(z)$ = bending moment in the column at depth z; E = modulus of the column material; I = moment of inertia around the bending axis; and y = horizontal deflection at depth z. The function d^2y/dz^2 represents the curvature of the profile at depth z and can be estimated by the finite-difference method.

$$\frac{d^2y}{dz^2} = \frac{y_{i+1} - 2y_i + y_{i-1}}{h^2} \qquad (3)$$

where y_{i+1}, y_i, and y_{i-1} = horizontal movements at stations $i + 1$, i, and $i - 1$, respectively; and h = distance between stations ($h = 0.61$ m for the profile of Fig. 13). Obtaining the bending moment profile requires a choice of modulus E. An average modulus of 300,000 kPa was chosen to obtain the profiles shown on Fig. 15; the bending moment profiles are shown for inclinometer 3-A22 and 3-C11, which was in the C row right behind 3-A22. The profiles show that the bending moment has two maximum moments: One negative, between 3- and 4-m deep due to the bowing of the piles; and one positive, at the top, due to the restraining effect of the relieving platform.

The maximum resisting moment of these unreinforced columns is controlled by the tensile strength f'_t of the soil-cement mix. If one assumes, as is usual for concrete, that f'_t is 1/10 of the compressive strength f'_c, the maximum resisting moment M_y before cracking occurs is

$$M_y = \frac{f'_c I}{10c} = \frac{\pi}{320} f'_c D^3 \qquad (4)$$

where c and D = radius and diameter of the column, respectively. Using the mean value of f'_c at 28 days (2,179 kPa) gives 16.11 kN·m, whereas using the lowest value (1,379 kPa) gives 10.20 kN·m. When comparing these M_y values to the maximum moments on Fig. 15, it appears desirable to measure routinely the tensile strength of the soil-cement mixture and
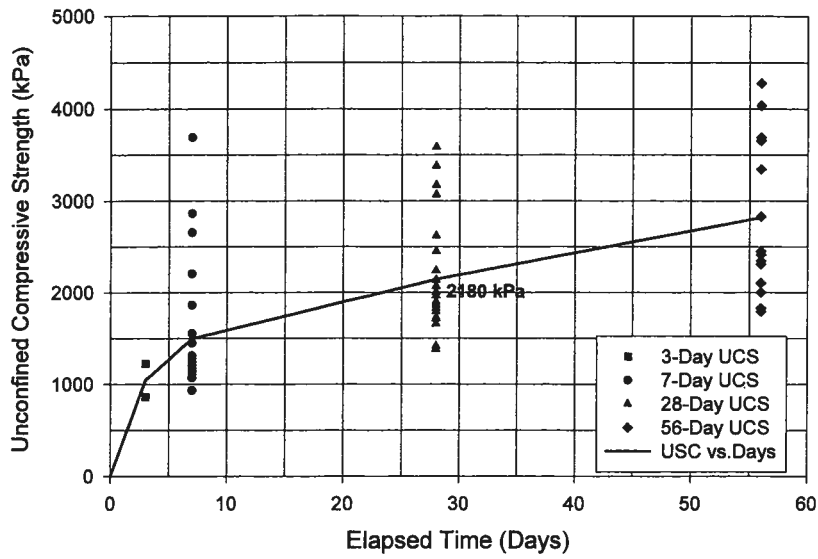
116

FIG. 10. Gain in Strength of Soil-Cement Mixture

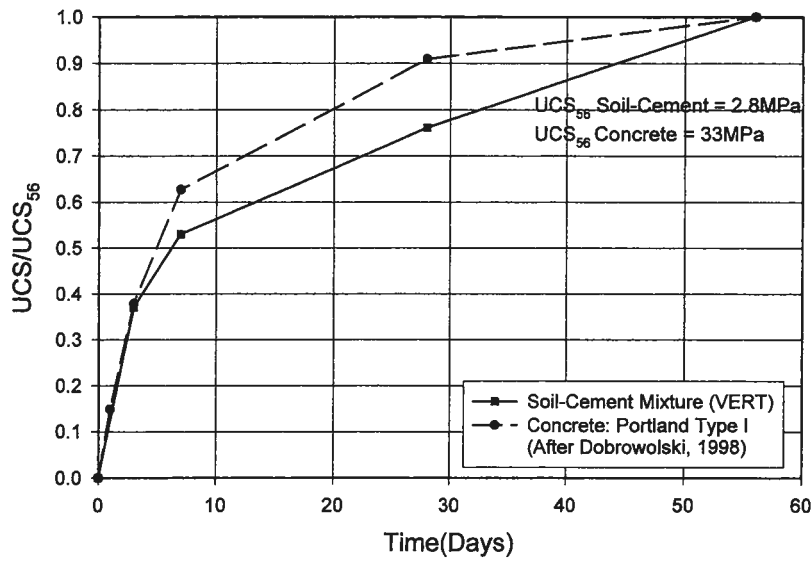
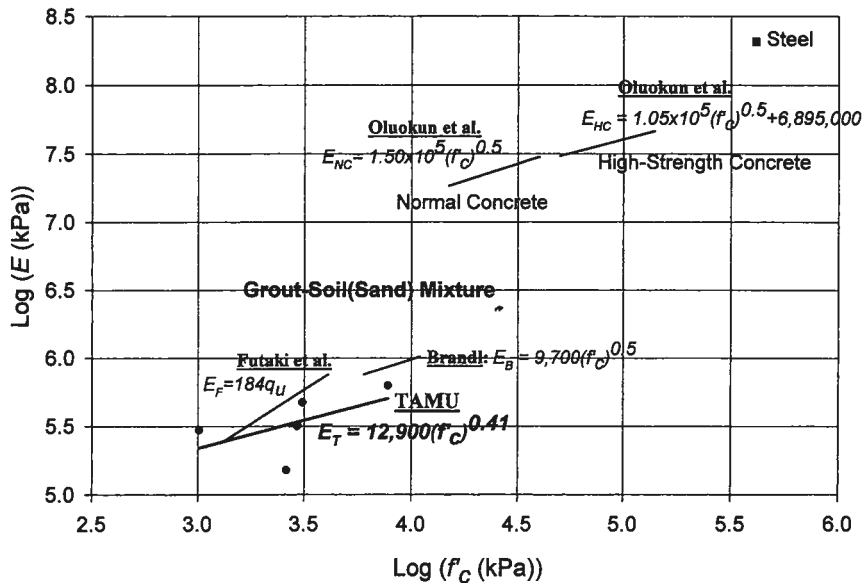FIG. 11. Normalized Gain in Strength of Soil-Cement Mixture and Concrete

FIG. 12. Modulus versus Compressive Strength for Soil-Cement and Concrete
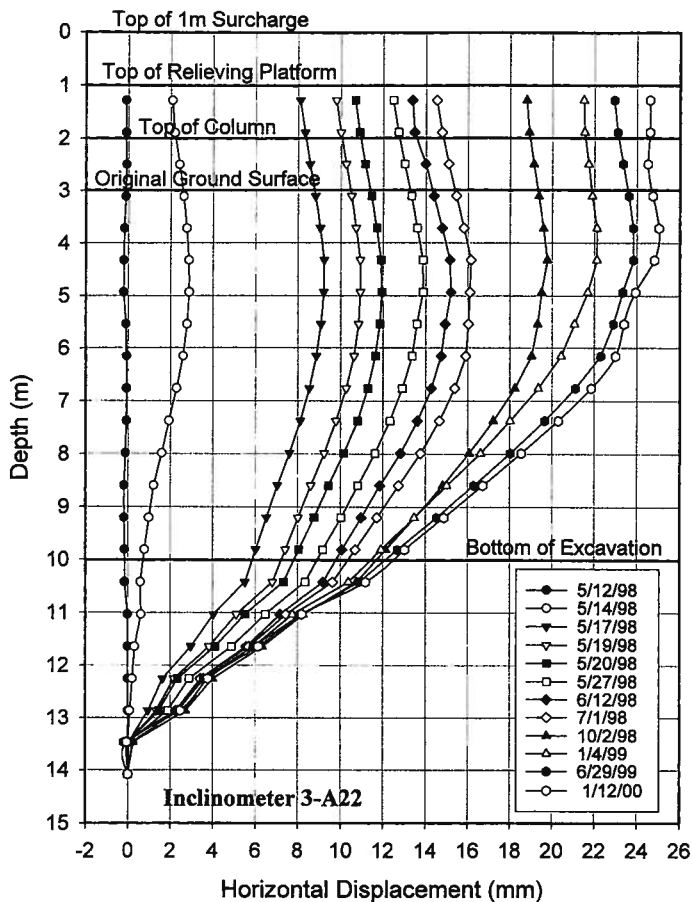
117

FIG. 13. Horizontal Movement versus Depth in Center of Front Face

to reinforce the columns, at least in the front row, to have reasonable safety against cracking.

The results for inclinometers 5-A36 and 1-A7 are shown in Fig. 16. Both inclinometers were on the front face of the wall and were symmetrical with respect to the center of the wall. However 1-A7 was in the part of the wall that had a relieving platform, and 5-A36 was in the part that did not have any. As can be seen, the relieving platform had a very beneficial effect because it decreased the maximum deflection by a factor of 2; on the other hand, the profile with the relieving platform shows
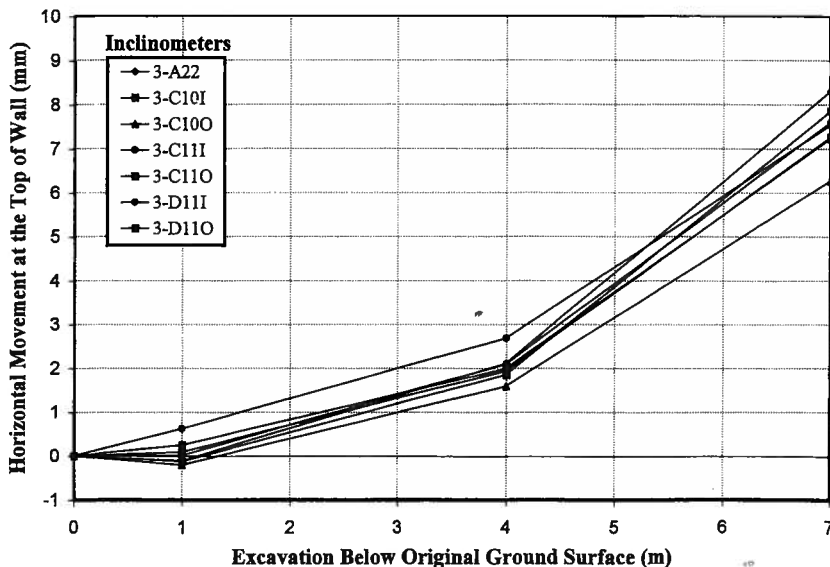
more curvature and therefore leads to a higher bending moment.

Fig. 17 is a comparison of the profile from inclinometers 3-C11I and 3-C11O. The letter I refers to the fact that the inclinometer casing was inside the column, and the letter O refers to the inclinometer outside the column in the natural soil. The two inclinometer casings were 0.91 m apart. Fig. 17 shows that the two profiles are almost identical. This is an indication that the columns and the soil between the columns deformed monolithically as one large gravity block.

Fig. 18 shows the evolution of the horizontal movement of the wall as a function of time. The increase in movement at the top of the wall was not negligible because the deflection had about doubled in 1-1/2 years, from 12.4 mm right after excavation and surcharge to 25 mm. However this time dependent movement is well in line with the time dependent movement of a similar size tieback wall built by the Schnabel Foundation at the same site (Soto and Briaud 1997).

The horizontal extensometers gave the horizontal movement of several points on the top surface of the wall (Fig. 19). Comparison of the extensometer results and inclinometer results at the top of the front face shows that the results from the two types of instruments are in agreement with the extensometer giving a displacement that is somewhat higher than the inclinometer (5 mm on the average). The discrepancy occurred right at the first 1-m excavation stage, yet there is no reason to doubt either measurement.

OBSERVED VERTICAL MOVEMENT AND GLOBAL BEHAVIOR

The vertical extensometer gave the settlement of various points in the wall during excavation and as a function of time thereafter. Fig. 20 shows the settlement of various points on the front face of the wall for extensometer 4-A26. The top and bottom of the wall settled approximately the same amount (9 mm). Extensometers 3-D12 (inside) and 3-D12 (outside) were 0.91 m from each other with one inside column D12 and one just outside column D12. These extensometers showed that the base of column D12 moved down 4 mm and the soil around the base of column D12 moved down 1 mm. Therefore, although such a difference is not significant, it appears that in the vertical direction the columns moved down slightly more than the soil.

The data from all instruments can be aggregated and used to describe the overall displacement of the wall (Fig. 21). This
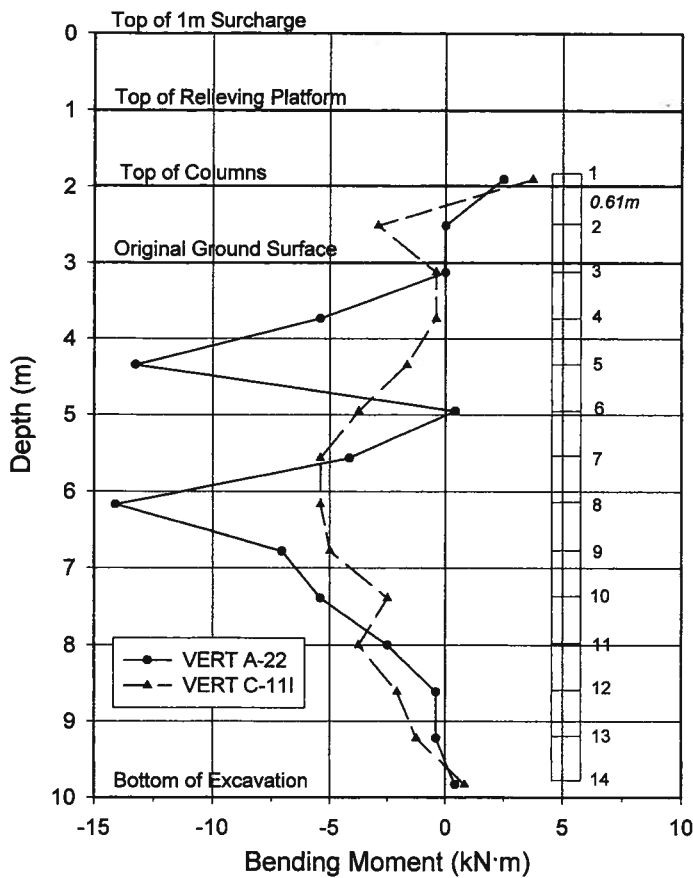

FIG. 14. Horizontal Movement at Top of Wall versus Excavation Depth

118

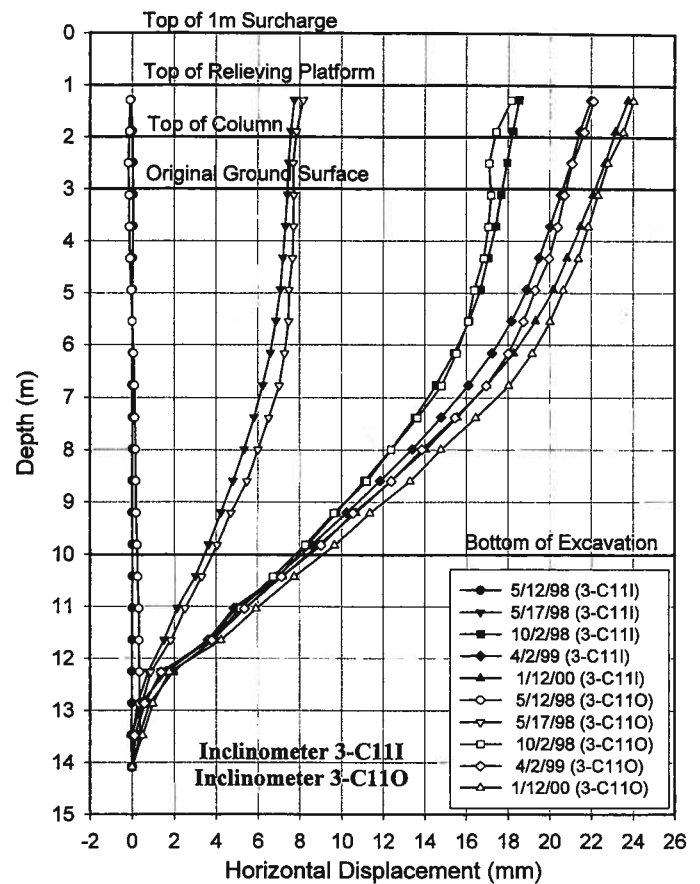**FIG. 15. Bending-Moment Profile from Two Inclinometer Profiles**

FIG. 17. Horizontal Movement versus Depth of Column and Soil between Columns
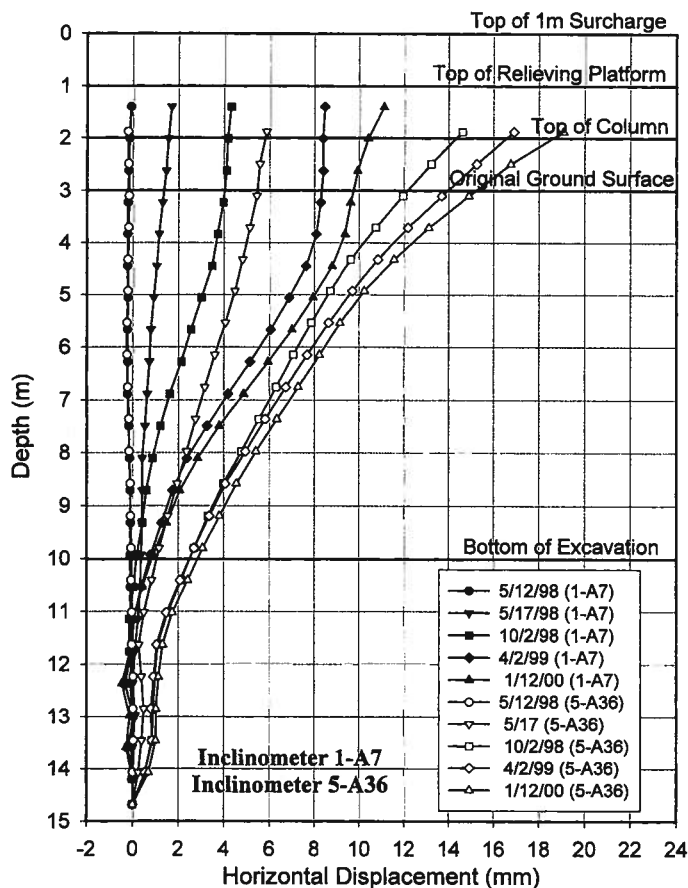

FIG. 16. Horizontal Movement versus Depth with and without Relieving Platform

movement can be decomposed into five components, as shown in Fig. 22: Rigid body translation (RBT), rigid body rotation (RBR), pure shear deformation (PSD), bending deformation (BD), and rigid body settlement (RBS). Each mode of deformation contributed to the horizontal and displacement at the top of the wall face Δ_T, except for RBS. These contributions can be evaluated as follows. The RBT created a $\Delta_{T(RBT)}$ that can be taken as the mean horizontal movement of the base [(5 + 11.1/2) = 8 mm], because theoretically the other modes of deformation do not affect it. Note that the bottom of the columns spread slightly apart, with a difference of 6.1 mm between the front column and the back column. The RBR can be taken as the rotation of the base of the wall {RBR = tan^{-1} [(8.5 − 3.9)/5,600] = 0.047°}, because theoretically the other modes of deformation do not affect it. The RBR created $\Delta_{T(RBR)}$ that is due to the RBR of the front face ($\Delta_{T(RBR)}$ = 8,500 tan 0.047 = 7 mm). The PSD can be taken as the rotation of the bottom of the front face of the wall minus the RBR. The rotation of the bottom of the front face is calculated as 0.168° on Fig. 13. The PSD is therefore 0.121° and the corresponding $\Delta_{T(PSD)}$ is 18 mm ($\Delta_{T(PSD)}$ = 8,500 tan 0.121 = 18 mm). The BD decreased the deflection at the top by an amount equal to ($\Delta_{T(RBT)} + \Delta_{T(RBR)} + \Delta_{T(PSD)}$) minus the measured deflection at the top ($\Delta_{T(meas)}$ = 23 mm on Fig. 13). Therefore $\Delta_{T(BD)}$ = 23 − 8 − 7 − 18 = −10 mm. To evaluate the relative contribution of each mode, one can calculate the deflection if there was no decrease due to bending (8 + 7 + 18 = 33 mm) and express each component as a percentage of 33 mm. Then, the RBT contributed 24%, the RBR 21%, the PSD 55%, and the BD − 30%; therefore, all of these modes of deformation contributed significantly to Δ_T.

119
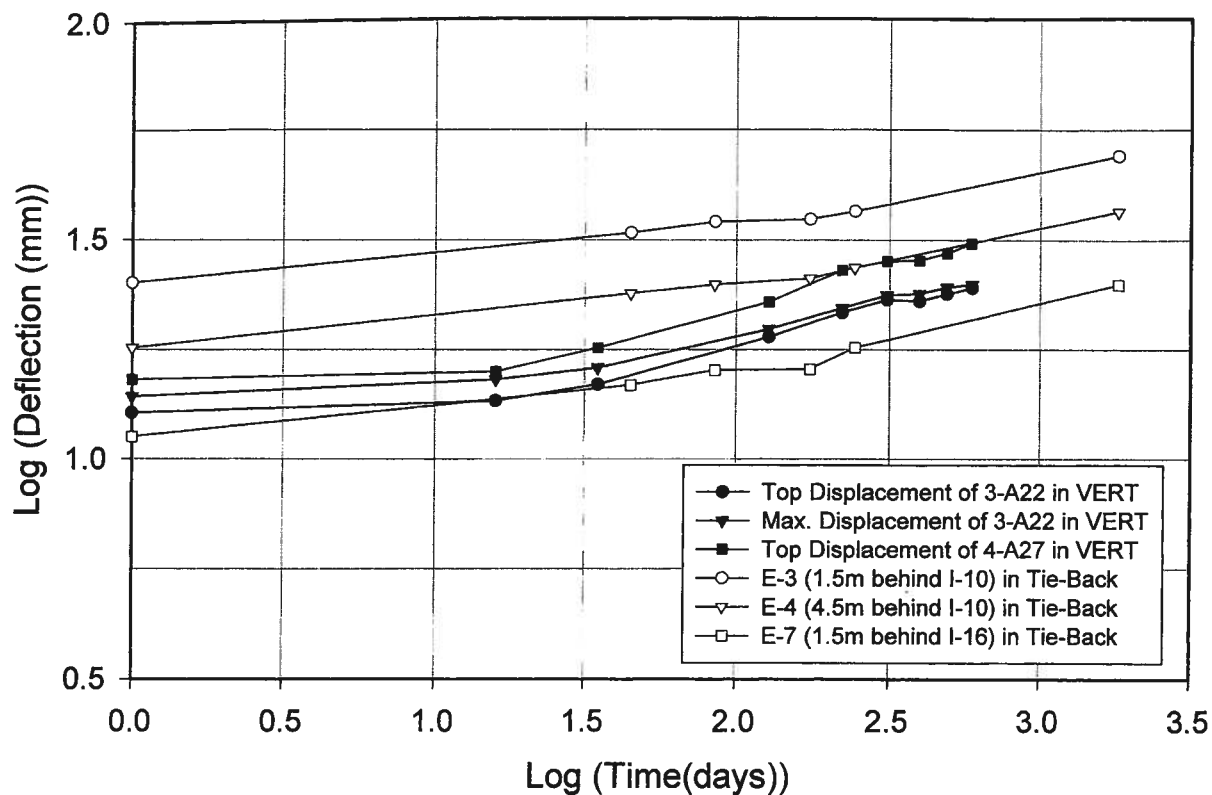
FIG. 18. Horizontal Movement versus Time for VERT Wall and Tieback Wall

Legend for FIG. 18:
- Top Displacement of 3-A22 in VERT
- Max. Displacement of 3-A22 in VERT
- Top Displacement of 4-A27 in VERT
- E-3 (1.5m behind I-10) in Tie-Back
- E-4 (4.5m behind I-10) in Tie-Back
- E-7 (1.5m behind I-16) in Tie-Back
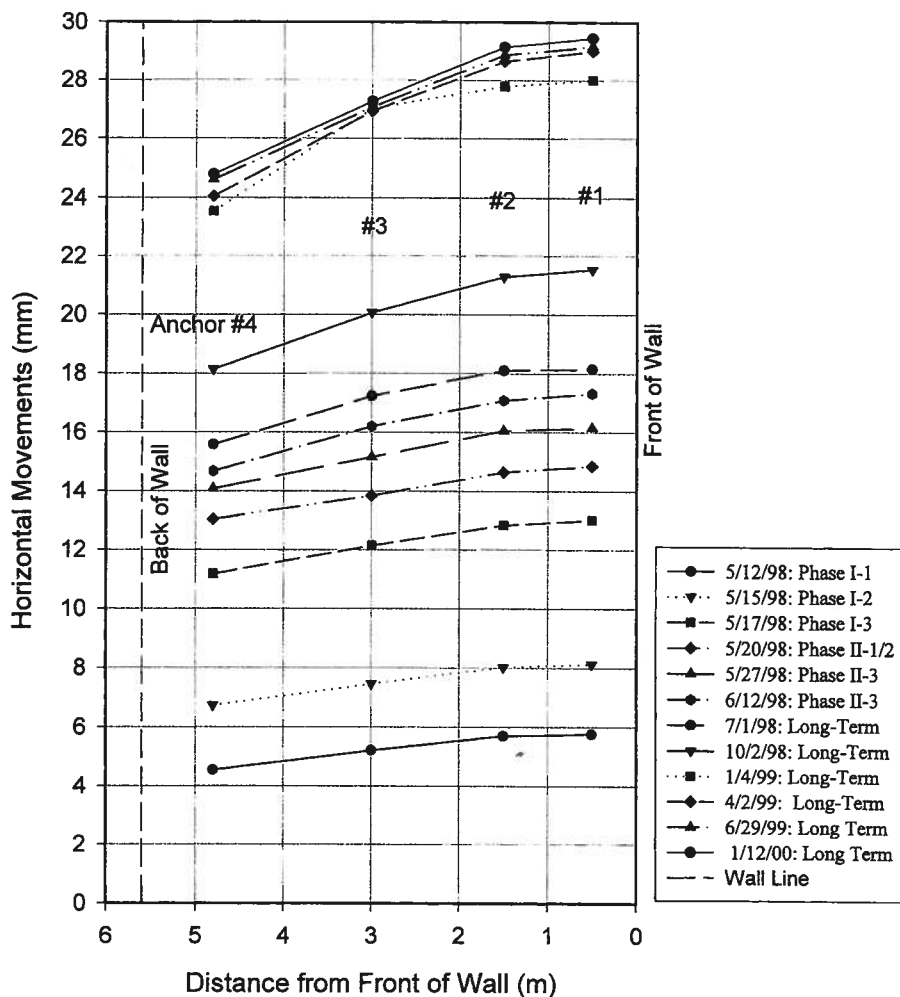
FIG. 19. Horizontal Movements from Horizontal Extensometers

Legend for FIG. 19:
- 5/12/98: Phase I-1
- 5/15/98: Phase I-2
- 5/17/98: Phase I-3
- 5/20/98: Phase II-1/2
- 5/27/98: Phase II-3
- 6/12/98: Phase II-3
- 7/1/98: Long-Term
- 10/2/98: Long-Term
- 1/4/99: Long-Term
- 4/2/99: Long-Term
- 6/29/99: Long Term
- 1/12/00: Long Term
- Wall Line

120
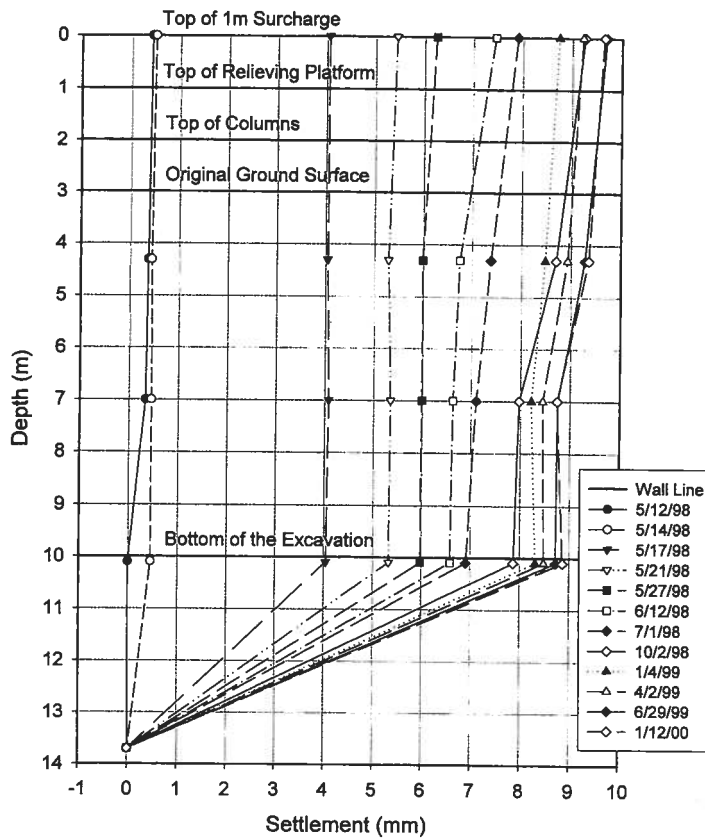
FIG. 20.   Settlement versus Depth from Vertical Extensometers
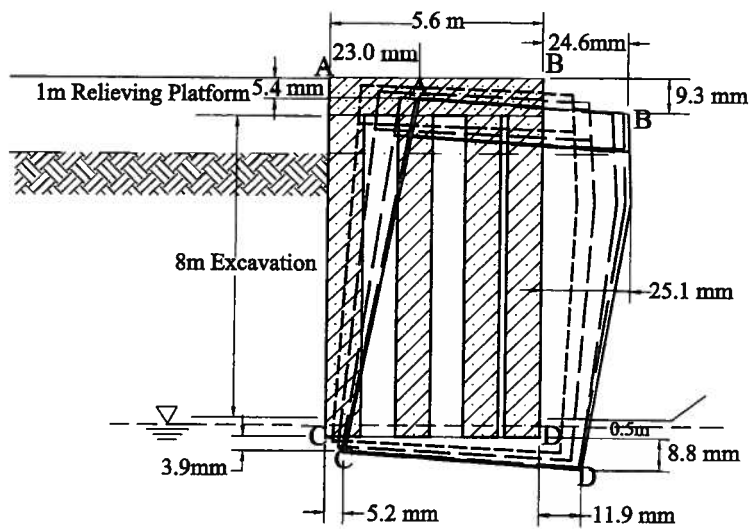
[SCALE] Displacement : Wall Size = 1:1000

LEGEND	
- - -	After 7m Excavation (5/17/98)
— —	After 3m Surcharge (5/27/98)
— —	Long Term Movement II (10/2/98)
——	Long Term Movement IV (4/2/99)
——	Long Term Movement VII(1/12/00)
▨	Soil-Cement Mixed Columns

FIG. 21.   Global Movement of Full-Scale VERT Wall

121

FIG. 22. Modes of Deformation of Full-Scale VERT Wall
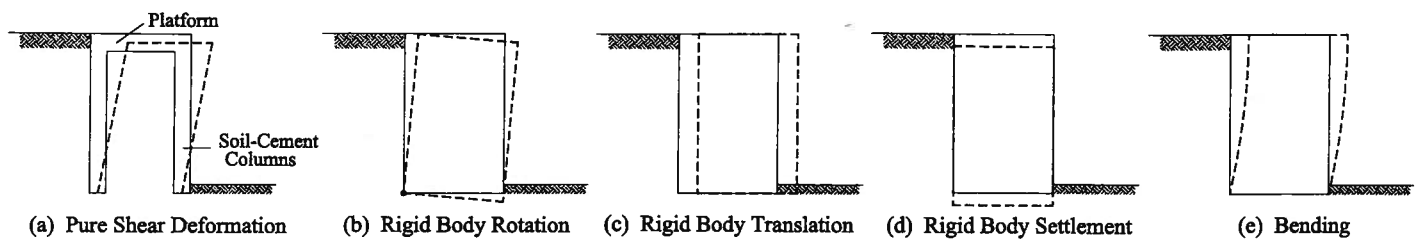
(a) Pure Shear Deformation (b) Rigid Body Rotation (c) Rigid Body Translation (d) Rigid Body Settlement (e) Bending

CONCLUSIONS

A new type of retaining wall called the VERT wall has been developed and tested at full scale at NGES-TAMU. The behavior of the full-scale wall was monitored for 1-1/2 years; the results are an indication that it is a viable retaining wall type. Indeed 1-1/2 years after construction, the horizontal deflection at the top of the 10-m high wall was 0.025 m and the vertical settlement of the same point was 0.0093 m; these movements are very similar to those of a same size tieback wall built next to the VERT wall.

The full-scale test also showed the following. The relieving platform played an important role in reducing deflections; a reduction factor of 2 was measured. The columns and the soil between the columns moved together in the horizontal direction. Although unreinforced columns behaved well, it was desirable to reinforce the front columns to ensure a factor of safety against bending and/or to determine a reliable lower bound of the tensile strength of the soil-cement mixture. The global behavior of the wall included RBT, RBR, PSD, BD, and RBS. The first four modes of deformation contributed to the horizontal deflection at the top of the wall, with PSD contributing the most.

ACKNOWLEDGMENTS

APPENDIX. REFERENCES

Brandl, H. (1998). "Foundation strengthening and soil improvement for scour endangered river bridge." *Geotechnical hazards*, Marie, Lisac, Szavits-Nossan, eds., Balkema, Rotterdam, The Netherlands.

Briaud, J.-L. (1997). "National geotechnical experimentation sites at Texas A&M University: Sand and clay, a summary." *Rep. No. NGES-TAMU-007*, Dept. of Civ. Engrg., Texas A&M University, College Station, Tex.

Briaud, J.-L., and Lim Y. (1999). "Tieback walls in sand: Numerical simulation and design implications." *J. Geotech. and Geoenvir. Engrg.*, ASCE, 125(2), 101–110.

Dobrowolski, J. A. (1998). *Concrete construction handbook*, 4th Ed., Mc-Graw-Hill, New York, 6-1–6-17.

Futaki, M., Nakomo, K., and Hagino, Y. (1996). *Design strength of soil cement columns as foundation ground for structures, grouting and deep mixing*, Yonekura, Terashi, Shibazaki, eds., Balkema, Rotterdam, The Netherlands, 481–484.

Jennings, S. P., Mathewson, C. C., Yancey, T. E., and Briaud, J.-L. (1996). "National geotechnical experimentation sites at Texas A&M University: Sand and clay, geology." *Rep. No. NGES-TAMU-005*, Dept. of Civ. Engrg., Texas A&M University, College Station, Tex.

Lin, K. Q., and Wong, I. H. (1999). "Use of deep cement mixing to reduce settlements at bridge approaches." *J. Geotech. and Geoenvir. Engrg.*, ASCE, 125(4), 309–320.

Oluokun, F. A., Burdette, E. G., and Deatherage, J. H. (1991). "Elastic modulus, Poisson's ratio, and compressive strength relationships at early ages." *ACI Mat. J.*, 88(1).

Soto, A., and Briaud, J.-L. (1997). "Observed long-term behavior of permanent ground anchors in clay and sand." *Res. Rep. to the Texas Dept. of Transp.*, Dept. of Civ. Engrg., Texas A&M University, College Station, Tex.

Should Grouted Anchors Have Short Tendon Bond Length?

By Jean-Louis Briaud,[1] Fellow, ASCE, William F. Powers III,[2] Associate Member, ASCE, and David E. Weatherby,[3] Member, ASCE

ABSTRACT: Field measurements associated with the behavior of ten low-pressure grouted anchors installed with a hollow stem auger at the National Geotechnical Experimentation Site at Texas A&M University are presented. The anchors were 0.3 m in diameter and embedded 13.8 m in a stiff to very stiff clay. Six anchors had a tendon bond length of 4.6 m and four had a tendon bond length of 9.2 m. All anchors were load tested to near failure, some were subjected to creep tests, and some to long-term relaxation tests. This study evaluates the load distribution in the soil, grout, and steel tendon; the shear strength of the soil-grout interface compared to engineering soil properties; the relationships between the ultimate load, the creep failure load, the creep threshold load, and the design load; the creep movement rate under load; and the load loss as a function of time. The results show that anchors with shorter tendon bond lengths have higher ultimate capacities and lower creep rates, and transfer the load further away from the supported structure.

INTRODUCTION

A grouted anchor and its components are shown in Fig. 1. In the United States the use of such anchors was common for temporary tieback walls in the 1970s. The increase in use of these anchors for permanent applications in the 1980s has prompted federal and state agencies to perform research on the long-term behavior of grouted anchors. This article summarizes one part of a research project sponsored by the Federal Highway Administration (FHWA), Washington, D.C., and Schnabel Foundation Company, Sterling, Va., aimed at improving the design of permanent tieback walls (Powers and Briaud 1993; Chung and Briaud 1993; Kim and Briaud 1994; Mueller 1996; Mueller et al. 1994; Long et al. 1996). The project started in 1989 and was completed in 1996. The part of the project reported here deals with the long-term behavior of grouted anchors in stiff clay (Powers and Briaud, 1993).

Satisfactory performance of a permanent ground anchor depends upon corrosion protection of the anchor tendon and its long-term load-carrying capacity. The objectives of this part of the project were to develop a better understanding of the time-dependent movement and load-carrying capacity of large-diameter ground anchors in clay, including the influence of varying tendon bond length and relative load level.

BACKGROUND

The topic of permanent grouted anchors has been reviewed in a sequence of publications by FHWA (Nicholson et al. 1982; Otta et al. 1982; Pfister et al. 1982; Weatherby 1982) that culminated with the summary report by Cheney (1988).

The steps involved in the design of low-pressure grouted, straight-shafted anchors in clay are as follows: first, the anchor direction and the design load Q_d are determined. For tieback walls, Q_d is determined from the earth pressure distribution exerted against the wall. Second, the required tendon cross section is established. Third, the anchor length L_a (Fig. 1) necessary to resist safely the design load Q_d is calculated as

$$L_a = \frac{Q_d \times F}{\pi D f_{max}} \quad (1)$$

where F = factor of safety; D = diameter of the anchor hole; and f_{max} = shear strength of the interface between the soil and the grout. Values of F reported in the literature vary from 1.6–3.0 (Bustamante and Doix 1985; Canadian 1985; Otta et al. 1982; Cheney 1988; Littlejohn 1990). It is important to ensure that the anchor bond length L_a is adequate to support the design load and the proof test load without transferring axial force into the active failure zone. Fourth, the tendon bond length L_b (Fig. 1) necessary to transfer the load from the steel tendon to the grout column is estimated. Fifth, the unbonded length L_u (Fig. 1) is calculated so that the anchor length L_a is entirely outside the mass of soil that would be associated with a failure of the structure. Sixth, the compressive stress in the grout of the unbonded length must be within acceptable limits; this last condition is rarely a problem and often is not checked in design.

The construction of a grouted anchor consists of creating a hole, inserting a steel tendon (single bar or multistrand), and injecting grout to fill the annulus between the tendon and the soil. The tendon is equipped with centralizers to keep the tendon in the center of the hole. The bottom part of the tendon length is bare and is directly bonded to the grout; this is the tendon bond length. The top part of the tendon length is in a grease-filled plastic sheath; this is the unbonded length. The grouting is performed under pressure for pressure grouted anchors; further distinction is made here between high pressure, low pressure, and gravity tremie. Regroutable anchors are subjected to repeated injections after partial curing of the grout. The anchors in this study are low pressure grouted anchors in
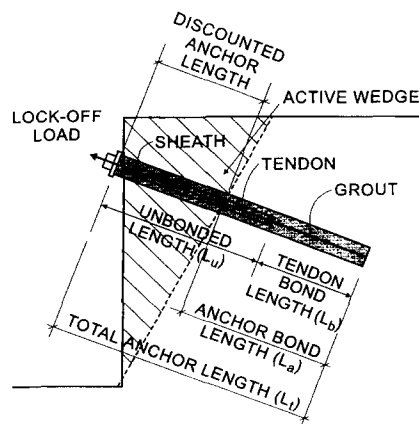
[1] Spencer J. Buchanan Prof., Dept. of Civ. Engrg., Texas A&M Univ., College Station, TX 77843-3136.

[2] Vice Pres. for Res., Schnabel Foundation, 45240 Business Court, Ste. 250, Sterling, VA 20166.

[3] Geotech. Engr., Reitz and Jens, Inc., 1055 Corporate Square Dr., St. Louis, MO 63132.

FIG. 1. Schematic of Grouted Anchor

stiff clay. Once the anchor is constructed and the grout has cured, the anchor is proof tested in tension to demonstrate that under 1.33 Q_d the creep movement as a function of time is less than 2 mm per log cycle of time. Note that this limit corresponds to about 15 mm of movement in a 100-yr period if the creep rate remains constant.

From the soil point of view, then, two aspects are important: the ultimate resistance Q_u of the anchor, which involves the maximum unit skin friction, f_{max}; and the creep movement as a function of time under 1.33 Q_d.

SHEAR STRENGTH OR SOIL GROUT INTERFACE, f_{max}

The following discussion is concerned with low-pressure grouted and tremie grouted anchors in clays. The load that will fail the anchor at the soil-grout interface during a pullout test mobilizes the shear strength, f_{max}, of that interface and is called here the ultimate load Q_u. An estimate of the anchor ultimate load Q_u is necessary before construction to ensure that the anchor design load Q_d can be carried safely by the soil. In design, the ultimate load Q_u is given by

$$Q_u = \pi D L_a f_{max} = F_{max} L_a \qquad (2)$$

where F_{max} = maximum friction load per unit length of anchor; and L_a = anchor bond length as shown in Fig. 1. The actual diameter of the grouted anchor is unknown, and typically the diameter of the drilling tool is used for D. Often in practice, the parameter F_{max} is used and quoted in references. This is misleading because F_{max} depends on D. The use of f_{max} is fundamentally correct and should be encouraged.

The shear strength f_{max} of the soil interface is correlated to the undrained shear strength s_u of the clay by quoting the factor α, which is the ratio of f_{max} over s_u. Fig. 2 gives examples of measured and recommended α values for low-pressure, straight-shaft grouted anchors; it is compared with data for drilled shafts by Kulhawy and Jackson (1989) and by Reese and O'Neill (1988). The parameter f_{max} can also be correlated to other soil properties such as the pressuremeter limit pressure p_L [Bustamante and Doix (1985), translated into English by Briaud (1992), Chapter 13].

CREEP MOVEMENT

Anchors are subjected to sustained tensile loads during the life of the structure. Under these loads, anchors exhibit time-
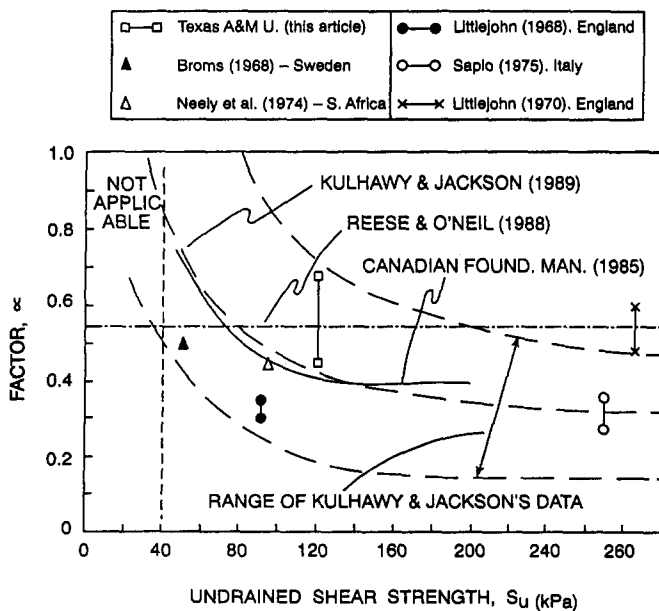
dependent or creep movements, which must be acceptably low for the structure to perform properly. Creep movement as a function of time is measured during the anchor testing program. Typically, graphs of creep movement versus log time are plotted for each load step (Fig. 3). The creep movement and the time are the ones occurring after the beginning of the load step. The slope s in mm per log cycle of time is calculated for each load step. In the United States, anchors are accepted when the slope s is less than 2 mm per log cycle of time for a load equal to 1.33 times the design load applied during 60 min (Weatherby 1982; Cheney 1988). This creep movement is due to the creep in the steel tendon, the progressive cracking of the grout in tension, and the creep of the soil in shear.

LOAD DISTRIBUTION

Figs. 4 and 6 are an illustration using simplifying assumptions and describing the load distribution in the various components of the anchor. The anchor considered in Figs. 4–6 is consistent with the actual anchors tested: it has a total length of 13.8 m, a tendon bond length of 4.6 m, and a tendon unbonded length of 9.2 m. The anchor diameter is 305 mm, the cross section area of the tendon A_T is 980 mm², and the grout cross-sectional area A_G is 72045 mm.² The modulus E_s used for the tendon is 2.07×10^8 kN/m², and the modulus E_G used

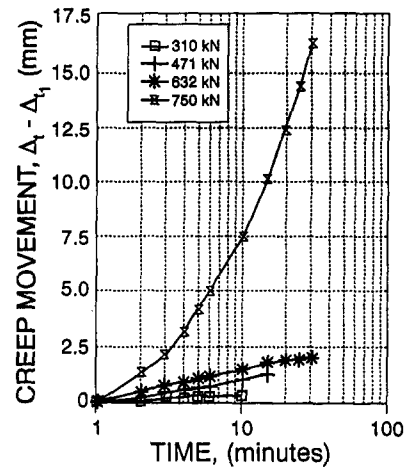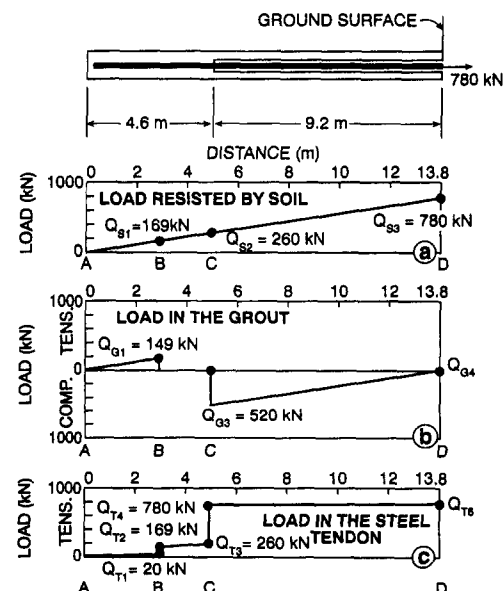FIG. 3. Creep Movement versus Time Curves for Anchor 8 (First Load)

FIG. 2. α Values for Low Pressure Grouted Anchors in Clay

FIG. 4. Schematic Load Distribution near Ultimate Load

JOURNAL OF GEOTECHNICAL AND GEOENVIRONMENTAL ENGINEERING / FEBRUARY 1998 / 111
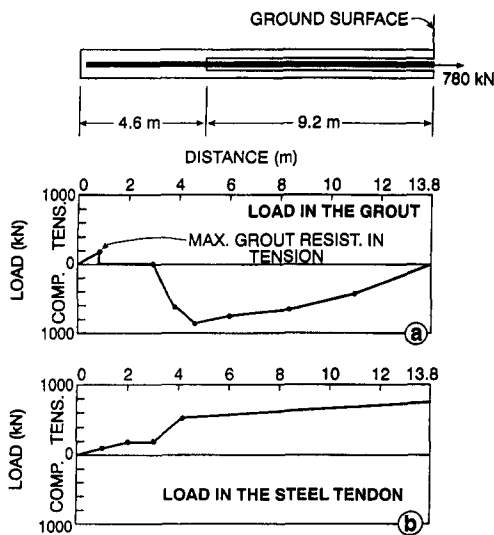
124

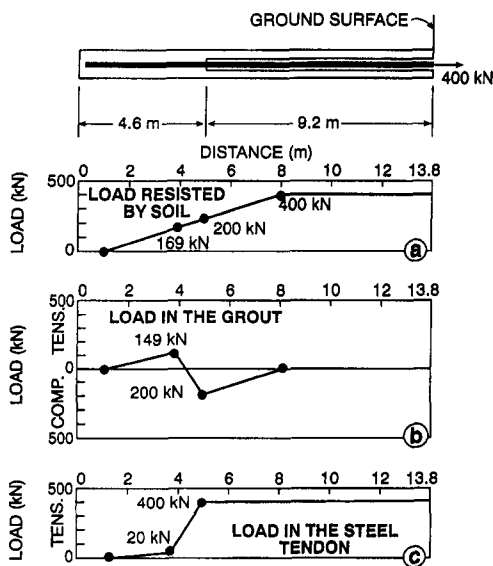FIG. 5. Measured Load Distribution for Anchor 1 near Ultimate Load

FIG. 6. Schematic Load Distribution at Design Load

for the grout is 2.07×10^7 kN/m². The undrained shear strength of the clay averages 125 kN/m² and the shear strength of the grout-soil interface f_{max} is considered to be constant and equal to 59 kN/m². Considering f_{max} to be constant along the shaft of the anchor is a simplifying assumption used for illustrative purposes only.

Two conditions are considered: the ultimate anchor load Q_u from the soil point of view, and the anchor design load Q_d. The ultimate load Q_u is the load that causes failure of the soil in shear at the grout-soil interface. At Q_u, the cumulative load resisted in shear by the soil may vary as shown schematically in Fig. 4(a). It is equal to zero at the bottom of the anchor and to the ultimate load Q_u at the ground surface (labeled $Q_{S3} = 780$ kN in the example). The linear variation shown assumes that the shear strength of the grout-soil interface f_{max} is constant along the shaft. This simplifying assumption is used for illustration purposes only and would not be true in nonuniform soil conditions. The cumulative load resisted in shear by the soil along the tendon bond length is 260 kN in the example [Q_{S2} in Fig. 4(a)]. At any point M along the anchor, the load in the steel tendon plus the load in the grout is equal to the load resisted in shear at the soil-grout interface between the bottom of the anchor and point M. At Q_u the load in the grout varies as shown in Fig. 4(b). It is equal to zero at the bottom

of the anchor and increases to the maximum tension load Q_{G1} that the grout can resist without cracking. This load can be estimated by

$$Q_{G1} = A_g E_g \epsilon_{crack} \qquad (3)$$

where A_g = grout cross section area; E_g = modulus of the grout; and ϵ_{crack} = failure strain for the grout in tension, which is about 10^{-4}. In the example Q_{G1} is 149 kN. Above that point the axial load in the grout drops to zero until the strain in the steel tendon becomes less than ϵ_{crack} again. Immediately above the boundary between the tendon bond length and the unbonded length, the grout is in compression. The load in the grout at that point is equal to the load that can be resisted in shear at the soil-grout interface between the tendon bond length/unbonded length boundary and the top of the anchor. In the example this is $780 - 260 = 520$ kN.

At Q_u, the load in the steel tendon varies as shown in Fig. 4(c). It is equal to zero at the bottom of the anchor and increases to a load Q_{T1} where the grout is at Q_{G1}. Compatibility of strain between the two materials leads to evaluating Q_{T1} as:

$$Q_{T1} = A_T E_T \epsilon_{crack} \qquad (4)$$

where A_T = cross section area of the steel tendon; and E_T = modulus of the steel tendon. In the example Q_{T1} is 20 kN. The sum $Q_{T1} + Q_{G1}$ is equal to the load Q_{S1} resisted by the soil between the bottom of the anchor and point B where Q_{G1} occurs. Point B in Fig. 4 is located at a distance l_1 from the bottom of the anchor such that

$$l_1 = \frac{Q_{S1}}{\pi D f_{max}} \qquad (5)$$

Above point B, the grout load is zero and the load in the steel tendon is equal to the load resisted by the soil. At the beginning of the unbonded length the load in the steel tendon is equal to the load at the top of the anchor, since there is no load transfer along the unbonded length.

Fig. 5 shows the load distribution obtained from the measurements on an actual test anchor, anchor 1, at a load near the ultimate load. The trends are similar to Fig. 4. At the design load Q_d, the load distribution is different and is as shown schematically in Fig. 6. Note that the soil zone that is the most stressed is around the bonded to unbonded length transition.

NATIONAL GEOTECHNICAL EXPERIMENTATION SITE

Ten anchors were constructed and load tested at one of the National Geotechnical Experimentation Sites located on the Texas A&M University Riverside campus. The soil at that site is predominantly a very stiff overconsolidated clay (Fig. 7),
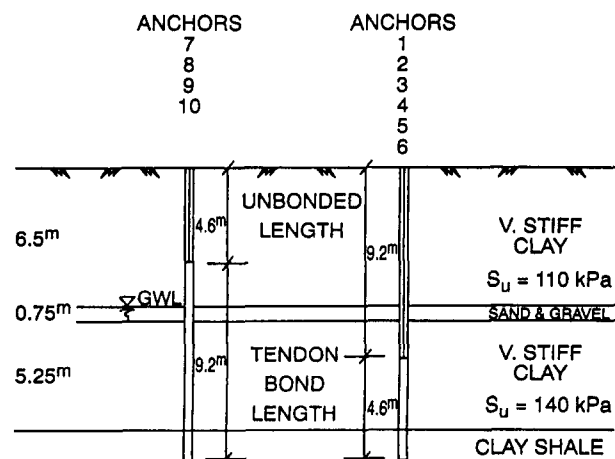

FIG. 7. Stratigraphy and Anchor Location

125

which has been tested numerous times starting in 1977 (Briaud 1993; Marcontell and Briaud 1994; Tao and Briaud 1995). The clay deposit at the location of the anchor project consists of a 6.5-m-thick layer of very stiff clay with the following average characteristics (Fig. 8 and 9): water content w = 24.4%; plastic limit w_p = 20.9%; liquid limit w_L = 53.7%; natural unit weight γ_t = 19.6 kN/m²; undrained shear strength s_u = 110 kN/m²; cone penetrometer tip resistance q_c = 2 MPa; pressuremeter limit pressure p_L = 0.8 MPa; and SPT blow count N = 12 blows/0.3 m. The overconsolidation of this layer is high as judged by the high ratio of modulus E_0 over limit pressure p_L for the pressuremeter (E_0/p_L = 25). A ratio of about 12 would be expected for a normally consolidated clay (Briaud 1992).

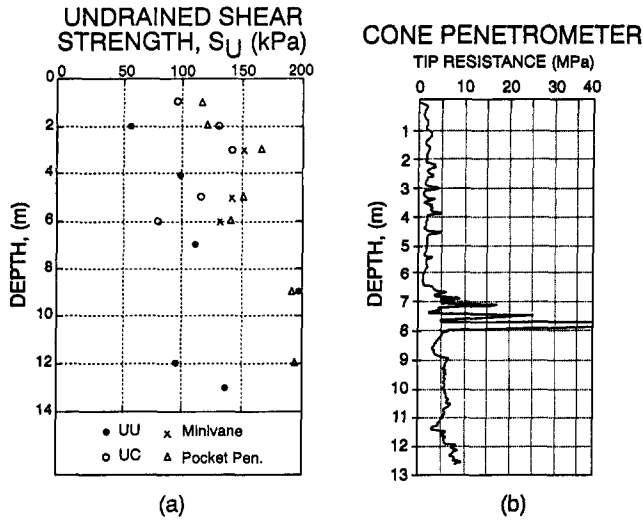The water table is 6 m deep and a 0.5-m- to 1-m-thick layer

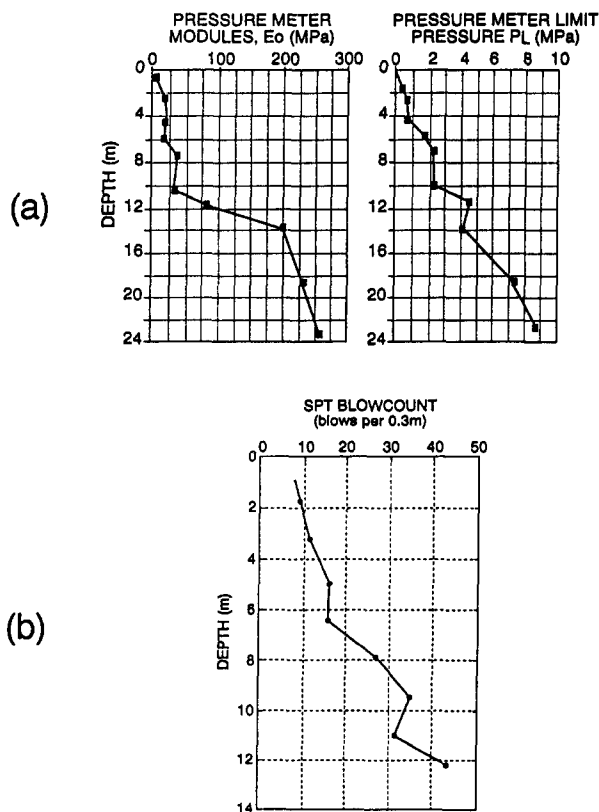FIG. 8. Soil Properties: (a) Undrained Shear Strength; (b) CPT Point Resistance

FIG. 9. Soil Properties: (a) Pressuremeter Results; (b) SPT Blow Count

of sand and gravel exists at a depth of around 6.5 m. Below this sand and gravel layer extends a layer of very stiff clay down to 12.5 m with the following average characteristics (Figs. 8 and 9): water content w = 24.5%; plastic limit w_p = 22%; liquid limit w_L = 65.5%; natural unit weight γ_t = 19.5 kN/m³; undrained shear strength s_u = 140 kN/m²; cone penetrometer tip resistance q_c = 6 MPa; pressuremeter limit pressure p_L = 2.2 MPa; and SPT blow count N = 32 blows/ 0.3 m. The overconsolidation of this layer is moderate as judged by the moderate ratio of modulus E_0 over limit pressure P_L for the pressuremeter (E_0/P_L = 16).

Below this layer is a layer of clay shale down to at least 30 m. This shale has average index properties similar to the hard clay, but a much higher stiffness and strength. The pressuremeter modulus E_0 averages 230 MPa and the limit pressure p_L = 6.5 MPa. The overconsolidation of this layer is very high as judged by a very high E_0/p_L of 35.

The top layer of clay is a flood plain deposit of Pleistocene age (Jennings et al. 1996). The next sand layer is a channel deposit, also of Pleistocene age. Both layers were deposited by the ancient Brazos River about 200,000 years ago. The two deeper layers of clay were deposited in a series of marine transgressions and regressions; they are of Eocene age, approximately 40 million years old. Erosion of the Eocene marine clay took place before the Pleistocene river sediments were deposited.

ANCHORS AND LOAD TESTS

Ten anchors were installed by drilling dry with a continuous flight hollow stem auger (Fig. 7). The outside diameter of the auger flight was 305 mm and the inside diameter of the hollow stem was 102 mm. Before drilling, the tendon equipped with a point was placed in the auger until the drill point was flush with the open drilling head on the auger. Drilling proceeded to a depth of 13.8 m. The auger was then slowly extracted without rotation while grout was pumped into the annulus between the soil and the tendons. A grout pressure of 0.7 MPa was maintained until the head of the auger was near the ground surface.

The grout slump varied from 165–254 mm, and the compressive strength at 26 days varied from 22–46 MPa. The steel tendon for each anchor consisted of seven strands of seven wires each for a total cross section area of 980 mm² with a guaranteed ultimate tensile strength of 1860 MPa. The tendons of anchors 1–6 were sheathed so as to have an unbonded length of 9.3 m, while the tendons of anchors 7–10 were sheathed so as to have an unbonded length of 4.6 m. All anchors were embedded 13.8 m in the clay deposit, going through the four soil layers as shown in Fig. 7.

Anchors 1, 2, 7, 8, 9, and 10 were instrumented with vibrating wire strain meters on the steel strands and vibrating wire embedment gauges in the grout mass. A total of 68 in-
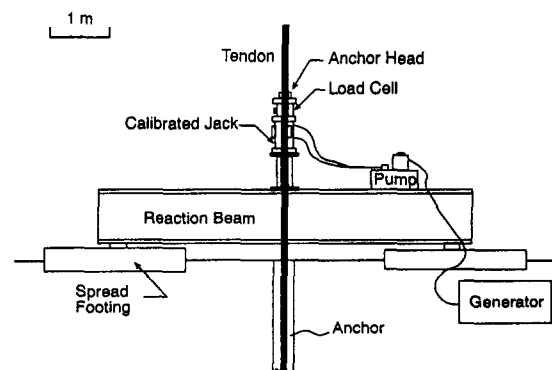

FIG. 10. Load Test Setup

JOURNAL OF GEOTECHNICAL AND GEOENVIRONMENTAL ENGINEERING / FEBRUARY 1998 / 113
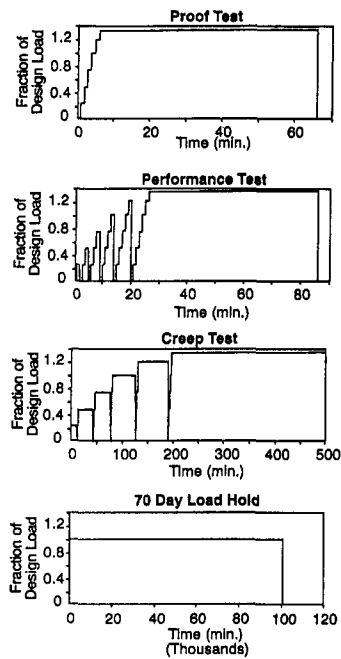
126

FIG. 11. Load History for Four Load Test Types

struments were installed in the bonded lengths and at the beginning of the unbonded lengths of the six anchors.

The installation of the 10 anchors and the subsequent load testing took place from Nov. 1990–July 1991. The load tests were tension or uplift tests performed by pulling on the tendons with a hollow jack (Fig. 10). The jack was placed above a steel frame against which it reacted. The steel frame rested on two spread footings approximately 2.5 × 2.5 m in size, embedded 1 m below the ground surface and with an edge-to-edge clear spacing of 2.3 m, or 7.5 anchor diameters. The load was recorded through a load cell placed above the jack, and the displacement was recorded with respect to a settlement beam for the short-term load tests and with respect to a deep benchmark anchored below the tip of the anchors and placed next to each anchor for the long-term load-hold tests.

Different types of load tests were performed: proof tests, performance tests, creep tests, and 70-day load-hold tests. The loading history for each of those types of tests is shown in Fig. 11. In the United States, every working anchor installed on a particular project is subjected to a proof test just prior to locking the anchor at its working load. Usually, 5% of all working anchors are subjected to a performance test to demonstrate the short-term cyclic load-carrying capacity of the anchors. Creep tests are performed occasionally to investigate the long-term load-carrying capacity of an anchor. A 70-day load-hold test was specific to this study.

LOAD TEST RESULTS AND MAXIMUM FRICTION

As an example of the results, Fig. 12(a) shows the load movement curve obtained for a proof test on anchor 5, Fig. 12(b) for a performance test on anchor 6, and Fig. 13(a) for a creep test on anchor 7.

The movement measured at the anchor head was the total movement including the elastic movement, mostly due to the elasticity of the tendon in the unbonded length, and the residual movement, mostly due to nonrecoverable movement and to the change in effective unbonded length. The residual movement is the movement read after unloading the anchor to a nominal alignment load of 20 kN from a given load step, and the elastic movement is the difference between the total movement and the residual movement [Fig. 13(b)]. Note that the elastic movement line is very close to the initial slope of the

total movement curve. The slope of that line (Δ/P) is equal to $L_e/A_T E_T$ where L_e is the equivalent elastic length of the anchor.

The ultimate load for each anchor was defined as the load obtained for a residual displacement of one-tenth of the anchor diameter ($B/10$) or for a total displacement of $B/10$ plus the elastic elongation of the anchor unbonded length. This large displacement was not reached for all load tests. The ultimate load was, therefore, obtained only for the anchors that reached that displacement or nearly reached that displacement (maximum load applied divided by extrapolated ultimate load $\geq$ 0.8) so that the ultimate load could be evaluated with reason-
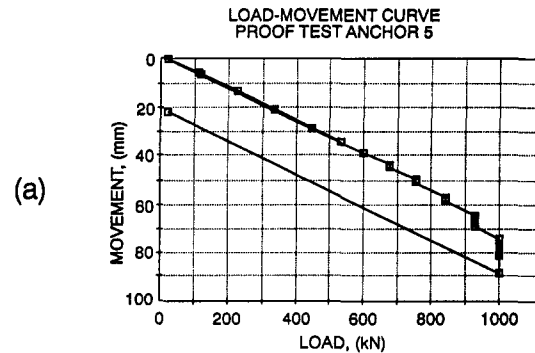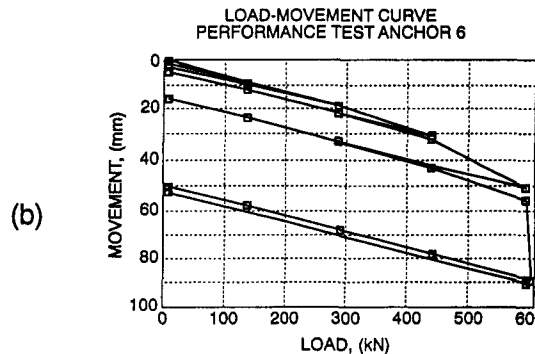
FIG. 12. Load Movement curves: (a) Anchor 5; (b) Anchor 6
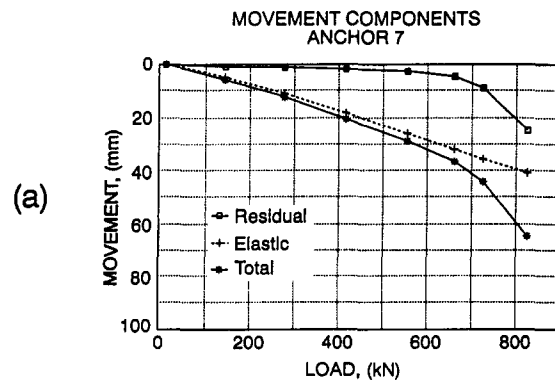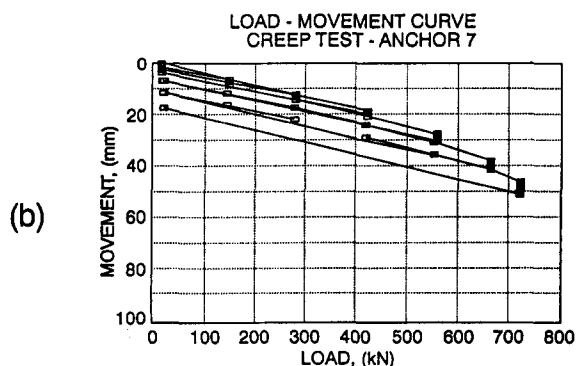
FIG. 13. Load Movement Curves for Anchor 7

127

TABLE 1. Data for 10 Anchors

Anchor number (1)	Ultimate load (kN) (2)	Bonded anchor length (m) (3)	Friction stress at failure (kN/m²) (4)	α values (5)
1	867	4.57	65.9	0.53
2	1080	4.57	82.1	0.66
3	ID[a]	4.57	—	—
4	934	4.57	71.0	0.57
5	ID[a]	4.57	—	—
6	712[b]	4.57	54.1	0.43
7	801	9.15	60.9	0.49
8	747	9.15	56.8	0.45
9	ID	9.15	—	—
10	801	9.15	60.9	0.49

[a]Insufficient displacement
[b]Installation difficulties encountered; 60% of anchor not grouted under pressure but simply free-fall.

able confidence. The ultimate loads are given in Table 1 together with the corresponding grout-soil interface shear strength f_{max} averaged over the length of the anchor.

Using the average properties of the clay deposit and the average f_{max} values, the following ratios are obtained;

- $\alpha = f_{max}/s_u$ varied between 0.43 and 0.66, and averaged 0.52
- f_{max}/q_c varied between 0.014 and 0.021, and averaged 0.016
- f_{max}/p_L varied between 0.036 and 0.055, and averaged 0.043
- f_{max}/N varied between 2.5 and 3.7, and averaged 2.9 (with f_{max} in kilopascals and N in blows per 0.3 m)

Some of these results are shown in Fig. 2.

INFLUENCE OF BOND LENGTH ON ULTIMATE LOAD

In Table 1, the average ultimate load for the anchors with a short bonded length (4.6 m) is 961 kN while the average ultimate load for the anchors with a longer bonded length (9.2 m) is 783 kN. Note that the ultimate load of anchor 6 was not used in the average because of the installation difficulties with this anchor; indeed, after a first unsuccessful installation attempt, a second location was selected. However, the hose broke after pressure grouting 6.1 m and the remaining 7.7 m were grouted by free-fall

The ultimate load for the anchors with a short bonded length is 23% larger on the average than the ultimate load for the anchors with a longer bonded length. This finding is consistent with the findings of Chaouch and Briaud (1991, 1992), who performed pullout load tests on two drilled and grouted piles at the same site; one drilled and grouted pile was pulled from the top, while the other was pulled from the bottom. The bottom-loaded pile carried 37.5% more load than the top-loaded pile. The anchors in this project penetrate through three different strata. However, the vertical variations of soil properties can not explain the results because at ultimate load, f_{max} is mobilized in all layers regardless of the tendon bond length.

The reason for the difference in capacity comes from the grout, which is mostly loaded in tension if the load is applied close to the top (long tendon bond length) and mostly in compression if the load is applied close to the bottom (short tendon bond length). Grout cracks at about 100 microstrains of tension. Under typical anchor loads, a certain length of grout will crack and the steel tendon will resist the tensile load within that zone. The axial stiffness (AE) of such a cracked section is much smaller than the axial stiffness of the same section
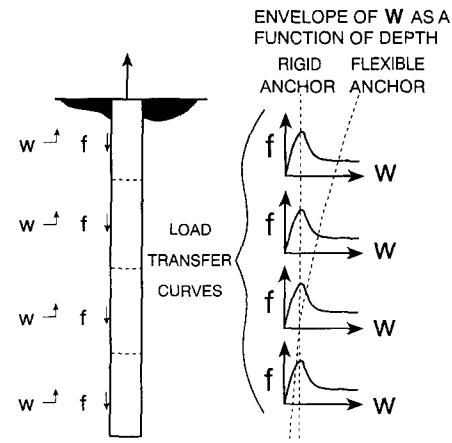
FIG. 14. Axial Stiffness Effect on Anchor Capacity
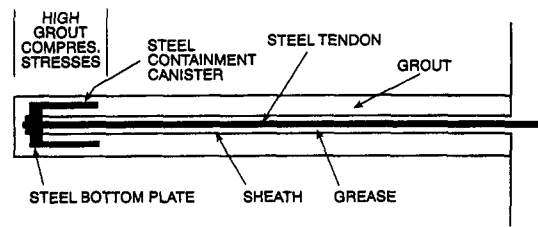
FIG. 15. Anchor Scheme for Zero Bonded Length

where the grout is in compression. The load transfer curves for stiff clays such as the one at this site exhibit post-peak strain-softening properties (Fig. 14). As a result, if the anchor is flexible (long bonded length), by the time the bottom of the anchor reaches its peak friction value, the top of the anchor is at the residual friction value and the friction along the anchor is somewhere between the peak value and the residual value. On the other hand, if the anchor is more rigid (short bonded length) the difference in movement between the top and bottom of the anchor is smaller than for the flexible case and all parts of the anchor can mobilize the peak friction at the same time, or close to it (Fig. 14).

This is known as the length effect on pile capacity (Murff 1980). This effect explains the 23% difference found in these anchor tests and leads to the conclusion that, all other dimensions being equal, the highest anchor capacity is reached for the shortest tendon bond length. This leads us to think that an anchor with a zero tendon bond length would be best. These anchors, known as compression anchors, give rise to different problems such as large grout compressive stresses and the possible need to reinforce the grout body. Therefore, it appears preferable at this time to aim for a short tendon bond length rather than a compression anchor such as the one shown in Fig. 15. Another advantage is that if two anchors in a tieback wall have the same overall length, the anchor with the short tendon bond length concentrates the soil stresses in a zone that is further away from the wall face since it is near the bottom of the anchor. This, in turn, reduces wall movement since the stressed zone is further away from the wall.

INFLUENCE OF BONDED LENGTH ON CREEP MOVEMENT

As pointed out earlier, it is common practice to plot creep results in the form of creep movement $(\Delta_t - \Delta_{t_1})$ versus the decimal logarithm of time (log t), where Δ_t is the upward movement of the anchor head (tendon) at a time t after applying the load Q, and Δ_{t_1} is the upward movement under the same load Q at the time t_1 equal to 1 min after the beginning of the load step. Such plots are presented for the first loading
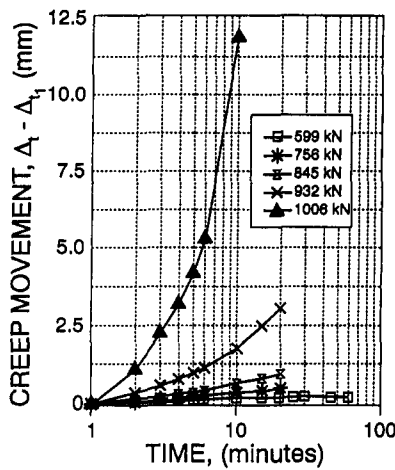
128

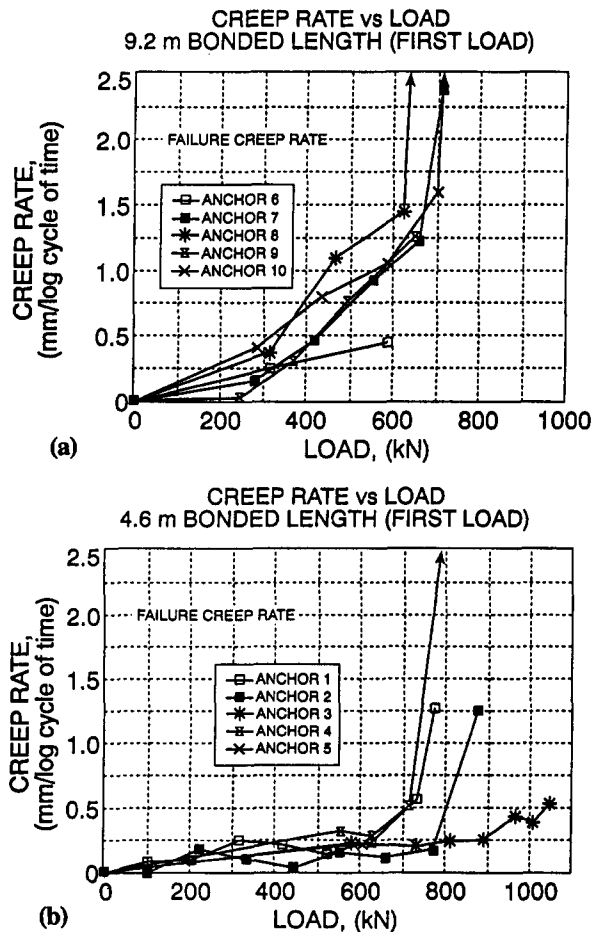FIG. 16.   Creep Movement versus Time Curves for Anchor 5

(a)

(b)

FIG. 17.   Creep Rate versus Load Curves for First Loading on (a) 9.2 m Bonded Length; and (b) 4.6 m Bonded Length

sequence on anchor 8 (Fig. 3) and for the reloading sequence on anchor 5 (Fig. 16).

The average slope of each line on these creep movement plots can be calculated; these slopes represent the creep rate s in millimeters per log cycle of time. A value of s can be obtained for each load level Q, and a plot of s versus Q can be prepared. Fig. 17(a) shows such a plot for all of the anchors with a long tendon bond length (9.2 m), while Fig. 17(b) is for the anchors with a short tendon bond length (4.6 m). As can be expected, the creep rate increases as the load increases.

A comparison of Figs. 17(a) and 17(b) shows clearly that the anchors with a short tendon bond length creep a lot less than the anchors with a long tendon bond length for similar

levels of axial load. At 400 kN, for example, the creep rate is about 0.56 mm per log cycle for the anchors with a long tendon bond length and only 0.2 mm per log cycle, or 2.8 times less, for those with a short tendon bond length. The reduction is significant and is possibly due to the grout being in compression over a longer portion of the anchor. The difference may also exist because the point of maximum soil stress (boundary between the unbonded and bonded tendon zone) is in the upper and somewhat softer clay for the anchors with a long tendon bond length while it is in the lower, somewhat stronger clay for the anchors with a short tendon bond length.

INFLUENCE OF RELOADING ON CREEP MOVEMENT

The anchors were subjected to a first loading test in March and April of 1991. The maximum load applied in this first loading series of tests varied from 600 kN to 1,000 kN. Anchors 5–10 were subjected to a reloading test hours after the first loading test was finished. The maximum load applied in this reloading series of tests was approximately the same as in the first loading tests.

Fig. 17(a) shows the creep rate versus load curve for the first loading tests on the anchors with the long bonded length. Fig. 18 shows the same graph for the reloading tests. Comparing Figs. 17(a) and 18 shows that the creep rate is significantly less during the reloading test. For example, at 400 kN, the creep rate is about 0.2 mm per log cycle for the first loading and only 0.1 mm per log cycle (or two times less) for the reloading tests. The reduction is significant and is attributed to the preloading effect of the first loading tests.

One very important question remains unanswered: is this preloading effect a permanent effect or a temporary one? If it is permanent, then reloading tests should be allowed to prove that anchors satisfy the acceptance criterion (less than 2 mm per log cycle under 1.33 × design load). If it is temporary, then reloading tests should not be allowed. Also, if it is temporary, how long does the preloading effect last? Research is needed in this area. Limited experience on anchor tests performed by Schnabel Foundation on one hand, and on spread footing tests performed at the Texas A&M University National Geotechnical Experimentation Site on the other hand, indicates that the effect is temporary.

OTHER OBSERVATIONS ON CREEP MOVEMENT

Several models were considered to fit the trends of the curves on the $(\Delta_t - \Delta_{t_i})$ versus log t graphs (Figs. 3 and 16). It was observed that at low load level these curves exhibit a
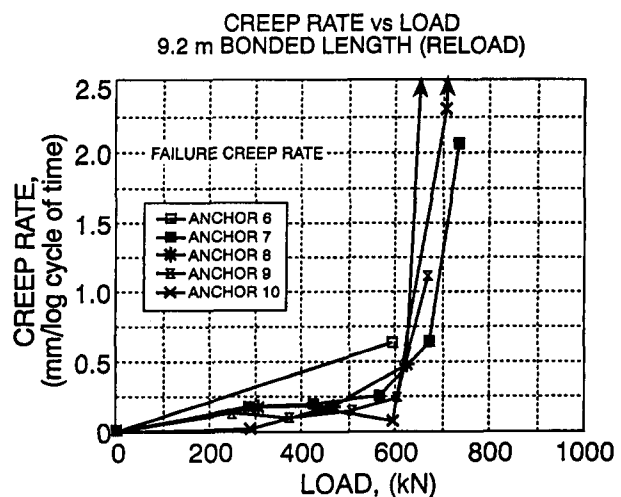

FIG. 18.   Creep Rate versus Load Curves for Reload on 9.2 m Bonded Length

slight downward curvature, that at medium load level the curves are straight lines, and that at high load level the curves exhibit an upward curvature. These observations lead to the following model recommendations:

$$\text{for } \frac{Q}{Q_f} \leq 0.5, \quad \frac{\Delta_t}{\Delta_{t_1}} = \left(1 + \log \frac{t}{t_1}\right)^n \qquad (6)$$

$$\text{for } 0.5 \leq \frac{Q}{Q_f} \leq 0.8, \quad \frac{\Delta_t}{\Delta_{t_1}} = 1 + \log\left(\frac{t}{t_1}\right)^n \qquad (7)$$

$$\text{for } \frac{Q}{Q_f} \geq 0.8, \quad \frac{\Delta_t}{\Delta_{t_1}} = \left(\frac{t}{t_1}\right)^n \qquad (8)$$

The viscous exponent n was found in these experiments to be approximately equal to 0.5 for (6) and (7) and between 0.5 and 1 for (8).

The ultimate load Q_u is defined as the load corresponding to a total displacement of one-tenth of the anchor diameter plus the elastic elongation of the anchor's unbonded length ($B/10 + PL/AE$). The failure load is defined as the load Q_f for which the creep movement accumulates at a rate equal to 2 mm per log cycle of time during the first loading of the anchor. The load Q_f was determined for anchors 4, 7, 8, and 10. The ratio Q_f/Q_u varied very little (0.83–0.89) and averaged 0.86.

Observation of Figs. 17 and 18 indicates that a creep load threshold Q_t exists; below Q_t the creep rate is small, and above Q_t the creep rate is much larger. This is particularly clear for Figs. 17(b) and 18. The ratio of Q_t/Q_u for these experiments was approximately 0.70. Since the design load Q_d is at most equal to $Q_f/1.33$, then the factors of safety would be at least 1.55 against the soil ultimate load, at least 1.33 against the creep failure load, and at least 1.09 against the creep threshold load.

The creep rate under the design load for these anchors was calculated. It averaged 0.9 mm per log cycle for the anchors with the long tendon bond length (9.2 m) and 0.22 mm per log cycle for the anchors with the short tendon bond length (4.6 m). This corresponds to 6.9 mm in 100 yrs and 1.7 mm in 100 yrs, respectively.

LOAD LOSS AS FUNCTION OF TIME

Once the anchor is locked off at the design load Q_d, the load varies as a function of time during the life of the structure. One of the concerns with anchors in clays is the creep of the soil around the anchor and the resulting decrease in load as time goes by. To investigate this load loss problem, the situation was simulated by locking off anchors 1, 2, 3, and 4 for 70 days with the same setup as the one used for the load tests (Fig. 10). During those 70 days, periodic measurements were made of the load in the load cell and of the displacement of the load cell with respect to a separate deep benchmark. The load cell moved down slightly during the 70 days, probably due to the creep settlement of the spread footings and the shrink-swell characteristics of the clay. The total movement of the load cell after 70 days varied from 0.75–2 mm and averaged 1.4 mm. The movement readings $\Delta(t)$ were used to correct the load read on the load cell (P_{UNC}) to the load that would have been read on the load cell had the load cell not moved (P_{COR}).

$$P_{\text{COR}} = P_{\text{UNC}} + \frac{\Delta(t)A_T E_T}{L_e} \qquad (9)$$

where A_T = cross section of the steel tendon; E_T = its modulus of elasticity; and L_e = elastic length of the anchor back calculated from the load test data. L_e is slightly larger than the unbonded length.
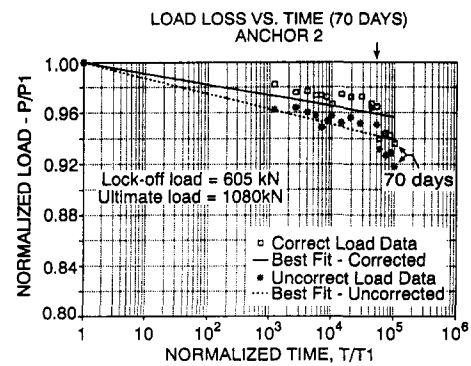
Fig. 19 shows a plot of the anchor load for anchor 2 (P_{UNC}

FIG. 19. Load Loss versus Time Curve for Anchor 2

or P_{COR}) normalized to the lock-off load read at time $t = 1$ minute after lock-off as a function of the time t normalized to $t_1 = 1$ min. This figure is typical and shows that the load loss is quite small, 0.88% of the lock-off load per log cycle of time in this case. Overall the percent load loss per log cycle of time varied from 0.5–1.4% per log cycle and averaged 0.9%. Such an average leads by extrapolation to a load loss of 7% of the lock-off load for a period of 100 yrs. This seems to be a very acceptable number. One of the reasons for this low load loss is that even if the displacement Δ of the anchor head or of the anchor bonded length is significant, the load loss will be small because the tendon is long and flexible. Indeed,

$$\text{Load loss} = \frac{\Delta \times A_T E_T}{L_e} \qquad (10)$$

in which $A_T E_T$ is small and L_e is large. In this respect, the anchors with the longest unbonded length will have the smallest load loss. This is another advantage of using anchors with shorter tendon bond length.

In Fig. 19, a change in slope can be observed after about 50,000 min (35 days), with an increase in the load loss rate after that time. This change in slope coincides with the beginning of the drilling process for an oil well located about 1 mi away from the National Geotechnical Experimentation Site. This change may also reflect the end of the preloading effect due to the earlier tests on anchor 2.

CONCLUSIONS

The following conclusions are based on the load testing of 10 full-scale low-pressure grouted anchors in a stiff to very stiff clay and on the analysis of the results. The anchors were 0.3 m in diameter and 13.8 m long, were installed dry with a hollow stem auger, and were grouted under 0.7 MPa of pressure.

1. The load distribution in the anchor is illustrated for the three elements involved: soil, grout, and steel tendon. At working loads, it shows that stresses in the soil are concentrated near the boundary between the bonded and the unbonded zone.

2. In the very stiff clay, the shear strength of the soil-grout interface f_{max} (kPa) averaged over the length of each anchor was related to the average soil properties by the following relationships:

$$\frac{f_{\text{max}}}{s_u} = 0.52; \frac{f_{\text{max}}}{q_c} = 0.016; \frac{f_{\text{max}}}{p_L} = 0.043; \frac{f_{\text{max}}}{N} = 2.9$$

3. The ultimate soil resistance Q_u was found to be 23% larger for the anchors with a short bonded length (4.6 m) than for the anchors with a long bonded length (9.2 m).
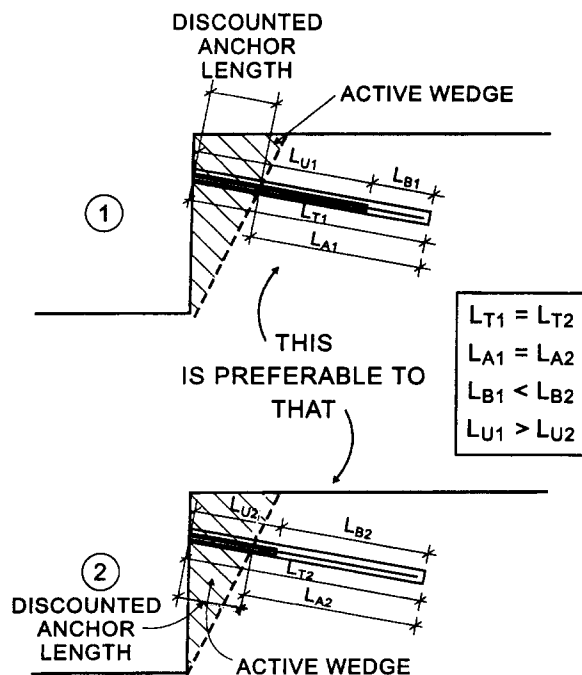
130

FIG. 20. Grouted Anchors Should Have Short Tendon Bond Length

4. The anchor failure load Q_f corresponding to a creep rate of 2 mm per log cycle of time was found to be equal to 0.86 times the soil ultimate load Q_u on the average.

5. The creep load threshold Q_t corresponding to the load at which the creep movement starts to accumulate much faster was clearly defined in most cases and corresponded to 0.7 times the soil ultimate load Q_u on the average.

6. Since the anchor design load Q_d is at most equal to 0.75 times Q_f, the following minimum factors of safety exist against Q_t, Q_f, and Q_u:

$$Q_d \le \frac{Q_u}{1.54} = \frac{Q_f}{1.33} = \frac{Q_t}{1.09}$$

7. The creep movement at the design load Q_d was 2.8 times less for the anchors with the short tendon bond length (4.6 m) than for the anchors with the long tendon bond length (9.6 m).

8. The creep rate under the design load averaged 0.9 mm and 0.22 mm per log cycle of time for the anchors with the long and short tendon bond lengths, respectively. This corresponds to 6.9 mm and 1.7 mm in 100 yrs.

9. The creep rate decreased drastically upon reloading. A typical case would be 0.2 mm per log cycle of time for the first loading and 0.1 mm per log cycle of time for the reloading. Retesting using the same creep failure rate should not be allowed until the load-history effects are better understood.

10. It was found that the current creep model, which consists of a straight line on a creep movement versus log time plot, fits the data well only for loads between 50 and 80% of the ultimate load Q_u. This range, however, covers the range of test loads and lock-off loads for most anchors.

11. The load loss of four anchors locked off for 70 days at a load Q equal to about $1/2$ Q_u averaged 0.9% of Q per log cycle of time. This corresponds to less than 7% of Q in 100 yrs.

12. For the same overall length, the grouted anchors with a short tendon bond length had the following advantages over the grouted anchors with a long tendon bond

length: higher ultimate load, lower creep rate, and lower time-dependent load loss. It also brings the soil stresses back further away from the wall. For tieback walls, it is essential to ensure that the anchor bond length L_a is adequate [(1) and Fig. 1] to support design and proof test loads without transferring axial force into the active failure zone. This study seems to indicate that, given L_a, the tendon bond length L_b should be as short as required to safely transfer the load from the steel tendon to the grout column (Fig. 20). Further testing to evaluate these findings would be valuable.

ACKNOWLEDGMENTS

APPENDIX. REFERENCES

Briaud, J.-L. (1992). *The pressuremeter*. A. A. Balkema, Brookfield, Vt.
Briaud, J.-L. (1993). "The National Geotechnical Experimentation Sites at Texas A&M University: clay and sand, data collected until 1992." *Res. Rep. NGES-TAMU-001 to the Fed. Hwy. Admin. and the Nat. Sci. Found.*, Dept. of Civ. Engrg., Texas A&M University, College Station, Tex.
Broms, B. B. (1968). "Swedish tieback system for sheet pile walls." *Proc., 3rd Budapest Conf. on Soil Mech. and Found. Engrg.*, 391–403.
Bustamante, M., and Doix, B. (1985). "Une Methode pour le Calcul des Tirants et des Micropieux Injectes." *Bull. de Liaison du Laboratoire des Ponts et Chaussees*, No. 140, Nov.–Dec., Laboratoire Central des Ponts de Chaussees, Paris, France.
Canadian foundation engineering manual, (1985). 2nd Ed., Canadian Geotechnical Society, c/o BiTech Publishers, Ltd., Vancouver, B.C., Canada.
Chaouch, A., and Briaud, J.-L. (1991). "Pull out test on a drilled and grouted pile loaded from the top." *Res. Rep. to UNOCAL Corp.*, Dept. of Civ. Engrg., Texas A&M University, College Station, Tex.
Chaouch, A., and Briaud, J.-L. (1992). "Pull out test on a drilled and grouted pile loaded from the bottom." *Res. Rep. to UNOCAL Corp.*, Dept. of Civ. Engrg., Texas A&M University, College Station, Tex.
Cheney, R. S. (1988). "Permanent ground anchors." *Rep. FHWA-DP-68-1R*, Federal Highway Administration, Washington, D.C.
Chung, M., and Briaud, J.-L. (1993). "Behavior of a full scale tieback wall in sand." *Res. Rep. to Schnabel Found. and the Fed. Hwy. Admin.*, Dept. of Civ. Engrg., Texas A&M University, College Station, Tex.
Jennings, S., Mathewson, C. C., Yancey, T., and Briaud, J.-L. (1996). "The National Geotechnical Experimentation Sites at Texas A&M University, clay and sand: geology," *Res. Rep. NGES-TAMU-005 to the Fed. Hwy. Admin. and the Nat. Sci. Found.*, Dept. of Civ. Engrg., Texas A&M University, College Station, Tex.
Kim, N.-K., and Briaud, J.-L. (1994). "A beam column method for tieback walls." *Res. Rep. to Schnabel Found. and the Fed. Hwy. Admin.*, Dept. of Civ. Engrg., Texas A&M University, College Station, Tex.
Kulhawy, F. H., and Jackson, C. S. (1989). "Some observations of undrained side resistance of drilled shafts." *Foundation engineering: current principles and practices*, Vol. 2, ASCE, 1011–1025.
Littlejohn, G. S. (1968). "Recent developments in ground anchor construction." *Ground Engrg.*, London, U.K., 1(3), 32–36, 46.
Littlejohn, G. S. (1970). "Soil anchors." *Ground Engrg., Proc. of an Inst. of Civ. Engrs. Conf.*, London, U.K., 36–40.
Littlejohn, G. S. (1990). "Ground anchorage practice." *Design and performance of earth retaining structures, Geotech. Spec. Publ. No. 25*, ASCE, 692–733.
Long, J. H., Cording, E. J., and Mueller, C. G. (1996). "Analysis and behavior of tieback walls." *Rep. to Schnabel Found. Co.*, Dept. of Civ. Engrg., University of Illinois, Urbana, Ill.
Marcontell, M., and Briaud, J.-L. (1994). "The National Geotechnical Experimentation Sites at Texas A&M University: clay and sand, data collected from January, 1993 to July, 1994." *Res. Rep. NGES-TAMU-003 to the Fed. Hwy. Admin. and the Nat. Sci. Found.*, Vols. 1–2, Dept. of Civ. Engrg., Texas A&M University, College Station, Tex.
Mueller, C. G. (1996). "Behavior of model-scale tieback walls in sand," PhD dissertation, Dept. of Civ. Engrg., University of Illinois, Urbana, Ill.
Mueller, C. G., Long, J. H., Cording, E. J., and Weatherby, D. E. (1994).

131

"Ground movements from tieback wall construction." *ASCE Conf. on Vertical and Horizontal Deformations for Foundations and Embankments, Geotech. Spec. Publ. No. 40*, 1337–1352.

Murff, J. D. (1980). "Pile capacity in a softening soil." *Int. J. Numer. and Analytical Methods in Geomech.*, 4, 185–189.

Neely, W. J., and Montague-Jones, M. (1974). "Pull-out capacity of straight-shafted and under-reamed ground anchors." *Die Siviele Ingenieur in Suid-Africa*, Jaargang 16, NR 14, 131–134.

Nicholson, P. J., Uranowski, D. D., and Wycliffe-Jones, P. T. (1982). "Permanent ground anchors: Nicholson design criteria." *Rep. FHWA/RD-81-151*, Federal Highway Administration, Washington, D.C.

Otta, L., Pantueck, M., and Goughnour, R. R. (1982). "Permanent ground anchors: stump design criteria." *Rep. FHWA/RD-81/152*, Federal Highway Administration, Washington, D.C.

Pfister, P., Evers, G., Guillaud, M., and Davidson, R. (1982). "Permanent ground anchors: stump design criteria." *Rep. FHWA/RD-81/150*, Federal Highway Administration, Washington, D.C.

Powers, W. F., and Briaud, J.-L. (1993). "Behavior of 10 full scale ground anchors installed in stiff clay." *Res. Rep. to Schnabel Found. and the Fed. Hwy. Admin.*, Dept. of Civ. Engrg., Texas A&M University, College Station, Tex.

Reese, L. C., and O'Neill, M. W. (1988). "Drilled shafts: construction procedures and design methods." *Rep. No. FHWA-41-88-042*, Federal Highway Administration, Washington, D.C., 564.

Sapio, G. (1975). "Comporamento di Tiranti de Ancoraggio in Formazioni de Argille pre Consolidate." *XII Convegno Nationale de Geotecnica*, Consenza, Italy.

Tao, C., and Briaud, J.-L. (1995). "The National Geotechnical Experimentation Sites at Texas A&M University: clay and sand, soil data in electronic form 1977–1995." *Res. Rep. NGES-TAMU-004 to the Fed. Hwy. Admin. and the Nat. Sci. Found.*, Dept. of Civ. Engrg., Texas A&M University, College Station, Tex.

Weatherby, D. E. (1982). "Tiebacks." *Rep. FHWA/RD-82/047*, Federal Highway Administration, Washington, D.C.

Tieback Walls in Sand: Numerical Simulation and Design Implications

By Jean-Louis Briaud,[1] Fellow, ASCE, and Yujin Lim[2]

ABSTRACT: A three-dimensional nonlinear finite-element analysis is used to study the influence of various design decisions for tieback walls. The numerical model simulates the soldier piles and the tendon bonded length of the anchors with beam elements, the unbonded tendon with a spring element, the wood lagging with shell elements, and the soil with solid three-dimensional (3D) nonlinear elements. The soil model used is a modified hyperbolic model with unloading hysteresis. The complete sequence of construction is simulated including the excavation and the placement and stressing of the anchors. The numerical model is calibrated against an instrumented case history. Then a parametric study is conducted. The results give information on the influence of the following factors on the wall behavior: Location of the tendon unbonded zone, magnitude of the anchor forces, embedment of the soldier piles, and stiffnesses of the wood lagging and the piles. The implications in design are discussed.

INTRODUCTION

Most commonly, tieback walls (Fig. 1) are designed on the basis of a simple pressure diagram (Terzaghi and Peck 1967) used to calculate the anchor loads and the bending moment profile in the piles. There is a growing trend in practice to design tieback walls by using the beam-column approach (Halliburton 1968; Matlock et al. 1981). This computer-based solution is used to predict the bending moment, the axial load, and the deflection profiles of the piles after the anchor loads have been chosen. Compared to the simple pressure diagram approach, the beam-column approach leads to deflection predictions and to improved bending moment profiles; however, the predicted deflections are not as reliable as the bending moments because the model ignores the mass movement of the soil. The finite-element method (FEM) represents another level of sophistication that better models the components involved (Clough 1984). The drawback is that the FEM approach is very time consuming; therefore, it is generally performed at the research level or for very large projects only.

A study on the use of the beam-column approach (Kim and Briaud 1994) led to detailed recommendations on how to best use that method. It also identified the inability of predicting reliable displacement profiles with this method because the model ignores mass movement. The FEM study described in this article was undertaken, after the beam-column study, to better simulate the deformation process and to evaluate the influence of various factors on the wall deflections. These factors include the location of the first anchor, the length of the tendon unbonded zone, the magnitude of the anchor forces, the embedment of the soldier piles, and the stiffnesses of the wood lagging and the piles (Lim and Briaud 1996).

The FEM has been used for the analysis of anchored retaining structures by Clough et al. (1972), Tsui (1974), Huder (1976), Desai et al. (1986), and Fernandes and Falcao (1988). Contributions on the simulation of the excavation process with the FEM have been made by Goodman and Brown (1963), Ishihara (1970), Christian and Wong (1973), Chandrasekaran

and King (1974), Ghaboussi and Pecknold (1984), and Brown and Booker (1985).

One of the first steps in any numerical simulation is to determine where to place the boundaries so that their influence on the results will be minimized. The next section addresses this issue.

MESH BOUNDARIES: HOW FAR IS FAR ENOUGH?

The boundary effect was studied while using a linear elastic soil. The bottom of the mesh is best placed at a depth where the soil becomes notably harder. The distance from the bottom of the excavation to the hard layer, is called D_b. It was shown (Lim and Briaud 1996) that when using a linear elastic soil in the simulation, D_b had a linear influence on the vertical movement of the ground surface at the top of the wall but comparatively very little influence on the horizontal movement of the wall face. For nearly all other analyses a value of D_b equal to 9 m or 1.2 times the wall height was used. This value of D_b came from the instrumented case history used to calibrate the FEM model because of the hard shale layer existing at that depth.

Considering the parameters H, W_e, B_e, and D_b as defined in Fig. 2, it was found in a separate study (Lim and Briaud 1996) that $W_e = 3D_b$ and $B_e = 3(H + D_b)$ were appropriate values for W_e and B_e; indeed beyond these values, W_e and B_e have little influence on the horizontal deflection of the wall due to the excavation of the soil. This confirms previous findings by Dunlop and Duncan (1970). For the instrumented wall to be simulated, H was 7.5 m, D_b was 9 m, B_e was 66 m or $4(H_e + D_b)$, and W_e was 10 m. The small value of W_e was chosen because the U-shaped excavation for the case history was 20-m wide.

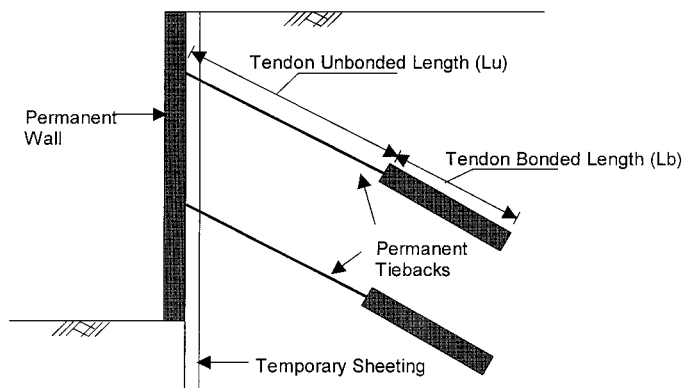[1]Spencer J. Buchanan Prof., Civ. Engrg., Texas A&M Univ., College Station, TX 77843-3136.

[2]Sr. Engr., Geotech. Div., Hwy. Res. Ctr., Korea Highway Corp., 293-1 Kumto-dong, Sujung-ku, Sungnam, S. Korea.

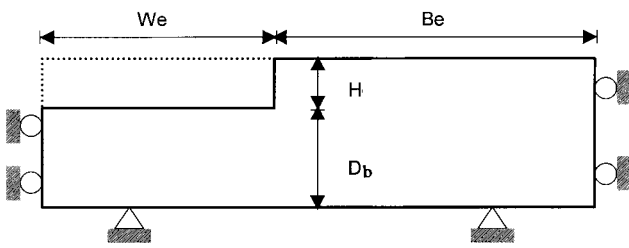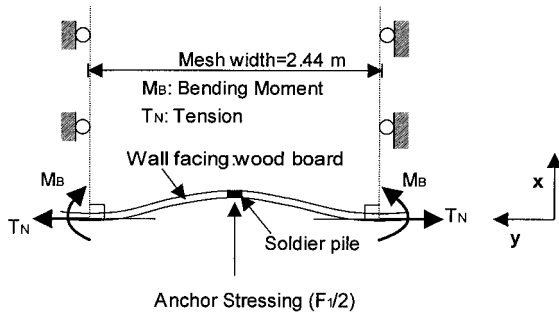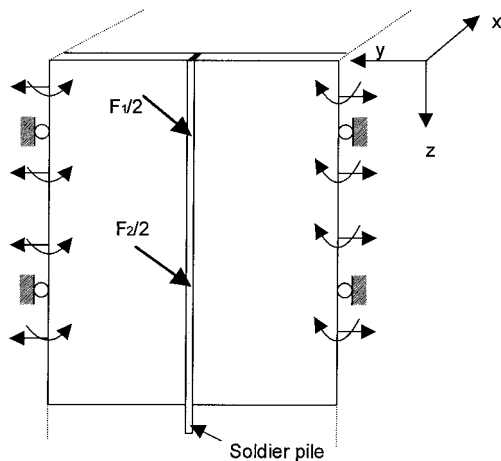**FIG. 1. Schematic of Tieback Wall**

FIG. 2. Definition of H_e, B_e, and D

(a) Force and boundary condition requirements: Plan view

(b) Force and boundary condition requirements: Front view

FIG. 3. Simulation Repetitive Wall Section

SIMULATED WALL SECTION

It would be possible to simulate the entire width of the wall in three dimensions. However, the size of the mesh would be prohibitively large. Instead, a repetitive section of the wall was chosen for the simulation. It was found that the best section (Fig. 3) would include one vertical pile at the center of the section, one stack of inclined anchors attached to the soldier pile and penetrating back into the soil, and the soil mass. The width of the mesh was equal to the pile spacing or 2.44 m for the case history. Special moment restraints were required on the vertical edge boundaries of the wall to maintain a right angle in plan view between the displaced wall face and the sides of the simulated wall section; namely, a tensile force T_n and a moment M_b were induced as shown in Fig. 3(a).

This wall section was chosen to simulate the three-dimensional behavior of a repetitive wall section toward the center of the excavation; it does not simulate the three dimensional arching effects at the corners of the excavation.

SOIL AND STRUCTURE ELEMENT MODEL

The general purpose code ABAQUS (*ABAQUS* 1992) was used for all the runs. The soldier piles and the tendon bonded

length of the anchors were simulated with beam elements; these are one-dimensional (1D) elements that can resist axial loads and bending moments. The stiffness for the pile elements was the *EI* and *AE* values of the soldier piles in the case history. These elements could resist bending in the three directions. The tendon bonded length was treated as a composite steel/grout section to get the *EI* and *AE* stiffness. A reduced grout modulus equal to 40% of the intact grout modulus was used to account for grout cracking; 40% was an educated guess. The wood lagging facing was simulated with shell elements; these are two-dimensional (2D) elements that can resist axial loads and bending moments in the two directions. The shell elements were given the thickness of the wooden boards and the modulus of wood. The steel tendon in the tendon unbonded length of the anchor was simulated as a spring element; this is a 1D element that can only resist axial load. This element was given a spring stiffness K equal to the initial slope of the load-displacement curve obtained in the anchor pullout tests.

The soil was simulated with 3D eight-noded brick elements. The soil model was a modified Duncan-Chang hyperbolic model (Duncan et al. 1980; Seed and Duncan 1984). This model is a nonlinear model that includes the influence of the stress level on the stiffness, strength, and volume change characteristics of the soil. With this soil model it was also possible to simulate the hysteresis of the soil by unloading and reloading the soil along a path different from the loading path. The parameters necessary for the soil model included seven parameters to describe the loading path tangent Young's modulus E_t, plus two parameters to describe the Poisson's ratio ν_t plus one parameter to describe the unloading-reloading path modulus E_{ur}. The seven parameters for E_t included the unit weight γ, the coefficient of earth pressure at rest K_0, the initial tangent modulus factor K, the stress influence exponent n for the tangent Young's modulus, the failure ratio R_f, the effective stress friction angle ϕ, and the effective stress cohesion C. The two additional parameters for ν_t were the bulk modulus factor K_B and the stress influence exponent n_B for the bulk modulus. The additional parameter for E_{ur} was the unload-reload modulus factor K_{ur}.

The tangent Young's modulus E_t is defined as the instantaneous tangential slope of the triaxial stress strain curve

$$E_t = \frac{\partial(\sigma_1 - \sigma_3)}{\partial \varepsilon_1} \tag{1}$$

where σ_1 and σ_3 = major and minor principal stresses in a soil element, respectively; and ε_1 = major principal strain for that same soil element. The expression that gives E_t for the hyperbolic model is

$$E_t = \left[1 - \frac{R_f(1 - \sin \phi)(\sigma_1 - \sigma_3)}{2(c \cos \phi + \sigma_3 \sin \phi)} \right]^2 Kp_a \left(\frac{\sigma_3}{p_a} \right) \tag{2}$$

where σ_1 and σ_3 have initial values of γz and $K_0 \gamma z$ (z = depth), respectively, and are updated as the loading and unloading takes place in increments; and p_a = atmospheric pressure.

The tangent Poisson's ratio ν_t is defined as

$$\nu_t = 0.5 - \frac{E_t}{6B_t} \tag{3}$$

where the tangent bulk modulus B_t is given by

$$B_t = K_B p_a \left(\frac{\sigma_3}{p_a} \right)^{n_B} \tag{4}$$

The relationship between E_t, ν_t, and B_t is given by

$$B_t = \frac{E_t}{3(1 - 2\nu_t)} \tag{5}$$

134

Seed and Duncan (1984) suggested a lower-bound value of B_t

$$B_{t\,min} = \frac{E_t}{3}\left(\frac{2 - \sin\phi}{\sin\phi}\right) \qquad (6)$$

This in essence forces the Poisson's ratio to remain higher than $K_0/(1 + K_0)$ and helps to prevent the tendency of the model to underestimate lateral stresses at small confining pressures. Poisson's ratio was also kept lower than 0.49. To avoid tension problems a lower bound for E_t was set at

$$E_{t\,min} = 0.25\ Kp_a(0.02)^n \qquad (7)$$

The unload-reload E_{ur} modulus is given by

$$E_{ur} = K_{ur}p_a\left(\frac{\sigma_3}{p_a}\right)^n \qquad (8)$$

At the point of unloading on the stress-strain curve, the modulus changes from E_t from (2) to E_{ur} from (7). The value of E_{ur}/E_t can be large (e.g., 20) and this sharp discontinuity in modulus value can lead to numerical instability. To prevent this problem, a smooth transition from E_t to E_{ur} is used on the unloading path (Seed and Duncan 1984; Lim and Briaud 1996).

To decide whether an element is on the loading or unloading path, a stress state (SS) coefficient is calculated at each step

$$SS = \frac{\sigma_1 - \sigma_3}{(\sigma_1 - \sigma_3)_f}\sqrt[2]{\frac{\sigma_3}{p_a}} \qquad (9)$$

If the current value of SS is larger or equal to the highest past value of SS (SS max-past) then E_t is used. If SS < SS_{max}, the unloading modulus is then used. This hyperbolic model was coded in FORTRAN and implemented into ABAQUS as a user-defined subroutine UMAT. The numerical values of the parameters used in the simulation of the case history are listed in Table 1.

TABLE 1. Parameters Used for FEM Simulation

Data (1)	Parameter (2)	Value (3)
Soil	Initial tangent modulus factor K	300
	Initial tangent modulus exponent n	0.85
	Strength ratio R_f	0.93
	Friction angle ϕ	32°
	Cohesion c	0
	Unloading-reloading modulus number K_{ur}	1,200
	Bulk modulus number K_B	272
	Bulk modulus exponent n_B	0.5
	Unit weight γ_s	18.5 kN·m³
	At-rest earth pressure coefficient K_0	0.65
Anchor	Tendon unbonded length	5.05 m
	Tendon bonded length	7.3 m
	Lock-off load—Row 1	182.35 kN
	Lock-off load–Row 2	160.0 kN
	Tendon stiffness—Row 1	19,846 kN·m
	Tendon stiffness—Row 2	19,479 kN·m
	Angle of inclination β	30°
Wall facing	Wall height	7.5 m
	Thickness of wall facing	0.1 m
	Elastic modulus of wood board	1.365×10^6 kN·m²
Soldier pile	Length of soldier pile	9.15 m
	Embedment	1.65 m
	Diameter of pipe pile	0.25 m
	Thickness of pipe pile	0.00896 m
	Horizontal spacing of piles	2.44 m
	Elastic modulus of steel pipe pile	2.1×10^8 kN m²
	Flexural stiffness EI	11,620 kN·m²
	Axial stiffness AE	1.47×10^6 kN

SIMULATING EXCAVATION SEQUENCE

The initial shape of the mesh was a rectangular parallelepiped (Fig. 4). The first step (Step 1 in Fig. 5) was to turn the gravity stresses on in the large brick, which was 76 m in length, 16.5 m in height, and 2.44 m in width. The second step (Step 2 in Fig. 5) was to install the piles; this consisted of activating the beam elements and allowing them to be stressed by the next steps. Therefore, driving stresses were not simulated. The third step (Step 3 in Fig. 5) was to excavate the first lift (2.4 m in the case history). This step induced initial deflections and a change in stress. The fourth step (Step 4 in Fig. 5) was to install the wood lagging and the first row of anchors. This step consisted of activating the shell elements simulating the wood lagging and activating the beam elements simulating the tendon bonded length of the anchor, thus allowing them to be stressed by the next steps. Therefore, the actual drilling and grouting process for the anchors was not simulated. The fifth step (Step 5 in Fig. 5) was to stress the anchor. This was simulated by applying on the soldier pile a force F equal to and in the direction of the anchor force and applying the same force F but in the opposite direction at the top of the tendon bonded zone. The sixth step (Step 6 in Fig. 5) consisted of activating the spring element simulating the unbonded tendon length. The seventh step was the excavation of the next lift (similar to Step 3 in Fig. 5). The process continued with repetitions of Steps 3–6 to simulate additional excavation lifts and anchor stressing. The final step was an excavation step to final grade below the last rows of anchor. Each run required about 6 h of central processing unit time on the Texas A&M University Super Computer. A total of ~100 runs was performed for a dollar value of $18,000.

Each excavation was simulated by applying on each element along the nth excavation boundary a stress vector $\Delta\boldsymbol{\sigma}_n$ in opposite direction to the stress vector that existed on that boundary at the end of the $(n - 1)$th excavation step. The stress vector $\Delta\boldsymbol{\sigma}_n$ was found by iteration until that vector and the stress vector existing on that boundary at the end of the previous step added to zero all along the nth excavation boundary. All elements above the nth excavation boundary were then deactivated. More precisely, the following procedure was used:

1. At each excavation step the unbalanced forces due to the excavation of the soil layers are

$$\mathbf{R}^n = P^n - I^{n-1} = \mathbf{K}^n\Delta U^n \qquad (10)$$

where $\mathbf{K}^n$ = tangent global stiffness matrix for the active element at the current increment or iteration; ΔU^n = increments of nodal point displacements; P^n = external loads for the current active elements, L^{n-1} = internal forces for active elements resulting from the previous excavation step; and $\mathbf{R}^n$ = residual force vector.
2. Solve for the residual force vector $\mathbf{R}$ assuming elastic behavior. For each excavation step, the force vector $\mathbf{R}$ is applied in several increments. Then equilibrium is found by iterating to reach a certain tolerance. For a system that is exactly in equilibrium $\mathbf{R}^n = 0$.
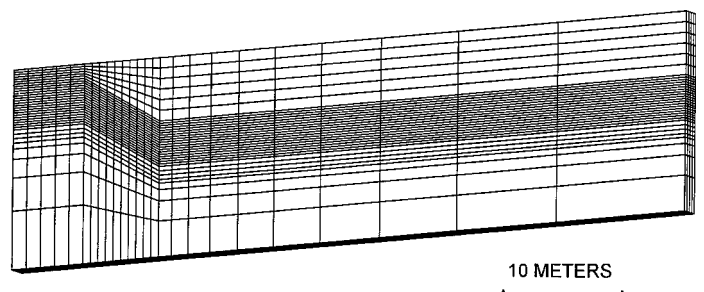

10 METERS

FIG. 4. Finite Element Mesh

STEP 1. Specify initial geostatic stress condition, and apply gravity load to the mesh and check equilibrium.

STEP 2. Install piles by activating the corresponding elements.

STEP 3. Excavate to the first Excavation level.

STEP 4. Install tendon bonded zone of the anchor, wall facing.

STEP 5. Apply lock-off load.

STEP 6. Activate spring simulating tendon unbonded length.
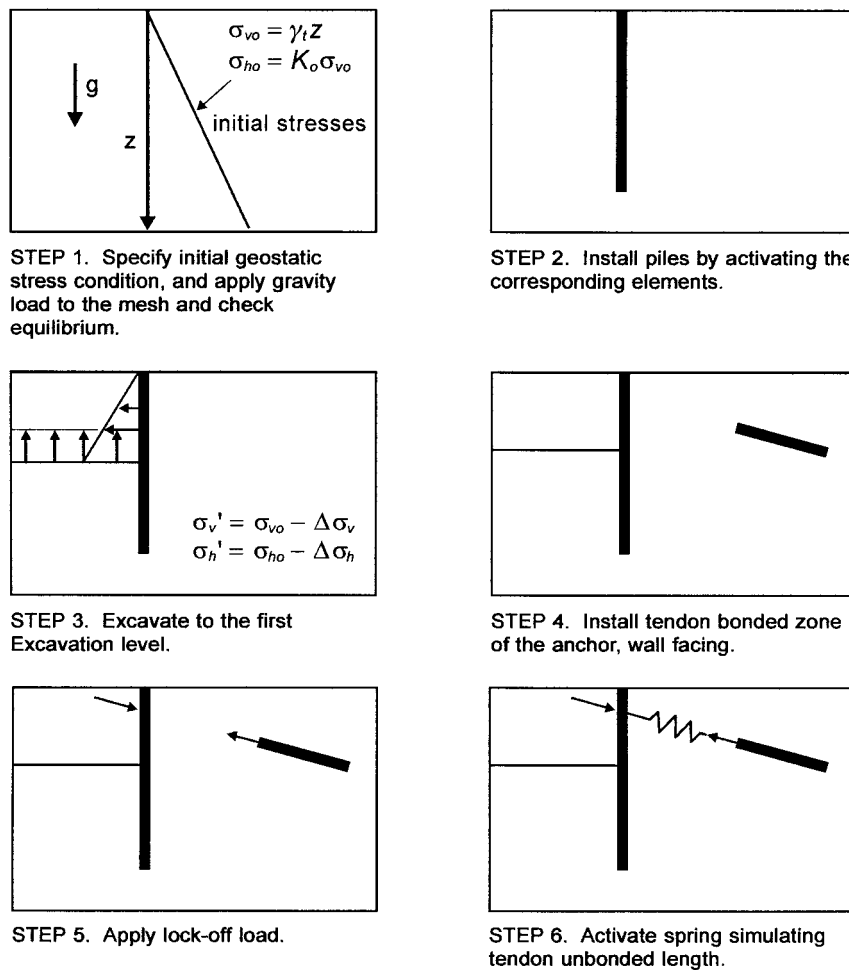
FIG. 5. Simulation of Excavation Sequence

3. Compute the internal force vector $\mathbf{I}^{n-1}$ for elements in the nth excavation stage by considering stress existing after the $(n - 1)$th excavation.
4. Compute the residual forces.
5. If convergence does not occur, apply the residual forces instead of $\mathbf{R}$ and repeat Steps 2–4.
   If convergence occurs go to Step 1; solve for the next step of excavation.

TEXAS A&M UNIVERSITY INSTRUMENTED TIEBACK WALL

The Federal Highway Administration and Schnabel Foundation sponsored the construction of a full-scale instrumented tieback wall in 1991 at the National Geotechnical Experimentation Site on the Riverside Campus of Texas A&M University (Fig. 6). This wall is 60 m in length and 7.5 m in height. It was built by driving H piles in a line on 2.44-m center for one part of the wall and by drilling and grouting H piles in a line on 2.44-m center for the other part of the wall. Half of the wall had only one row of anchors while the other half had two rows of anchors. The two-row anchor wall was used to calibrate the FEM model. The steel H piles were HP 6×24 section, 9.15 m in length embedded 1.65 m below the bottom of the excavation. The wood lagging boards were 2.4 m in length, 0.3 m in height, and 75 mm in thickness. The high pressure grouted anchors were inclined 30° with the horizontal and located at 1.8 and 4.8 m below the top of the wall; they were 89 mm in diameter, 12.35 m in length with a 7.3-m tendon bonded length. The steel tendon itself (Dywidag bar) was 25 mm in diameter.

The soil consists of a 13-m-thick layer of medium dense fine silty sand deposited in a river environment $\sim$50,000 years ago and underlain by a 40,000,000-years-old hard shale. The engineering properties and the geology of this sand deposit have been determined in detail as part of the National Geotechnical Experimentation Site program (Briaud 1993; Marcontell, and Briaud 1994; Tao and Briaud 1995; Fugro-McClelland 1996; Jennings et al. 1996; Simon and Briaud 1996). The following average properties of the sand are a total unit weight of 18.5 kN/m^3, standard penetration test blow count increasing from 10 blows per 0.3 m at the surface to 27 blows per 0.3 m at the bottom of the piles, borehole shear friction angle of 32° with no cohesion, cone penetration test point resistance of 7 MPa, PMT modulus of 8 MPa, and PMT limit pressure of 0.5 MPa. The water level is 9.5 m below the top of the wall.

The wall was instrumented with vibrating wire strain gauges on the soldier piles to obtain bending moment profiles, with inclinometer casings to obtain horizontal deflection profiles, and with load cells at the anchor heads to monitor the anchor forces.

CALIBRATION OF MODEL AGAINST CASE HISTORY

The TAMU two-row anchor tieback wall was used to calibrate the FEM model. The H piles were replaced with pipe piles of equivalent stiffness (AE and EI) because the H-type beam element in the ABAQUS library created some numerical instabilities while the pipe type did not. For the anchors, the grout annulus with a modulus equal to 0.4 times the intact modulus of grout was included with the steel tendon to compute the stiffness AE and EI of the tendon bonded length. The spring constant for the unbonded tendon length is given by
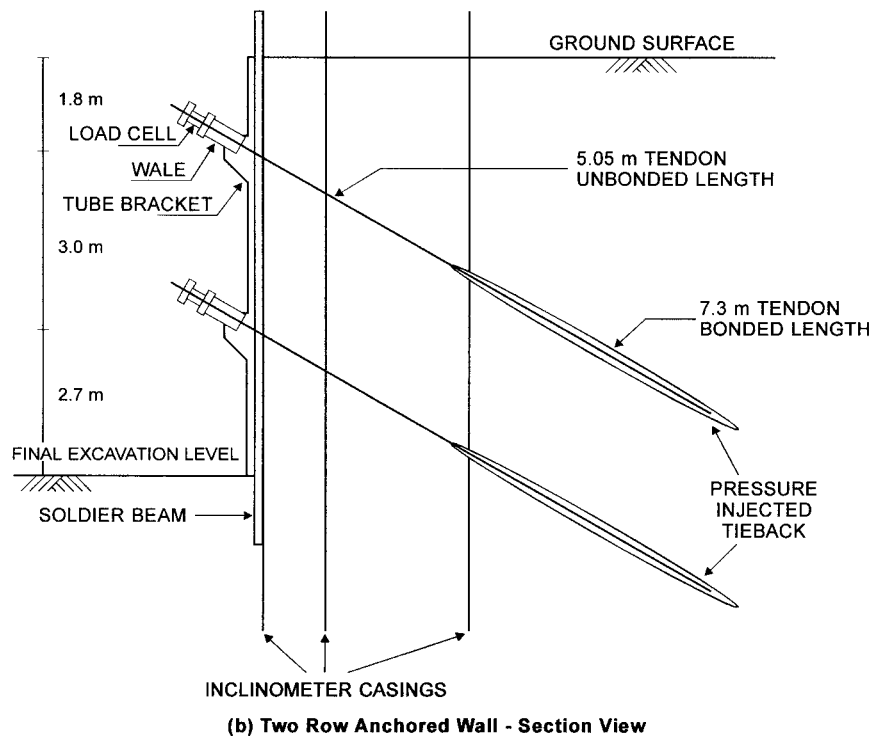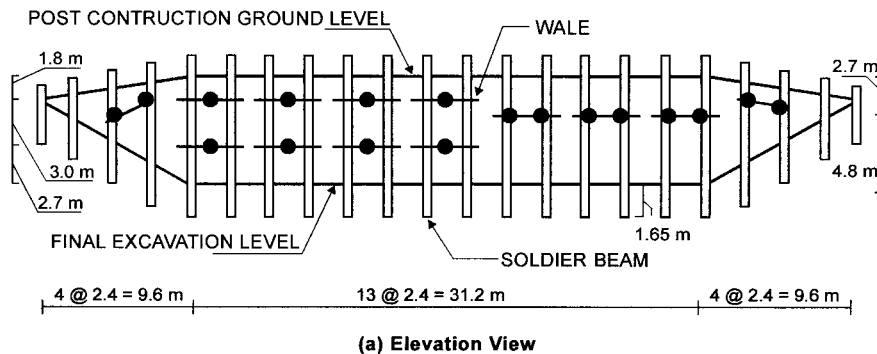
(a) Elevation View

(b) Two Row Anchored Wall - Section View

FIG. 6. Texas A&M University Tieback Wall

AE/L, where A and E are the cross section area and modulus of the steel tendon, and L is the unbonded length. Actually this spring constant was obtained from the anchor load tests as the slope of the load versus movement curve. The 10-parameter hyperbolic model was used for the soil.

The calibration process consisted of finding the set of those 10 parameters that led to the best match between the measured and calculated deflection u, bending moment M, and axial load Q profiles of the soldier piles. Among the soil parameters it was found that the most influential ones were K and K_0 for the deflections, K_0 for the bending moment in the soldier piles, and γ_t for the axial load including the downdrag load. All other parameters had a relatively small impact on the calculated values.

The comparison between measured and calculated u, M, and Q profiles are shown on Fig. 7. As can be seen the bending moment profile and the deflection at the top of the wall are well matched, while the deflection profile and the axial load below 5 m were not. Within the constraints of the project the writers could not match the three profiles (deflection, bending moment, and axial load) equally well. This is due in part to the limitation of the model. The writers decided to concentrate on matching the bending moment profile and the top deflection ($K = 300$) while erring on the conservative side for the other parameters. A K of 600 led to better matching of the deflection profile but underpredicted severely the top deflection. The final model parameters are presented in Table 1.

PARAMETRIC ANALYSIS

A number of factors were varied from the initial values of the case history to evaluate their influence on the wall response. These factors were the location of the first anchor, the length of the tendon unbonded zone, the magnitude of the anchor force, the embedment of the soldier piles, and the stiffnesses AE and EI of the wood lagging and the soldier piles.

The location of the first anchor was varied from $Y = 0.6$ m to $Y = 1.8$ m below the top of the wall while keeping the angle of the anchors constant. The second anchor was kept in 3 m below the first anchor. The results show (Fig. 8) that a position of $1.2-1.5$ m leads to lower deflections and lower bending moments with a 25% reduction in u and M compared to the 1.8-m anchor position. The results also show that the position of the first anchor has very little influence on the axial load distribution including the downdrag load.

The length of the tendon unbonded zone L_u was ~5 m for the case history. This length L_u was varied from 1.375 to 16.2 m while keeping the tendon bonded length constant and the anchor load constant; also the stiffness of the spring that represents the unbonded length of the tendon was kept constant (Table 1). While this may not be a good representation of the actual situation it was used to isolate the influence of the location of the tendon bonded length. The distance D in Fig. 9 is the horizontal distance from the top of the wall to the intersection with the ground surface of a line passing through
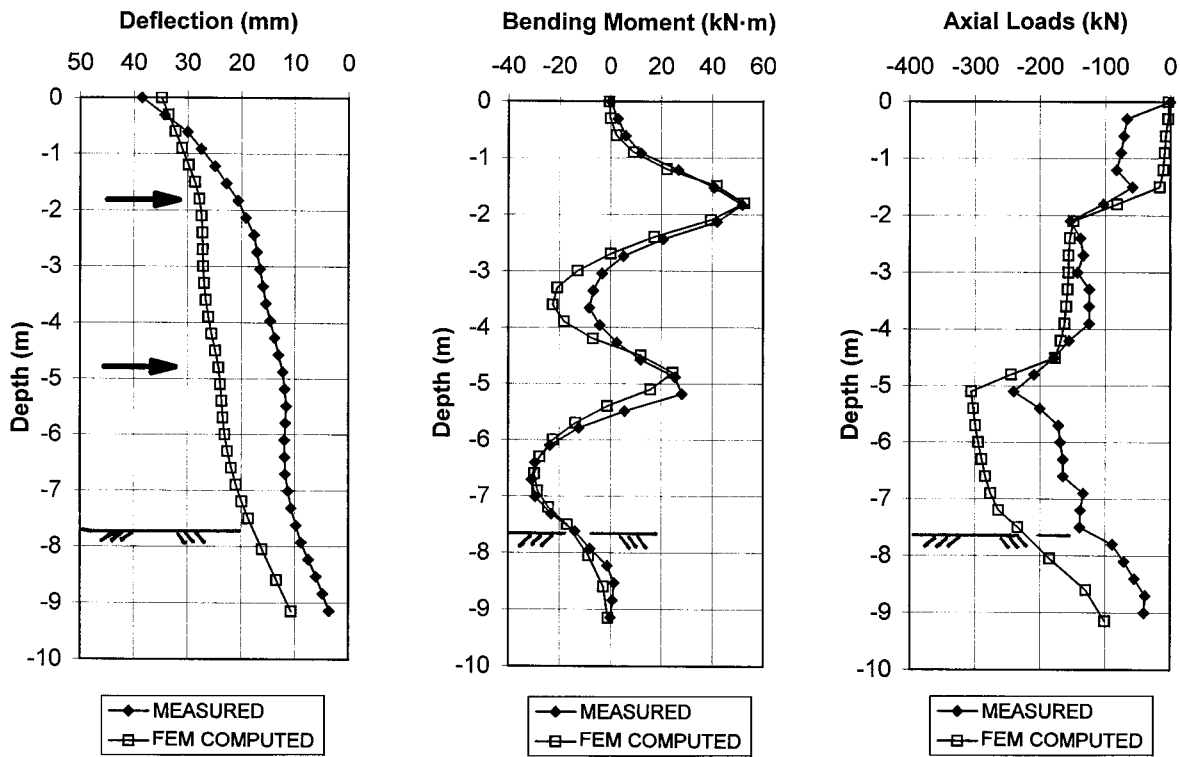
FIG. 7.   Measured and Calculated Displacements, Bending Moments, and Axial Loads
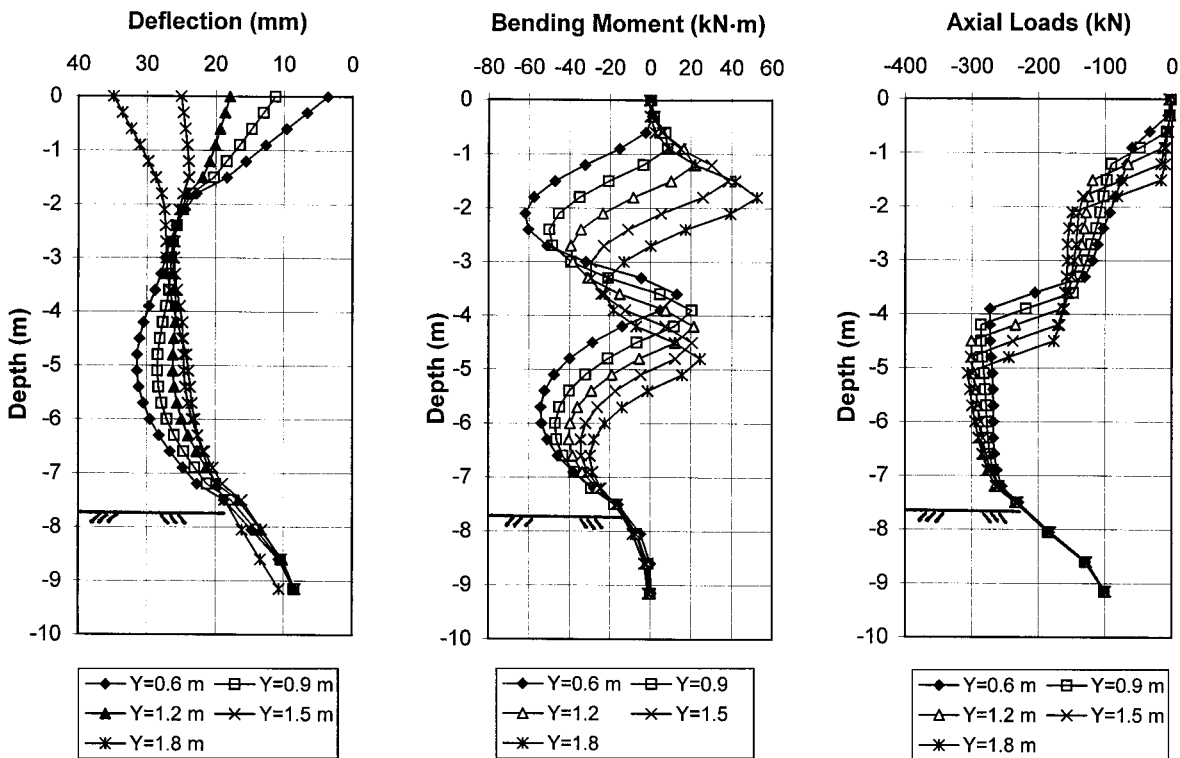
FIG. 8.   Influence of First Anchor Location

the end of the tendon unbonded length and parallel to the failure plane of the classical failure wedge $(45 + \phi/2)$ starting at the bottom of the excavation. The distance H is the wall height. The results show (Fig. 9) that the location of the tendon bonded length only has a small influence on the bending moment and the axial load in the soldier piles as long as the beginning of the tendon bonded zone is outside the failure wedge. The location of the tendon bonded length has an influence on the deflection at the top of the wall u_{top}; when L_u was 3 times longer than in the case history the deflection at

the top of the wall u_{top} was equal to 0.57 times the value of u_{top} for the case history. At first glance, this result may seem surprising if one thinks that the longer the unbonded length the larger the elongation of the anchor. Of course this did not occur in the simulation because the spring stiffness was kept constant. The fact that the anchor is prestressed to the lock-off load and that there is very little change in anchor load as the excavation proceeds (as observed in the case history) minimizes the influence of the unbonded length elongation as the large elongation takes place during prestressing. On the other
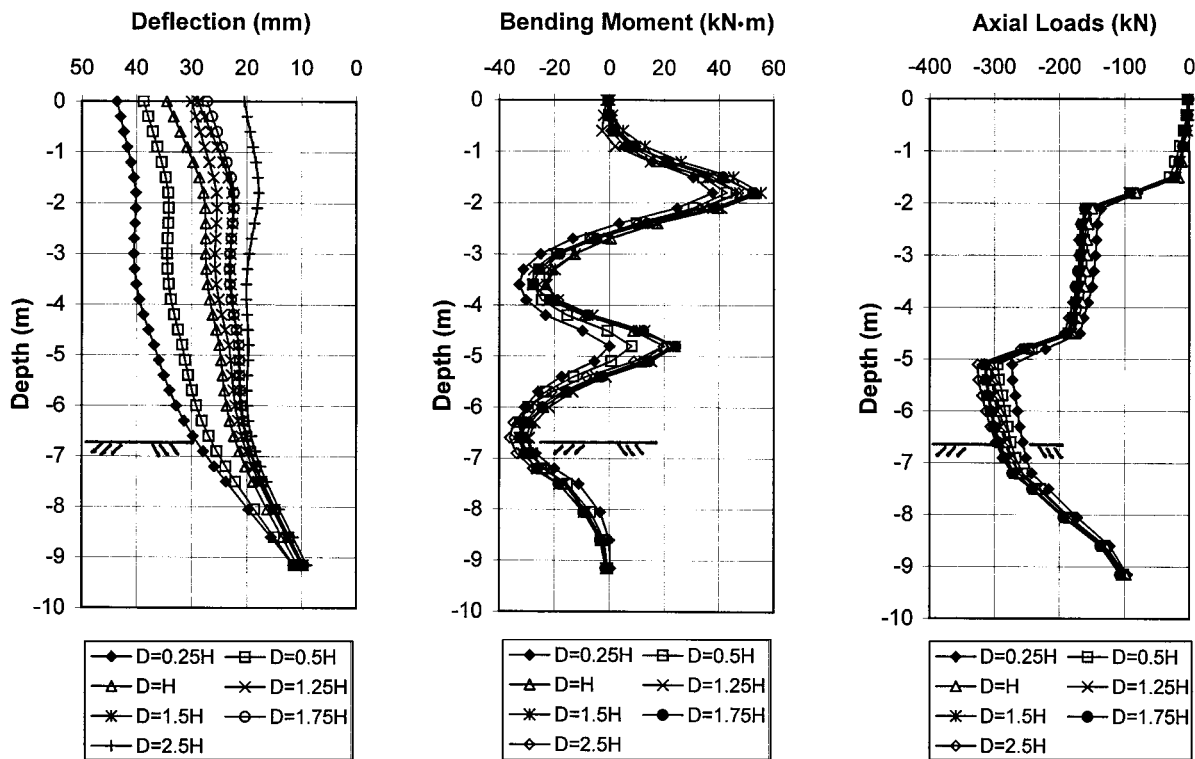
FIG. 9. Influence of Tendon Unbonded Length
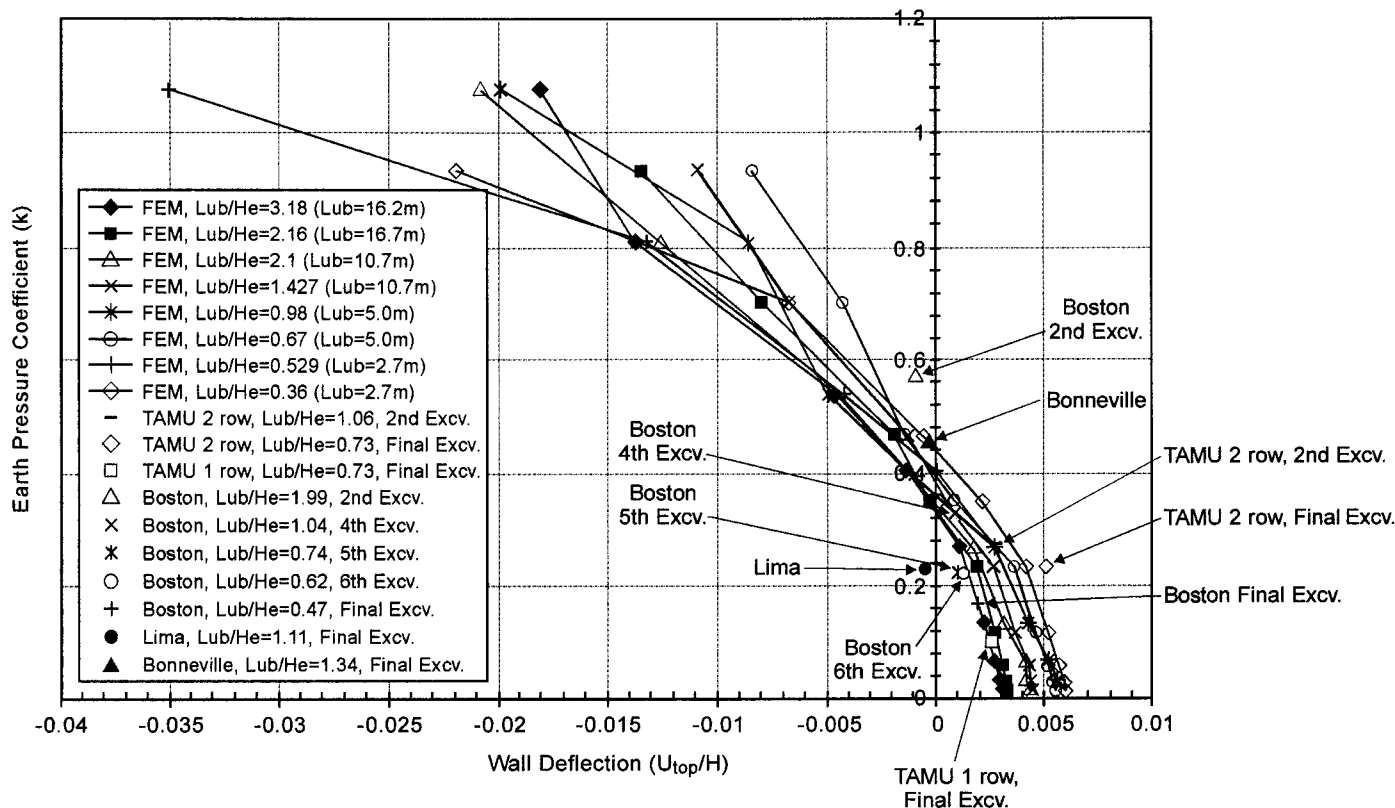
FIG. 10. Influence of Anchor Force on Deflection at Top of Wall

hand long tendon unbonded lengths place the tendon bonded length further away from the wall in a soil zone that moves less when the wall is further excavated; also for inclined anchors the tendon bonded length is located deeper in the soil mass and therefore, usually, in a stronger less deformable mass. It was found that L_u had no influence on the deflection at the bottom of the wall, which remained equal to 10 mm. It was also found that increasing L_u for the first anchor alone it

was much more effective to reduce the deflection at the top of the wall than increasing L_u for the second anchor.

The magnitude of the anchor force was varied. The sum of the horizontal components of the anchor forces divided by the frontal area of the wall is the average pressure p corresponding to a constant pressure diagram against the wall. Alternatively the anchor load is p times the tributary area. The ratio of p over γH is the earth pressure coefficient k; γ is the effective

soil unit weight; and H is the total height of the wall. The value of k was varied in the parametric analysis from 0.02 to 1.1 by varying the anchor loads correspondingly, and the deflection at the top of the wall u_{top} was calculated by the FEM. Case histories were also collected to obtain measured values of k and corresponding measured values of u_{top}. The Boston case history was obtained from Houghton and Dietz (1990); the Bonneville case history was obtained from Munger et al. (1990); the Lima case history was obtained from Lockwood (1988); and the Texas A&M University case history was obtained from Chung and Briaud (1993). The relationship between k and (u_{top}/H) is presented in Fig. 10, while the relationship between k and (u_{mean}/H) is in Fig. 11, where u_{mean} is the average wall deflection over the wall height; it is obtained from the deflection profile. These figures show that, for the common value of k equal to $0.65k_a = 0.2$ often used in design and for the data shown, the ratio (u_{top}/H) varies from 1/500 to 1/225. For the same value of k, the ratio (u_{mean}/H) varies from 1/1,000 to 1/300. The figures also show that for k values of ~0.4 the deflections are close to zero and that for k values higher than 0.4 the wall moves inward.

The embedment of the soldier piles was varied from 0 to 10 m. The results show that u_{top} decreases with increasing embedment (Fig. 12), that the bending moment profiles does not change significantly, but that the downdrag load increases significantly with increasing embedment.

The modulus of the wood lagging E_{wood} was varied. With the E_{wood} value equal to the wood modulus, the wooden boards bow between the soldier piles, and the center of the wooden boards deflects more than the piles. As E_{wood} increases the boards become more rigid, and the boards and soldier piles tend toward a common deflection; as a result the pile deflection increases. The bending moment also increases, but the axial load is relatively unaffected. Varying the stiffness EI of the soldier piles from $11,000-41,000$ kN·m^2 had only a small influence on the deflections, bending moments, and axial loads.

DESIGN IMPLICATIONS

The following recommendations are based on the data from four case histories, on a detailed 3D nonlinear FEM simulation of one of these case histories (the TAMU wall) and on an extensive FEM parametric analysis. The application of these recommendations is limited by the range of parameters studied.

The best position for the first anchor appears to be between 1.2 and 1.5 m below the top of the wall. In current practice the first anchor tends to be placed deeper than that. Significant deflections can accumulate during this step, and it is very difficult to eliminate them by further construction. By comparison, in soil nailing the first nail is placed at a much shallower depth. A vertical spacing of 3 m between anchor rows below the first anchor was the only spacing used. It appeared to work well as there was no excessive deflections nor bending moment between anchors.

The length of the unbonded length proposed by Cheney seems to work well. Longer unbonded length particularly for the first anchor leads to somewhat smaller deflections. Cheney's unbonded length for an anchor is equal to the length from the wall to the failure surface plus 1.5 m or one-fifth of the wall height, whichever is greater. The failure surface is taken as the plane having a $45° + \phi/2$ angle with the horizontal starting at the bottom of the wall.

The magnitude of the anchor loads is the most important factor influencing all variables. It has a direct influence on deflections and bending moments. In the case of mechanically stabilized earth walls and soil nailed walls the reinforcing strips or the nails are not prestressed; as a result there is less control over the deflection of the wall. In the case of tieback walls, the engineer can now use the proposed k versus (u_{top}/H) relationship to select anchor lock-off loads that will approximately generate a chosen deflection. The use of the k versus (u_{top}/H) relationship should be limited to cases that are similar to the cases used to generate that relationship. Zero deflection can be reached for a constant pressure diagram with a pressure
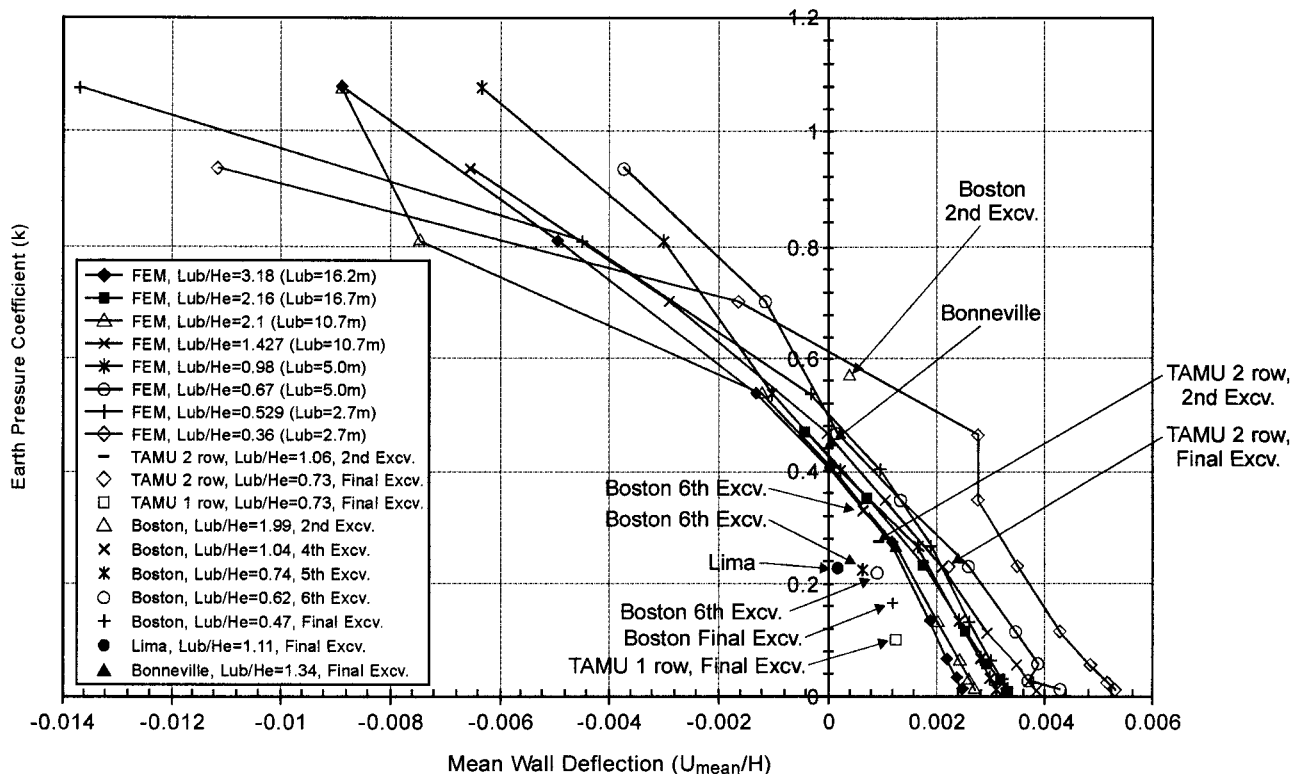

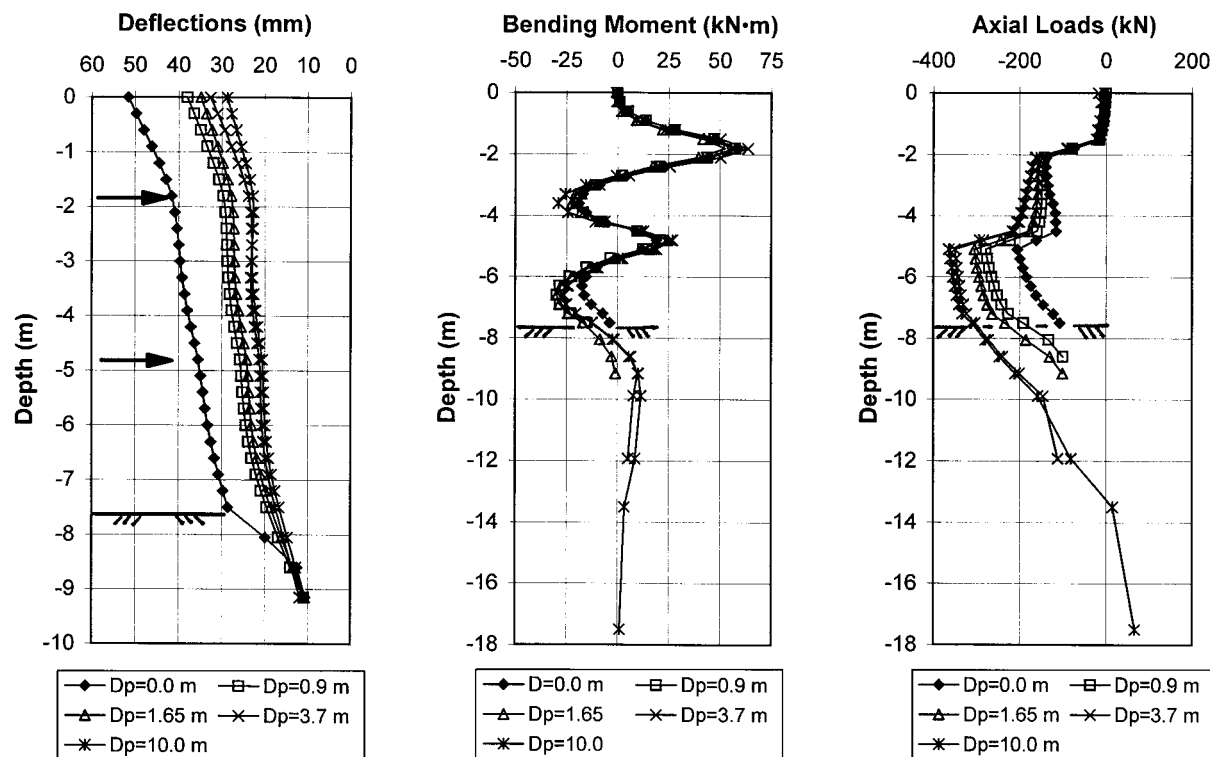**FIG. 11. Influence of Anchor Force on Mean Wall Deflection**

140

FIG. 12. Influence of Soldier Pile Embedment

intensity equal to $0.4\gamma H$. This pressure is ~ 2 times larger than Terzaghi and Peck's intensity of $0.65K_a\gamma H$.

Providing no embedment for the soldier piles is not recommended even if bottom heave and slope stability are not a problem. No embedment leads to larger deflection. An embedment of 1.5 m decreased the top deflection significantly in this study. Larger embedment depths were rather ineffective.

ACKNOWLEDGMENTS

APPENDIX. REFERENCES

ABAQUS User's and Theory Manuals. (1992). Version 5.2, Hibbit, Karlson & Sorensen Inc., Pawtucket, R.I.

Briaud, J.-L. (1993). "National geotechnical experimentation site at Texas A&M University: Data collected until 1992." *Rep. No. NGES-TAMU-001*, Department of Civil Engineering, Texas A&M University, College Station, Tex.

Brown, P. T., and Booker, J. R. (1985). "Finite element analysis of excavation." *Res. Rep. No. 532*, School of Civil and Mining Engineering, University of Sydney, Sydney, Australia.

Chandrasekaran, V. S., and King, G. J. W. (1974). "Simulation of excavation using finite elements." *J. Geotech. Engrg. Div.*, ASCE 100(9), 1086–1089.

Christian, J. T., and Wong, I. H. (1973). "Errors in simulating excavation in elastic media by elements." *Soils and Found.*, Tokyo, 13, 1–10.

Chung, M., and Briaud, J.-L. (1993). "Behavior of a full scale tieback wall in sand." *Rep. to Schnabel Foundation and the Federal Highway Administration*, Department of Civil Engineering, Texas A&M University, College Station, Tex.

Clough, G. W. (1984). *User's Manual for Program SOIL STRUCT*. Department of Civil Engineering, Virginia Polytechnic Institute and State University, Blacksburg, Va.

Clough, G. W., Weber, P. R., and Lamont, J. (1972). "Design and observation of a tie-back wall." *Proc., ASCE Spec. Conf., Perf. of Earth and Earth Supported Struct.*, Vol. 1, ASCE, New York, 1367–1389.

Desai, C. S., Muqtadir, A., and Sheele, F. (1986). "Interaction analysis of anchor-soil systems." *J. Geotech. Engrg.*, ASCE, 112(5), 537–553.

Duncan, J. M., Byrne, P. M., Wong, K. S., and Marby, P. (1980). "Strength, stress-strain and bulk modulus parameters for finite element analysis of stresses and movements in soil mass." *Rep. No. UCB/GT/80-01*, University of California, Berkeley, Calif.

Dunlop, P., and Duncan, J. M. (1970). "Development of failure around excavated slopes." *J. Soil Mech. and Found. Div.*, ASCE, 96(2), 471–493.

Fernandes, M. M., and Falcao, J. C.-B. (1988). "The nonlinear behavior of ground anchors and its consideration in finite element analysis of tied-back walls." *Proc., Num. Meth in Geomech.*, Balkema, Rotterdam, The Netherlands, 1243–1248.

Fugro-McClelland. (1996). "National geotechnical experimentation sites at Texas A&M University: Clay and sand laboratory test data." *Rep. No. NGES-TAMU-007*, Department of Civil Engineering, Texas A&M University, College Station, Tex.

Ghaboussi, J., and Pecknold, D. A. (1984). "Incremental finite element analysis on geometrically altered structure." *Int. J. Numer. Methods in Engrg.*, 20, 2051–2064.

Goodman, R. E., and Brown, C. B. (1963). "Dead load stresses and instability of slopes." *J. Soil Mech. and Found. Div.*, ASCE, 89(3).

Haliburton, T. A. (1968). "Numerical analysis of flexible retaining structures." *J. Soil Mech. and Found. Div.*, ASCE, 94(3), 1233–1251.

Houghton, R. C., and Dietz, D. L. (1990). "Design and performance of a deep excavation supports in Boston, Massachusetts." *Proc., ASCE Spec. Conf. on Des. and Perf. of Earth Retaining Struct.*, ASCE, New York, 795–816.

Huder, I. J. (1976). "Deformation and earth pressure." *Proc., Panel Discussion, 6th ECSMFE*, Vol. 4, 37–40.

Ishihara, K. (1970). "Relations between process of cutting and uniqueness of solution." *Soils and Found.*, Tokyo, 10(3), 50–65.

Jennings, S. P., Mathewson, C. C., Yancey, T. E., and Briaud, J.-L. (1996). "National geotechnical experimentation sites at Texas A&M University: Clay and sand. Geology." *Rep. No. NGES-TAMU-005*, Department of Civil Engineering, Texas A&M University, College Station, Tex.

Kim, N. K., and Briaud, J.-L. (1994). "A beam column method for tieback walls." *Rep. to Schnabel Foundation and the Federal Highway Administration*, Department of Civil Engineering, Texas A&M University, College Station, Tex.

Lim, Y., and Briaud, J.-L. (1996). "Three dimensional non linear finite element analysis of tieback walls and of soil nailed walls under piled bridge abutment." *Rep. to the Federal Highway Administration and the Texas Department of Transportation*, Department of Civil Engineering, Texas A&M University, College Station, Tex.

Lockwood, M. E. (1988). "Retention system monitoring demonstration

project no. 68.'' *Rep. for the Ohio Department of Transportation*, Cincinnati, Ohio.

Marcontell, M., and Briaud, J.-L. (1994). ''National geotechnical experimentation sites at Texas A&M University: Clay and sand. Data collected Until 1994.'' *Rep. No. NGES-TAMU-003*, Department of Civil Engineering, Texas A&M University, College Station, Tex.

Matlock, H., Bogard, D., and Lam, I. (1981). ''BMCOL 76: A computer program for the analysis of beam-columns under static axial and lateral loading.'' Program developed at the University of Texas at Austin and documented at Ertec Inc., Long Beach, Calif.

Munger, D. F., Jones, P. T., and Johnson, J. (1990). ''Temporary tieback wall, Bonneville navigation lock.'' *Proc., ASCE Spec. Conf. On Des. and Perf. of Earth Retaining Struct.*, ASCE, New York, 778–794.

Seed, R. B., and Duncan, J. M. (1984). ''SSCOMP: A finite element analysis program for evaluation of soil structure interaction and compaction effects.'' *Rep. No. UCB/GT/84-02*, University of California, Berkeley, Calif.

Simon, P. A., and Briaud, J.-L. (1996). ''National geotechnical experimentation sites at Texas A&M University: Clay and sand. Soil data in electronic form 1995–1996.'' *Rep. No. NGES-TAMU-006*, Department of Civil Engineering, Texas A&M University, College Station, Tex.

Tao, C., and Briaud, J.-L. (1995). ''National geotechnical experimentation sites at Texas A&M University: Clay and Sand. Soil data in electronic form 1995–1996.'' *Rep. No. NGES-TAMU-004*, Department of Civil Engineering, Texas A&M University, College Station, Tex.

Terzaghi, K., and Peck, R. B. (1967). *Soil mechanics in engineering practice*, 2nd Ed., Wiley, New York.

Tsui, Y. (1974). ''A fundamental study of tied-back wall behavior,'' PhD thesis, School of Engineering, Duke University, Durham, N.C.

Predicting, monitoring and controlling ground movements during excavation

R.J. Finno

Dept of Civil and Environmental Engineering, Northwestern University, USA
r-finno@northwestern.edu

ABSTRACT: This paper summarizes an adaptive management approach for predicting, monitoring, and controlling ground movements associated with excavations in urban areas. Successful use of monitoring data to update performance predictions of supported excavations depends equally on reasonable numerical simulations of performance, the type of monitoring data used as observations, and the optimization techniques used to minimize the difference between predictions and observed performance. This paper summarizes each of these factors and emphasizes their inter-dependence. Example applications of these techniques from case studies are presented to illustrate the capabilities of this approach.

1. INTRODUCTION

This paper describes an adaptive management approach to predict, monitor and control ground movements associated with excavations in urban areas. The goal of such an analysis is to allow one to use the observed performance at early stages of a project to objectively calibrate a predictive model so that reliable predictions of subsequent performance can be made. The successful application of such techniques depends on the predictive model, in this case a finite element simulation of construction, the monitoring data and the inverse technique itself. This paper will illustrate this approach as applied to supported excavations made through soft to medium clays. Comments are made regarding how details of the finite element simulations, the instrumentation and data collection, and the inverse technique affect the results of the methodology. Several examples of excavations where these techniques were applied are presented.

2. ADAPTIVE MANAGEMENT METHOD

Developments in sensor technology, information technology and numerical analyses allow one to automate the cycle of observation and performance prediction updating.

This automated observational approach can be thought of as adaptive management, and is summarized in Figure 1. The left hand column represents calculations made during the design and updating phases, and includes finite element computations when applied to deep excavations.
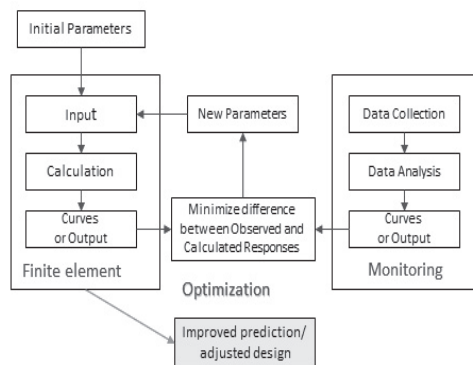

Figure 1. Adaptive Management Method

The center column is the optimization needed to update predictions based on the measurements. The right hand column represents the field observations, usually inclinometer data, but also optical survey, pore water pressure and strain gage data. These data can be incorporated into

the optimization routine as observations against which the numerical predictions are evaluated.

Examples of this approach applied to supported excavations are described by Finno and Calvello (2005) and Finno and Langousis (2007). Ideally, this process works automatically, all data collected in the field is transferred in real time to a host computer where it can be processed into format compatible with the numerical analyses, and updated performance predictions can be made in near real time.

Optimization is central to the process of adaptive management of geotechnical systems. Therein, various parts of a model are changed so that the measured values are matched by equivalent computed values until the resulting calibrated model accurately represents the main aspects of the actual system. Optimization tools are readily available. For example, MATLAB contains tool boxes with optimization routines, and these can be linked with commercial finite element codes as well.

Successful use of this approach depends equally on reasonable numerical simulations of performance, the type of monitoring data used as observations, and the optimization techniques used to minimize the difference between predictions and observed performance, as subsequently discussed.

2.1 Numerical analyses

A key to a successful finite element simulation is to reasonably represent within a numerical simulation pertinent field activities during construction. In addition to replicating construction procedures, there are several other important factors that have an impact on the computed responses, including the constitutive model, dimensionality of the problem and initial ground stresses. These factors have been described by Finno (2010) for application to supported excavations.

2.2 Optimization

Use of an inverse model provides results and statistics, offers powerful tools for model analysis and, in many instances, expedites the process of adjusting parameter values. The fundamental benefit of inverse modeling is its ability to calculate automatically parameter

values that produce the best fit between observed and computed results.

A common method of inverse analysis that has been applied to geotechnics is optimization by the gradient method. This approach employs a local parameter identification of a specific constitutive law. Many of the early evaluations of performance data using this approach were conducted with very simple soil models that severely restricted the ability of the computations to accurately reflect the observed field performance data, irrespective of employing inverse techniques. Clearly, unless the constitutive model has the capability to represent the response of the soil at the point of measurement to the particular loading condition, the approach will not be successful.

When applying the optimization technique to field problems, the underlying assumption is that the only uncertainty is the material response, and all other factors are known and contain no errors. When making a prediction of response, this is clearly not true. However, if field observations of performance are used to calibrate the model during construction, then the construction procedures are known exactly and this source of uncertainty is removed.

2.3 Observations

One must carefully select the types of data and locations of the measuring points when applying an inverse technique. Inclinometer data based on measurements close to a support wall are most useful when typical elasto-plastic constitutive models are assumed to represent soil behavior, as is the case when employing commercial finite element codes. These data can be supplemented by ground surface settlements when using a constitutive model that accounts for small strain nonlinearities and dilation (e.g., Finno 2010).

Advances in sensor technology allow measurements to be collected autonomously and sent to a host computer for processing, real time display and use in an inverse analysis. For example, remotely sensed total survey stations can be established to monitor the displacement of optical prisms (e.g. Finno and Blackburn 2005). In-place inclinometers can be deployed to remotely measure lateral movements of the walls of the support system and the adjacent

ground. Vibrating wire piezometers can be installed to monitor pore water pressures in the adjacent ground. Strain gauges can be mounted on structural supports to measure strains at discrete points in internal braces of temporary support systems due to earth loading, self-weight, temperature changes, and unexpected construction loading. Tiltmeters can be mounted on structural elements and results used to compute the angular distortion of an affected structure.

2. EXAMPLES OF CAPABILITIES

3.1 Parameter Optimization at Early Stages of Excavation

The ability of the approach to provide optimized parameters at an early stage of excavation which leads to good predictions of subsequent performance is illustrated by the Chicago Ave. and State St. subway renovation project in Chicago (Finno and Calvello 2005). This project involved the excavation of 12.2 m of soft to medium clay within 2 m of a school supported on shallow foundations. Figure 2 shows the FE mesh used in the analysis. The support system consisted of a secant pile wall with three levels of support, which included pipe struts (1st level) and tieback anchors (2nd and 3rd levels). The subsurface conditions consisted of an urban fill, mostly medium dense sand but also containing construction debris, overlying four strata associated with the advance and retreat of the Wisconsin-aged glacier. The upper three are ice margin deposits deposited underwater, and are distinguished by water content and undrained shear strength. With the exception of a clay crust in the upper layer, these deposits are lightly overconsolidated as a result of lowered groundwater levels after deposition and/or aging.

A complete record of performance of the excavation can be found in Finno et al. (2002). Figure 3 summarizes lateral movements to excavation and support on the east side of the excavation. Both lateral movements and settlements are shown, although optimization was based solely on the former. The movements that

occurred as the secant pile wall extend through all compressible layers. This is important when
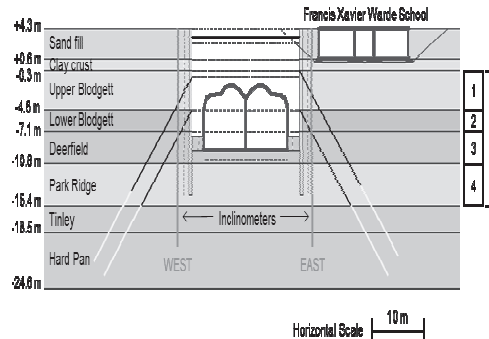
Figure 2. FE mesh for Chicago-State excavation

using these observations to calibrate parameters using inverse techniques in that these movements occur at an early stage of the excavation.

These observations were sufficient to optimize parameters in all layers so that movements could be "predicted" at subsequent stages of excavation. It is important to realize that the H-S model used for this analysis did not include effects of small strain non-linearity and hence relatively large movements were needed before any adjustments could be made to the model parameters.

Very little movement beyond that which occurred during wall installation were observed until the excavation was lowered below EL. – 1.4 m CCD; a maximum of 4 mm additional lateral movement occurred as a result of excavating to this elevation. This behavior suggests that the upper clays initially are relatively stiff, and provide field indications of the small strain nonlinearity of these soils. The secant pile wall incrementally moved toward the excavation in response to excavation-induced stress relief. When the excavation reached final grade, the maximum lateral movement was 28 mm. The school settled as the secant pile wall moved laterally. The maximum settlement at the school at the end of excavation also was 28 mm when the excavation bottomed out.

Figure 3. Movements at Chicago-State project

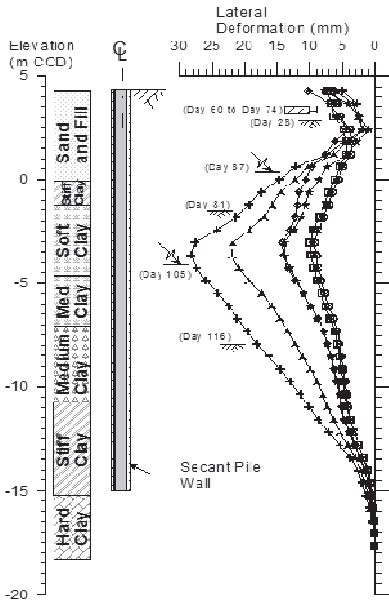Table 1 shows the calculation phases and the construction stages used in the finite element simulations. Note that the tunnel tubes and the school adjacent to the excavation were explicitly modeled in the first 12 phases of the simulation to take into account the effect of their construction on the soil surrounding the excavation. Stages 1, 2, 3, 4 and 5 in the optimization process refer to the construction stages for which the computed results were compared to inclinometer data taken from two inclinometers on opposite sides of the excavation. Construction steps not noted as "consolidation" on Table 3 were modeled as undrained. Stiffness parameters for the hardening soil model (Schanz et al. 1999) were optimized for each of the compressible clay layers. Details about the definition of the finite element problem, the calculation phases and the model parameters used in the simulation can be found in Calvello (2002). Visual examination of the horizontal displacement distributions at the inclinometer locations provides the simplest way to evaluate the fit between computed and measured field response. When computations were made based on parameters derived from results of drained

Table 1. FE Simulation of construction

Phase	Construction step	Stage
0	Initial conditions	
1-4	Tunnel construction (1940)	
5	Consolidation	
6-10	School construction (1960)	
11-12	Consolidation	
13	Drill secant pile wall (1999)	
14	Place concrete in wall	1
15	Consolidation (20 days)	
16	Excavate and install struts	2
17	Excavate below first tieback level	
18	Prestress first level of tiebacks	3
19	Excavate below second tieback level	
20	Prestress second level of tiebacks	4
21	Excavate to final grade	5

triaxial tests, the finite element model computed significantly larger displacements at every construction stage (Finno and Calvello 2005). The maximum computed horizontal displacements were about two times the measured ones and the computed displacement profiles result in significant and unrealistic movements in the lower clay layers. As one would expect, these results indicated that the stiffness properties for the clay layers based on conventionally-derived triaxial data were less than field values.

Figure 4 shows the comparison between the measured field data from both sides of the excavation and the computed horizontal displacements when parameters are optimized based on stage 1 observations. The improvement of the fit between the computed and measured response is significant. Despite the fact that the optimized set of parameters is calculated using only stage 1 observations, the positive influence on the calculated response is substantial for all construction stages. At the end of the construction (i.e. stage 5) the maximum computed displacement exceeds the measured data by only about 15%. These results are significant in that a successful recalibration of the model at an early construction stage positively affects subsequent "predictions" of the soil behavior throughout construction.
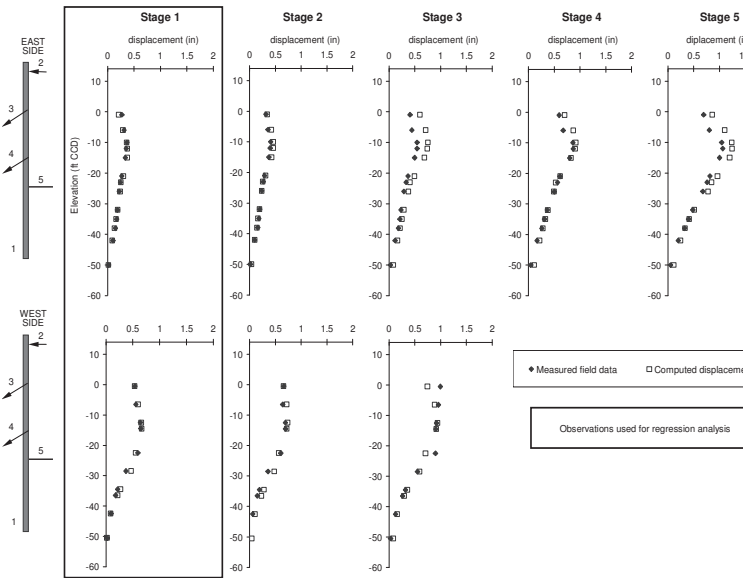
Figure 4. Observed and computed horizontal displacements based on optimization at stage 1

Analyses also were made wherein parameters were recalibrated at every stage until the final construction stage (stage 5). At every new construction stage, the inclinometer data relative to that stage were added to the observations already available. Results indicated that difference between the fit shown in Figure 4 and with those calibrated after every increment was not significant. In essence, the inverse analysis performed after the first construction stage "recalibrated" the model parameters in such a way that the main behavior of the soil layers could be accurately "predicted" throughout construction.

3.2 Applicability of Optimized Parameters in Similar Geology

To illustrate the applicability of the optimized parameters that formed the basis of the good agreement in Figure 4 to other excavation sites in these soil deposits, the results of numerical simulations are presented in Figures 5 on these optimized parameters for the conditions at the Lurie (Finno and Roboski 2005). The geologic origin of the most compressible material is similar at both sites, but the sites are located about 2 km apart. Consequently one

should expect some variability in the actual parameters at each site.

Examining the comparisons in the clay layers below EL. –5 m CCD for the Lurie data on Figure 5, reasonable agreement is observed at stages 5 and 6, with significant differences seen at stage 4. This is likely caused by the fact that the H-S model used herein does not include provisions to represent the large stiffness degradation with small strains. As discussed previously, one must select moduli that represent the average strains within the soil mass, and when the movements are small, the average modulus should be higher in a model that does not consider the small strain modulus degradation. As noted, the agreement between computed and observed responses was good for the latter stages of excavation where the lateral movements were larger.

Similar agreement was noted using the same optimized parameters at the excavation for the Ford Design Center (Blackburn and Finno 2007). As indicated in Figure 6, the numerical results followed similar trends as the observed data, but with larger magnitudes. The parameters used in the analysis again were based on the larger deformations that were present at the Chicago-State site, and hence resulted in larger

147

deformations than were observed at the Ford Center. In any case, the application of the Chicago-State based optimized parameters to both the Lurie and Ford sites resulted in reasonable agreement with the observed lateral movements, within the limitations of the analyses. Application of the inverse techniques to these data resulted in improved fit with minor changes to the parameters.
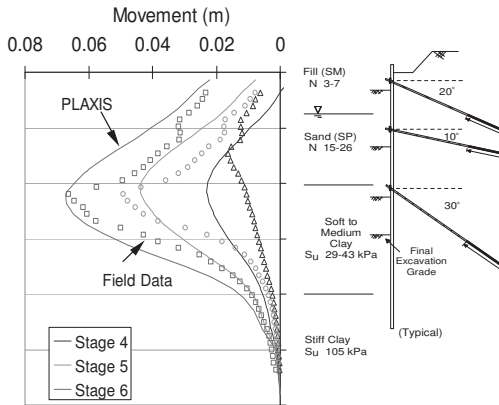

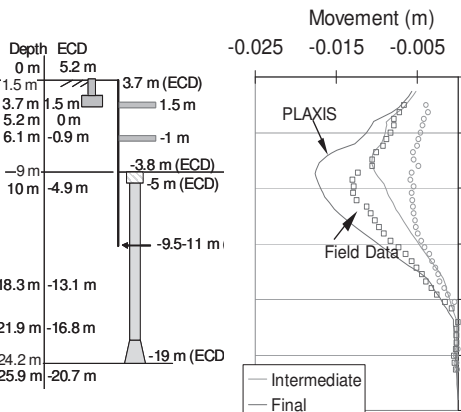Figure 5. Computed and observed displacements: Lurie excavation

Figure 6. Computed and observed displacements: Ford Center excavation

4. CONCLUDING REMARKS

The calibration by inverse analysis of the various simulations presented herein indicated that the numerical methodology developed to optimize a finite element model of an excava-

tion can be very effective in minimizing the errors between the measured and computed results. However, the convergence of an inverse analysis to an "optimal solution" (i.e. best-fit between computed results and observations) does not necessarily mean that the simulation is satisfactorily calibrated. A geotechnical evaluation of the optimized parameters is always necessary to verify the reliability of the solution. For a model to be considered "reliably" calibrated both the fit between computed and observed results must be satisfactory (i.e. errors are within desired and/or accepted accuracy) and the best-fit values of the model parameters must be reasonable.

5. REFERENCES

Blackburn, J.T. and Finno, R.J., (2007). "Three-Dimensional Responses Observed in a Braced Excavation in Soft Clay," *J. Geot. Geoenvir. Engrg.*, ASCE, 133 (11), 1364-1373.

Calvello, M. (2002). "Inverse Analysis of a Supported Excavation through Chicago Glacial Clays," PhD. thesis, Northwestern University

Finno, R., "Evaluating Excavation Support Systems to Protect Adjacent Structures," (2010). DFI Journal, Deep Found. Inst, 4(2), 3-19.

Finno, R.J. and Blackburn, J.T. (2005). "Automated monitoring of supported excavations," *Proc., 13th Great Lakes Geot. Geoenv. Conf.,* GPP 3, ASCE, Milwaukee, WI., 1-12.

Finno R.J., Bryson L.S. and Calvello M. (2002). "Performance of a stiff support system in soft clay." *J. Geot. Geoenvir. Engrg.*, ASCE, 128(8), 660-671.

Finno, R.J. and Calvello, M. (2005). "Supported excavations: the observational method and inverse modeling." *J. Geot. Geoenvir. Engrg,.* ASCE, 131 (7).

Finno, R.J. and Langousis, M., (2007). "Real Time Monitoring at the Olive 8 Excavation," *Proceedings, FMGM 2007*, Int'l. Symp. on Field Meas. in Geomech., GSP 175, ASCE, Boston, September.

Finno, R.J. and Roboski, J.F., (2005). "Three-dimensional Responses of a Tied-back Excavation through Clay," *J. Geot. Geoenvir. Engrg*, ASCE, Vol. 131, No. 3, 273-282.

Schanz,T., Vermeer, P.A., and Bonnier, P.G. (1999), "The hardening soil model – Formulation and Verification," *Proc. Plaxis Symp.: Beyond 2000 in Comp. Geotechnics,* Balkema, 281-296.

Response of piled buildings to deep excavations; hypothesis of soil structure interaction

M. Korff

Deltares / Cambridge University, *mandy.korff@deltares.nl*

ABSTRACT: This paper explores the influence of the piled foundation on the building response to excavation-induced deformations. A hypothesis of the influence of the type of foundation, positive and negative skin friction and the flexibility of the piles is described resulting from soil deformations attributed to the deep excavation. A case study is described about the subway construction in Amsterdam, the Netherlands, in typical soft soil conditions with historic buildings on timber pile foundations.

1. INTRODUCTION

The response of piled buildings near deep excavations is governed by the effect of the deep excavation on the soil, the interaction between the soil and the pile and the interaction between the pile and the building. In general, the unloading effect of the deep excavation will lead to deformations and changes in stresses behind the wall. Due to these excavation-induced changes, the nature of the interface between the pile and the soil changes.

The soil-structure interaction for buildings adjacent to deep excavations has been studied by several researchers, such as Goh (2010), El-Shafie (2009), Finno et al. (1991), Ong (2004) and Xu and Poulos (2000). Many other authors studied the green field displacement related to deep excavations or the building response to these deformations.

The interaction between these topics is still under development since many real life situations are difficult to assess. The impact of the presence of pile foundations; the combination of initial stresses in/under the foundation with effects resulting from the deep excavations; load transfer within the building or foundation slab and the combinations of different loads/displacements are not known very well. If these effects are not considered, the current estimates may be too conservative or too optimistic, leading to costly measures being taken unnecessary or at a late stage in the project.

Some cases describing the behaviour of piled buildings due to horizontal and vertical ground deformations can be found in the literature.

2. CASES INCLUDING PILE RESPONSE

2.1. Tunnels

Jacobsz et al. (2005) describe the effects of tunnelling on piled structures for the Channel Tunnel Rail Link. A difference is found between end bearing and friction piles. End bearing piles were found to follow the green field settlement at the pile base for small volume losses. A reduction in the pile base capacity and subsequent load (due to stress relief caused by tunnelling) will result in the mobilisation of additional positive shaft friction. The soil and pile will settle the same amount as the neutral level. Friction piles alter the green field subsurface displacements and can be assumed to follow more or less the surface settlements as a conservative approach.

Kaalberg et al. (2005) describe the results of an extensive programme in the Netherlands to find

the influence of tunnelling on piles, for which measurements and a field test were performed. Deformation of piles due to shield tunnelling consists of settlement of the soil layer around the pile toe and settlement caused by stress relief around the pile toe.

The general movement of the pile for both tunnels and excavations is in the direction of the construction with a downward component. An approximately triangular zone of influence behind the wall or beside the tunnel is expected. Specific for tunnels are the heave that occurs below the mid height of the tunnel and the 3D effect for a passing TBM. Specific for deep excavations are the 3D effect of corners, installation effects of retaining walls.

2.2. Deep Excavations

Some papers describe cases with the response of piled buildings due to excavations. Davies & Henkel (1982) showed for a Hong Kong case that piles adjacent to a deep excavation experienced serious settlements due to negative skin friction caused by the lowering of the water table. Lee et al. (2007) showed for a Bangkok case that very long piles settled about 30% of the surface settlement, probably caused by an increase in negative skin friction.

In Korff et al. (2011) two Dutch cases have been described where negative skin friction clearly plays an important role in the response of piled buildings to deep excavations.

Elshafie (2008) studied the soil structure inter-action for deep excavations with experimental modelling and concludes that buildings with individual spread footings experience significant distortions and tensile strains concentrating at the weak parts of the buildings. Ong (2004) performed similar work focusing on lateral displacements of single piles and pile groups showing a clearly time-dependent behaviour and reduction of bending moments in piles in groups compared to single piles. In a case presented by Finno et al (1991) observed movements of a deep excavation were twice as large as expected. A pile group located closely behind the wall was not significantly affected either in lateral or axial capacity and the actual moments in the piles were not large enough to cause cracking.

The described cases indicate that both the horizontal and vertical effects on pile founda-tions are relevant in the soil-structure interac-tion related to deep excavations. This paper mainly deals with the vertical effects.

3. CASE STUDY NORTH-SOUTH LINE

3.1. Deep excavation and soil conditions

The North-South Line in Amsterdam passes under the historical centre of the city in twin tunnels. Three main underground stations built by means of a top down construction are under construction in the historic city centre. Details of the construction can be found in Kaalberg et al. (2005). A cross section of Ceintuurbaan Station with soil profile and monitoring instru-ments is shown in Figure 1.
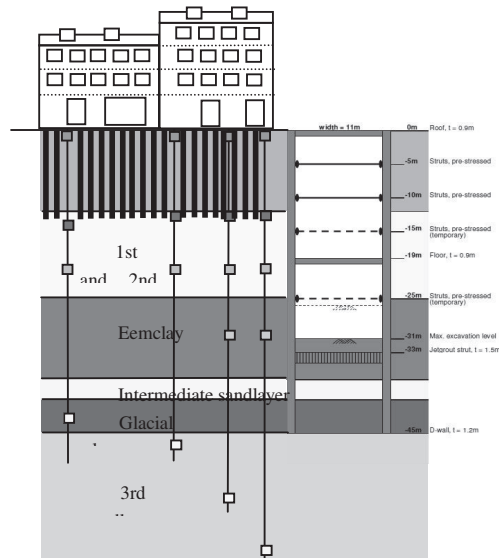

Figure 1 Cross section of Ceintuurbaan Station with soil profile and extensometer locations

The subsoil consists of a layer of fill of about 3 m underlain by soft Holocene deposits to a level of about NAP -11.0m (ground level around NAP +1.0m). These are underlain by the 1st sand layer. The 2nd sand layer is found at about NAP -16m, extending to NAP -25m. Below the

150

2nd sand layer a stiff clay layer of around 15m thickness (the Eem clay) is underlain by the 3rd sand layer.

The monitoring instruments include extensometers behind the wall, inclinometers in the soil and in the wall, manual levelling of the surface and the build-ings and automatic monitoring of the buildings. Details about the construction and monitoring of Ceintuurbaan Station are given in De Nijs & Buykx (2010).

3.2. Pile foundations

Most buildings in the historic centre of Amsterdam are built with masonry walls, wooden floors and timber pile foundations, reaching into the First Sand Layer at about 12m below the surface level. More recent buildings with 1-4 storeys are built with concrete walls and floors and prefabricated concrete or steel piles. Foundations for some recent buildings are in deeper layers such as the second sand layer.

The buildings considered in this paper are from the older type, see Figure 2.

Figure 2 Historic buildings at Vijzelgracht (left) and Ceintuurbaan Station (right), dated 1880-1920

The wooden piles are installed in pairs, see figure 3, with 0.8m between the pairs. Pile diameters for the timber piles vary from 160 - 300 mm (typical 180-200 mm) at the head and usually diminish by 8 mm/m to about 70-200 mm (typical 120-140 mm) at the toe. Based on several pile load tests in the historic centre it is known that the wooden pile foundations have low factors of safety
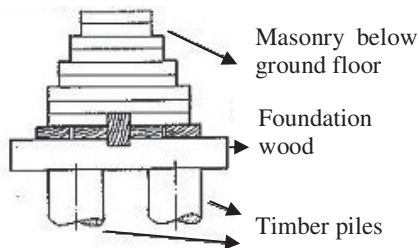
Figure 3 Typical cross section of base of the wall in masonry buildings (Zantkuyl, 1993)

A typical load-displacement curve is shown in Figure 4. The timber piles generally find between 80 % or 90 % of their capacity at the tip according to Kaalberg et al. (2005) and Van der Stoel (2001). Up to 15% of the buildings of this age in Amsterdam are not up to standards according to Van Tol (1994). A large number of timber piles deteriorate due to decay of the wood, which may lead to a different kind of building response; this effect is not described here.
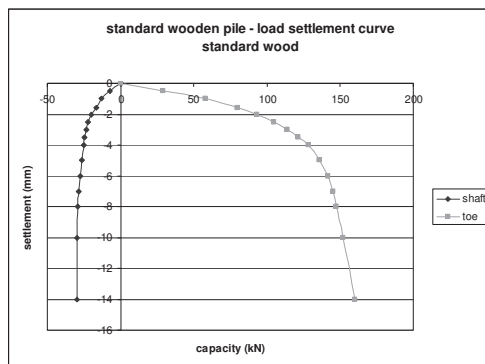
Figure 4 Representative load-settlement curve for timber piles in Amsterdam after TNO (1995)

The high horizontal flexibility assures that the piles can move rather easily with the soil in horizontal direction, if compared to concrete piles.

3.3. Subsidence in Amsterdam

The presence of soft soil layers combined with earlier city developments which included raising of the ground level causes ongoing subsidence due to consolidation and creep. Old

151

cities in the Western part of the Netherlands, including Amsterdam, in general experience ground surface settlements of about 10 to 20 mm/year due to this effect. This is comparable to other soft soil cities in the world such as Bangkok with 10-30 mm/year (Aobpaet et al. 2010), but less than cities like Mexico City or Jakarta, which settles 50-70 mm per year according to Hirose et al. (2001).

In Amsterdam, most of the surface settlements are attributed to the Holocene layers, which are located above the pile tip and only to a lesser extent to layers below the pile tip.

3.4. Initial state of the piles

To determine the response of piled buildings to excavations the current state of the piles is essential. Most piles in the historic centre of Amsterdam will already have experienced the maximum negative skin friction possible over time.

Negative skin friction can develop along the shaft of a pile when the soil surrounding the pile settles more than the pile itself. This happens for example when soft clay layers settle due to the weight of overburden, ground water lowering or other causes and the pile remains stable in the foundation layer. Positive skin friction occurs in opposite circumstances; the pile settles more than the surrounding soil. Both forces are likely to act on the timber piles in Amsterdam, see Figure 5.
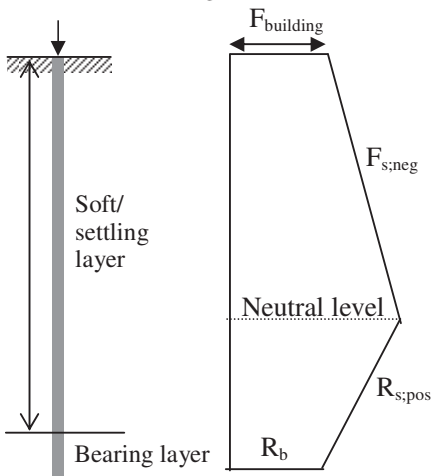
For end bearing piles with sufficient factor of safety the neutral level is found close to the location of the bearing layer. For the most historic Amsterdam foundations, the reserve capacity is smaller, and positive skin friction is also found in the soft or settling layers. The maximum force in the pile is found at the neutral level.

Subsequent raising of the street level over the last 100 years caused the piles under the facades to attract most of the external loading. The man made layer is usually thicker in the streets than under the houses, leading to larger negative skin friction and also horizontal displacements at the position of the facades.

Negative skin friction can be calculated according to Zeevaert - de Beer (1969, 1971) or the slip method from Eurocode 7. Several opinions on the development of skin friction are available in literature. Some, such as Fellenius (2006) have found that negative skin friction is already fully mobilized at a few millimeter differential deformation. Others find an increasing negative skin friction up to several hundreds of millimeters. Shen (2008) found in centrifuge tests that the degree of mobilization of negative skin friction along piles varied between 35% and 95% depending on the soil deformation, the pile slenderness and the relative stiffness of the pile to the soil. Possible skin friction profiles with depth are presented in Figure 6.

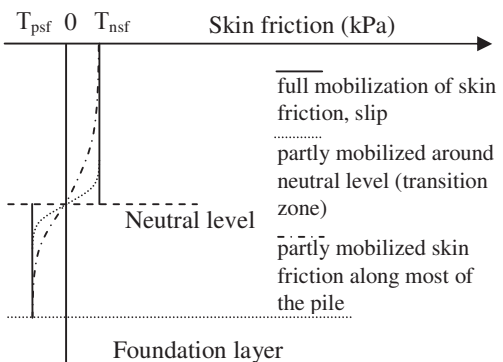
Figure 5 Development of negative and positive skin friction along a pile with low factor of safety

Figure 6 Mobilization of positive and negative skin friction along the pile with Tnsf = negative skin friction and Tpsf = positive skin friction

Usually in Amsterdam, it is considered that the negative skin friction is already fully mobilized before the excavation takes place. This means that a fictive Factor of Safety (FOS*) based on characteristic values including negative skin friction can be determined as:
FOS* = $(R_b + R_{s;pos})/ (F_{building} + F_{nsf})$. If FOS* is around 1, the factor of safety based on the partial factors from EC7 is smaller than 1.

4. HYPOTHESIS RESPONSE PILED BUILDINGS TO DEEP EXCAVATION

The buildings in the influence zone of the excavation may experience several phenomena:

1. reduction of pile capacity due to lower stress levels
2. settlement of the pile tip due to soil deformations below the base of the pile
3. development of negative (or positive) skin friction due to relative movements of the soil and the pile shaft
4. redistribution of pile load over the piles under the building slab, the building wall or a foundation cap or beam
5. horizontal deformations of the piles (causing bending of the pile).

The settlement of the pile head is determined by the combination of the first four effects described above:

$$s = s_1 + s_2 + s_3 + s_4 \qquad (1)$$

S_1 for end bearing piles is significant if the pile tips are in the active zone. Stress relief around the pile tip can lead to mobilisation of positive shaft friction. If this situation occurs, a new load-settlement curve will be established due to relaxation at the tip.
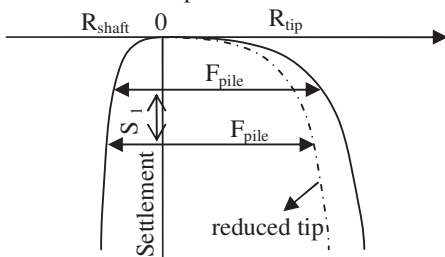

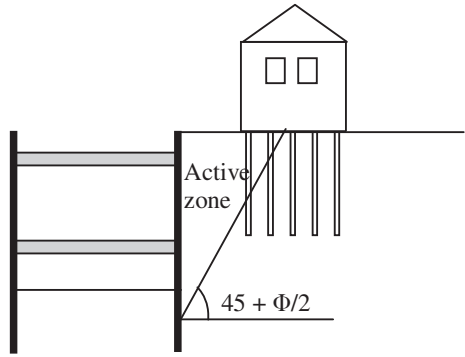Figure 7 Load –settlement curve for a pile with constant load Fpile, and subsequent settlement S_1.

Figure 8 Active zone behind the wall

For an average angle of internal friction of the soil of 25 degrees and 30m excavation, the active zone shown in Figure 8.is at least 12 m wide at pile tip level (at ~1/3 of the excavation depth). This means some relaxation should be expected for buildings located within this distance, which is the majority of the buildings along the stations. The amount of relaxation can be determined based on the method of Figure 7. The load-settlement diagram of Figure 4 could be used or specific pile load tests. The reduced bearing capacity of the tip could be related to the reduction of the cone resistance linearly with the stress level determined from FEM analysis.

S_2 may be calculated without interaction with the piles, for example with a FE-analysis or by using the Aye et al. (2006) method for deeper soil deformations due to excavations:
$S_2 = S_{w0} * (x/D_y)^2$ with S_{wy} is $4V_y/D_y$, $D_y = 2.5 * y *$ the excavation depth/wall height, x is the distance from the wall, y is the depth of the pile tip and V_y is the deflected volume of the wall below pile tip level.

S_3 is a true interaction component. For end bearing piles complying with current standards negative skin friction development will not cause additional settlements, which means $S_3 = 0$. For all other piles S_3 depends on the amount of negative skin friction mobilized in the initial state. Fellenius (2006) describes the concept of the pile moving with the neutral plane. For the Amsterdam piles with FOS* of about 1 and the assumptions that the pile load and the tip resistance remain constant ($S_1=0$ and $S_4 =0$), the

resulting skin friction (F_{neg} – R_{pos}) can not change either. The neutral level will remain at about the same level and the pile follows the settlement of the soil at this level. If the piles have more reserve capacity, the neutral level is found closer to the bearing layer and the settlement will be less. For friction piles the neutral level is found close to the surface and S_3 is about equal to the surface settlement.

An important issue thus is to determine the level of the neutral plane. This could be done theoretically based on CPT data or from historic data of relative building settlements to surface settlements. In case of the Amsterdam subway it is possible to determine the neutral level based on the base monitoring before construction activities started, since both the building settlements as well as the soil deformations at surface and pile tip level have been measured.

$$S_3 = FSR * (S_{z;\ surface} - S_{z;\ tip\ level}) \qquad (2)$$

With: $S_{z;\ tiplevel}$ is the settlement of the soil at the tip level , $S_{z;\ surface}$ is the settlement of the ground surface, FSR is the Factor of Settlement Response, which determines the relative percentage of the soil settlement between surface and tip level;

$$FSR = (S_{z;neutral\ level} - S_{z;tip\ level}) /\ (S_{z;surface\ level} - S_{z;tip\ level}) \qquad (3)$$

Assuming a linear relationship between the ground settlement at surface and pile tip level, the FSR can be determined as from the relative position of the neutral level to the surface and the tip level, see Figure 9. FSR = (neutral level – tip level) / (surface level – tip level). The FSR by definition is 0 for end bearing piles and 1 for full friction piles.
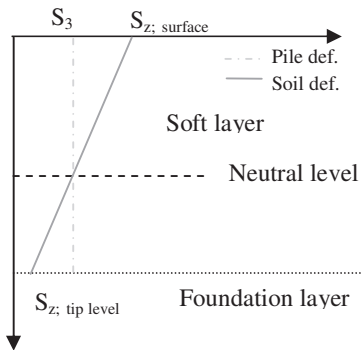
Figure 9 Settlement profile and neutral level, assuming linear relationship

A different S_3 will be found for the same surface settlement and settlement of the foundation layer, when the 'shape' of the settlement with depth is not linear, for example due to the nature of the settlement origin, such as dewatering, tunnelling or excavation. See figure 10.
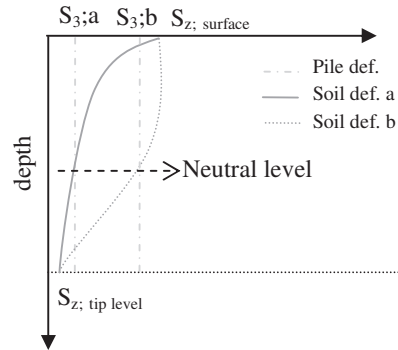
Figure 10 S_3 based on a non-linear settlement profile and known neutral level

If the negative skin friction is not fully mobilized at the initial state or the tip resistance reduces, the skin friction will further mobilize, which will raise the neutral level. S_3 might also include an elastic component of the shortening of the pile if the total stress in the pile increases with increasing negative skin friction.

Due to the S_3 settlement a small amount of extra shaft resistance could be obtained for the extra embedment in the bearing layer. When the cone resistance in the bearing layer is not constant, also the tip resistance might be affected. Both these effects are considered to be second order and should be neglected in normal conditions.

If the pile redistributes it load, S_4 needs to be determined together with S_3. This could occur if the piles closest to the excavation settle more than the piles further away. The building stiffness will prevent the building from following the different pile movements and the pile load will redistribute accordingly. If this happens, the external load on the pile changes, leading to a new equilibrium. This effect should be determined by a coupled analysis for a pile group, such as with a boundary element method as described by Xu and Poulos (2000).

5. TESTING AND DISCUSSION OF HYPOTHESIS

The described effects causing the piles and subsequently the buildings to settle, will be evaluated by analyzing the substantial amount of monitoring data present for the Amsterdam case study. This will include the determination of the neutral level from the base monitoring and the analysis of the relative settlement of the building to the soil deformations at surface and pile tip level. This will make it possible to determine the interaction factor FSR for the specific buildings. To distinguish between the contributions of S_1, S_3 and S_4, different locations need to be compared and additional analysis performed. S_2 can be directly evaluated against the results of the extensometer measurements at pile tip level.

Several questions specific for the response of piled buildings to deep excavations remain to be answered by comparing the ground deformations with the building deformations, such as:
- Is there a load transfer between the piles?
- How large is the group effect?
- To what extent does the presence of the piles reinforce the soil?

6. SUMMARY AND CONCLUSIONS

The hypothesis for the behavior of piled buildings influenced by deep excavations includes:
- Stress relief around the pile tip can lead to mobilisation of positive shaft friction.
- Piled buildings tend to follow the soil deformations at the neutral plane, leading to a difference in response of end-bearing and friction piles; end bearing piles follow the soil deformations at pile tip level, friction piles as a conservative approach relate more to ground settlement at the surface.
- Piles might settle by an extra amount due to draw down of the ground water and/or diaphragm wall installation, depending on the shape of the subsequent soil deformation.
- Load redistribution will influence the settlement depending on the building stiffness.
- The presence of the piles influences the subsurface ground displacements.

- Piles are rather flexible in horizontal loading and tend to follow the soil deformations.
- Disturbing effects on the piles should be added to the existing loading and stresses in the piles.

The North-South Line project presents possibilities to investigate the vertical interaction, but unfortunately not the horizontal interaction, due to the limited availability of reliable inclinometer data. The results of this will be described in future papers.

REFERENCES

Aobaet, A., Caro Cuenca, M., Hooper, A., Trisirisatayawong, I. 2010. Land subsidence evaluation using INSAR time series analysis in Bangkok metropolitan area. *Proceedings Fringe* 2009 Workshop, Frascati, Italy, ESA SP-677.

Aye, Z.Z., Karki, D. and Schulz, C., 2006. Ground Movement Prediction and Building Damage Risk-Assessment for the Deep Excavations and Tunneling Works in Bangkok Subsoil. *International Symposium on Underground Excavation and Tunnelling* 2-4 February 2006, Bangkok, Thailand

Davies, R.V. & Henkel, D. 1982. Geotechnical problems asso-ciated with the construction of Chater Station, Hong Kong. *The Arup Journal* 17(1): 4-10.

Elshafie. M. Z. E. B. 2008. Effect of building stiffness on exca-vation induced displacements. *University of Cambridge*. PhD.

Fellenius, B.H. 2006. Results from long-term measurement in piles of drag load and downdrag. *Canadian Geotechnical Journal,* Vol. 43, No. 4, pp. 409 – 430

Finno, R. J., Lawrence, S. A., Allawh, N. F., and Harahop, I. S. (1991) Analysis of performance of pile groups adjacent to deep excavation. *J. Geotech. Eng.*, 117(6), 934–955.

Hirose, K., Maruyama, Y., Murdohardono, D., Effendi, A. and Abidin, H.Z., 2001. Land subsidence detection using JERS-1 SAR Interferometry. *2nd Asian conference on remote sensing.*

Centre for remote imaging, sensing and processing (CRISP), NUS, Singapore.

Jacobsz, S. W.; Bowers, K.H.; Moss, N.A.; Zanardo, G. (2005). The effects of tunnelling on piled structures on the CTRL. *Geotechnical Aspects of Underground Construction in Soft Ground*, Amsterdam, Taylor&Francis Group, Lon-don.

Kaalberg, F.J., Teunissen, E.A.H., van Tol, A.F., Bosch, J.W. , 2005. Dutch research on the impact of shield tunnelling on pile foundations. *Geotechnical Aspects of Underground Construction in soft ground* (pp. 123-131). London: Taylor & Francis.

Korff, M., Mair, R.J., Van Tol, A.F., Kaalberg, F.J.(2011) The response of piled buildings to deep excavations; *Proceedings of TC28 conference, Roma* (in print)

de Nijs. R.E.P. & Buykx. S.M. 2010. Instrumentation and Monitoring at Deep Excavation in Historic City of Amster-dam. *Design and Performance Analysis of Monitoring Sys-tem at Ceintuurbaan Station. ITA 2010*. Vancouver

Ong, D.E.L. 2004. Pile behaviour subject to excavaton-induced soil movement in clay. PhD thesis from NUS

Poulos, H.G. and Chen, L.T., 1996, Pile response due to unsupported excavation˜ induced lateral soil movement. *Canadian Geotechnical Journal*, Vol.33, pp.670-677.

TNO (1995) Onderzoek naar te verwachten zettingschade bij de aanleg van de Noord/Zuidlijn in Amsterdam, Diana studies, fase 1.

Shen, R.F., 2008, Negative skin friction on single piles and pile groups, PhD thesis from NUS

Stoel A.E.C. van der, Grouting for Pile Foundation Improvement, 2001, TU Delft

Xu, K.J. and Poulos, H.G., 2000, Theoretical Study of Pile Behaviour Induced by a Soil Cut. *Proceedings GeoEng 2000*, CD volume.

Zantkuijl, H. J. (1993). *Bouwen in Amsterdam - Het woonhuis in de stad (Building in Amsterdam).* Amsterdam, Architectura & Natura.

Zeevaert, L., 1959. Reduction of point bearing capacity because of negative friction. *Proc.First Pan American Conference on Soil Mechanics and Foundation Engineering,* Vol. 3,pp. 1145-1152.

Zeevaert, L. *Foundation Engineering for difficult subsoil conditions*. Van Nostrand Reinhold Company, Chapter 8, pp. 335-423.

Current status on research, execution and international design codes on geosynthetic reinforced retaining walls

L. Vollmert

BBG Bauberatung Geokunststoffe GmbH & Co. KG, Germany, *lvollmert@bbgeo.com*

ABSTRACT: Cost effects on international infrastructural projects as well as on local masonry sites require modern construction techniques, easy to execute and reducing the required level of maintenance. Therefore retaining structures using reinforced soil as backfill material in combination with various facing techniques have become more and more popular. The design and execution processes for several techniques have already been fixed in international design codes. The paper gives an abridgement on the current situation of geosynthetic reinforced walls with a focus on Europe with a link to overseas developments, experience and topics.

1. INTRODUCTION TO REINFORCED RETAINING STRUCTURES

These days geosynthetic reinforced retaining walls are installed in considerable heights and have become very popular design elements. With their nature-orientated visual appearance using e.g. gabion facings they are an economic alternative to common heavy weight or concrete constructions. Additionally they allow the use of secondary construction material (e. g. recycled concrete) or by-products from steel production like furnace slag for use in the steel grid baskets and in the backfill. The geosynthetic reinforced structure itself forms the main part of the retaining structure (Figure 1), fulfilling the requirements on the internal and external stability.

The main difference to a concrete cantilever wall therefore is given by the situation, that a failure within the structure of a cantilever wall leads to a failure of the whole structure. In opposite to this, a failure of the facing linked to a reinforced soil structure does not lead to a general failure necessarily due to the fact, that the structure remains stable. Figure 2 shows the original remaining parts of the Ziggurat Aqar-Quf, reinforced by reed, after approx. 3500 a of erosion and demolition and a partly reconstruction near Bagdad, Iraq, with a height of 57 m.

(i) Reinforced soil wall

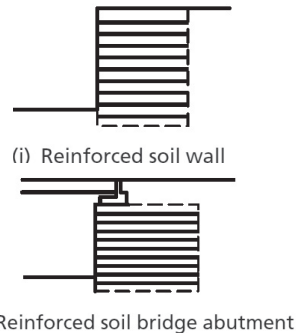(ii) Reinforced soil bridge abutment

Figure 1. Examples for Reinforced Retaining Walls as given by DIN EN 14475

Figure 2. Ziggurat Aqar-Quf, 3500 year old reinforced soil structure near Bagdad (picture by unknown reference)

2. GEOSYNTHETICS

Geosynthetics used for reinforced soil structure as modern construction material are relatively new in terms of understanding and are still not part of the standard education. Problems of understanding synthetics are often linked to the fact, that synthetics behave different compared to well known materials as concrete and are not ideal elastic as e.g. steel.

On the other hand, synthetics and wood, one of the eldest construction material ever used by civil engineers, are both polymers and comparable in many aspects. Additionally, synthetics are already used in many applications where concrete is not suitable and has to be protected against chemicals e.g. in pipelines. The material behaviour of geosynthetics is primarily characterised by the thermoplastic properties. The initially essential three values for the description of the thermoplastic behaviour are:

- Load (F)
- Temperature (T)
- Time (t)

Giving an impression on the influence of creep, tested in air, is compiled by Jones (1996), see Figure 3. For a certain design-lifetime, a reduction is required. Additional factors and influences to be considered by installation and in service lead to a significant reduction of the ultimate strength (T_{ult}) in comparison to the design strength (T_d), see Figure 4. Comparing the actual load (L_a) and the ultimate tensile strength, reduced by installation damage, a low range of stress is valid right at the beginning of the period in service, leading to a low strain rate. This effect has been documented by several strain measurements on site and discussed by e.g. Heerten et al. (2009).

Certain research has been done by several authors, coming up with the tendency, that creep in soil will be less compared to tests in air. Nevertheless, creep has to be taken into consideration worldwide to be on the safe side.

On the other hand, the Japanese design codes allow for the usage of the strength characteristic of "fresh" material for temporary and exceptional loading conditions e.g. by earthquake even after years in service due to the fact, that the material remains elastic (Figure 5).
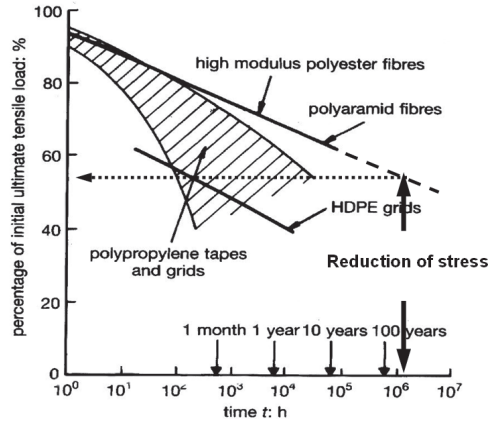

Figure 3. Time and load dependence of different raw materials (according to Jones, 1996)
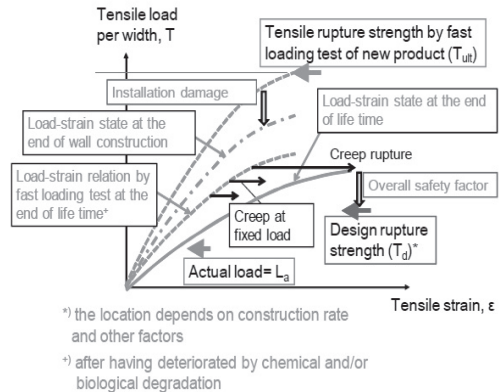

Figure 4. Typical procedure to obtain the design rupture strength (T_d) of geosynthetic reinforcement under long-term static loading conditions (Tatsuoka et al., 2010)

158

Figure 5 shows typical tensile loading tests on a PET geogrid. In one test, sustained loading (SL) was applied for 30 days during otherwise monotonic loading (ML) at a constant strain rate. The rupture strength from this test is essentially the same as those obtained by two continuous ML tests without an interruption of SL at an intermediate stage. This data set clearly indicates that, upon the restart of ML at a constant strain rate, the load-strain relation soon rejoins the one during continuous ML loading and the rupture strength does not decrease by SL at an intermediate stage, but it is rather unique function of the strain rate at rupture (Tatsuoka et al., 2010).
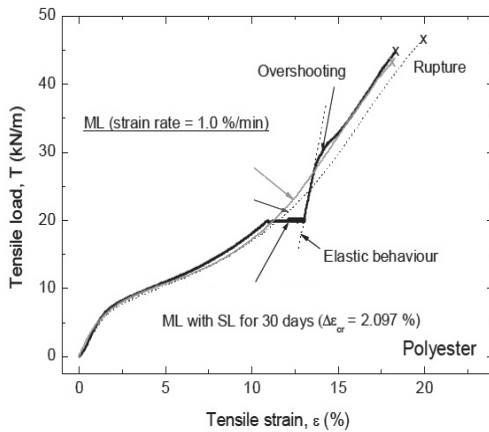

Figure 5. Comparison of tensile load - strain relations from three ML tests with and without creep loading for 30 days at an intermediate load level (Tatsuoka et al., 2010).

3. LONG-TERM EXPERIENCE ON GEOSYNTHETIC REINFORCED WALLS AND CONCLUSIONS FOR DESIGN

Herold (2007) documented seven high loaded structures that are under continuous supervision. The documented strain within the geosynthetic reinforcement is measured within the range of 0.05 % … 0.4 %. The strain therefore is less as expected by Ultimate Limit State Design (ULS), but in accordance with scientific approaches and actual understanding of compound material (Heerten et al., 2009).

Ruiken et al. (2010) managed to visualize the shear rotation of granular material in the front of a reinforced wall (Figure 6). The required deformation of the facing is very low and is depending on the degree of reinforcement respectively the vertical layer distance of the reinforcement. Secondary shear planes develop during deformation, showing significant differences as to be expected by active earth pressure theory. EBGEO has already used these findings on the basis of the publication by Pachomow (2007), allowing for a reduced earth pressure on the facing of a reinforced earth wall.

From back analysis of the constructions measured by Herold (2007), taking the actual design codes into consideration, general conclusions can be drawn and recommendations for further design are given concerning the expected deformation of a construction, see Table 1.
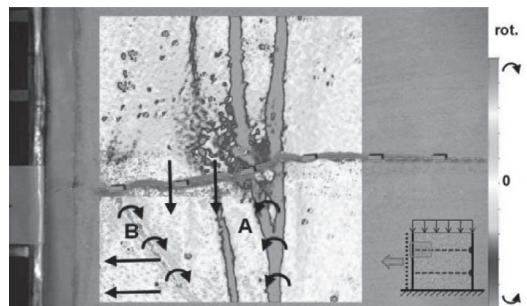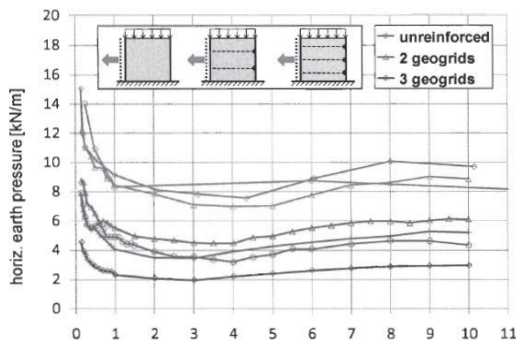

Figure 6. Large-scale biaxial testing on geogrid reinforced walls; reduced deformation by geogrids (not fixed to the facing) (left) and particle rotation and shear-zone development at the front of the wall (right) (Ruiken et al., 2010)

159

Table 1. Deformations to be expected for reinforced walls (according to Herold, 2007)

Max. horizontal deformation:
- Total: $h_{total} = 0.005 \ldots 0.01 * H$
- Post-construction: $h_{post} = 0.15 \ldots 0.3 * h_{total}$
  $= 0.00075 \ldots 0.003 * H$

Max. vertical deformation:
- Total: $v_{total} = 0.01 \ldots 0.02 * H$
- Post-construction: $v_{post} = 0.15 \ldots 0.4 * V_{total}$
  $= 0.0015 \ldots 0.008 * H$

- H: max. height of construction; h: horizontal deformation; v: vertical deformation
- all deformations within the construction
- to be added by subsoil settlements
- lower boarder for walls without surcharge, upper boarder with surcharge

4. DESIGN CODES AND STANDARDS

4.1. Designing with geosynthetics

In the case of the planning and dimensioning process especially high constructions require a specific static system as well as a corresponding execution. Several design codes and recommendations dealing with geosynthetic reinforcements exist in Europe, e.g. Norway and Switzerland, but BS 8006 and EBGEO are commonly used and in line with the Eurocode 7 (EC7). Figure 7 shows the range of codes in line with the EC7 for one country, here Germany, starting with the general code EC1, to EC7, the national annex and the recommendation of the German Geotechnical Society. Additionally, the harmonised European codes as national documents have to be considered for testing and execution, e.g. DIN EN 14475.

4.2. Approach of soil pressure distribution

For reinforced soils the soil pressure is indifferent in consequence of the dowelled shear zone. However, the active soil pressure can be considered as established reference value. According to EBGEO the horizontal stress which affects the gabions is calculated as reduced active soil pressure depending on the stiffness of the facing system defined in DIN EN 14475 (non-deformable, partially deformable, deformable), Equation (1) and Table 2
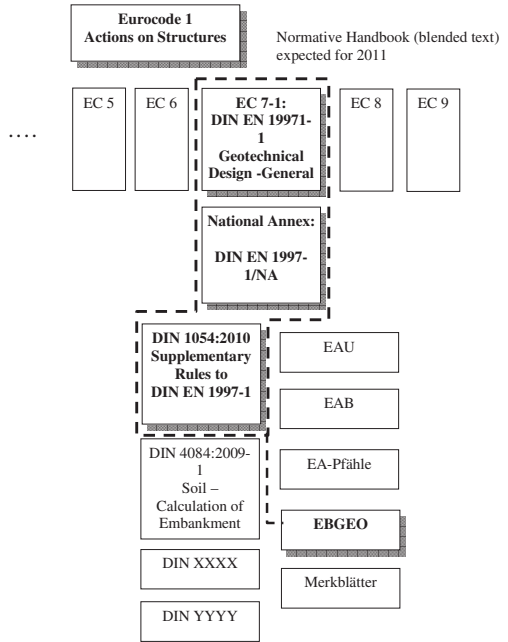
Figure 7. Normative range designing with geosynthetics in Germany (Heerten, 2011).

This requires an effect of the total system as compound structure. The distance of the vertical reinforced layers should not be larger than 0.8 m. Soil pressures resulting from loads have additionally to be considered without reduction as well as loads given by compaction.

$$E_{Facing} = (\eta_g \cdot k_{agh,k} \cdot \gamma_k \cdot H_i \cdot \gamma_G + \eta_q \cdot k_{aqh,k} \cdot q \cdot \gamma_Q) \cdot l_v \quad (1)$$

where

E_{Facing}	resulting load on the facing, horizontal component, acting on the facing between two layers of reinforcement
η_g, η_q	Matching coefficient [-]
$k_{agh,k}$, $k_{aqh,k}$	Coefficient active earth pressure [-]
γ_k	Weight per unit area of the soil [kN/m³]
H_i	Covering [m], measured from the top to the middle of two reinforcing layers
q	Traffic load [kN/m²]
γ_G, γ_Q	Partial safety factor DIN 1054 [-]
l_v	Vertical space between layers [m]

160

Table 2. Calibration factor η_g, η_q (EBGEO)

	Calibration factor			Earth pressure angle
	η_g		η_q	δ
	$0 < h \leq 0.4\,H$	$0.4\,H < h \leq H$		
Non-deformable facing elements	1.0	1.0	1.0	Analogous to DIN 4085
Partially deformable facing elements	1.0	0.7	1.0	$1/3\,\varphi'$ to $1.0\,\varphi'$ (see [11])
Deformable facing elements	1.0	0.5	1.0	0

Notes: 1) In the contact zone h = H.
   2) The calibration factors are derived from literature evaluations and large-scale tests [18].

Earth pressures from bounded surcharges are also considered without redistribution. Compaction earth pressures to DIN 4085 are adopted additionally for design

5. WORKED EXAMPLE: RETAINING WALL IN LENNESTADT, GERMANY

5.1. Structure

For the development of an industrial park the new construction of a road in Alten-hundem/Sauerland, Germany, was required. In the course of the approx. 400 m long section, which bridges an altitude difference of 28 m, amongst others a 115 m long retaining wall with a slope filling of approx. 20,000 m³ and a height of 25 m was constructed. In order to preserve the cross-section of the adjoining river Hundem a retaining wall with an inclination of 65° was chosen.

A massive steel concrete base which is founded on the stable rock level and which is interlocked with the rock by means of a skid is installed at the toe of the construction to ensure the global bearing capacity. The massive foundation also prevents the retaining wall from scouring in case of flood waters.

5.2. Geosynthetic reinforcement

In order to guarantee the internal stability of the superimposed back-anchored gabion wall or the bearing resistance of the top slope areas, respectively, the steep slope has been carried out as reinforced soil. The geosynthetic reinforcement has been continuously installed in layer distances of 0.8 m over their entire length.

Up to a construction height of 12.4 m a reinforcement carried out with Secugrid® 200/40 R6 was chosen for static reasons. In the top layers a reinforcement with Secugrid® 120/40 R6 could be used at lower required tensile strengths.

In the case of the choice and dimensioning of the geogrids among others the resistance against increased pH-values has to be evaluated together with the operational demands. Due to the monolithic structure of the geogrids the single bars only show a very small surface compared to the used raw material. The high sensibility of polyester towards the pH-value dependant external hydrolysis which is well known for wovens and geogrids manufactured of monofilaments is thus much lower. For the used Polyester geogrids only a reduction of 18% for the influences resulting from the increased pH-values had to be charged.

5.3. Recycling material and wrapping

Recycling material which was available and which consisted of bituminous road construction material was used as fill material. This was treated with adhesive agents and approved for installation according to the life-cycle resource management act, the waste avoidance and management act as well as the federal water act. A geomembrane Carbofol® HDPE 406 Megafriction/Megafriction with a thickness of 2 mm was installed to fulfil guidelines of the water law.

In the front area the geomembrane was installed in wrap-around sections, in order to realize a connection between slope surface (gabions) and the reinforced steep slope. The top layer of the wrap-around was in this case carried out with a slight cross-fall in the outer direction, in order to prevent surface water from penetrating into the construction.

On the slope side a drainage mat Secu-drain® XX8 combined with gravel infiltration ditches for the collection of layer and seepage water was installed. The lining was also carried out by means of a geomembrane which was protected in this area by means of a 10 cm thick concrete protection layer C15/20 from unintentional damages.

5.4. Facing System / Gabions

For the gabions a height of 0.8 m was chosen according to the layer distances of the geogrids dimensioned in the calculations. The gabion baskets were statically proven and were filled with coarse grain. The connection of the gabions to the geogrids is carried out by means of friction. To achieve a better shear transmission an interlocking layer consisting of fine grain material is installed between the gabion layers.

Figure 8. Retaining wall in Lennestadt (Vollmert & Orth, 2009)

6. FINAL REMARKS

Following the results gained by international research teams not named here since the 1970s, especially in the late 1980s significant progress has been made in understanding soil structure interaction of reinforced soil and design. Design codes are available in several countries taking the specific experience into consideration, but following the same principles. Up to now, retaining structures from geosynthetic reinforced soil have become standard structures.

7. REFERENCES

BS 8006-1, 2010-10: Code of practice for strengthened/reinforced soils and other fills.

DIN EN 14475, 2006-04: Execution of special geotechnical works - Reinforced fill.

EBGEO. Recommendations for Design and Analysis of Earth Structures using Geosynthetic Reinforcements – EBGEO (English version). 2nd Edition. Pubished by German Geotechnical Society (DGGT). Ernst & Sohn, Berlin, 2011.

EN 1997-1:2004/AC 2009. (German Version: DIN EN 1997, Eurocode 7): Geotechnical design - Part 1: General rules.

Heerten, G., Vollmert, L. & Klompmaker, J. 2009. The geomechanical behaviour of geogrids. Proc. Geotechnical Monitoring, Bratislava, Slovakia.

Heerten, G., Vollmert, L. & Herold, A. 2011. Modern geotechnical construction methods for important infrastructural buildings. Proc. Geotechnical Problems of Engineering Constructions, Bratislava, Slovakia.

Herold, A. 2007. 10 Jahre Verformungsbeobachtung an KBE-Bauwerken – Ist die Dehnsteifigkeit der Geokunststoffe der Schlüssel zur korrekten Prognose des Verformungsverhaltens von KBE-Stützbauwerken? geotechnik, Heft 30.

Jones, C. J. F. P. 1996. Earth Reinforcement and Soil Structures. Thomas Telford.

Pachomow, D., Vollmert, L. & Herold, A. 2007. Der Ansatz des horizontalen Erddrucks auf die Front von KBE-Systemen. Tagungsband zur 10. FS-KGEO 2007, München.

Ruiken, A., Ziegler, M., Vollmert, L. & Duzic, I. 2010. Recent findings about the confining effects of geogrids from large scale laboratory testing. 9th International Conference on Geosynthetics, Brazil.

Tatsuoka, F., Koseki, J. & Tateyama, M. 2010. Introduction to Japanese codes for reinforced soil design. 9th International Conference on Geosynthetics, Brazil, pp. 247 – 255.

Vollmert, L. & Orth, W. 2009. Reinforced High Gabion Walls – Specific Characteristics and Design Assessments. Darmstädter Geotechnik-Kolloquium, Darmstadt, Germany.

Deformations of soil in deep excavations: comparing calculation results with in-situ measurements

V.M. Ulitsky
St. Petersburg State Transport University, Russia, *ulitsky.vladimir@gmail.com*

A.G. Shashkin, K.G. Shashkin, M.B. Lisyuk, V.A. Vasenin
Georeconstruction Engineering Co, St. Petersburg, Russia, *mail@georec.spb.ru*

ABSTRACT: The paper deals with the issue of realism, such as may or may not be displayed by various models and calculation methods when used to calculate retaining structures of deep excavations. This issue is crucial for development of underground construction in areas of soft soils distribution and congested urban areas. Based on a series of large scale in-situ testing in deep excavations St. Petersburg geotechnical engineers have drawn certain conclusions on applicability and usefulness of deformation and settlement prediction methods used to assess movement of cofferdams and existing buildings. The paper describes one of the several test pits in St. Petersburg, where a series of in-situ monitoring was carried out.

1. INTRODUCTION

In the congested conditions of modern cities the issue of building underground structures that can be used for parking, shopping arcades, or motorway junctions becomes more and more important. Conditions for underground construction in such maritime cities as Amsterdam, Stockholm, or St. Petersburg are not favourable. In St. Petersburg typical soil profile consists of 15-20 m deep layer of soft plastic and liquid soils. These soils have low strength and high density, which justifies for higher pressure values onto retaining structures.

The analysis of failures in underground construction demonstrates the scope of research in the sphere of subsoil behaviour during excavation works to be insufficient. The shortage of such studies is readily illustrated by the work of Schweiger (2002). Besides, the existing calculation methods for cofferdams focus mainly on their strength and stability (in this case the calculations are based on the ultimate limit states).

In congested urban areas it is important to limit permissible deformations of the adjacent buildings, and consequently of the cofferdam. Thus the calculations based on the serviceability limit states become crucial. Apart from the deformations of subsoil caused by excavation works there are also deformations conditioned by construction method. Technology-related settlements can cause unacceptable deformation of the adjacent buildings.

Emergency situations may appear when the experience of construction of excavations on a site not surrounded by adjacent buildings is used for construction in congested urban areas. When existing buildings are situated in the close proximity to the site, the loads onto the cofferdam increase considerably while permissible settlements of historical buildings are as a rule limited to 2-3 cm according to St. Petersburg Codes.

To facilitate development of underground construction in difficult geological conditions of St. Petersburg it is required to carry out complex research of soil behaviour that would include instrumented monitoring of cofferdam and soil displacements both in the ground and on the surface.

In 2006 authors initiated big-scaled instrumental studies of cofferdam and subsoil behaviour at several deep excavations in St. Petersburg. Instrumented measurements of cofferdam displacements during construction of deep underground structures in soft soils were also performed by other specialized companies. The present paper contains the monitoring data from the test pit located in the central part of St. Petersburg.

2. REVIEW OF THE MAIN APPROACHES TOWARDS CALCULATIONS OF DEEP EXCAVATION COFFERDAMS

Most of the existing methods of cofferdam calculation are focused on assessment of cofferdam strength and stability. The simplest analytic calculation methods assume full realization of active and passive pressures.

To reduce the flexibility of the cofferdam in congested urban areas it is required to apply such technologies as would allow minimizing its displacements. In such circumstances the assumption as to full realization of both active and passive pressures becomes not exactly correct.

Under these conditions the approach using coefficients of subgrade reaction is widely applied to calculations. Therefore we will refer to it as a subgrade reaction method. In this case certain nonlinear dependence between pressure of the soil on the cofferdam and cofferdam displacement is replaced by piecewise-linear dependence, with a slope of the line in the pre-limit state determined by a coefficient of subgrade reaction. The main disadvantage of this approach is the uncertainty of values of the subgrade reaction coefficient K_h. Determination of coefficients encounters difficulties, in this connection a range of empirical formulae exists. In particular, Schmitt formula can be used (Schmitt, 1995):

$$K_h = 2.1 \frac{E_{oed}^{4/3}}{EI^{1/3}} \tag{1}$$

where E_{oed} is constrained deformation modulus, E – Young modulus, I – moment of inertia

Another drawback of the subgrade reaction method is the lack of possibility to predict the movement of subsoil.

To overcome the shortcomings of this method of calculation it is possible to use an elasto-plastic model with a strength criterion, described by Mohr-Coulomb equation. This model was also realized in many local and international software products.

Application of this model may sometimes lead to erroneous results. In this model soil behaviour both at the stage of loading and unloading is described by the same deformation modulus, which does not correspond to the real

soil behaviour. When modelling excavations in soft soils, the model predicts abnormal uplift of the excavation bottom which leads to a distortion of the overall deformation picture. Instead of ground settlement outside the excavation within a considerable area, it shows uplift of the surface (see Fig. 6, 7).

When modelling the movements of the subsoil of the underground structure the most important thing is to define soil deformations during the unloading phase and deformations of form change that occur when stress deviator increases. Hence, in compression test results closer attention should be paid to unloading curve. In case of clay soils with a low seepage ratio it would be prudent to carry out undrained triaxial test, because the time of excavation is not enough for consolidation to occur. The soil model should be able to describe soil behaviour during the unloading phase and non-linear behaviour of the soil when the stress deviator increases. To meet these requirements it is necessary to use more complicated soil models, accounting for soil form change deformations.

In reality deformations of cofferdam and of soil mass develop over a time (see Fig. 8). When excavation for underground structures is carried out in stages, the deformations often are not stabilised during the undergoing works of each stage. To give the actual values of movements the model should take into account a possibility of incomplete deformation realization on each stage. The model should include rheological parameters that describe the development of deformations in time. In many models the delay in time of deformations of form change is either not described at all (the deformation of form change is considered to be instantaneous), or is connected to consolidation and volume creep through the effect of dilatancy or contraction. Shear creep of soil should be taken into account

In Russia geotechnical researchers traditionally give prominence to the issue of shear creep (Maslov, 1977, Vyalov, 1978). To describe the deformation of clay soils a visco-elasto-plastic model was proposed (Shashkin et al., 2005, 2007) which accounts for deformation development in time in terms of shear creep.

3. DEFINITION OF THE PARAMETERS OF THE VISCO-ELASTO-PLASTIC MODEL

Majority of the parameters of the model may be determined through results of standard oedometric and triaxial tests.

The biggest challenge is to set rheological parameters of the soil. Clay soils that are typical for St. Petersburg demonstrate clearly pronounced thixotropic properties. When their natural structure is disturbed they can transform from solid to liquid state. And as the result the soil viscosity considerably decreases (by several orders of magnitude). In the process of coring the natural structure of the samples is disturbed to a certain degree. Hence, during the laboratory tests considerable deformations of the samples develop within several minutes. In reality deformations of structures appear within rather a long period (ranging from several days to several months or years).

To test in-situ properties of soils, samples were taken while excavating the test pits. The samples were directly placed in the rings for corresponding tests which ensured the minimal disturbance of their natural structure. During the triaxial tests the samples of liquid consistency exhibited a brittle failure pattern at vertical deformation of 5-7%, (the samples from boreholes exhibited yield without failure till the value of deformations of about 15%). Creep tests with low stress demonstrated rather prolonged development of deformations in time (Fig. 1). In this manner laboratory data prove the presence of considerable viscosity in natural undisturbed soils, the fact that should be taken into consideration at calculations.
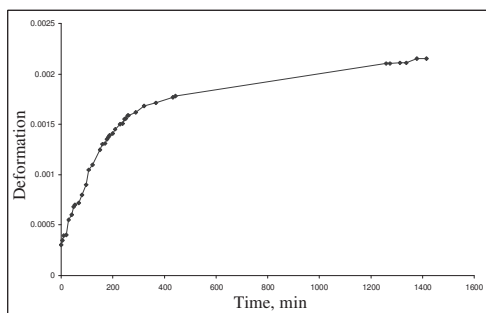

Figure 1. Unconfined creep test of the undisturbed sample of liquid loam at constant vertical normal stress of 5.4 kPa.

To derive rheological parameters for deformation of form change back analysis of the monitoring data of deformations of buildings and structures was used. The first information about the viscosity values local soils was obtained from the monitoring of deformations of the dyke structures. It was then adjusted based on the collected data of monitoring of the settlements of 15 buildings in St. Petersburg (Shashkin et al., 2007). Subsequent adjustment was made based on monitoring of underground works at the test pit.

4. COMPARISON OF THE CALCULATION RESULTS WITH THE DATA OF INSTRUMENTED MONITORING AT THE TEST PIT

The test pit has dimensions of 31m × 11.5m. The wailings of the strutting system were manufactured of H-beams, while H-beams of another type were used as cross bracings. The cofferdam was constructed of sheet piles type cut out of tubes with the diameter 1208 mm and thickness of 12 mm. The layout of the test pit is presented at Fig. 2, 3.
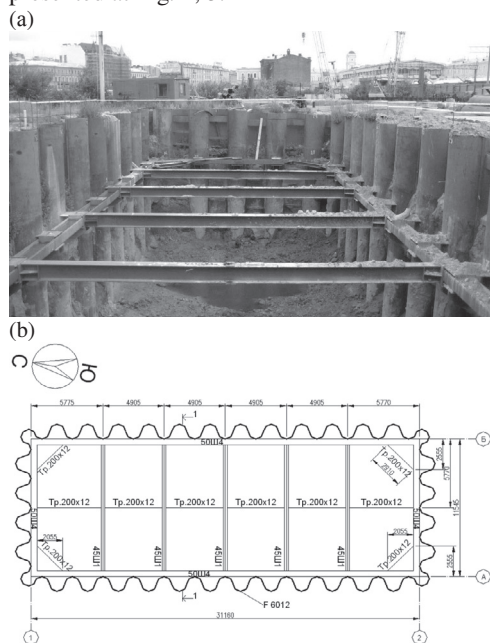
(a)

(b)

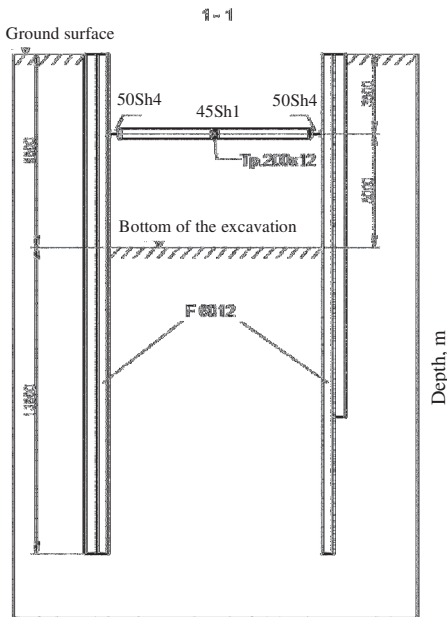Figure 2. Overview (a) and (b) layout of sheet piles and beams at the level of -3.5 m from the sheet piles top at the test pit.

Figure 3. Cross-section of the excavation at the test pit.

Figure 4. Geotechnical profile and results of SPT test carried out at the test pit.

Fig 4 shows soil profile as revealed by site investigation. Prior to installation of sheet piles at the test pit, trenches of 1.5-2 m deep were excavated. When sheet piling was completed the internal volume of soil within the cofferdam was excavated down to -4m from the ground surface following which the struts were installed and the test pit gaps were backfilled. Thus, accompanying monitoring at the test pit started at the second stage of excavation, at the reference level of –4 m and down to the level of the bottom of excavation at –8.5 m (See Fig. 5).

Analysis of the monitoring readings evidences that the sheet pile wall generated displacement up to 5 cm, and the settlement of non-loaded soil surface at the distance of 15-20 m totalled 18-30 mm as of the moment when the monitoring was completed. In this manner it was proved that the technical solution of the cofferdam and struts system that was used at the test pit does not limit additional settlement of the adjacent buildings to the permissible values (2 cm for buildings of the third category of technical condition in St. Petersburg).
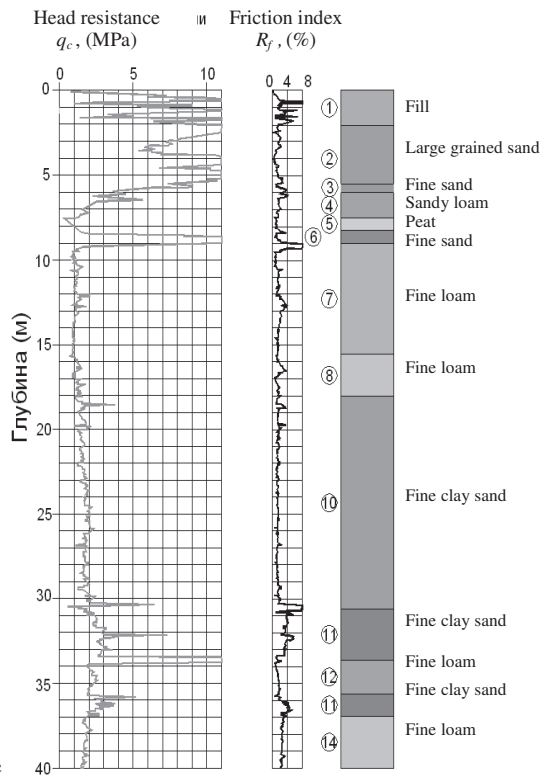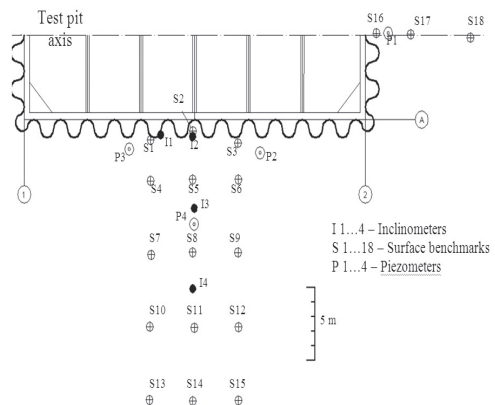

Figure 5. Position of monitoring equipment near the test pit.

Monitoring equipment was installed on the side of the pit where the sheet pile wall was completed down to the depth of 22 m (See Fig. 6). On the opposite side the pile toes had alternating levels of 16-22 m.
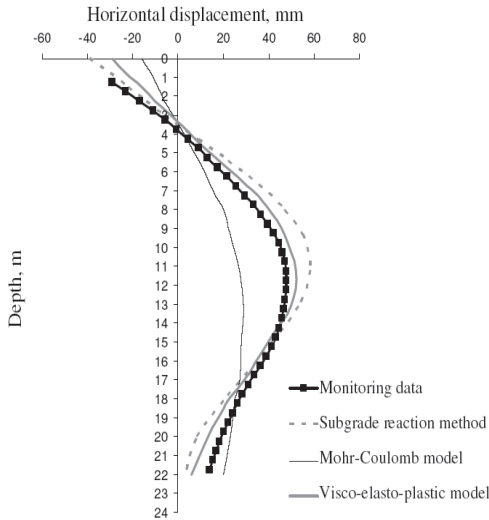

Figure 6. Comparison of the monitoring data of the cofferdam movements with the calculations based on various models.

Three various approaches were used to calculate the test pit in question: subgrade reaction method, Mohr-Coulomb and the visco-elasto-plastic model. Fig. 6 shows that the subgrade reaction method allows to accurately predict deformations of the sheet pile wall. In Mohr-Coulomb model standard soil properties were used. Fig. 6, 7 demonstrate that in general this model describes the behaviour of the soil incorrectly, which can be explained by the above-mentioned shortcomings of the model itself. When visco-elasto-plastic model was applied with the parameters based on the results of oedometric and triaxial tests, the resulting prediction was close to the monitoring data. Therefore, the model allows to describe correctly soil behaviour in time (Fig. 8).
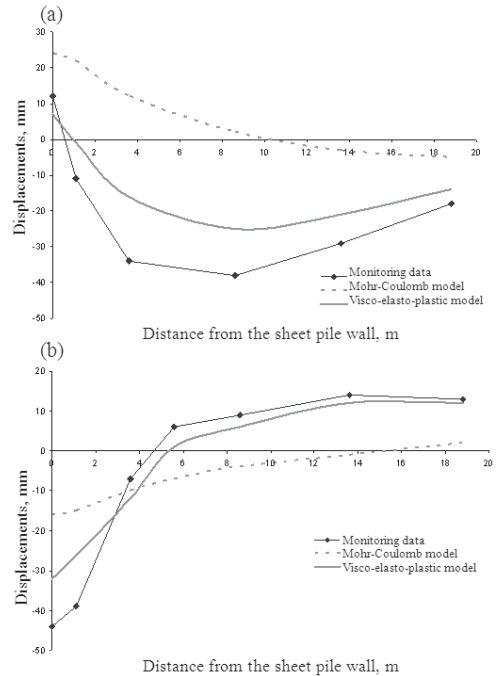
Figure 7. Comparison of vertical (a) and horizontal (b) displacement of the benchmarks as obtained during monitoring and as was predicted by calculations using different models.

CONCLUSIONS

In-situ tests on deep excavations conducted in St. Petersburg provided unique material for scholarly analyses as well as a chance of developing a most realistic calculation methodology for underground structures. Here we studied the observation data and the calculation results obtained from one of the test pits in downtown St. Petersburg. The observations obtained from that project proved typical for other sites also.

Figure 8. Comparison of the deformations development in various locations of the soil with the calculations made with the Visco-elasto-plastic model.

When developing calculation methodologies for deep pits cofferdams two approaches are possible. These approaches are radically different: (1) development of simple empirical methods, which would allow one to approach most closely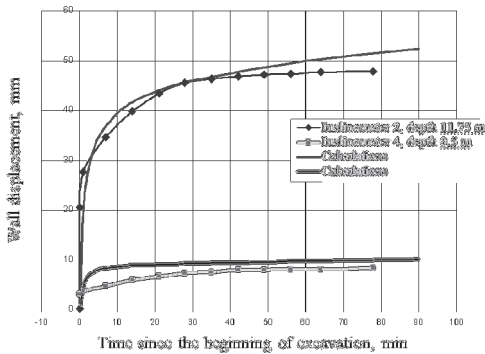 the results of in-situ measurements and (2) development of computation methods based on analyses of physical regularities observed in silty clay soils' behaviour.

The advantage of the first approach is simplicity of calculation method. However, in that case possibilities of accurate soil deformation predictions are limited. Based on the observations of the test pits, as an example of the first approach one may recommend the half-analytical method defining co-efficient of subgrade reaction based on formula (1).

The advantage of the second approach is considerable universality of the computation methodology.

When assigning standard soil behaviour parameters, the simplest elasto-plastic model with a limited Mohr-Coulomb surface does not provide an adequate definition of subsoil behaviour. To achieve a correct representation of soil behaviour it is necessary to use models depicting a difference in soil behaviour during loading and unloading, as well as non-linear character of soil response under form change deformations in triaxial tests. Additionally, for computation of underground structures it is highly important to work with realistic values of subsoil deformation rate. As demonstrated by comparison of calculations and the in-situ measurements the visco-elasto-plastic model of soil behaviour produces a good accuracy of prediction, including time-dependant deformations. This allows to recommend the presented approach for calculating retaining structures in soft soils and congested urban conditions.

REFERENCES

Schweiger, H.F. 2002. *Benchmarking in geotechnics*. Computional geotechnics group

Schmitt, P. 1995. *Méthode empirique d'évaluation du coefficient de réaction du sol vis-à-vis des ouvrages de soutènement souples*. Revue Française de Géotechnique, Vol. 71, pp. 3-10

Maslov, N.N. 1977. *Soil mechanics in practice of construction*. Moscow. Stroyizdat (in Russian)

Vyalov, S.S. *Rheological aspects of soil mechanics*. 1978. Moscow. "Vysshaya Shkola" (in Russian)

Shashkin A.G., Shashkin K.G. 2005. *Basic regularities of soil-structure interaction*. Proceedings of the international geotechnical conference on Soil-structure interaction. Vol. 1. pp. 11-38. Saint Petersburg, 26-28 May.

Shashkin, A.G., Shashkin, K.G., Ulitsky, V.M., .and Lutchkin, M.A.. 2007. *Design of buildings on soft clays with account of shear strains development in time*. Development of Urban Areas and Geotechnical Engineering. Vol.11, pp. 11-55 (in Russian)

Three-dimensional slope stability analysis

I.K. Fomenko
«Centergeology», Moscow, Russia, *ifolga@gmail.com*

O.V. Zerkal
Geological Faculty, Moscow State University, Moscow, Russia, *igzov@mail.ru*

ABSTRACT: Presents the results of the beta testing software SVSlope 3D (SoilVisionSystems, Ltd (Canada)) on three-dimensional simulation of slope stability.

Three-dimensional modeling has currently become a regular practice in geotechnical investigation, which includes numerical model study of ground massive stressed-deformed state, and is extensively used in ecological and geological problems solving. Slope stability analysis has remained one of the few major application fields based on two-dimensional analysis in geological engineering. However, two-dimension modeling effectiveness has recently begun to weaken in this field too. A number of application-dependent software producers (SoilVisionSystems, Inc. (Canada), TAGAsoft, Inc. (the USA), Itasca International, Inc. (the USA), O.Hungr Geotechnical Research, Inc. (Canada), etc.) have already been using three-dimensional slope stability modeling software modules. It appears probable that such well-known companies as GEO-SLOPE International, Inc. (Canada) and Roscience, Inc. (Canada) may put analogous production into effect in the near future. 3D solutions are also implemeted as part of multi-functional software systems (for example, Geotechnical Module of ANSYS/CivilFEM (ANSYS, Inc.) programme). Consequently, if 3D revolution in slope stability analysis has not been initiated yet, it can be expected in the coming years.

Moreover, slope stability analysis extention from two-dimensional to three-dimensional solution cannot be treated as a simple task completed by adding one more dimension. For instance, slip surface shape description concept changes completely in the transition process from two-dimensional to three-dimensional solution. Slip surface is treated as round-cylindrical in planar scenario, while in extensional, three-dimensional setting slip surface should be treated as spherical (ellipsoidal). Three-dimension slope stability modeling is indisputably more correct and perspective in comparison with two-dimension models, and extensional analysis advantages are evident. We shall illustrate some of them.

In the first place, three-dimension slip surface version is modeled (under condition of properties homogeneity) in the form of a sphere segment. Round-cyllindrical slip surface is not anologous to it in two-dimensional solution. From the mechanical point of view, the task under consideration cannot be treated as planar and, consequently, cannot be solved correctly, without significant suppositions, in two-dimension solution.

In the second place, even in case of two-dimension slope stability analysis application, a number of conditions are to be considered

during problem solving, for instance, such as geological structure homogeneity and topographical homgneity in the direction of the slope's trend. At the same time a number of cases may be found in practice when exactly these factors affect stability significantly (for instance, tectonic fault, crossing slope on the angle or slope part shearing during roads and pipelines construction). All this can be taken into complete account only in three-dimension modeling.

In the third place, an important advantage of three-dimension slope stability analysis is the fact that such analysis allows to project landslide process development not only in depth (in the massive) but also on the surface. It allows to assess risks connected with extensional landslide activization process more effectively, to render more constructive decisions on landslide protection.

In the forth place, two-dimension slope stability modeling has almost exhausted its potential in the view of further development. Basic ideas and principles to two-dimension slope stability estimate were completely established by the middle of 1960s, and significant scientific breakthrough in slope modeling methodology development (2D) has not been registered lately. Particular features detalization of previously developed methods can only be detected.

In many cases two-dimension landslide slopes schematization presents significant and not always well-founded simplification of the real situation. Therefore, it may seem uncommon that two-dimension modeling practice in slope stability estimate was that successful. However, it should be noted that it has had its grounds.

At first, in 1987 S. Cavounidis illustrated that three-dimension slope stability coefficient was much higher in comparison with its two-dimension analogue (Cavounidis, 1987). Thus, problem solving in plain setting is more conservative and possesses a factor of safety (Fs) in comparison with extension analysis.

Secondly, mathematical two-dimension methods realization made a step forward and at present three-dimension modeling is deficient of such significant instruments as probability

analysis, sensitivity analysis, slip surface optimization by means of dynamic programming method, etc.

Thirdly, three-dimension analysis methods are numerically less sensitive in comparison with two-dimension methods, especially when they are based on the condition of forces equilibrium, and much more labour-intensive.

Three-dimension slope stability analysis experience, aquired by the authors, is based on SVSlope 3D software (SoilVisionSystems, Ltd. (CANADA)) beta-testing. A slope model presented in Fig. 1 was studied as a test case. Ground properties, considered in the analysis, are presented in Table 1.

In three-dimension setting the following slope stability estimate methods were applied during modelling process:

- Janbu method referring to the group of methods that meet forces equilibrium condition;
- Bishop method referring to the group of methods that meet moment balance condition;
- Spencer method referring to the group of methods that meet overall moment and forces equilibrium.

EntryandExit method was applied as algorithm of critical slip surfaces search in three-dimension setting. Spencer method modeling results are presented in Fig. 2 an 3. Comparison of three-dimension and two-dimension analysis results is presented in Table 2 and illustrated in Fig. 4 and 5 respectively.

Resulting data analysis allows to state:

- critical slip surface obtained as the result of three-dimension modeling differs from slip surface obtained as the result of two-dimension modeling;
- three-dimension modeling slope stability coefficients are higher than that of two-dimension.

Table 1. Ground properties building up estimated slope

Number of a geological layer	Cohesion (kPa)	Internal friction angle (degrees)	Density (kN/m3)
1	80	25	20
2	60	35	20

Table 2 Comparison of three-dimension and two-dimension analysis results

Calculation variant	Calculation method Spencer	Bishop	Janbu
3D	1.339	1.292	1.256
2D	1.272	1.256	1.224
Relation Fs3D/2D	1.053	1.029	1.026

Therefore, obtained results can prove A.W. Skempton conclusion that in simple cases to contrast three-dimension and two-dimension analysis results the following function can be applied (Skempton, 1985):

$$Fs(3D)=1.05*Fs\ (2D) \qquad (1)$$

The function implies that in case of three-dimension slope stability modeling safety is shifted 5% higher. Obtained beta-testing data on slope stability estimate by Spencer method are in agreement with the function (1). However, it should be noted that for slopes with complex planar geometry, geological structure and hydrogeological situation, difference between two-dimension and three-dimension estimate may exceed 20-30 % (Starkand, 1998, Gitirana, 2008).

It should be expected that three-dimension principles realization in quantitative slope stability estimation in the near future will be implemeted in Russian application-dependent software, and three-dimension stability estimate methods will become a regular practice of geotechnical research.
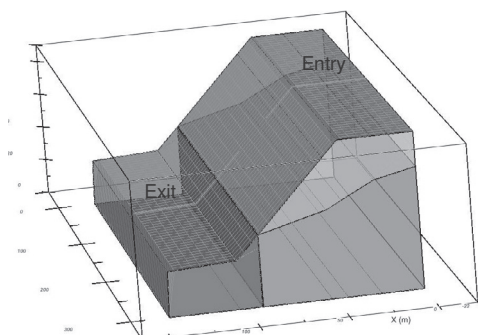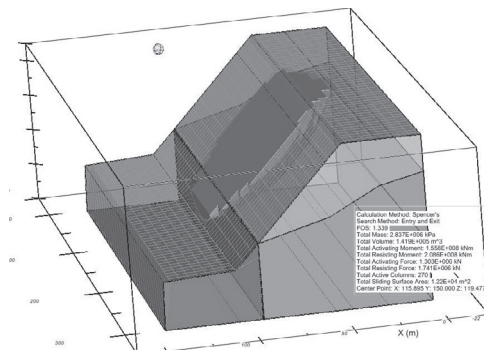

Fig. 2 Spencer method slope stability analysis results

Fig. 3 Spencer method slope stability analysis results (plan arrangement)

Fig. 1 Slope model general view (red lines mark Entry-Exit slip surface zones)

Fig. 4 Two-dimension modeling results (Spencer method)

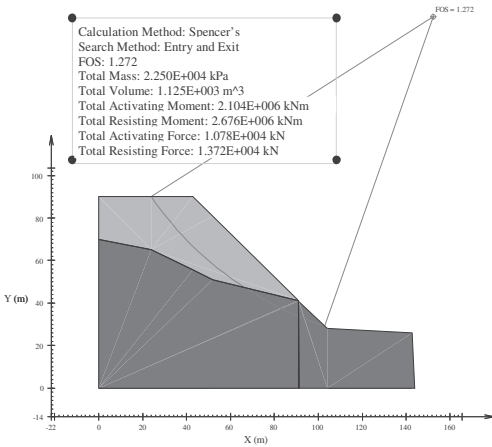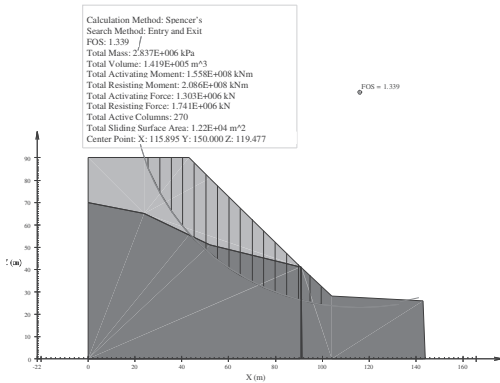Fig. 5 Three-dimension modeling results in two-dimension projection (Spencer method)

REFERENCES

Cavounidis S. On the ratio of factor of safety in slope stability analyses//Geothnique, 1987, v.37, №2, p.p. 207-210

Gitirana G.(Jr.), Santos M.A., Fredlund M. Three-Dimensional Analysis of the Lodalen Landslide//Proc. of the GeoCongress'2008 (New Orleans, 9-12.03.2008). - New Orleans, 2008

Skempton A.W. Residual strengths of clays landslides, folded strata and the laboratory//Geotechnique, 1985, v. 35, №1, p.p. 3-18.

SVOffice 2006 User's and Theory Guide. - Saskatoon, SoilVision Systems Ltd., 2007

Stark T., Eid H. Performance of Three-Dimensional Slope Stability Methods in Practice//Journal of Geotechnical and Geoenvironmental Engineering, 1998, v.124, №11, p.p. 1049-1060.

Monitoring the behavior of anchored retaining walls of RAINIER III building– MONACO

C. Jacquard,
Fondasol, *Catherine.jacquard@fondasol.fr*

R. Vallentin
Fondasol, *romain.vallentin@fondasol.fr*

ABSTRACT:
This papers presents the behaviour of an embedded wall during deep excavation, and compares the measurements of the instrumentations, and the calculated deformations, using back analysis. Its shows how the analysis of the measurements, during excavation, gave the opportunity to reinforce one part of the wall, to limit its deformation.

1. THE PROJECT

This project in Monaco was to build 9 floors of underground car parks within the empty space between existing tunnels and a car park. Above these buried floors, 4 buildings with accommodations, shops, and technical premises are under construction. The excavation includes also two connection tunnels.

The topography of the site is typical to Monaco, sharply sloping toward the sea. The excavation of 16,5 m to 21,5m high (Fig.1 and fig.2), was carried out in fills, slope deposits of fallen rocks in silty and clayey matrix, and cretaceous marl or Jurassic limestone. The contact between marl and limestone, was expected to consist of a crushed zone with beige to green gravel clay and blocks with raw fragments cuskittle-alleys. There is water flowing in slope deposits.

Along the existing car park "La Colle" (downhill side), micropiles of 350mm section, reinforced with 252/17,5mm section metal tubes were bored to excavate 14,5m high under existing car park level. Along the existing road tunnel (uphill side), reinforced concrete piles of 800mm diameter had already been bored, to enable construction of the tunnel. Beams were

prestressed between La Colle car park, and the existing tunnel, to prevent horizontal displacements. During excavation, anchors were bored in the soils and pre-stressed, and reinforced concrete was performed between piles and micropiles.

All the retaining structures of the excavation and the tunnels were submitted to very strong limits of deformation (10mm) because of the proximity of existing constructions.
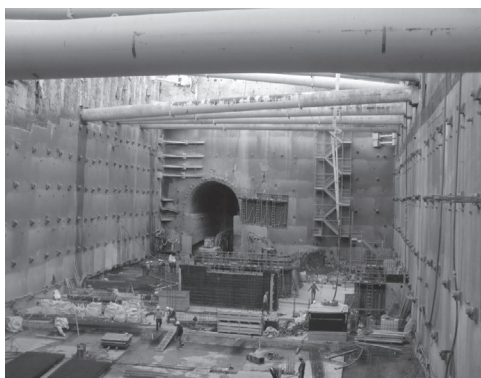

Figure 1. Overview of the excavation

2. THE INSTRUMENTATION

The excavation was carried out according to the interactive method in order to optimize or reinforce the retaining structure in the case of discrepancies between theoretical calculations and observation. Therefore, 8 cross-sections (see Fig. 2) were equipped with a piezometric tube behind the retaining structure, an inclinometer bored 5 meters under the bottom of piles or in the micropiles, one strain gauge on beams and one on anchors, and extensometric gauges fixed in a bore hole in the soil, 6m longer than the lenght of the longest anchor. Moreover, general topographic control of existing buildings behavior was performed with several acquisition targets embedded on facades.
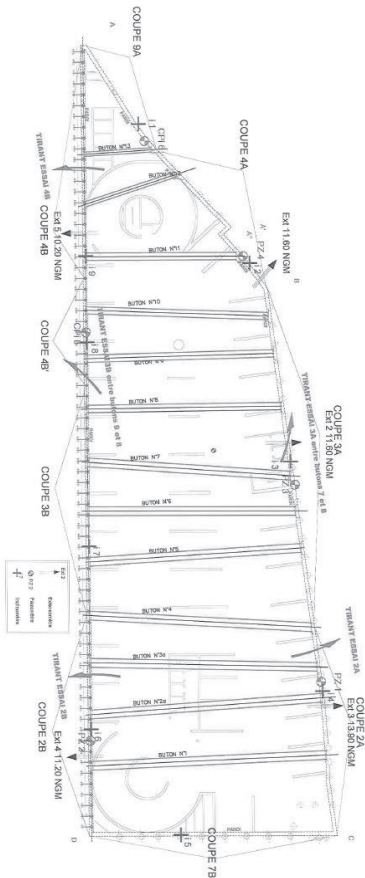

Figure 2. Plan view of the instrumentation

3. BEHAVIOUR DURING EXCAVATION

On existing tunnel side, the measurements of deformation along the retaining structure by inclinometers and targets, tension in anchors, and extension of extensometers, were in good accordance with what was expected.

On existing La Colle car park side (see Fig. 3), the behaviour of the retaining structure, which should have been equipped with five levels of anchors (respectively 19- 16- 13-13 - 13m length), began to be obviously different from the prediction when excavating to put the 3rd level of anchoring.

It was then decided to make further investigations: one core drilling and two pressiometer drillings found out that under the existing park, at the expected geological contact between Cretaceous marl and Jurassic limestone, there was a rather plastic clay thin layer (see Fig.9).
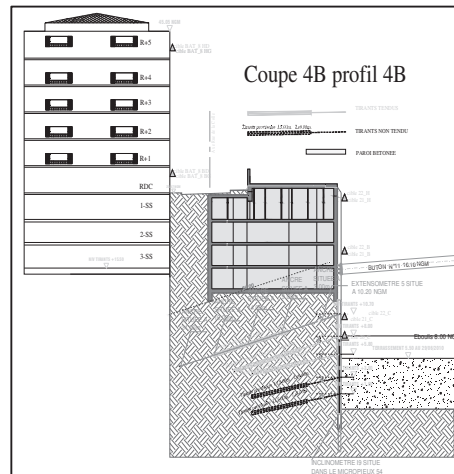

Figure 3. Cross-section 4B under existing car park La Colle

It was also observed that the anchors already in tension, should be anchored in the plastic clay.

It was then decided to reinforce the retaining structure by:
-    A second beam level pre-stressed on the car park wall

- An additional level of anchors, which length is 23m,
- One level of long bored drains (20m)

It was also decided that the excavation would continue by sections instead of full level, before tensing the anchors.

The excavation was then continued. The displacements of the retaining structure under the existing car park went on increasing in a reasonable manner, until the excavation reached the bottom level at -1.5 NGM at the end of October 2010. The structures of the underground floors were then built up, and the construction is now in the upper levels. No damage was observed in the surroundings. It is to say that the foundation of the existing car park is a thick reinforced concrete basement with two direction ground beams.

4. ANALYSIS OF INSTRUMENTATION

The maximum authorized horizontal displacement of the embedded wall, was 10mm; but it was asked the contractor to start to reinforce the retaining wall, as soon as the displacement reaches 8.5mm!

4.1. Inclinometers

It is first interesting to notice that on the side constituted of 800mm piles (existing tunnel side), the inclinometric and topographic measurements indicated small displacements, close to those expected. (see Fig. 5).

On the contrary, the inclinometers on La Colle car park side indicated horizontal displacements obviously greater than those expected. On figure 5, is presented horizontal deformation of the embedded wall, calculated by elasto-plastic method, also called "reaction modulus" method, for the cross-section that had to be reinforced. This method takes into account the successive steps and levels of excavation and pre-stressing beams or anchors.

Compared to the deformation measured by the inclinometer installed in one micropile of the wall, it can be seen that as soon as the excavation begins, the real horizontal displacement is greater in the upper level of the wall. By

increasing in the model the values of reaction modulus for passive reaction of the soil (id when the anchors are pre-stressed), we should better compare the calculated model and observed behaviour.
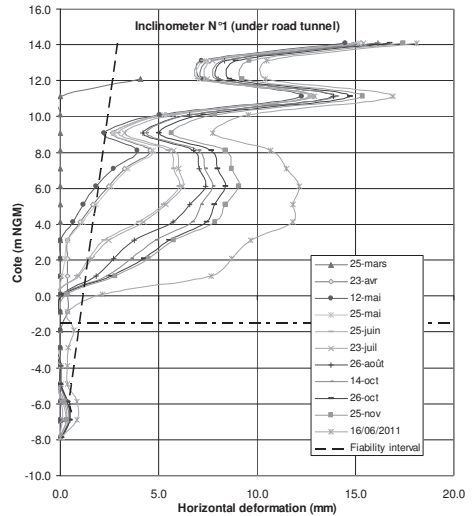

Figure 4. Section 9A- Measured horizontal deformations under road tunnel (800mm piles wall)
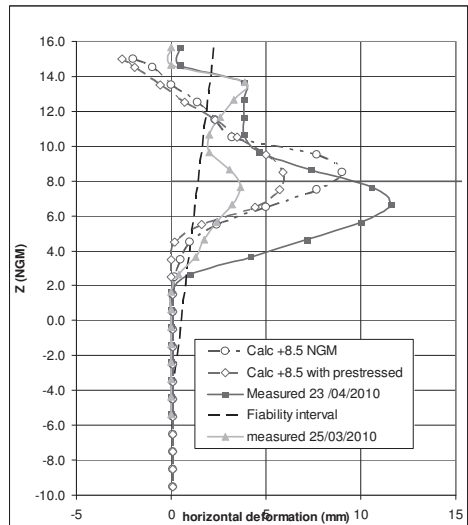

Figure 5. Section 4B- Calculated and measured horizontal deformations (350mm piles wall)

175

One part of the explanation for this horizontal displacement in the upper part of the wall (between 14 and 12 NGM), is that the shortening of the beams due to decrease of temperature during night wasn't taken into account in the model; during the measurement period, the scale of temperature variation between 8.00 AM and 01.00 PM is up to 13 °C on one day, but it is probably not the maximum between night and day, which was not measured. For instance Beam N°11 was pre-stressed at 94 Tonnes, but the first measurements were under this value, probably due to decrease of temperature, that could lead to horizontal movement of the car park structure (see Fig.7). The fact is that until 4th April 2010, the only movement was indicated by inclinometer (see figures 4 and 5), as extensometric head or prism didn't indicate any movement.

But this is not enough to explain why there was so much deformation, even after reinforcing the embedded wall, and after reaching the bottom of the excavation (-1,5 NGM), as the stress in the anchors and beams didn't obviously increase. On figure 6, it can be seen that displacement under the excavation was nearly the same than the one calculated, but at +5 NGM, there was around 18.5 mm of difference. Six months later, the deformation of soil was measured until 3m beneath the excavation, and the deformation was 6mm more at + 5 NGM, and 9mm at -1.5 NGM. In the same time, the inclinometer N°1, on the opposite side of the excavation, indicated a deformation of 3mm more at + 6 NGM, and 5mm at +1.0 NGM (see Fig. 4).

4.2. Extensometers

The extensometric measurements consisted of measuring the displacement between the anchor point at 24m far from the excavation wall, and the anchors respectively at 19, 14, 9 and 3m far from the excavation. On existing tunnel side, it indicated that the ones anchored at 19m far from the excavation didn't have significant movements. On car park side, the extensometric anchors at 19m length from the excavation, had a significant displacement of 4mm when it was decided to reinforce the wall

(see fig. 7). During the same period, the anchor tension decreased of 6 % (see fig. 8).

The displacement of 19m extensometer anchor can be explained by the fact that the 3 anchor lines were not longer enough to go ahead the geological contact between limestone and marl   (see fig. 8).
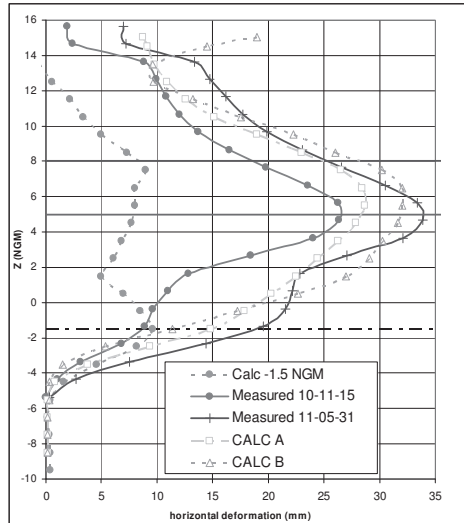

Figure 6. Section 4B- Calculated and measured horizontal deformations (350mm piles wall)
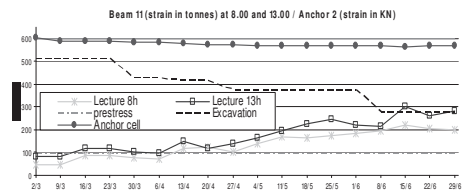

Figure 7. Section 4B- Strain measured on beam 11, at +16,1 NGM, and anchor at 10.7 NGM
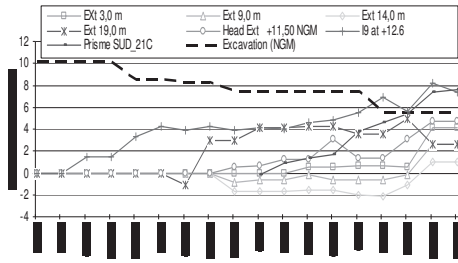
Figure 8. Section 4B- deformation measurements on extensometer, and on inclinometer, at +12,6 NGM
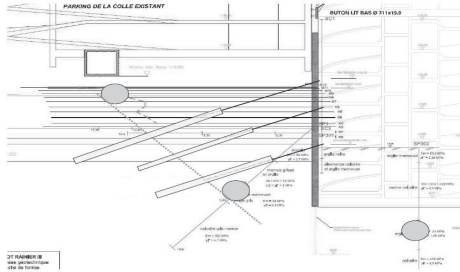

Figure 9. Section 4B- geological section after further investigations

4.3. Creeping

After the excavation completion, and the building of concrete infrastructure levels, it is to be noticed that the embedded wall constitutes of 350mm piles registered further horizontal movements, which amplitude wasn't predicted by preliminary calculations, as 800mm piles registered small deformations. These amplitudes can be explained by creeping movements, which parameters were not correctly appreciated.

5. GEOTECHNICAL PARAMETERS

The investigations consisted of 7 core boreholes and 2 pressiometer bore-holes (see table 1). There were no identification tests, and no mechanical tests in laboratory, before the reinforcement. There were also 2 boreholes and 6 pressiometer bore-holes on the close tunnel road site.

Table 1. Parameters measured from pressiometer tests

Soil Type	Pl* (MPa)	E_M (MPa)
Fill and weak slope deposits	0.4	3
Slope deposits	1.0	8
Alterated marl	2.0	18
Hard Marl	6.0	100
Alterated limestone	4.0	30
Unfracturated limestone	> 6.0	> 200

On sample of plastic clay encountered at the contact between marl and limestone , it was measured:
- C' = 49 kPa et ϕ' = 22° (direct shear test) ;
- Ip = 31 %, WL= 62 % ;
- γ = 21 to 21.7 kN/m3 ;
- Wn = 20 to 25 % ;

The parameters taken into account to calculate section 4B are in tables 2 and 3.

Table 2. Parameters for calculation before reaching the base of excavation

Soil Type	γh (kN/m3)	Φu (°)	Cu (kPa)	KhC MN/m3
Dense slope deposits	20	30	10	52
Alterated marl	20	20	30	75.6
Hard Marl	24	20	70	244

Table 3. Parameters for calculation after reaching the base of excavation

Soil Type	Cote (NGM)	Φ' (°)	C' (kPa)	KhL MN/m3
Dense slope deposits	+17	30	8	32.5
Alterated marl	+8	30	5	47.3
Hard Marl	+5	30	20	122

It was not possible to simulate the same deformation as those measured, when changing only one of the following parameters:
- plastic parameters;
- elastic parameters;
- water level
- creeping of anchors.

On tables 4 and 5, are parameters used in elasto-platic model to have similar deformations than those measured at 23th April 2010.

The model that leads to equivalent displacements that those measured is:
- with groundwater being considered at +5 NGM instead of (-1,5 NGM)
- with plastic parameters being indicated in tables 4 and 5 (respectively before and after reaching the bottom of excavation
- with lowering gradually 50% of the tension of the 3 top anchor lines.

The graphic curves A and B, on Fig.6 show the calculation before and after replacing the anchors by concrete floors.

Table 4. Parameters used for retro-analysis before reaching bottom of excavation

Soil Type	Cote (NGM)	Φu (°)	Cu (kPa)	KhC MN/m3
Dense slope deposits	+17	30	15	52
Alterated marl	+8	20	10	75.6
Hard Marl	+0.9	20	70	244

Table 5. Parameters used for retro-analysis after reaching bottom of excavation

Soil Type	Cote (NGM)	Φ' (°)	C' (kPa)	KhL MN/m3
Dense slope deposits	+17	30	8	32.5
Alterated marl	+8	20	5	47.3
Hard Marl	+0.9	30	37	122

6. CONCLUSION

The most important observations were:
- The phenomena of creeping of anchors, which was also observed in other profiles of the same side of excavation. Only the extensometric measurements enable this interpretation. The anchors were probably not enough long, considering the plastic clay layer encountered. But their length was limited by the authorization given to bore only under the car park "La Colle"!
- The phenomena of creeping of soils after reaching the bottom of excavation. This is not often measured, because often measurement ends after reaching the bottom of excavation. But in hard clay, or marl, this phenomena should be better taken into account.

It finally is to be said that the instrumentation obviously helped the contractor to adapt the embedded wall reinforcement to insure satisfying behaviour, and to enable the construction to be carried out without delay.

7. REFERENCES

Allagnat, D. 2005. La méthode observationnelle pour le dimensionnement interactif des ouvrages. *Presses de l'Ecole Nationale des Ponts et Chaussées*

Marten, S. & Delattre, L. & Magnan, J.P. 2005. Etude expérimentale et méthodolgique sur le comportement des écrans de soutènement. *Presses de l'Ecole Nationale des Ponts et Chaussées*

NF EN 1997-1 juin 2005. *Afnor,* Eurocode 7 : Calcul géotechnique- partie 1 : règles générales (Eurocode 7 : geotechnical design- part 1 : general rules)

NF P 94-282 mars 2009. *Afnor,* Calcul géotechnique- ouvrages de soutènement- écrans (geotechnical design- retaining structures- embedded walls)

Methodology and technology of underground floor construction underneath an historic building (Kamennoostrovsky Theatre in St. Petersburg)

V.M. Ulitsky
Chair of TC207 "Soil-Structure Interaction and Retaining Walls" ISSMGE
State Transport University, Saint Petersburg, Russia, *ulitsky.vladimir@gmail.com*

A.G. Shashkin, K.G. Shashkin, M.B. Lisyuk
Georeconstruction Engineering Co, Saint Petersburg, *Lisyuk@gmail.com*

ABSTRACT: The paper presents a case-history of full-scale underground development underneath a listed historic building in St. Petersburg where the construction method known as 'top-down' was used in the area for the first time in its unique restoration-oriented modification. The chosen method of analyzing underground structures and existing buildings based on two limit states using a visco-elasto-plastic soil model proved quite effective, of which the described case history is an apt illustration.

1. HISTORICAL BACKGROUND

Kamennoostrovsky (Stone Island) Timber Theatre was constructed in 1828, designed by architect S. Shustov to provide a temporary floor for the Imperial Opera and Ballet Troupe whilst reconstruction of the Larger Masonry Theatre was ongoing (the latter was subsequently rebuilt into the St. Petersburg Conservatoire). The critics noted rare elegance of the structure and it was due to that elegance that following a decade and a half a decision was taken to preserve it by means of adding rubble-work foundations (prior to that the lowest courses of the building rested directly on timber piles). The Russian-Italian architect Alberto Cavos believed he had managed to prolong the building's life by about 50 years. However the building was able to withstand the passage of time for as long as 180 years, surviving the tempestuous years of revolutions and wars. Until the 1930s the Stone Island Theatre was used as a warehouse, when it was renovated and converted into a television theatre and later to a dance studio. In Russia only two timber theatre-structures have remained, the Stone Island Theatre being a world heritage site protected by the UNESCO (Fig. 1).

Figure 1. Stone Island Theatre during reconstruction.

2. DEVELOPMENT OF PLAN TO RENOVATE THE THEATRE

The Stone Island Theatre was revived in 2006 when the Russian President decreed for it to serve as Second House of Tovstonogov Academic Drama Theatre to commemorate the 80th anniversary of a famous Russian actor Cyril Lavrov.

Over the two centuries, however, thespian field has developed more sophisticated requirements regarding comforts of the audience. Indeed, these days there are codes and standards envisaging roomy foyers and cafes, convenient wardrobes and lavatories. A contemporary theatre is like an iceberg, inasmuch as its bigger part is not visible to the audience. That invisible space houses stagecraft facilities – upper and lower stage mechanics (e.g. stage terracing, orchestra pit, lighting arrangements, backdrop hoists, etc). Likewise, the theatre goers are unable to see set and props storages. A lot of volume is taken up by air ducts as the air has to be fed into auditoria at low speed ensuring noise-free environment. There are also other innumerable maintenance and utility rooms.

The General Designer «Georeconstruction» Institute was given a highly complicated task featuring what at the time seemed as two mutually exclusive requirements – to convert an old timber building into a contemporary theatre with all the necessary technical sophistication without altering the original historic appearance in any way. The only way to make it happen was to locate all new addenda and enhancements required by a modern state-of-the-art theatre underground, immediately underneath the historic superstructure.

A similar project was realized by A. Pinto in Portugal (Pinto, 2003), where a second stage was provided underneath the historic Theatro Circo in Lisbon, immediately under the main auditorium. The building was underpinned with piles which were joined together by means of reinforced concrete pile caps following the progress of excavation. Over the entire period the settlement was never in excess of 8 mm. Such remarkable result was achieved in reasonably favourable ground conditions – relatively deep ground water level, sandy subsoil, and hard bedrock at shallow depth to embed the underpinning piles.

There had been a similar positive case history of an underground development underneath a historic monument in St. Petersburg, viz. Grand Vestibule construction at Konstantinovsky Palace in the suburb of Strelna to provide access from the lower park. Old grottoes and loggias serving as retaining structures in the natural slope on which the palace had been built were underpinned with bored piles whereby the historical levels in the centre of the building were lowered by 5 m to enable construction of the grand staircase (Ulitsky et al, 2003).

The geotechnical challenge at the Stone Island Theatre was considerably more serious primarily due to a high ground water level. The absolute levels at Stone Island are rather low and the area is subject to flooding. Additionally, the subsoil is compounded largely by soft clay. To make matters worse there is a listed building in the vicinity – the Dacha of Baron Kleinmichel.

To ensure safety of the existing historic buildings, the following criteria were set: (1) additional settlement of the theatre on account of all types of extraneous influences should not be in excess of 20 mm, which is the official requirement for the 3-rd category of reconstructed buildings according to Russian Technical Code TSN 50-302-2004; (2) additional settlement of Kleinmichel' Summer Mansion and it fence should not be in excess of 10 mm over the entire period of construction works on the adjacent site, which is a far more strict requirement than necessary because the building has a restored décor; (3) the ground water level around the underground structure should not vary from the natural by more than 15 cm; (4) the level of dynamic impact through vibration acceleration during construction should not exceed 0.15 m/c^2, as per Russian Technical Code TSN 50-302-2004. The last two criteria could be met on the only condition that near-perfect water-tightness of the cofferdam was ensured and that works were carried out at sparing regimes and accompanied by constant monitoring. The first two criteria could be ensured solely by means of a computer-simulated and analyzed underground structure model.

The area of the theatre's location was levelled with made up ground, the absolute levels

being in the order of 1.930…2.270 m BS (Baltic Datum). Made up ground is 0.8…4.5 m thick. Underlain by lacustrine and marine deposits, it is compounded by silty sand, medium grained sand, light silty loams, and silty sand clay. The underside of this stratum is at 5.5…11.0 m. Underneath down to 10.8…17.0 m the site is compounded by lacustrine and glacial deposits of the Baltic Glacial Lake – silty loams with consistency ranging from liquid to liquid-plastic. Directly underneath there are glacial deposits of the Luga Moraine, compounded by silty sand-clay and loams with gravel and pebbles, as well as boulders which are encountered down to the level of 21.0…26.5 m. Underlying the latter lacustrine and glacial deposits are identified – varved silty loams, stiff-plastic and liquid-plastic in consistency. Quaternary deposits extend down to 24.2…30.3 m, corresponding to absolute levels of -22.27… -28.27 m BS, and are underlain by Wendian stratum, being light firm silty clay.

The area has an aquifer located around the boundary of quaternary deposits. Site investigation in October and November 2007 identified ground water at 1.3…1.8 m from the surface, corresponding to the absolute levels of 0.75…0.30 m BS. Ground water associated with the first aquifer is supplied by the Srednyaya Neva and the Krestovka rivers. The first aquifer system of made up and marine deposits is underlain by relatively water tight marine loams and varved loams of lacustrine and glacial deposits), whose high content of clay particles and dust (in excess of 80%) allows to consider them an aquifer.

Reconstruction implies provision of underground facilities under the entire footprint of the building and extending beyond its perimeter by 6.8 to 25 m (the size of the underground space is 80×40 m). The relative level of the underground structure is at minus 6 m (minus 2.9 m BS). In order to construct the underground area, excavation was necessary down to relative level -6.7 m (absolute level -3.6 m BS). The absolute planning level is at 2.0 m BS. Therefore, an excavation down to 5.6 m from the surface was necessary to accommodate the underground structure.

3. STAGES OF THE THEATHRE RECONSTRUCTION

The sequence of works adopted for the project is shown in Figures 2-9. The works can be subdivided into 6 stages:
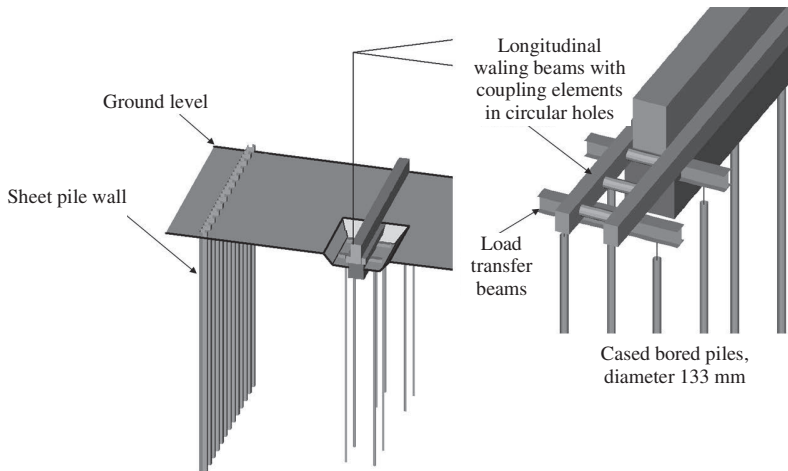

Figure 2. Construction of sheet piles, bored piles, and the unit transferring the load from the walls to the piles.

Figure 3. Introduction of beams underneath the waling and transferring loads onto piles.

1. Stage 1. Drilling holes in existing walls to accommodate transverse beams of the unit responsible for temporary walls-to-piles loads redistribution.
2. Stage 2. Construction of bored piles, introduction of the transverse steel beams, preparation of rebar cages and concreting for reinforced concrete waling beams to facilitate load transfer. (Fig. 2, 3). Simultaneous construction of the sheet pile cofferdam. Bored piles were of 2-step construction "Titan" type: initiated with oscillation of the casing down to the level of the underground structure subsequently followed with pile construction as such. The casing was necessary to improve bending strength of the top half of the pile, which was needed during excavation for the underground structure.
3. Application of jacking devices on the transverse beams, tightening retaining nuts on bars of the underpinning bored piles thereby engaging the piles to assume loads. Following this the lower sections of the building's rubblework foundations could be removed (Fig. 4). These works were to be carried out using maximum sparing methods, ruling out dynamic loading onto existing buildings. Following removal of the lower parts of the rubblework foundations a slab is to be cast directly underneath, forming a rigid disc at the level of the founda-

tions (Fig. 5). Stiffness strips are cast under the existing foundations to redistribute loads onto the slab. Bored piles also are embedded into the rigid disk slab. Following this step, the units described in 2 above are no longer required as the loads from the walls of the building are now transferred directly onto piles through the medium of the rigid disk.
4. Excavation of the pit for the underground structure down to the designed level. Excavation is performed by layers starting from the strips closer to the outer perimeter. Thereat symmetry of excavation on various sections of the building is to be strictly observed. To provide for stability of the sheet pile cofferdam a waling beam and a shoring system are provided; those are to be supported by the rigid disk and mounted on special embedded elements in the slab (Fig. 6, 7). Following excavation of the perimeter strips light-duty machinery is introduced into the pit and excavation begins directly underneath the theatre building. To ensure access of the machinery to the areas under the theatre the bored piles are grouped by four or more always leaving sufficient gaps to allow plant passage. As the soil is excavated the piles are propped by struts to form through-section columns and enhance stability.

5. Construction of bottom slab for the underground structure. Forming embedment slots for the bored piles in the bottom slab.

Concreting for the exterior walls, interior walls and columns of the underground structure (Fig. 8). After concreting for the exterior wall of the underground structure and construction of the intermediate slabs at the perimeter sections the spaces between the sheet piles and the underground structure are backfilled. Following completion of the underground structure and backfilling the struts are taken down (Fig. 9). As soon as supports are introduced under the rigid disk slab, temporary through-section columns of bored piles are dismantled at which point the loads come to be transferred through the bottom slab.

Figure 4. All loads have been redistributed. Old foundations removed.
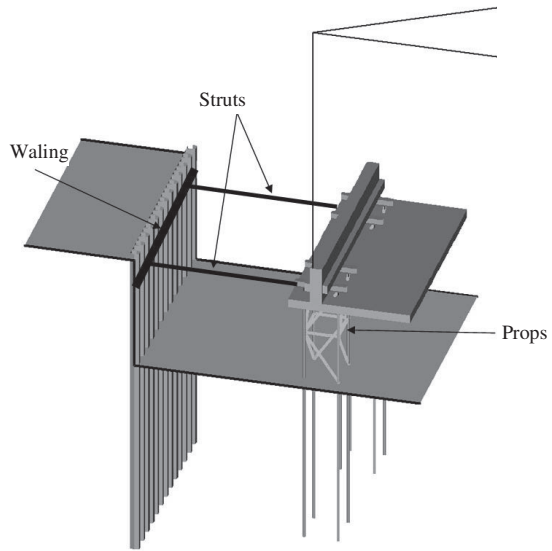

Figure 5. Construction of the top slab.

Figure 6. Excavation down to design level with struts.

Figure 7. Strutting tubes are installed between the top slab and the sheet pile wall.
Excavation for the underground space under the theatre below and around the footprint.
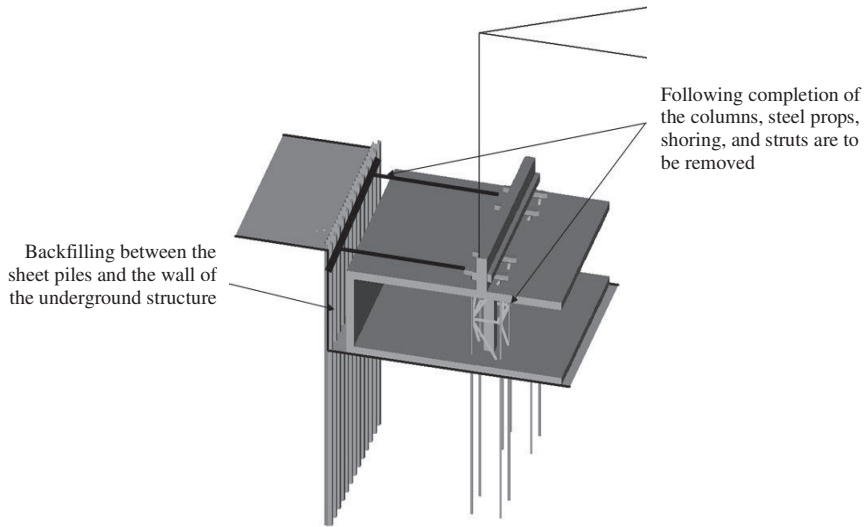
Figure 8. Concreting for the walls and columns of the underground structure.

Figure 9. Constructing the underground structure.

The project featured the first (2008) implementation of the famous "top-down" construction method in its particular restoration-oriented modification: structural restoration of historic elements proceeded upwards, whereas the new underground areas were excavated downwards.

4. CALCULATIONS OF THE UNDERGROUND STRUCTURE

The underground structure was analysed for two groups of limit states, both for the actually designed structure and for the existing buildings, according to a method developed by the second author (Ulitsky et al, 2010).

Calculations for the second group of limit states (in the deformation domain) were performed based on the permissible values of additional deformations of the adjacent buildings caused by the entire scope of impact related to theatre reconstruction. Based on this analysis, a cofferdam layout and a system of shoring were identified, such as would ensure observance of the permissible deformation values of the adjacent buildings for the adopted sequence and rate of works, staying also within prescribed working regimes. In this case it is important to accurately predict subsoil deformation rate, adopting adequate rheological models. At this point a necessity appears of proper connection between solutions obtained by the geotechnical engineer with the contractor's deadlines for each type of works, important for safety of the adjacent buildings. The deadlines are to be agreed as early as at the stage of forming the geotechnical concept. Evidently, the most reasonable and viable solution of retaining structures and shoring is obtainable through preserving the natural soil texture. In this case soil behaviour can be represented through a visco-elasto-plastic model (Ulitsky et al, 2010), whereas the initial viscosity parameter according to our analysis (Shashkin & Shashkin, 2005), can be identified based on the following relation $\eta_0 \approx 100c_u$ [kP year], where c_u – undrained strength of soil. Rheological behaviour of soil here can be represented by:

$$\eta(\tau) = \eta_0 \, \frac{\tau_{\lim} - \tau}{\tau_{\lim}} .$$

This relation allows to combine within one model various types of soil behaviour: slow strain development at insignificant shear stresses and fast deterioration at peak stress values.

It is the authors' contention that a design based entirely on the assumption that natural soil texture is going to stay intact and having no instruments to withstand a failure scenario may not be used. An error or a delay in works implementation should not lead to a calamitous loss of adjacent buildings and structures. Therefore the buildings around the theatre had been analyzed also for the first group of limit states (in strength and stability domains) for an impact of works associated with the underground structure with indefinite delays and with rupturing of natural soil texture. In a visco-elasto-plastic model complete loss of natural texture or a maximum suspension of works can be represented by a nought value of initial viscosity. In other words each subsequent stage of works is assumed as being infinitely long or deformation realized at each stage is taken as limitless (which is the same).

To identify the geotechnical situation for the reconstruction project in question analyses were performed in three settings:

- Analytical solution with one level of shoring;
- Semi-analytical model with coefficients of subgrade reaction, calculated using Schmitt's formula (1995):

$$K_h = 2.1 \frac{E_{oed}^{\,4/3}}{EI^{1/3}} ;$$

- Visco-elasto-plastic soil finite element model with problems being solved in plane strain mode (Ulitsky et al 2010).

Analytical solutions showed the necessary cofferdam length of 15 m, which with the local lowering of moraine deposits had to be at least 17 m.

Semi-analytical solutions (Fig. 10) practically correspond to analytical ones. This was because of similarity of settings and a vast area of limit state realization in soil when values of coefficients of subgrade reaction do not significantly affect calculation results.

Visco-elasto-plastic calculations were performed in stages with excavation time taken to be in order of 6 months. Reduced excavation was modelled at the first stage down to the level below the shoring. At the second stage – construction of shoring and bulk excavation. The analysis assumed loads outside the excavation to be 20 kPa. Analyses were performed for two groups of limit states for the existing historic buildings: 1 – with subsoil remoulding; 2 – assuming intact subsoil texture.

As the analyses performed for the first group of limit states showed, cofferdam displacement values and bending moments in it when computed through the visco-elasto-plastic model with ruptured texture are close to calculation results obtained through analytical and semi-analytical settings. The maximum moment in the cofferdam was 1006 kNm/linear m (101 tonne-m/linear m). To assume a moment like

this a heavy duty sheet piling profile was needed which was achieved using coupled Larsen V piles installed as every second sheet pile in the cofferdam. Calculations showed loads at the propping level to be 446 kN/linear m (45 tonne/m).
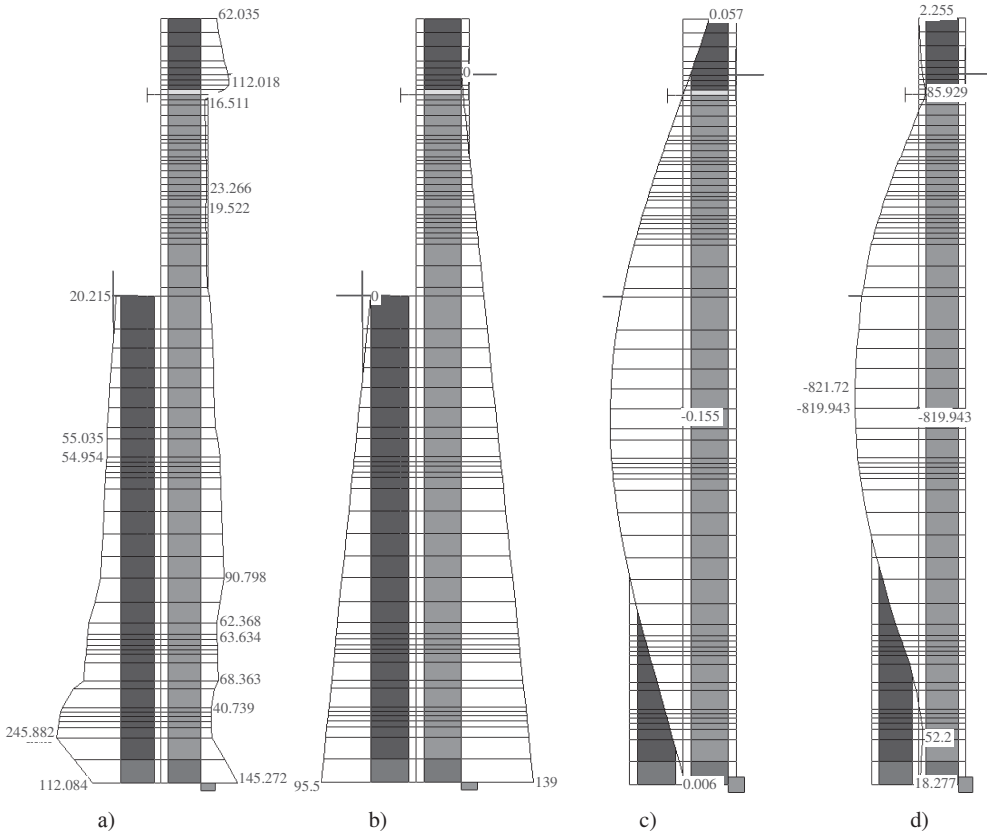

Figure 10. Cofferdam analysis using the semi-analytical method: a – earth pressure contours (kPa), b – water pressure contours in drained setting (kPa), c – cofferdam displacement (m), d – contour of moments in sheet piles (kN)

As can be seen from Fig. 11, the expected displacement of the cofferdam is somewhere in the region of 20 cm. As the building is underpinned with bored piles prior to excavation and its rigidity is provided by means of a rigid disk, movement of the exterior contour is not detrimental for its structures.

The analysis showed the area over which settlement extended on account of soil remoulding to be around 20 m (Fig. 12) in which case Kleinmichel's Summer Mansion can develop settlement of 20 mm, which is not dangerous for its structures but may damage the décor. Loads in the elements of the cofferdam and in the shoring, defined based on first group of limit states analyses for the adjacent buildings, were taken into account during definitions of cross-sections of those structural elements.

Analyses for the second group of limit states for the historic buildings (with assumption of the natural texture being intact) allowed to establish that horizontal displacement of the cofferdam over a period of 6 months would total 30 mm, whereas additional settlement of Kleinmichel's Summer Mansion would not exceed 10 mm, which satisfies the established safety requirements necessary to preserve the décor.

In order to retain natural subsoil texture, monitoring programme envisaged constant consideration of vibration parameters during construction of underpinning piles, removal of rubblework foundations, and sheet pile driving for the cofferdam. Apart from that, monitoring also included regular checks of groundwater level in the area around the site, measurements of settlement and tilts of the theatre, Kleinmichel's Summer Mansion and its fence, and observations of horizontal displacements of the cofferdam.
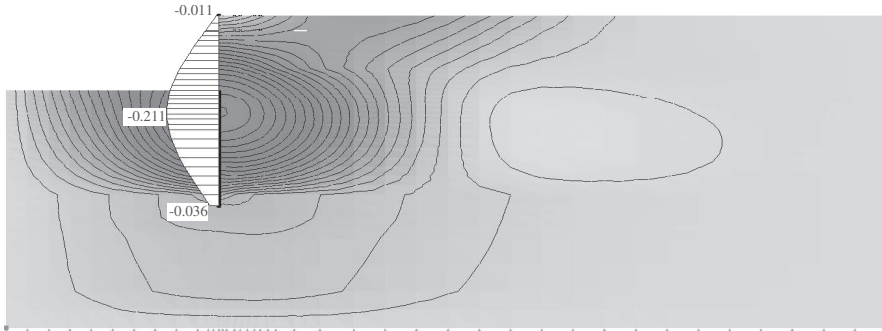

Figure 11. Epure and contours of horizontal displacements of the cofferdam and the soil (m)
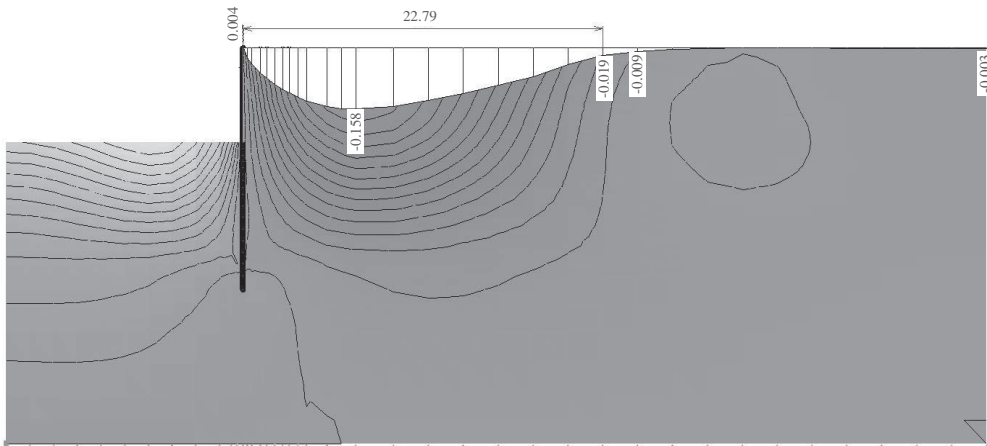

Figure 12. Epure and contours of vertical movement of soil (m)

5. MONITORING OF THE THEATRE

Monitoring in situ allowed to assess workability of the suggested design methodology as well as efficiency of the entire concept of geotechnical supervision.

It is worthy of notice that owing to geotechnical monitoring which was ongoing throughout the entire period of construction works the project team managed to rule out any influence of exceeding the permissible level of vibration acceleration (0.15 m/s^2). Cofferdam had been constructed with a very high quality and made it possible to keep the ground water at its natural level. Maximum settlement of the theatre building reached 24 mm, whereat no dangerous

differential was ever registered (Fig. 13). Following redistribution of loads from the building onto the piles settlements became fully manageable as it had been made possible to adjust the entire building by means of retaining nuts on bars of the underpinning bored piles. Owing to a high culture of works implementation and a reliable design this was never implemented.

Figure 13. Settlements of Stone Island Theatre (mm)

Lost

As of 2010.04.06
As of 2010.05.19

Figure 14. Settlement of Kleinmichel's Summer Mansion (mm)

Horizontal displacement of the sheet piles reached 25…30 mm, and settlement of Klein-michel's Summer Mansion were never in excess of 9 mm (Fig.14). It is interesting to point out that the biggest danger to the Dacha was not the nearby excavation for the theatre project but seasonal fluctuations of the foundations related to frost heave in winter followed by spring thaw.

Therefore design, of the underground structure based on two groups of limit states for the existing buildings ensured not only safety of historic structures, but also safety of their interiors, whereas geotechnical monitoring ensured safety of soil in terms of remoulding during all types of construction works.

REFERENCES

1. Pinto A., Gouveia M. Teatro Circo: Underpinning works for the underground enlargement of a Centenary Theatre – *Reconstruction of historical cities and geotechnical engineering.* St.Petersburg, Volume 1, 2003. pp. 169–174.

2. Ulitsky, V.M, Shashkin, A.G., Orshansky, S.B. Strengthening of Konstantinovsky palace subsoils and foundations. 2003. *Reconstruction of Konstantinovsky palace.* Published by 'Gore-construction-Fundamentproject' Engineering Co. Saint Petersburg, pp.134–141 (in Russian).

3. Ulitsky, V.M, Shashkin, A.G., Shashkin, K.G. 2010. Main regularities of soft clays soil behavior during deep excavations. *Proc. of International Geotechnical Conference 'Geotechnical Challenges in Megacities'*. Moscow, Volume 1, 2010 (in Russian).

4. Shashkin, A.G., Shashkin, K.G. 2005. Elasto-viscoplastic model of structurally unstable soils. 2005. *Reconstruction of Cities and Geotechnical Engineering*. Saint Petersburg, Volume 9, pp. 221–228 (in Russian).

5. Schmitt, P. Méthode empirique d'évaluation du coefficient de réaction du sol vis-à-vis des ouvrages de soutènement souples. *Revue Française de Géotechnique 71*. 1995. C. 3–10.

A geotechnical study of failure mechanism during installation of an underground reservoir in soft soils

K.G. Shashkin
Georeconstruction Engineering Co, St. Petersburg, Russia, *cshashkin@yandex.ru*

T.V. Maslak
Georeconstruction Engineering Co, St. Petersburg, Russia, *mail@georec.spb.ru*

ABSTRACT: The paper presents a study of a complicated geotechnical situation which appeared during installation of an underground reservoir in soft soils.

1. INTRODUCTION

Failure study is an interesting area both for the purposes of both practical design and verification as regards methodologies of structural and geotechnical numerical analyses. The situation described herein is interesting, inasmuch as it shows typical errors in design organization (e.g. incomplete and imprecise site investigation), as well as errors in design of an underpinning structure (related to incomplete understanding and analysis of the geotechnical situation.

The project we have studied is an installation of an underground reservoir for the purposes of construction of an underground sewer pumping station. The reservoir is a circular monolith reinforced concrete structure 22 m in diameter, with design level of 12 m and wall thickness 1.2 m (Figure 1).

Site investigation revealed hard moraine deposits at about 12 m from the ground level. It was intended to immerse the reservoir to the borderline of those hard deposits, reaching which it had been supposed the advancement of the reservoir would be self-arrested; following that it had been planned to construct the bottom slab around the level of the reservoir cutting edge. However, upon reaching the intended design level, self-advancement of the structure persisted. As evidenced by surveying, uncon-

trolled progressive differential settlement of the structure (with tilt reaching approx. 0.15 m) continued at the rate of 3-5 cm a week.

Figure 1. The reservoir after underpinning with bored piles and the tilt having reached 1200 mm

Repeated site investigation revealed soft deposits reaching down to approximately 30 m from the ground surface. Thus, the first link in the following series of unfortunate events is erroneous site investigation data, as those were used as foundational information for the entire project. Sadly, the tendency to save money on the initial stage of the project characterization, i.e. site investigation, is to be recognized as typical for the larger proportion of all construc-

tion projects. The following calamitous sequence of events clearly show the dangers hidden behind this kind of thrift-guided psychology.
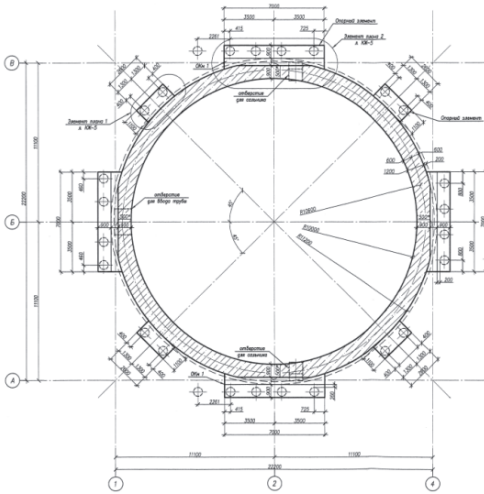

Figure 2. Underpinning the reservoir with bored piles (design detail)

2. UNDERPINNING DESIGN

In order to arrest self-advancement of the reservoir some kind of underpinning solution had to be devised. The contracting company addressed by the client specialized chiefly in design and construction of piled foundations. The task set to the contractor was "to arrest uncontrolled sinking of the underground reservoir in order to complete the underground section of the sewer pumping station (i.e. to be able to excavate down to the cutting edge of the underground reservoir)".

The contractor put forward the following underpinning option: to redistribute the loads from the reservoir to bored piles, using a pilecap to link them with the upper part of the reservoir ring. The design featured 26 no. 30 m long 630 mm diameter piles to be constructed along the circumferential perimeter of the structure (Figure 2) with toes embedded in hard moraine deposits. Static load tests performed on the piles showed their bearing capacity to be adequately strong (up to 100 t).

However, the underpinning design failed to consider the situation which would technically appear at the moment of the reservoir excavation. Meanwhile, it is evident that excavation of soft material down to the cutting edge of the reservoir may have potentially led to soil intake inside the reservoir. This soil intake phenomenon has been well studied using bored piles as an example; it would have been unreasonable to suppose that such conditions would not manifest in a large diameter well.

So, as expected, following to engagement of the piles, sinking of the reservoir stopped. However, subsequent excavation resulted in considerable soil intake inside the reservoir, around which a visible settlement trough began to form. It is to be noted that there had been no significant transport of ground water inside the excavation, the bottom of the reservoir was inundated with semi-liquid water-retaining soil. This soil intake phenomenon inside the reservoir resulted in its rapid movement (up to 80 cm per day) with tilt reaching 1200 mm.

3. ANALYTICAL AND NUMERICAL ANALYSES

To understand the reasons for such dramatic developments and in order to work out a methodology of the reservoir stabilization we carried out analytical and numerical analyses using various software.

Let us view a detail of the reservoir – a sector with an angle α. Now we define the most probable slip radius r.
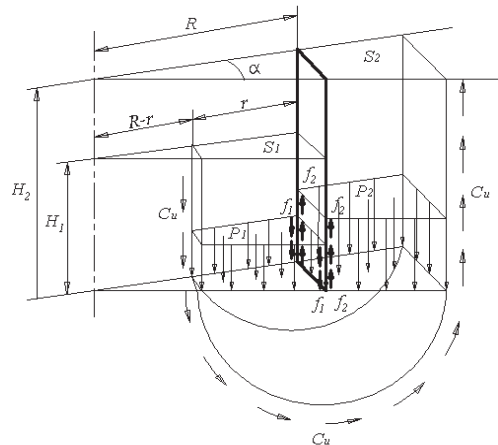

Figure 3. Analysis profile for analytical calculation of subsoil stability

Square area of sector inside the reservoir:

$$S_1 = \frac{R^2 \cdot \alpha}{2} - \frac{(R-r)^2 \cdot \alpha}{2} = \frac{(R-r) \cdot \alpha + R \cdot \alpha}{2} \cdot r =$$
$$= \frac{1}{2}(R - r + R) \cdot \alpha \cdot r = \frac{2 \cdot R - r}{2} \cdot \alpha \cdot r$$

Total force counteracting upwardly directed soil pressure (constraining force):

$$G_1 = \gamma \cdot S_1 \cdot H_1 + C_u \cdot H_1(R-r) \cdot \alpha + f_1 \cdot H_1 \cdot R \cdot \alpha$$

Constraining pressure:

$$P_{G1} = \frac{G_1}{S_1} = H_1 \left(\gamma + 2 \cdot C_u \cdot \frac{R-r}{(2 \cdot R - r) \cdot r} + \right.$$
$$\left. + 2 \cdot f_1 \cdot \frac{R}{(2 \cdot R - r) \cdot r} \right)$$

Square area of sector outside the reservoir:

$$S_1 = \frac{R^2 \cdot \alpha}{2} - \frac{(R-r)^2 \cdot \alpha}{2} = \frac{(R-r) \cdot \alpha + R \cdot \alpha}{2} \cdot r =$$
$$= \frac{1}{2}(R - r + R) \cdot \alpha \cdot r = \frac{2 \cdot R - r}{2} \cdot \alpha \cdot r$$

Total force conducive to upwardly directed soil pressure (displacement force):

$$G_2 = \gamma \cdot S_2 \cdot H_2 - C_u \cdot H_2 \cdot (R+r) \cdot \alpha - f_2 \cdot H_2 \cdot R \cdot \alpha$$

Displacement pressure:

$$P_{G2} = \frac{G_2}{S_2} = H_2 \cdot \left(\gamma - 2 \cdot C_u \cdot \frac{R+r}{(2 \cdot R + r) \cdot r} - \right.$$
$$\left. - 2 \cdot f_2 \cdot \frac{R}{(2 \cdot R + r) \cdot r} \right)$$

Let us now define function of points of a circular cylindrical slip surface:

$$y(x, r) := \sqrt{r^2 - (x - R)^2}$$

Assuming loads in a profile considering a sector of an axisymmetrical problem it is necessary to account for the moment generated by normal forces applied perpendicularly to its outermost sloping surface. Otherwise, at low c_u values sector may turn out to be unstable even if there is no differential of pressures P_{G1} and P_{G2}.

Dividing moment of soil cohesion by moment of forces related to weight and initial applied differential of pressures, and further reducing the result by value of small angle α, analogous to the elementary Terzagi plain problem method, we obtain the safety factor:

$$K(r, P) := \frac{\displaystyle\int_{R-r}^{R+r} c_u \cdot \frac{r^2}{y(x, r)} \cdot x \, dx}{\displaystyle\int_{R-r}^{R+r} (p(x, P, r) + \gamma \cdot y(x, r)) \cdot x \cdot (x - R) \, dx - \int_{R-r}^{R+r} \frac{1}{3} \cdot \gamma \cdot y(x, r)^3 \, dx - \int_{R-r}^{R+r} \frac{1}{2} \cdot p(x, P, r) \cdot y(x, r)^2 \, dx}$$

As evident from the analysis the safety factor decreases as r increases, therefore the most unfavourable pattern of instability development would be $r = R$.

In this case the formula to obtain the safety factor becomes considerably more simple and is reduced to

$$K = \frac{2\pi c_u}{P_{G2} - P_{G1} - P} \qquad (1)$$

Further analysis was performed at undrained soil strength of 26 kPa and soil density of 19.3 kPa derived from laboratory testing (Figure 4). Let us now consider excavation down to the cutting edge, as initially assumed in the design. In this case $P_{G1} = 0$, $P_{G2} = 194.5$ kPa, whereat soil friction against the reservoir walls is discounted, as, one may say, the reservoir advances and moves together with the soil. Then the safety factor according to Formula (1) is 0.84. Not discounting friction against the outer wall of the reservoir the safety factor is 0.93.
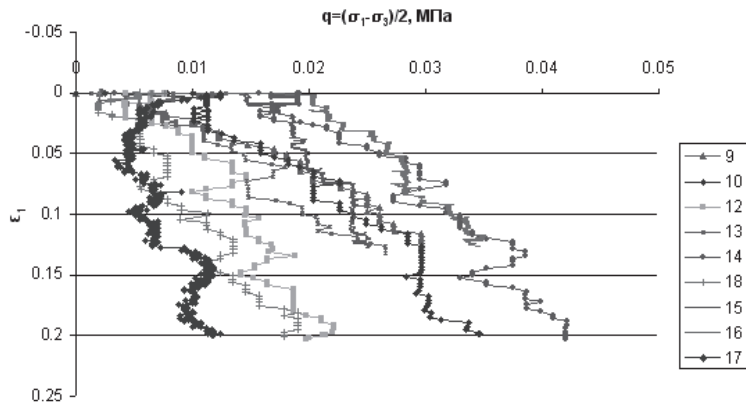
Figure 4. Results of triaxial unconsolidated-undrained tests of the reservoir subsoil

Numerical analysis of soil stability performed using PLAXIS and FEM models produced results similar to the analytical (Figure 5,6).
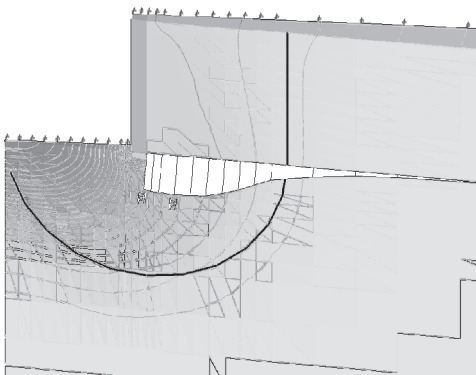

Figure 5. Soil failure around the reservoir (indeterminate movement values). Numerical analysis with FEM models. Safety factor at C_u=26 kPa is 0.93

Analysis of the reservoir stability with account of the constructed underpinning piles was carried out in spatial setting using FEM models 2.0 software. We analyzed 1/8 of the spatial profile of the reservoir and surrounding soil (with account of symmetry axes). The piles were modelled with their relevant longitudinal rigidity and flexural stiffness, considering also their possible loading beyond failure: for bending stresses exceeding the ultimate we

modelled plastic hinges. For piles with designed degree of reinforcement the taken ultimate bending moment was 260 kNm.
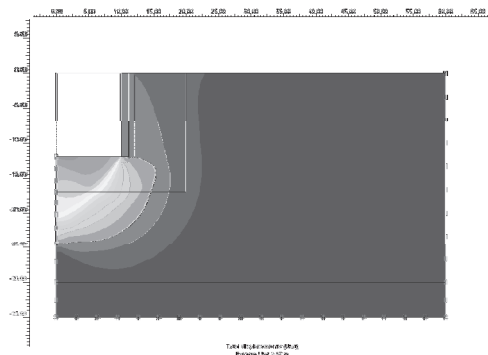

Figure 6. Soil failure around the reservoir (indeterminate movement values). Numerical analysis with PLAXIS. Safety factor at C_u=26 kPa is 0.87

Analysis showed the numerical calculations not to tally, which is significant of ultimate stress in the subsoil being exceeded and of stability loss. The pattern of instability development is in agreement with the analytical and the numerical solutions (Figure 7). The pattern of piles failure is shown in Figure 7.
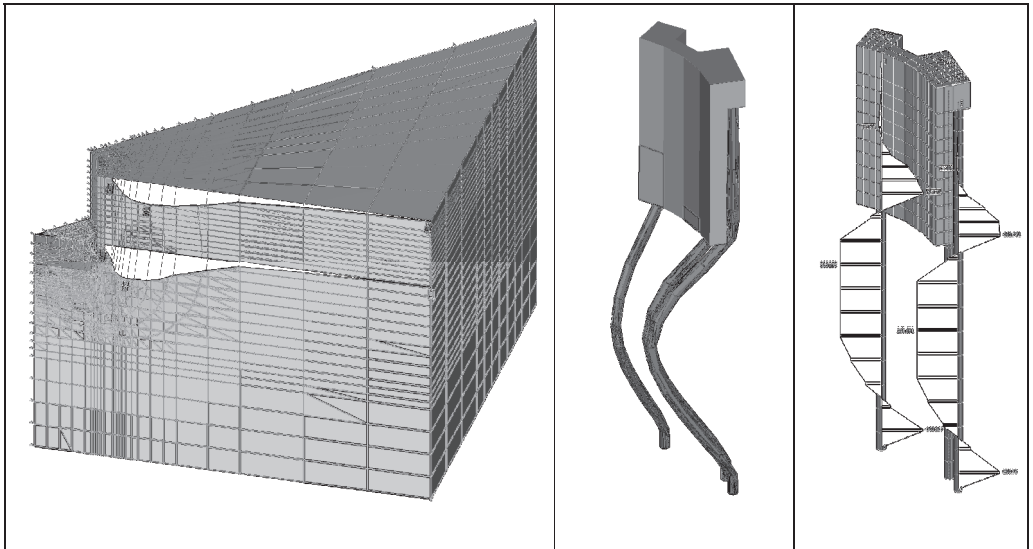
194

Figure 7. Pattern of instability development in spatial setting and the pattern of piles failure

The analysis showed also that underpinning the reservoir with bored piles had not accommodated the possibility of excavating soil down to design level. Bored piles of 620 mm diameter are impossible to be reinforced to such an extent that they would withstand instability development in subsoil. The tilt of the reservoir was most probably related to nonsimultaneous failures of the piles.

Thus, the underpinning phase was geotechnically unsubstantiated which ultimately resulted in the underpinning measures going to waste.

To make possible excavation of the reservoir it was necessary first and foremost to rule out loss of bearing in the soil as outlined in Figure 3.

As the most expedient option we came forward with soil strengthening by jet grouting with application also of vertical anchors. Jet grouting alone was obviously insufficient to exclude the possibility of loss of bearing in the soil. Soil/cement mixture, being the final result of jet grouting, does not possess sufficient bending strength and would have inevitably failed, if instability developed along circular cylindrical surface, which would have rendered it useless in keeping the soil out of the reservoir. Therefore the main measure to counteract bearing failure in soil was construction of anchors embedded in relatively hard deposits. The anchors, possessing tensile strength, would act against stability loss in soil (Figure 8).
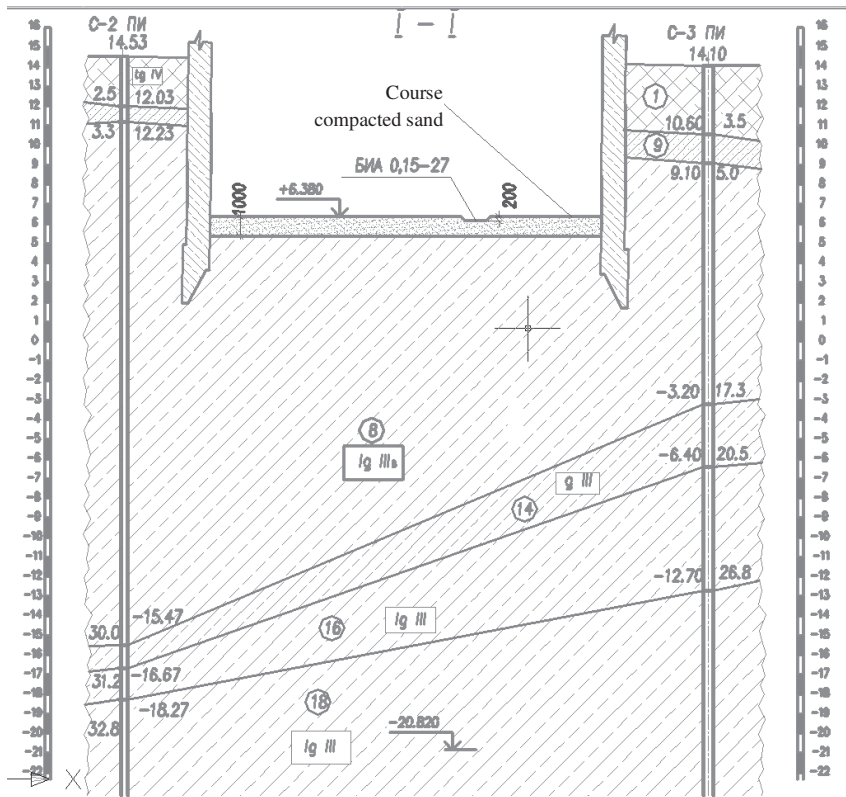
Figure 8. The anchors working against development of soil instability and soil intake into the reservoir

Currently the soil has been successfully strengthened as described above, whereby settlement of the reservoir has been arrested.

The case history described herein clearly shows dangers hidden behind design practice with insufficient site investigation data, as well as repercussions occurring due to incomplete geotechnical analysis of structures behaviour at the strengthening/underpinning stage.

The geotechnical bases of microtunneling in urban conditions

V.M. Ulitsky
St. Petersburg State Transport University, Russia, *ulitsky.vladimir@gmail.com*

V.N. Paramonov, A.G. Shashkin
Georeconstruction Engineering Co, St. Petersburg, Russia, *parvn@georec.spb.ru*

ABSTRACT: In the report there are presented description of microtonneling technology, requirements to technology of works in conditions of large cities and the main principles of working out the theoretical methods for geotechnical forecast of the technology. There are presented example of design forecast the technology of microtonneling and construction of vertical technological pit.

The construction of deep engineering communications is the essential necessity for all large cities of the world. The problem of lining the deep collectors appears with the special importance in St.-Petersburg, the engineering infrastructure of which much lags behind the level of European capitals.

The complexity of the problem appears because of the special engineering-geological conditions of St.-Petersburg. The contours of historical city center with high accuracy coincide with area of distribution the soft clayey soils.

This territory is characterized with the following geological conditions. From the surface the absolute mark of which seldom exceeds +3,0...+3,5 m the average 2-meter layer of a bulk ground is situated, and lower there are delth mainly fine and silty sand (capacity from 2 up to 10 m), which are spread by 10...20-meter layer of weak Baltic loam and sandy loam. The root of rather strong moraine adjourment is on depth up to 20...30 м from the surface

The microtunneling technology is rather perspective and, basically, the most safe method of construction the communications.

It assumes construction of vertical shafts in tops of a broken line on an axis of a line with alternation of working and reception shafts. The sizes of shafts in the plan are defined by dimensions of jack station and microtunneling machine. The depth of shafts is usual on 1 m exceeds design depth of a line. Microtunneling comes true by cave-in of rock-exploiting body, in a forward part of which there is four-beam rotor, equipped with core cutters and knifes.

The microtunneling process is conducted practically with closed face. The ground, getting to a rotor, is pounded by cutters, reduces to the pulp with the help of water, submitted to front of microtunnel, and is pumped out on the surface.

At carrying out the works in compact urban conditions the detailed geotechnical bases is required for two components of technology, namely:

– for construction of the vertical technological shafts;

– for the horizontal microtunneling process including carrying out the works in the soft clayey soils.

The geotechnical substantiation can be carried out proceeding from the information about the engineering-geological conditions of territory; data of topographical shooting of the site; the items of information on a type, storey, date of construction and degree of safety of the neighbor buildings; about a construction and state of the foundations, average loads at the

foundation; about a category of safety of the neighbour buildings, determining necessity of realization of work on strengthening their ground and underground constructions.

The most perfect way of keeping this information are geotechnical maps. These maps give the important information basis for lining the engineering networks, tunnels, underground lines in urban conditions. With their help it is possible to establish precisely, which buildings get in a zone of raised risk at carrying out that or other kind of civil work. The maps become the base for creation of detailed system of supervision (monitoring) for deformations of these buildings and control for carrying out the civil work close to them. The maps allow to formulate the requirements to technology of work, ensuring minimization of adverse influence on existing buildings. With the help of the maps the specific requirements on water protection of pits can be exposed also.

When the vertical shafts are constructed the next geotechnical and geoecological requirements should be assured:

– to ensure static and filtration stability of the vertical barriers and bottom of the shaft;

– to bear the necessary horizontal load from the jack station by the shaft wall;

– to keep natural structure of soils in the foundation of the neighbor buildings;

– to exclude inadmissible dynamic influence on buildings and soils of the foundations;

– to keep the natural ground water level at the surrounding territory.

The safe approach to the existing buildings should be determined for the microtunneling process. The velocities of the shield moving and removing of the soil pulp should be correlated so that to exclude the work of the machine in the condition of «cave-in», on the one hand, and to exclude extraction of the soil volume exceeding geometrical volume of the tunnel, on the other hand. Partly the latter is provided by the computer programs, incorporated in the block of management.

The structure of the shaft barrier is calculated in view of its joint work with the surrounding soil massive and neighbor buildings. The feature of such calculations is determined by complexity of geometry of the designed scheme and the geological bedding, with presence of media with essentially various proper-ties (soils and constructions), and at last with the nonlinearity of the media properties. This feature stipulates the application of numerical methods, in particular, the finite element method, with use the traditional in the geomechanics measure of indefinitely small strains.

The other aspect of the considered technology – the microtunneling process - required the other approach at the mathematical modeling. When any geotechnological operations follow to significant local displacements of the soil, in particular, relatively to the shield, the mathematical models should be constructed with the account the kinematics of media with use the measures of large strains.

We shall consider a geotechnical substantiation of a lining the engineering communications on an example of a collector on a line pr. Nastavnikov – pr. Kosygina in Petersburg.

For the first time the question on such substantiation has arisen in connection with deforming of three buildings at lining near them on usual technology the trench canalization collector at the depth 5,0 m from the surface.

The peculiarity geological conditions at the site consists that here are clayey soils of various durability up to depth 13...19 m, containing only lenses and seams of saturated sand, water in which are not connected with the head horizon. The head waters are dated to the thick layer of sand, spreading the clay layer.

At working the trench an attempt of downturn this deep head horizon, unsuccessful due to extensiveness the territory of its meal, was undertaken. This attempt has resulted only to suffosion carrying out the silt particles from the foundation of the existing buildings into the water lowering chinks. The struggle with inflow of water has appeared practically impossible, water lowering was soon stopped. Fortunately, it has not put irreparable damage the buildings, constructed on piles: floors and the partitions, erected on a ground have suffered only. Carried out the hereinafter geotechnical mapping by four hundred chinks at the territory has resulted to the paradoxical conclusion: just the emergency site of the line had the most favorable conditions for lining the trench by depth up to 5,5 m. The analysis of geotechnical situation has shown, that piezometric level, revealed in limits of the emergency site, did not exceed the water level in sand lenses and layers and was on the

depth no less than 6,0 m from the surface. Whereas the root of sand layer, containing pressure head waters, does not rise above mark −13 m from the surface, during excavation the trench on given depth is lower than its bottom there was the layer clayey soil, the thickness of which is sufficient for prevention of break the head waters. The receipt of head waters in a trench could be created only by an artificial way – through the chink or lengthways sheet pile, cutting through the clayey soil. The inflow of water from sand lenses and seams, contained in the clayey stratum, could not essentially complicate excavation of trenches. Lining of the communications on an emergency site it was possible to carry out practically dry in trenches, protected by short (not cutted the clay) sheet pile at the opened overflow.

The described soil conditions jointly with offered technology of construction the trench make the first geotechnical type at the map of considered line (fig. 1). The second type, similar in a geological structure with first, but described by absence of sand lenses and seams in the top clayey stratum, in the technological relation is easier, as does not require any construction the water-proof protection of the trench. To the third and fourth type there corresponds presence in the zone the layers of sand, containing head waters, connected to the basic head horizon, or alternation of sands, containing inter-strata head waters, and clayey sediments at all depth of the geological section. In these conditions an application of special technologies, excluding water lowering outside the trench is necessary.
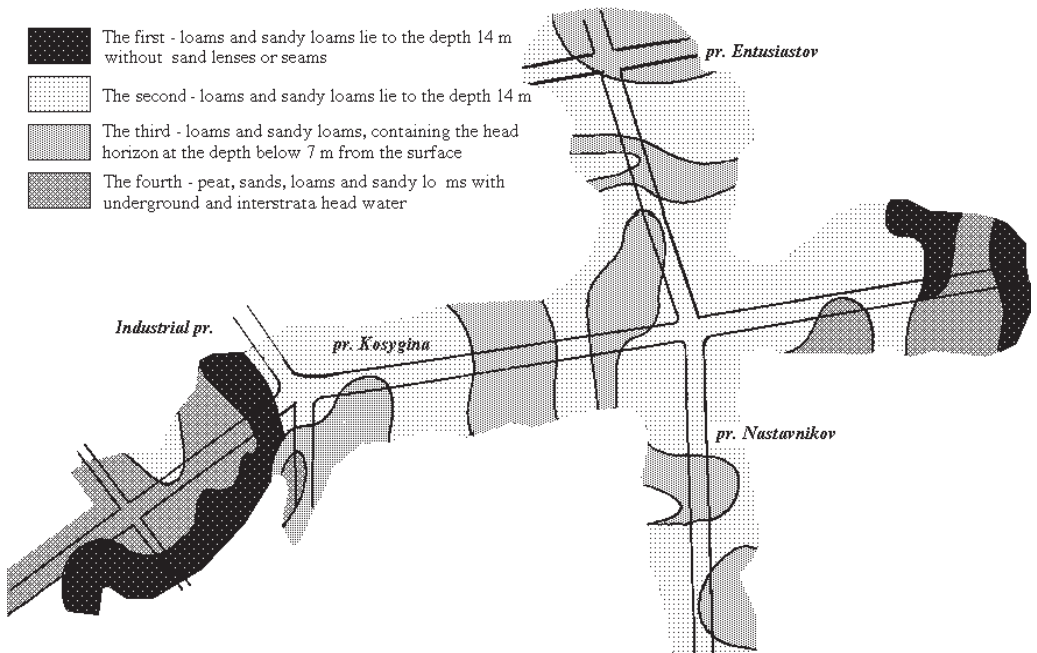

Fig. 1. Fragment of a geotechnical map for lining the engineering communications on depths up to 5 m from the surface.

The carried out calculations have allowed to recommend application in the given conditions the technology of microtunneling. The vertical technological shafts are expedient to place on sites of territory, characterized by the first or second type of soil conditions, the sites with the third and fourth types geological conditions were offered be to was passed by microtunnels.

The complexity of the geotechnical situation in a considered case is much reduced by significant distance of the line from existing buildings (about 30 m). Thus, the main problems, deci-

sion of which it is necessary to give the basic attention, are following:

– maintenance of stability the walls of shaft, perceiving pressure of the soil and the bottom, on which hydrostatic pressure of head waters acts;

– recognition the horizontal effort from the jack station during pressing the elements of a collector;

– changement the stress-strain state of the soil massive during microtunneling (which can be reflected in this case only at the nearly located communications.

Two first problems were investigated by elastic – plastic model, realized in the program complex "Geomechanics" (Fadeev and others), last – with use the measure of large strains geometrically and physically nonlinear statement (Paramonov, Shashkin).

The first series of problems was devoted to research the problem of stability the natural clayey bottom of the shaft excavation at presence the head horizon in spreading sand. The scheme of the problem is represented on the fig. 2. In the series of the decisions the thickness of the soil bottom, sufficient to percept the pressure of head horizon was determined. The stability of the bottom relied supplied in the event that in elements of a ground there were not enough stretching stresses, which could lead to infringement the continuity of soil and its break by water pressure. The depth of excavation was accepted equal to 7,0 m, i.e. by 1 m lower than designed, taking into account over-excavation of soil and construction the sublayer. The stability of walls of excavation in this series of problems was considered deliberately supplied (condition of maintenance of stability were considered in the second series of problems). Silty loams and loams were considered as relative waterproof (on period of running the works).The influence of head waters was simulated by the application the appropriate vertical pressure at the bottom of waterproof.

The carried out calculations have allowed to define, that the stability of pit bottom is provided at the minimum thickness of the clayey layer 2,0 м below than bottom. The first and second types of soil conditions on a geotechnical map of area correspond to this condition(see fig. 1).
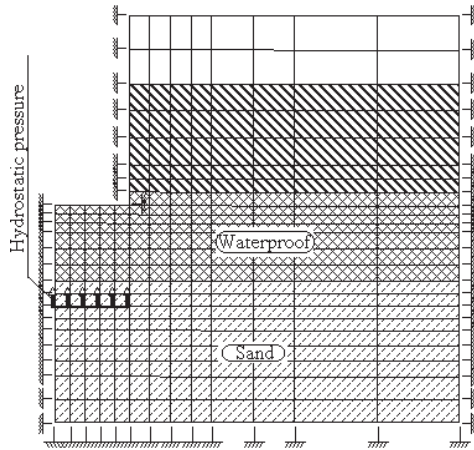

Fig. 2. The FE scheme of problem of stability the soil bottom of the shaft.

The second series of problems consist in determination the efforts in the construction of shaft and stress-strain state of soil massive around the shaft walls by jet effort from the jack (2880 KN for the machine M 288-M- A VN 1200c of German firm "Herrenkneht"). Erection of the shaft walls was supposed with bored piles with trust system in two levels. The calculations allowed to established, that the maximum moment in sections of shaft wall makes 177 KN·m (fig. 3). Thus the maximum horizontal displacement of the wall does not exceed 5 mm. Results of the calculations problem allow to recommend the construction of the shaft walls with the piles of length 10 m and the diameter of 460 mm with reinforcing 6∅28AIII.
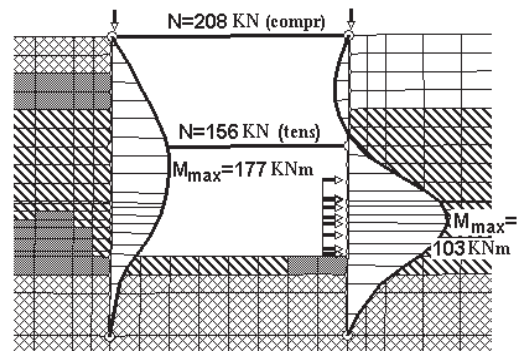

Fig. 3. Loads in the shaft elements from jack

At last, in the last series of calculations the microtonneling process was considered. The

decision of problems came true in the most unprofitable elastic-plastic statement, allowing to consider two extreme situations: outstripping of cave-in of the working body in comparison with exploitation of the soil and return situation, resulting to overexcavation of soil at the face.
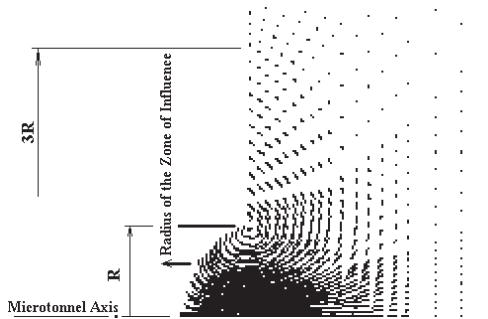

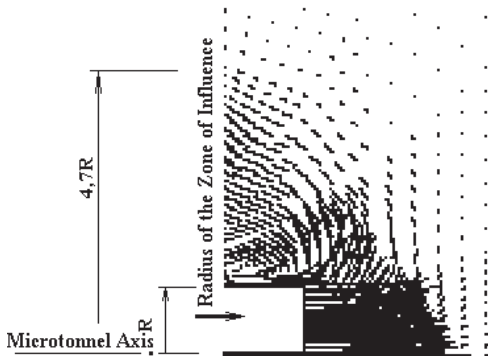Fig. 4. Trajectories of the movement the soil particles at overexcavation.

Рис.5. Trajectories of the movement the soil particles at outstriping cave-in in comparison with development of a ground.

The decision of the problem in large strains allows to estimate these two cases movement of the soil particles, which is represented by moving of the nodes of FE grid. Th calculations show, that for the given technology the greatest influence to the soil can render effect of cave-in, resulting to lift the surface and appreciable displacement of the soil in a zone of radius 5R, where R - radius of tonnel.

Real picture of soil movement is possible to present by entering to account the parity of rheological properties and microtonneling speed.

REFERENCES

Paramonov V.N., Shashkin V.N. Modeling The Technological Processes at the Construction the Bored Piles in Soft Clays // Problems of Foundation Engineering in Conditions of New Capital. *Proc. of I Kazakhstan national geotechnical conference*. Akmola, 1997. Vol. II. - pp. 462-466. (In Russian).

Fadeev A.B., Paramonov V.N., Repina P.I., Glybin L.A., Shashkin A.G. The FEM at Working Out the Students Works in Engineering Disciplines: *The Manual*. SPbGASY. SPb, 1997. – 60 p. (In Russian).